SYNTHESIS OF MAIN GROUP MOLECULES AND MATERIALS EXHIBITING UNIQUE REACTIVITY AND OPTOELECTRONIC BEHAVIOR

By

JEROD M. KIESER

Submitted in partial fulfillment of the requirements for the degree of

Doctor of Philosophy

Thesis Advisor: Dr. John D. Protasiewicz

Department of Chemistry

CASE WESTERN RESERVE UNIVERSITY

January 2020

Case Western Reserve University

School of Graduate Studies

We hereby approve the thesis/dissertation of

Jerod M. Kieser

candidate for the degree of Doctor of Philosophy.*

Committee Chair

Dr. Thomas Gray

Committee Member

Dr. Geneviève Sauvé

Committee Member

Dr. Gregory Tochtrop

Committee Member

Dr. David Schiraldi

Defense Date

August 07, 2019

*We also certify that written approval has been obtained

for any proprietary material contained therein

For Dan and Lora

Your continued encouragement made this possible

Table of Contents

List of Figures

List of Schemes

List of Abbreviations

Ac	acetyl
Anal. Calcd.	combustion elemental analysis, calculated
anhyd.	anhydrous
APT	attached proton test
Ar	aryl
BAP	1,3-benzazaphosphole
BOP	1,3-benzoxaphosphole
br	broad
CAAC	cyclic (alkyl)(amino)carbene
Cat.	catalyst
cod	1,5-cyclooctadiene
COSY	correlated spectroscopy
Cp	cyclopentadienyl
d	doublet
deg	degrees
Dipp	2,6-diisopropylphenyl
DMAP	4-dimethylaminopyridine
DME	dimethoxyethane
DMSO	dimethylsulfoxide
DOSY	diffusion ordered spectroscopy
ESPT	excited state proton transfer
Et	ethyl

^{Et}CAAC	(2,6-diisopropylphenyl)-4,4-diethyl-2,2-dimethyl-pyrrolidin-5-ylidene
Eq.	equilibrium
EXSY	exchange spectroscopy
Fp	cyclopentadienyliron dicarbonyl
FWHM	full-width half-maximum
GFN2-xTB	geometry, frequency, noncovalent, extended tight binding
hept	heptet
HMBC	heteronuclear multiple bond correlation
HOMO	highest occupied molecular orbital
hr	hour
HSQC	heteronuclear single quantum correlation
IMes	1,3-bis(2,4,6-trimethylphenyl)imidazol-2-ylidene
^{i}Pr	isopropyl
IPr	1,3-bis(2,6-diisopropylphenyl)imidazol-2-ylidene
IPrBr	1,3-bis(2,6-diisopropylphenyl)-4,5-dibromoimidazol-2-ylidene
K_d	association constant
K_{eq}	equilibrium constant
KS-MO	Kohn-Sham molecular orbital
LDA	lithium diisopropylamide
LUMO	lowest unoccupied molecular orbital
m	multiplet
MAS	magic angle spinning
Me	methyl

MeCN	acetonitrile
Mes	2,4,6-trimethylphenyl
Mes*	2,4,6-tri-t-butylphenyl
MW	molecular weight
^{n}Bu	*n*-butyl
NHC	*N*-heterocyclic carbene
NMR	nuclear magnetic resonance
NOE	nuclear Overhauser effect
NOESY	nuclear Overhauser spectroscopy
OCP	phosphaethynolate, $[O\text{-}C{\equiv}P]^{-}$
ORTEP	Oak Ridge thermal ellipsoid plot
OTf	trifluoromethanesulfonate
Ph	phenyl
Ph-BIM	2-phenylbenzimidazole
ppm	parts per million
Pr	propyl
q	quartet
RT	room temperature
s	singlet
sep	septet
Solv.	solvent
t	triplet
*t*Bu	*tert*-butyl

^{t}Bu-BAP	2-*tert*-butyl-1,3-benzazaphosphole
TD-DFT	time-dependent density functional theory
Th	thiophenyl
Th-BAP	2-(thiophen-2-yl)-1,3-benzazaphosphole
THF	tetrahydrofuran
TMB	tetramethylbutane
TMS	trimethylsilyl
Ts	toluenesulfonyl
TTS	tetrakis(trimethylsilyl)silane
UV	ultraviolet
δ	chemical shift
λ_{em}	emission wavelength
λ_{ex}	excitation wavelength
Φ	quantum yield

Synthesis of Main Group Molecules and Materials Exhibiting Unique Reactivity and Optoelectronic Behavior

Abstract

by

JEROD M. KIESER

The development of π-conjugated organic materials has become an important research field due to the wide variety of potential device applications. Heteroatom substitution within the π-conjugation of these materials allows for substantial tunability of materials properties. Our focus has been on the integration of phosphorus into π-conjugated systems to take advantage of the similarities of C=C and P=C bonds. One of the materials we used to advance this goal is sodium phosphaethynolate Na[OCP]. Using a zirconium-benzyne complex, $Cp_2ZrC_6H_4(PMe_3)$, we discovered unique insertion chemistry, previously not known for this synthon, which produced a metallophosphaalkene dimer bound within a coordination polymer. Additionally, a number of organometallic complexes were further derived from this.

In a separate project, we also studied the photophysical response of isolable carbenes on NH-containing fluorophores. Based on the emission quenching we observed upon combining 1,3-bis(2,6-diisopropylphenyl)imidazole-2-ylidene (IPr) with the luminescent 2-(thiophen-2-yl)-1,3-benzazaphosphole, we began work on expanding this phenomenon to cover more common fluorophores, such as carbazole and 2-phenylbenzimidazole. Both of these fluorophores also exhibited a qualitative quenching

upon mixing with IPr, however the products were highly labile and dissociated into their constituent parts at low concentration. We examined this reversibility via NMR experiments across a range of concentrations as well as through diffusion ordered spectroscopy and both analyses provided evidence for the adducts being held together through weak hydrogen bonding interactions. This was further evidenced through single-crystal X-ray diffraction. We further tested the breadth of these results by employing a more reactive cyclic (alkyl)(amino)carbene, (2,6-diisopropylphenyl)-4,4-diethyl-2,2-dimethyl-pyrrolidin-5-ylidene (^{Et}CAAC), which underwent an N-H insertion reaction with each of the N-H containing fluorophores. Due to the increased steric profile of 2-phenylbenzimidazole, we found that this insertion was reversible and could transfer the carbene *in situ* to another substrate. Based on all of the combinations, we found that the reactivity and photophysical response could be tuned based on the electronic and steric properties of both carbene and fluorophore, giving a neutral hydrogen bonding complex, proton transfer salt, or N-H insertion reaction depending on combination of materials used.

Chapter 1: Introduction

Section 1.1: Heteroatom Substitution for Tunable, Functional Materials

One overarching goal of our work is the development of new tunable, functional molecules and materials. One of the key methods we utilize to work toward this goal is the use of heteroatom substitution, specifically phosphorus. Although phosphorus resides in group 15 and is most chemically similar to nitrogen, a very strong comparison can also be made to carbon. The first of two main points that make up this argument is due to the diagonal relationship between phosphorus and carbon on the periodic table. Because of this, the difference in Pauling electronegativity between carbon (2.55) and phosphorus (2.19) is relatively small, smaller than differences between either carbon and silicon (1.90) or carbon and nitrogen (3.04). The second main point, as shown in **Figure 1.1**, is based on the comparison of frontier orbitals of the simplest alkene ($H_2C=CH_2$) and phosphaalkene ($HP=CH_2$).

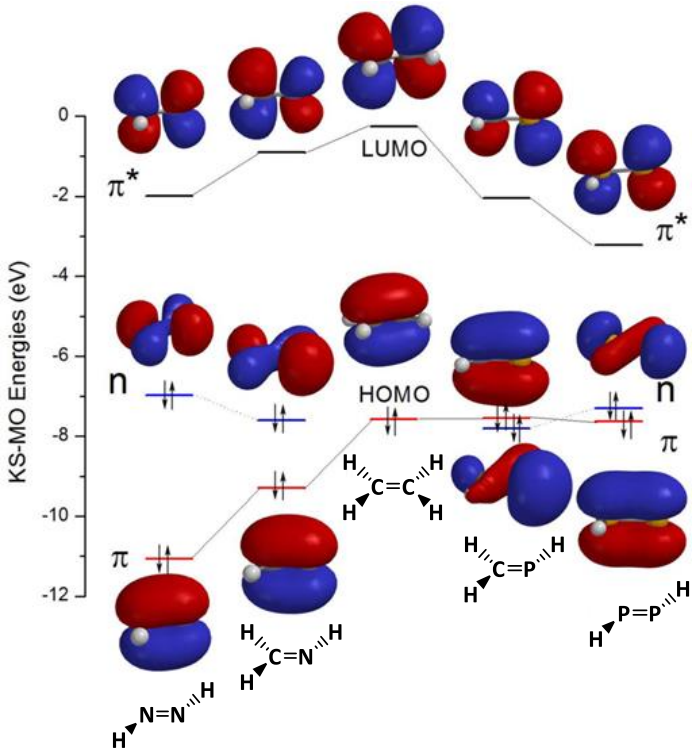

Figure 1.1: Calculated frontier orbitals for simplest C, N, and P analogs of ethylene.[1]

Comparison of the HOMO and LUMO orbitals for ethylene and phosphaethylene reveals them to be isolobal, however the phosphaalkene has a significantly lower energy LUMO and thus reduced HOMO-LUMO (π-π*) gap. This is in contrast to the nitrogen analogs which exhibit a larger π-π* transition and significantly more lone-pair character for the HOMO. These two points provide arguments for calling phosphorus a "carbon copy".[2] This comparison, however, does not take into account the additional non-bonding electrons which represents a change from the all carbon system. This allows for the phosphorus-substituted material to exhibit added functionality that was not possible in the fully organic material. Coupled with the reduced π-π* gaps, substitution for phosphorus into a conjugated material would allow for both tunability and added functionality.

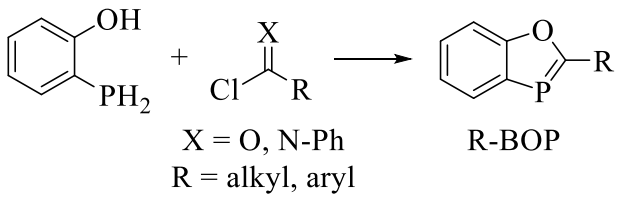

Scheme 1.1: Typical synthesis for 1,3-benzoxaphopholes (BOPs).

The current area of interest in our group concerns 1,3-benzoxaphospholes (BOPs), heterocyclic systems incorporating P=C bonds into fused rings. These materials had previously been synthesized by Heinicke, however we expanded on his work due to the inherently strong luminescence observed with 2-aryl-BOPs.[3–6] Compared to earlier work studying acyclic phosphaalkenes, BOPs presented significantly stronger luminescence.[7,8]

Section 1.2: Sodium Phosphaethynolate, Na[O-C≡P], an Important Synthon in Phosphorus Chemistry

One major drawback in studying compounds containing heavier main-group elements, such as the low coordinate (λ^3-σ^2) phosphaalkenes discussed above, lies in the limited availability of chemicals and reactions compared to the wide array that are used in more common synthetic organic chemistry. This is particularly true for pπ-pπ bonded phosphorus as the limited orbital overlap was thought to make this inherently too unstable until the first P=C and P=P containing molecules were isolated.[9,10] Even still, many systems containing P=C or P=P bonding require the addition of sterically large groups nearby to kinetically stabilize this bond from oligomerization. A notable exception used in our work, as discussed in **Section 1.1**, is the stable yet relatively non-bulky 1,3-benzoxaphosphole. For further development in this field, it is important to continue developing new or easier methods to access these types of materials.

One important example of this type of breakthrough is the recent work involving the phosphaethynolate anion, the phosphorus analog of cyanate. Unlike widely available cyanate, phosphaethynolate, $[OCP]^-$, was not discovered until Becker isolated its lithium salt in 1992.[11] Though it was a very non-bulky, C≡P containing molecule, very little research was performed on it for another decade. At that point, other group 2 analogs were synthesized, though only the calcium salt was found stable enough for isolation.[12] Once again, very little research was devoted to this material until 2011 when Grützmacher isolated $Na[OCP]\cdot(dioxane)_x$.[13] Not only was this salt shown to be exceptionally stable, but the synthesis, as provided in **Scheme 1.2**, was developed to minimize the amount of pyrophoric materials that needed to be handled, such as tris(trimethylsilyl)phosphine or lithium bis(trimethylsilyl)phosphide as in earlier reports.

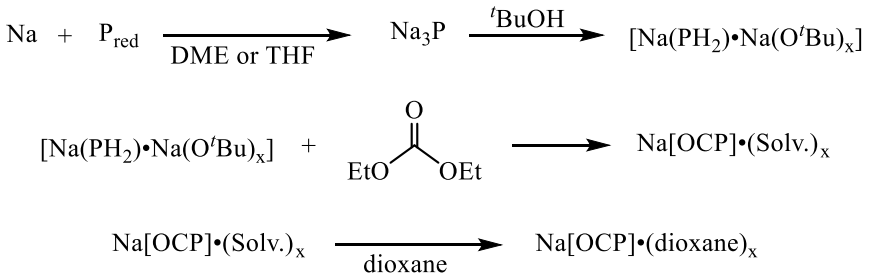

Scheme 1.2: Synthesis of Na[OCP].

This salt was found to be remarkably stable to heat (110 °C for 2.5 days) and ambient conditions (decomposes over days in degassed water). Furthermore, multiple resonance contributors (phosphaethynolate, phosphaketenide, and a CO adduct of P^-, as shown in **Scheme 1.3**) allow for broad reactivity. From this material, now obtainable as a stable compound in large scale, a number of heterocycles were synthesized as shown in **Scheme 1.4**. Included are examples of [2+2] and [4+2] cycloaddition products, phosphorus analogs of important materials such as urea or cyanuric acid, and a highly tunable

chromophore.[14–17] Additionally, the resonance contributors resulted in obtaining, for instance, either P- or O- bound products from the reaction with a trialkylsilyl halide.[18]

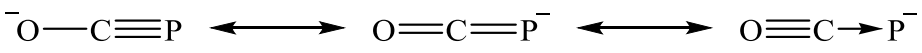

Scheme 1.3: Resonance structures of Na[OCP]

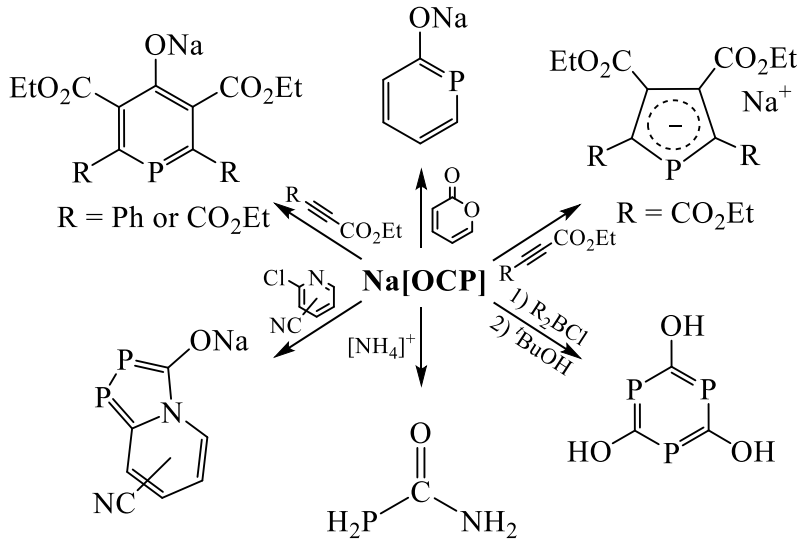

Scheme 1.4: Representative reactivity of Na[OCP].

One area that has not seen as broad development with Na[OCP] in the few years that this material has been widely available is reactivity towards transition metal complexes. Unlike the sudden and broad array of reactions observed with main-group systems, metal centered reactions with Na[OCP] remain limited to salt metathesis with a metal halide or pseudohalide as shown in **Scheme 1.5**.[19–22] While this does not diminish the importance of studying $[OCP]^-$ as a ligand, and it should be mentioned that some of the referenced complexes undergo additional reactions once the $[OCP]^-$ ligand is present, the lack of broader reactivity for Na[OCP] in this field is unexpected. This is particularly true due to the large amount of metal complexes formed from similar phosphaalkyne ligands (R-C≡P).[23,24]

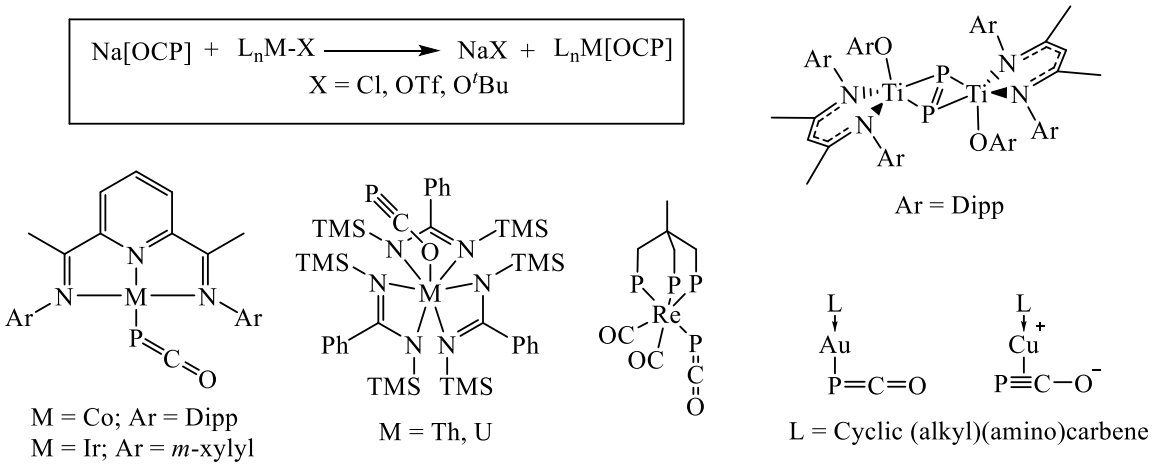

Scheme 1.5: Representative transition metal chemistry involving Na[OCP].

Section 1.3: *N*-Heterocyclic Carbenes and Their Use in Luminescent Materials

Singlet carbenes are a class of main-group compounds which include a divalent carbon center and both a filled and empty non-bonding orbital, as shown in **Scheme 1.6**. Due to their ambiphilic nature and high degree of electronic and steric tunability, they find use as stabilizing ligands in transition metal catalysis, organocatalysis, and other fields.[25–28]

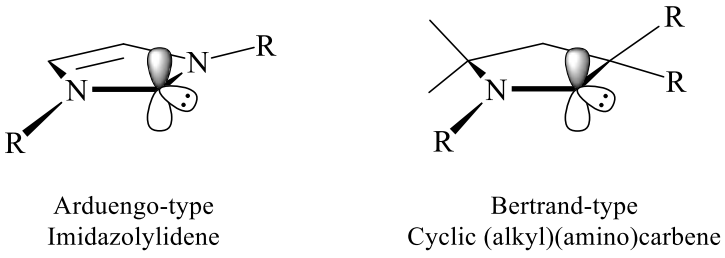

Scheme 1.6: Representative singlet carbene types used in this work.

The field of carbene chemistry has exploded since a 1991 report detailing the isolation of 1,3-bis(adamantyl)imidazol-2-ylidene.[29] Though reports had previously cited carbenes or carbene complexes,[30–32] Arduengo maintains the title of having first isolated a "bottleable" free carbene. Since those early reports, there has been no end to the extent at

which carbenes can be both utilized and have their properties tuned through various design strategies. [33,34] One recent review details at least 39 different types of isolable carbenes.[35]

Our interest with *N*-heterocyclic carbenes is primarily based on potential for use in tunable optoelectronic materials, similar to our interest in heteroatom substitution. For the most part, carbenes are not typically photophysically interesting on their own. However, a few examples of photo-switchable carbenes exist. [36–39] In an example by Yam, shown in **Scheme 1.7**, the photochemical quantum yield of a gold complex is directly affected by a photochemical reaction on the carbene backbone.[40]

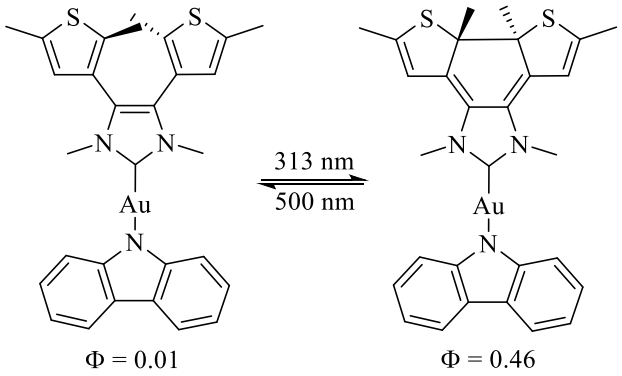

Scheme 1.7: Example of photochemically active carbene complex.

Regardless of their lack of inherent photophysical properties, carbenes have a wide array of applications such as organic photovoltaics, organic light-emitting diodes, and sensors.[41–45] Of particular interest for our work is the comparison between copper-carbene complexes in **Scheme 1.8**. In this case, complexes of the form CuL_2^+ have vastly different photophysical properties depending on the type of carbene used.[46] Similarly, recent reports have shown carbene-copper(I)-carbazolide complexes used as promising materials in organic light-emitting diodes.[47,48] However, as should be apparent, the breadth of work involving luminescent materials that include carbenes remains generally focused on late

transition metal complexes and considerably less interest in expanding this field to main-group or metal-free systems.

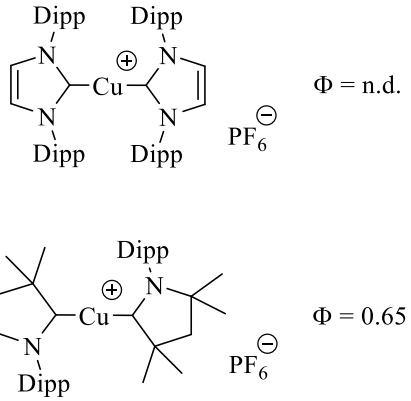

Scheme 1.8: Effect of carbene, IPr or CAAC, on the quantum yield of a Cu(I) complex.[46]

Section 1.4: References

(1) Simpson, M. C.; Protasiewicz, J. D. Phosphorus as a Carbon Copy and as a Photocopy: New Conjugated Materials Featuring Multiply Bonded Phosphorus. *Pure Appl. Chem.* **2013**, *85*, 801–815.

(2) Dillon, K. B.; Mathey, F.; Nixon, J. F. *Phosphorus : The Carbon Copy : From Organophosphorus to Phospha-Organic Chemistry*; 1998.

(3) Heinicke, J.; Tzschach, A. 1,3-Benzoxaphosphole-Heterocyclen Mit Phosphor Der Koordinationszahl 2. *Phosphorus Sulfur Relat. Elem.* **1985**, *25*, 345–356.

(4) Washington, M. P.; Gudimetla, V. B.; Laughlin, F. L.; Deligonul, N.; He, S.; Payton, J. L.; Simpson, M. C.; Protasiewicz, J. D. Phosphorus Can Also Be a "Photocopy." *J. Am. Chem. Soc.* **2010**, *132*, 4566–4567.

(5) Laughlin, F. L.; Deligonul, N.; Rheingold, A. L.; Golen, J. A.; Laughlin, B. J.; Smith, R. C.; Protasiewicz, J. D. Fluorescent Heteroacenes with Multiply-Bonded Phosphorus. *Organometallics* **2013**, *32*, 7116–7121.

(6) Wu, S.; Rheingold, A. L.; Protasiewicz, J. D. Luminescent Materials Containing Multiple Benzoxaphosphole Units. *Chem. Commun.* **2014**, *50*, 11036–11038.

(7) Smith, R. C.; Protasiewicz, J. D. Systematic Investigation of PPV Analogue Oligomers Incorporating Low-Coordinate Phosphorus Centres. *Eur. J. Inorg. Chem.* **2004**, No. 5, 998–1006.

(8) Smith, R. C.; Protasiewicz, J. D. Conjugated Polymers Featuring Heavier Main Group Element Multiple Bonds: A Diphosphene-PPV. *J. Am. Chem. Soc.* **2004**, *126*, 2268–2269.

(9) Becker, G. Bildung Und Eigenschaften von Acylphosphinen. I. Monosubstitutionsreaktionen an Substituierten Disilylphosphinen Mit Pivaloylchlorid. *Z. Anorg. Alleg. Chem.* **1976**, *423*, 242–254.

(10) Yoshifuji, M.; Shima, I.; Inamoto, N.; Hirotsu, K.; Higuchi, T. Synthesis and Structure of Bis(2,4,6-Tri-Tert-Butylphenyl)Diphosphene: Isolation of a True "Phosphobenzene." *J. Am. Chem. Soc.* **1981**, *103*, 4587–4589.

(11) Becker, G.; Schwarz, W.; Seidler, N.; Westerhausen, M. Acyl- Und Alkylidenphosphane. XXXIII. Lithoxy-methylidenphosphan · DME Und -methylidinphosphan · 2 DME — Synthese Und Struktur. *Z. Anorg. Alleg. Chem.* **1992**, *612*, 72–82.

(12) Westerhausen, M.; Schneiderbauer, S.; Piotrowski, H.; Suter, M.; Nöth, H. Synthesis of Alkaline Earth Metal Bis(2-Phosphaethynolates). *J. Organomet. Chem.* **2002**, *643–644*, 189–193.

(13) Puschmann, F. F.; Stein, D.; Heift, D.; Hendriksen, C.; Gal, Z. A.; Grützmacher, H.-F.; Grützmacher, H. Phosphination of Carbon Monoxide: A Simple Synthesis of

Sodium Phosphaethynolate (NaOCP). *Angew. Chem. Int. Ed.* **2011**, *50*, 8420–8423.

(14) Heift, D.; Benko, Z.; Grützmacher, H. Redox-Triggered Reversible Interconversion of a Monocyclic and a Bicyclic Phosphorus Heterocycle. *Angew. Chem. Int. Ed.* **2014**, *53*, 6757–6761.

(15) Jupp, A. R.; Goicoechea, J. M. Phosphinecarboxamide: A Phosphorus-Containing Analogue of Urea and Stable Primary Phosphine. *J. Am. Chem. Soc.* **2013**, *135*, 19131–19134.

(16) Suter, R.; Mei, Y.; Baker, M.; Benkő, Z.; Li, Z.; Grützmacher, H. 2,4,6-Tri(Hydroxy)-1,3,5-Triphosphinine, P 3 C 3 (OH) 3 : The Phosphorus Analogue of Cyanuric Acid. *Angew. Chem. Int. Ed.* **2017**, *56*, 1356–1360.

(17) Suter, R.; Benkő, Z.; Bispinghoff, M.; Grützmacher, H. Annulated 1,3,4-Azadiphospholides: Heterocycles with Widely Tunable Optical Properties. *Angew. Chem. Int. Ed.* **2017**, *56*, 11226–11231.

(18) Heift, D.; Benkő, Z.; Grützmacher, H. Is the Phosphaethynolate Anion, (OCP)−, an Ambident Nucleophile? A Spectroscopic and Computational Study. *Dalt. Trans.* **2014**, *43*, 5920.

(19) Alidori, S.; Heift, D.; Santiso-Quinones, G.; Benkå, Z.; Grützmacher, H.; Caporali, M.; Gonsalvi, L.; Rossin, A.; Peruzzini, M. Synthesis and Characterization of Terminal [Re(XCO)(CO) 2(Triphos)] (X=N, P): Isocyanate versus Phosphaethynolate Complexes. *Chem. - Eur. J.* **2012**, *18*, 14805–14811.

(20) Camp, C.; Settineri, N.; Lefèvre, J.; Jupp, A. R.; Goicoechea, J. M.; Maron, L.; Arnold, J. Uranium and Thorium Complexes of the Phosphaethynolate Ion. *Chem. Sci.* **2015**, *6*, 6379–6384.

(21) Liu, L.; Ruiz, D. A.; Dahcheh, F.; Bertrand, G.; Suter, R.; Tondreau, A. M.; Grützmacher, H. Isolation of Au-, Co-η [1] PCO and Cu-η [2] PCO Complexes, Conversion of an Ir–η [1] PCO Complex into a Dimetalladiphosphene, and an Interaction-Free PCO Anion. *Chem. Sci.* **2016**, *7*, 2335–2341.

(22) Grant, L. N.; Pinter, B.; Manor, B. C.; Suter, R.; Grützmacher, H.; Mindiola, D. J. A Planar Ti2P2 Core Assembled by Reductive Decarbonylation of −O−C≡P and P−P Radical Coupling. *Chem. - Eur. J.* **2017**, *23*, 6272–6276.

(23) Weber, L. Metallophosphaalkenes—from Exotics to Versatile Building Blocks in Preparative Chemistry. *Angew. Chem. Int. Ed.* **1996**, *35*, 271–288.

(24) Weber, L. Recent Developments in the Chemistry of Metallophosphaalkenes. *Coord. Chem. Rev.* **2005**, *249*, 741–763.

(25) Scott, N. M.; Nolan, S. P. Stabilization of Organometallic Species Achieved by the Use of N-Heterocyclic Carbene (NHC) Ligands. *Eur. J. Inorg. Chem.* **2005**, No. 10, 1815–1828.

(26) Wolfgang A. Herrmann. N-Heterocyclic Carbenes: A New Concept in Organometallic Catalysis. *Angew. Chem. Int. Ed.* **2002**, *41*, 1290–1309.

(27) Enders, D.; Niemeier, O.; Henseler, A. Organocatalysis by N-Heterocyclic Carbenes. *Chem. Rev.* **2007**, *107*, 5606–5655.

(28) Mercs, L.; Albrecht, M. Beyond Catalysis: N-Heterocyclic Carbene Complexes as Components for Medicinal, Luminescent, and Functional Materials Applications. *Chem. Soc. Rev.* **2010**, *39*, 1903–1912.

(29) Arduengo, A. J.; Harlow, R. L.; Kline, M. A Stable Crystalline Carbene. *J. Am. Chem. Soc.* **1991**, *113*, 361–363.

(30) Igau, A.; Grutzmacher, H.; Baceiredo, A.; Bertrand, G. Analogous α,α'-Bis-Carbenoid Triply Bonded Species: Synthesis of a Stable Λ3-Phosphinocarbene-Λ5-Phosphaacetylene. *J. Am. Chem. Soc.* **1988**, *110*, 6463–6466.

(31) Wanzlick, H. -W; Schönherr, H. -J. Direct Synthesis of a Mercury Salt-Carbene Complex. *Angew. Chem. Int. Ed.* **1968**, *7*, 141–142.

(32) Öfele, K. 1,3-Dimethyl-4-Imidazolinyliden-(2)-Pentacarbonylchrom Ein Neuer Übergangsmetall-Carben-Komplex. *J. Organomet. Chem.* **1968**, *12*, P42–P43.

(33) Hopkinson, M. N.; Richter, C.; Schedler, M.; Glorius, F. An Overview of N-Heterocyclic Carbenes. *Nature* **2014**, *510*, 485–496.

(34) Martin, D.; Melaimi, M.; Soleilhavoup, M.; Bertrand, G. A Brief Survey of Our Contribution to Stable Carbene Chemistry. *Organometallics* **2011**, *30*, 5304–5313.

(35) Melaimi, M.; Jazzar, R.; Soleilhavoup, M.; Bertrand, G. Cyclic (Alkyl)(Amino)Carbenes (CAACs): Recent Developments. *Angew. Chem. Int. Ed.* **2017**, *56*, 10046–10068.

(36) Neilson, B. M.; Lynch, V. M.; Bielawski, C. W. Photoswitchable N-Heterocyclic Carbenes: Using Light to Modulate Electron-Donating Properties. *Angew. Chem. Int. Ed.* **2011**, *50*, 10322–10326.

(37) Neilson, B. M.; Bielawski, C. W. Photoswitchable Organocatalysis: Using Light to Modulate the Catalytic Activities of N-Heterocyclic Carbenes. *J. Am. Chem. Soc.* **2012**, *134*, 12693–12699.

(38) Teator, A. J.; Tian, Y.; Chen, M.; Lee, J. K.; Bielawski, C. W. An Isolable, Photoswitchable N-Heterocyclic Carbene: On-Demand Reversible Ammonia Activation. *Angew. Chem. Int. Ed.* **2015**, *54*, 11559–11563.

(39) Peris, E. Smart N-Heterocyclic Carbene Ligands in Catalysis. *Chem. Rev.* **2018**, *118*, 9988–10031.

(40) Yam, V. W.-W.; Lee, J. K.-W.; Ko, C.-C.; Zhu, N. Photochromic Diarylethene-Containing Ionic Liquids and N-Heterocyclic Carbenes. *J. Am. Chem. Soc.* **2009**, *131*, 912–913.

(41) Di, D.; Romanov, A. S.; Yang, L.; Richter, J. M.; Rivett, J. P. H.; Jones, S.; Thomas, T. H.; Abdi Jalebi, M.; Friend, R. H.; Linnolahti, M.; et al. High-Performance Light-Emitting Diodes Based on Carbene-Metal-Amides. *Science* **2017**, *356*, 159–163.

(42) Föller, J.; Marian, C. M. Rotationally Assisted Spin-State Inversion in Carbene-Metal-Amides Is an Artifact. *J. Phys. Chem. Lett.* **2017**, *8*, 5643–5647.

(43) Elie, M.; Renaud, J. L.; Gaillard, S. N-Heterocyclic Carbene Transition Metal Complexes in Light Emitting Devices. *Polyhedron* **2018**, *140*, 158–168.

(44) Sun, J.-K.; Zhang, W.; Guterman, R.; Lin, H. J.; Yuan, J. Porous Polycarbene-Bearing Membrane Actuator for Ultrasensitive Weak-Acid Detection and Real-Time Chemical Reaction Monitoring. *Nat. Commun.* **2018**, *9*, 1–8.

(45) Bąk, K. M.; Chabuda, K.; Montes, H.; Quesada, R.; Chmielewski, M. J. 1,8-Diamidocarbazoles: An Easily Tuneable Family of Fluorescent Anion Sensors and Transporters. *Org. Biomol. Chem.* **2018**, *16*, 5188–5196.

(46) Gernert, M.; Müller, U.; Haehnel, M.; Pflaum, J.; Steffen, A. A Cyclic Alkyl(Amino)Carbene as Two-Atom π-Chromophore Leading to the First Phosphorescent Linear Cu I Complexes. *Chem. - Eur. J.* **2017**, *23*, 2206–2216.

(47) Shi, S.; Jung, M. C.; Coburn, C.; Tadle, A.; Sylvinson, D. M. R.; Djurovich, P. I.; Forrest, S. R.; Thompson, M. E. Highly Efficient Photo- and Electroluminescence

from Two-Coordinate Cu(I) Complexes Featuring Nonconventional N-Heterocyclic Carbenes. *J. Am. Chem. Soc.* **2019**, *141*, 3576–3588.

(48) Hamze, R.; Peltier, J. L.; Sylvinson, D.; Jung, M.; Cardenas, J.; Haiges, R.; Soleilhavoup, M.; Jazzar, R.; Djurovich, P. I.; Bertrand, G.; et al. Eliminating Nonradiative Decay in Cu(I) Emitters: >99% Quantum Efficiency and Microsecond Lifetime. *Science* **2019**, *363*, 601–606.

Chapter 2: Reactivity of Sodium Phosphaethynolate, Na[O-C≡P], Towards Arynes and Metal-Aryne Complexes

Section 2.1: Introduction

Please note, the results discussed in **Chapter 2** represent this author's contributions to a previously published work.[1]

Based on our group's continuing work with 1,3-benzoxaphospholes, BOPs, as discussed in **Section 1.1**, we became interested in studying sodium phosphaethynolate given that both materials share a similar O-C-P arrangement of atoms. BOPs have often been synthesized through condensation of 2-phosphinophenol and an acid or imidoyl chloride, as shown in **Scheme 2.1**.[2]

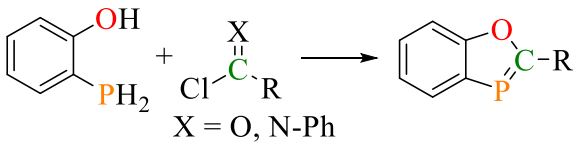

Scheme 2.1: Synthesis of 1,3-benzoxaphospholes.

While this is an effective way to synthesize luminescent BOPs, particularly those where R = aryl, this reaction is limited to only those substituents that can incorporate the required acid or imidoyl chloride functionality. We therefore sought to develop a different synthesis for BOPs, whereby additional functionality could be added or where the BOP could be attached to another substrate. Given the previously mentioned similarity to the phosphaethynolate anion, we envisioned a reaction whereby Na[OCP] could be added to benzyne in order to form an anionic BOP, as shown in **Scheme 2.2**. From this, we could install completely new functionality on the BOP that was otherwise unavailable given the currently used synthesis. A similar reaction to this between an organic azide (valence isoelectronic to phosphaethynolate) and benzyne had already been reported.[3]

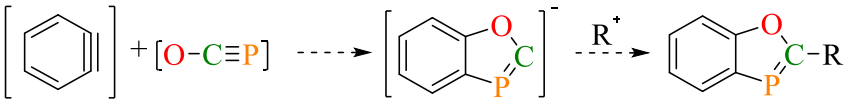

Scheme 2.2: Proposed synthesis of anionic BOP from Na[OCP].

Furthermore, the isolation of an anionic BOP would allow for a direct comparison to a similar heterocycle, 1,3-benzazaphospholes (BAPs). These heterocycles are structurally similar to BOPs except for the substitution of an NR group instead of O, however BAPs were not known to be luminescent unlike BOPs which are highly emissive.[2,4,5] Conversely, and of importance for this work, BAPs have been synthesized which incorporate completely different functionality than BOPs, particularly *N*-methyl-2-lithio-1,3-benzazaphosphole.[6] As shown in **Scheme 2.3**, this BAP can react with a wide range of electrophiles and acts as an example for the potential of a similar anionic BOP.

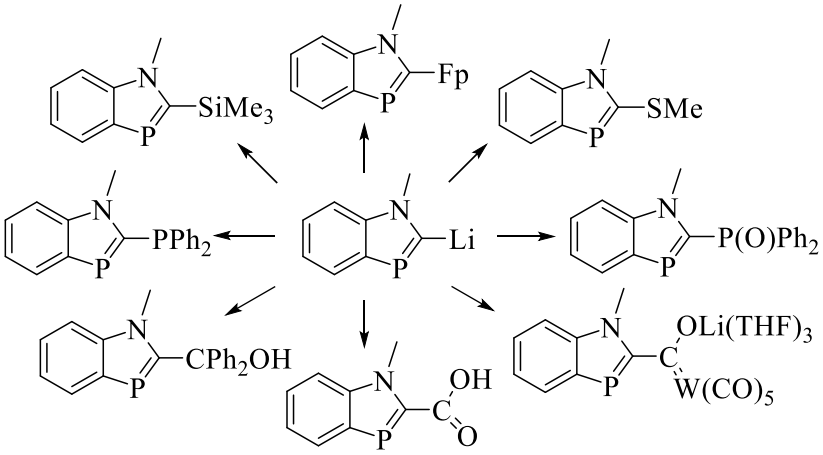

Scheme 2.3: Reactivity of *N*-methyl-2-lithio-1,3-benzazaphosphole.[6]

Section 2.2: Results and Discussion

Section 2.2.1: Reactions of an Aryne with Na[O-C≡P]

One common method towards the formation of an aryne intermediate is the thermal decomposition of an *ortho*-halogenated-metallo-arene, such as 2-chlorophenyllithium. This reagent must first be synthesized at cryogenic temperatures, with aryne formation

occurring upon warming due to elimination of lithium chloride. This reactivity is well studied and has been used previously in our research involving *m*-terphenyl ligands.[7,8] Our initial reactions utilizing Na[OCP] to trap benzyne from the decomposition of these highly basic and nucleophilic intermediates, as shown in **Scheme 2.4 (a)**, were met with failure.

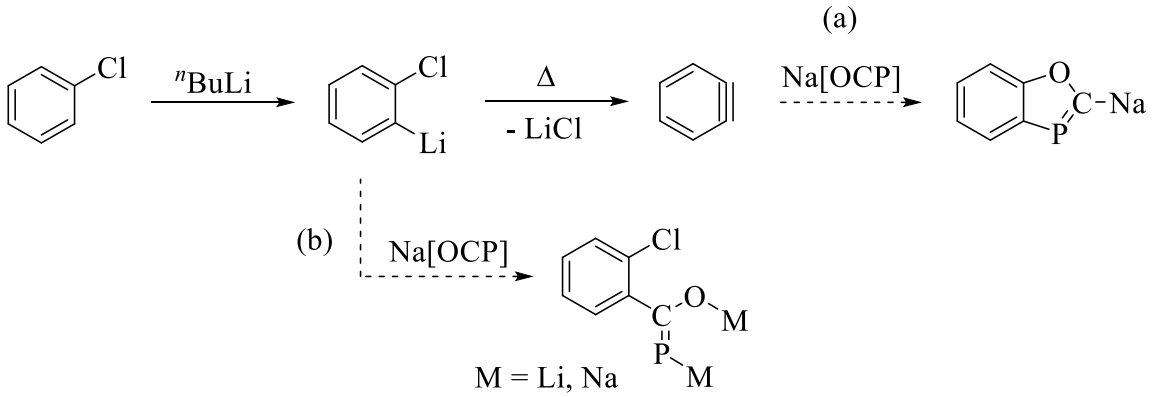

Scheme 2.4: (a) Proposed reaction between Na[OCP] and benzyne and (b) potential competing side reaction of Na[OCP] with aryllithium.

We then decided to study a simplified reaction between phenylmagnesium bromide and Na[OCP] followed by quenching of the reactive mixture with trimethylsilyl chloride in order to trap the potential product given by **Scheme 2.4 (b)**. We detected a pair of ^{31}P NMR signals at 133.88 and 131.08 ppm, shown in **Figure 2.1**, similar to a trimethylsiloxy-substituted polyphosphaalkene reported by Gates (^{31}P NMR δ = 132 and 152 ppm, for *Z* and *E* isomers respectively) as shown in **Scheme 2.5**.[9] This product could be attributed to nucleophilic attack on the carbon within Na[OCP] and indicates that our first choice for aryne source does not allow for the intended reactivity. Furthermore, the ^{31}P NMR signal associated with unreacted $[OCP]^-$ in this mixture shifted from -392 ppm to a set of signals centered around -368 ppm. Coincidentally, this result was the first indication of what we

would eventually report as MgCl[OCP] and Mg[OCP]$_2$ (^{31}P NMR δ = -369.5 and -367.9 ppm, respectively), though this discovery went unnoticed at the time.[10]

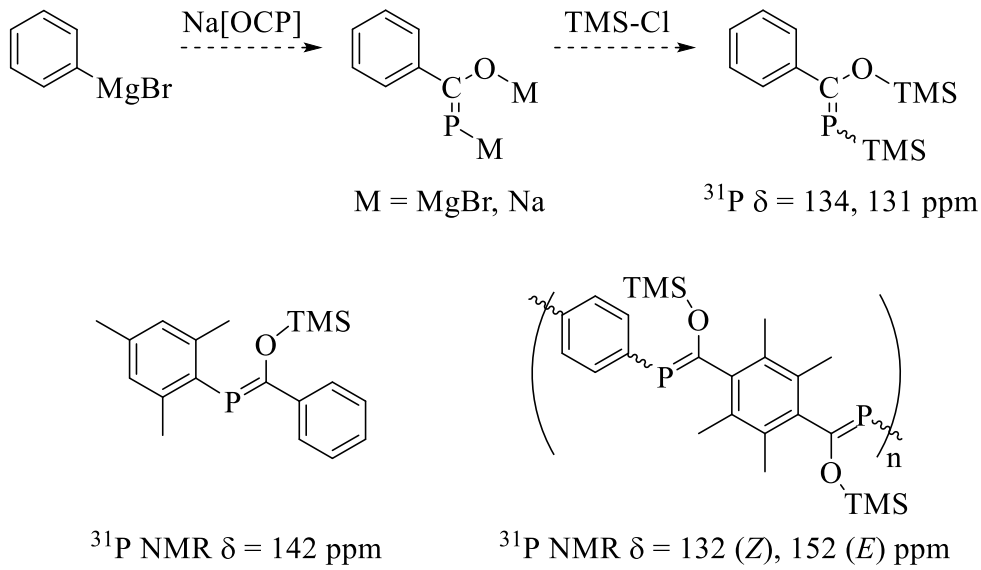

Scheme 2.5: (top) Proposed reaction between Na[OCP] and phenylmagnesium bromide and subsequent addition of trimethylsilyl chloride. (bottom) Reference ^{31}P NMR chemical shifts of comparable phosphaalkenes.[9]

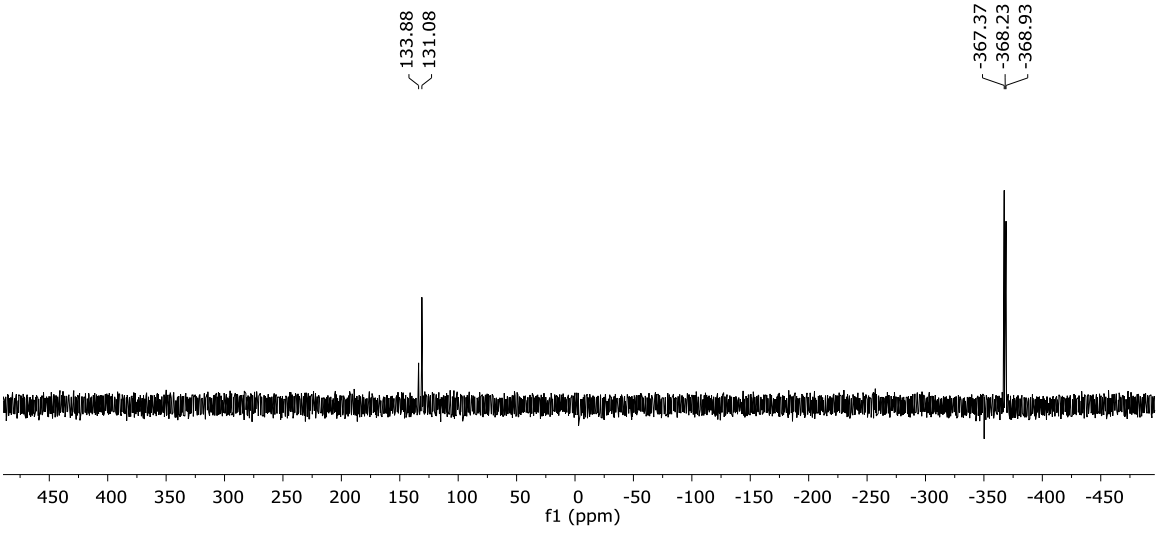

Figure 2.1: ^{31}P NMR (162 MHz, THF) of reaction between Na[OCP] and PhMgBr, followed by addition of TMS-Cl.

Upon realizing these pre-aryne intermediates which were inherently strong nucleophiles could not be utilized in this reaction, we examined other sources of arynes. One popular reagent that has both milder reactivity as well as greater stability is 2-trimethylsilylphenyl triflate. Addition of cesium fluoride produces a cascading loss of trimethylsilyl fluoride and cesium triflate to produce the desired aryne. This approach was explored due to assumed compatibility between Na[OCP] and the starting arene, as well as the other components in solution.

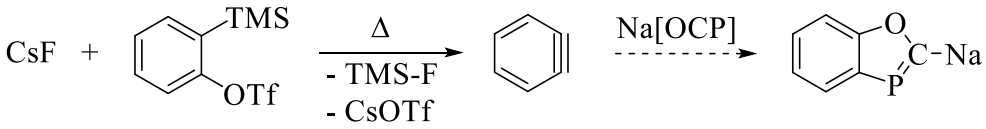

Scheme 2.6: Proposed reaction between Na[OCP] and benzyne to form an anionic BOP.

The reaction between Na[OCP], 2-trimethylsilylphenyl triflate, and CsF (used as fluoride source) did not proceed as desired, and investigation of reactions of Na[OCP] with each compound separately gave evidence of specific problems. First, a mixture of Na[OCP] and 2-trimethylsilylphenyl triflate heated at 80 °C showed a new set of ^{31}P NMR signals after only a few minutes associated with the oxidative tetramerization of the $[OCP]^-$ anion, previously reported by Becker.[11]

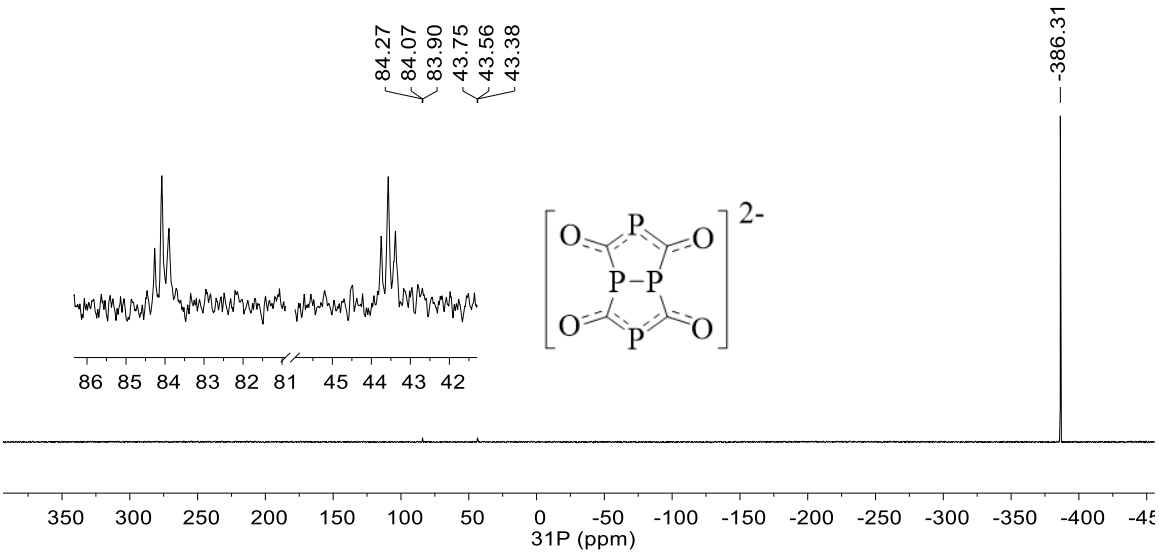

Figure 2.2: ^{31}P NMR (162 MHz, THF) spectrum of reaction between Na[OCP] and 2-trimethylsilylphenyl triflate.

Furthermore, throughout our studies of Na[OCP], we had noticed that the ^{31}P NMR signal of the $[OCP]^-$ anion was not consistently observed at -392 ppm in THF, but often was shifted downfield in some reaction mixtures, particularly when employing other cations such as Cs^+ (as previously mentioned, this was also observed with Grignard reagents though unexplored). This was confirmed by mixing Na[OCP] and CsF in THF within an NMR tube, then adding a small capillary filled with Na[OCP] in THF to this tube. NMR analysis provided two distinct ^{31}P NMR signals, assumingly associated with Cs[OCP] and Na[OCP] (-381 ppm and -392 ppm, respectively).

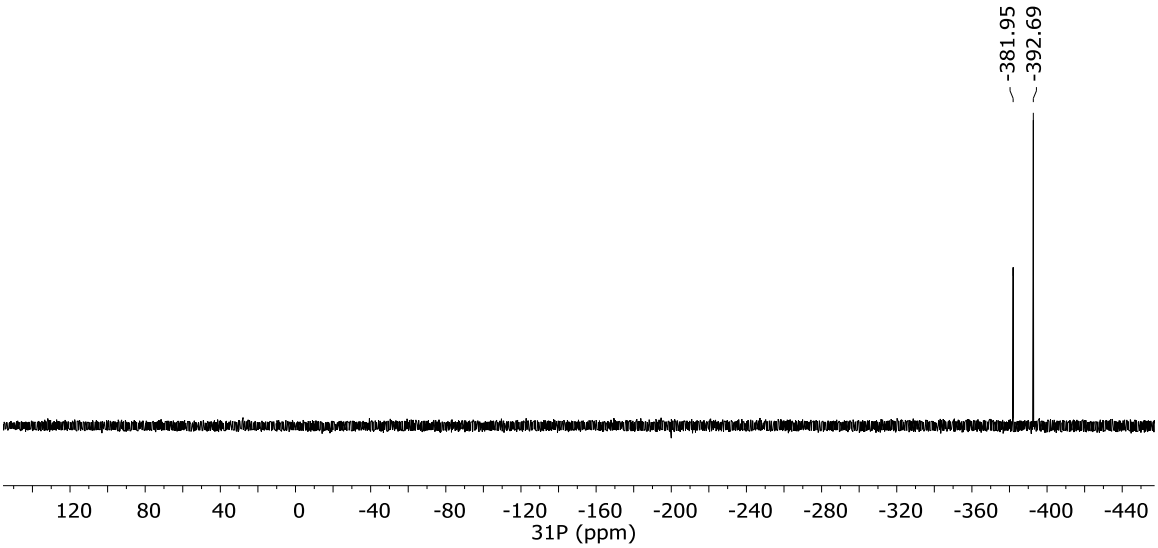

Figure 2.3: ^{31}P NMR (202 MHz, THF) spectrum of mixture of Na[OCP] and CsF with capillary containing Na[OCP] in THF used as internal standard.

Attempts to isolate Cs[OCP] from this mixture were unsuccessful. While this cation exchange should not have resulted in significant problems for this reaction, literature precedent at the time provided that Na[OCP] was considerably more stable compared to other $M[OCP]_n$ compounds. For example, the lithium salt was rarely studied after its discovery and salts of M = Mg, Ca, Sr, Ba were reported as extremely sensitive towards air, moisture, heat, and loss of coordinating solvent, with $Ca[OCP]_2DME_3$ reported as the only other isolable phosphaethynolate salt prior to Grützmacher's work.[12–14] We later showed that $Mg[OCP]_2{\cdot}THF_4$ could be isolated as a crystalline solid.[10] However, at this time the examination of both the stability and reactivity of potentially a new Cs[OCP] synthon was not pursued.

Section 2.2.2: Insertion of Na[O-C≡P] into a Zirconium-Benzyne Complex

Due to the difficulties encountered in **Section 2.2.1**, primarily the side reactions of aryne precursor chemicals and Na[OCP] before the reactive aryne intermediate could even form, we chose another strategy. A number of transition metal complexes have been

isolated and reported which contain aryne ligands. For our purposes we examined Buchwald's zirconium benzyne complex due to its known reactivity with unsaturated molecules such as alkynes, nitriles, or *tert*-butylphosphaalkyne as shown in **Scheme 2.7**.[15–17]

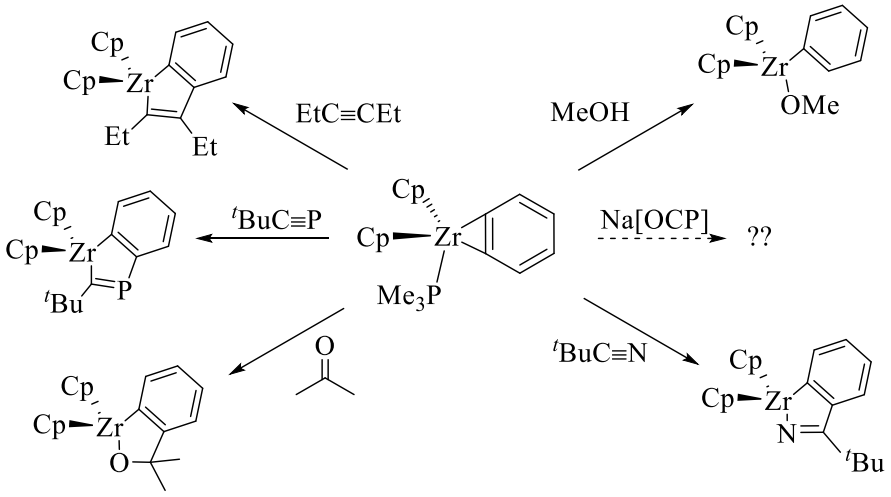

Scheme 2.7: Representative reactivity of zirconium-benzyne complex with unsaturated molecules.[15–17]

Our first attempt to study the reaction between Na[OCP] and the zirconium-benzyne complex was performed at a small scale within an NMR tube. One of the benefits of working with phosphorus-substitued materials is the ability to track reaction progression through ^{31}P NMR spectroscopy. The wide spectral window and opportunity to use non-deuterated solvents makes this analysis both highly diagnostic and facile for use in quick reaction monitoring.

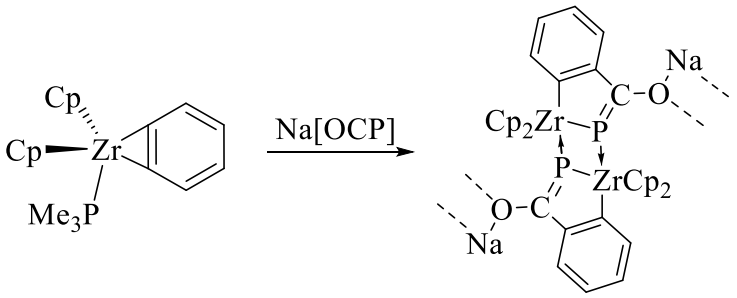

2.1

Scheme 2.8: Insertion reaction of Na[OCP] to yield coordination polymer **2.1**.

For the reaction shown in **Scheme 2.8**, each of the starting compounds has a unique ^{31}P chemical shift in THF, -392 ppm for Na[OCP] and -3 ppm for the trimethylphosphine ligand in the zirconium-benzyne complex. Upon mixing THF solutions of each in an NMR tube and mixing, an extremely dark red solution was obtained. Analysis of this solution by ^{31}P NMR (**Figure 2.4**) showed a large resonance for free trimethylphosphine at -62 ppm signifying that most of the benzyne complex had reacted and shed its phosphine ligand. Interestingly, no resonance was observed to account for the portion of Na[OCP] that had reacted, although inspection of the tube after a few minutes revealed a red, crystalline solid which would account for the unobservable NMR signal if all of this material was insoluble.

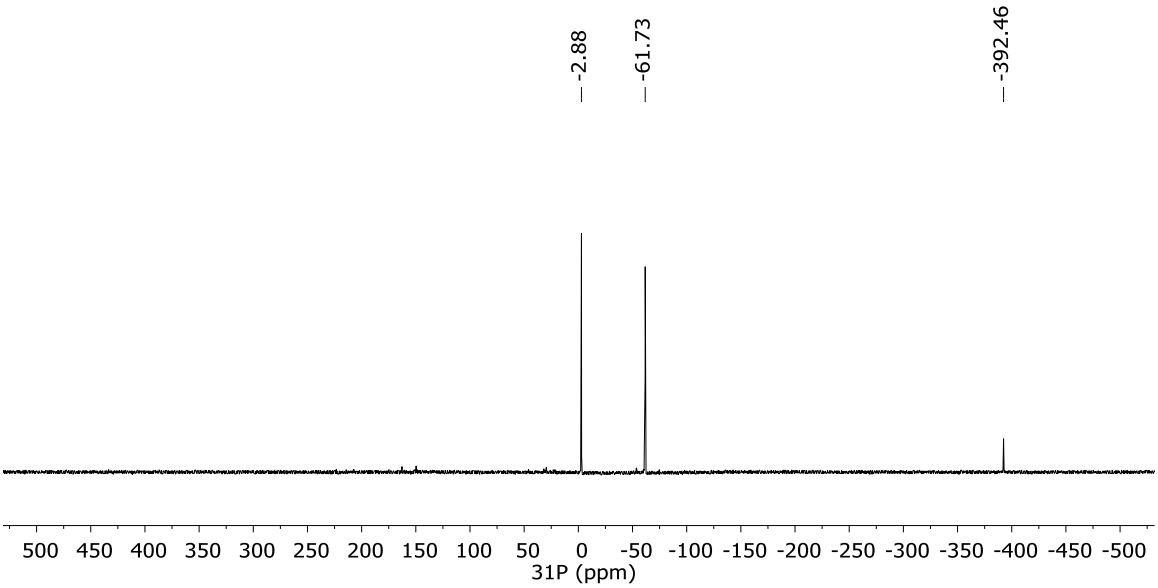

Figure 2.4: ^{31}P NMR (162 MHz, THF) spectrum of incomplete reaction between Na[OCP] and zirconium-benzyne complex.

Since NMR analysis suggested a relatively clean reaction between Na[OCP] and the zirconium-benzyne complex, we attempted to isolate single crystals of this red solid from the reaction mixture in order to identify the new material. A dilute solution of Na[OCP] in THF was carefully layered on a concentrated solution of zirconium-benzyne complex in THF that had been previously added to an NMR tube. This produced a very dark red solution at the interface between layers. After standing undisturbed for 24 hours, small red crystals were obtained that were suitable for X-ray diffraction. The molecular structure of this red solid, compound **2.1**, revealed that Na[OCP] had inserted into one of the Zr-C bonds of the zirconium-benzyne complex as shown in **Figure 2.5**. Even though zirconium is highly oxophilic, **2.1** was assembled through new Zr-P bonds and not Zr-O bonds. Furthermore, each phosphorus atom was coordinated to two metal centers and the remaining alkoxide unit formed a coordination polymer through bridging sodium cations.

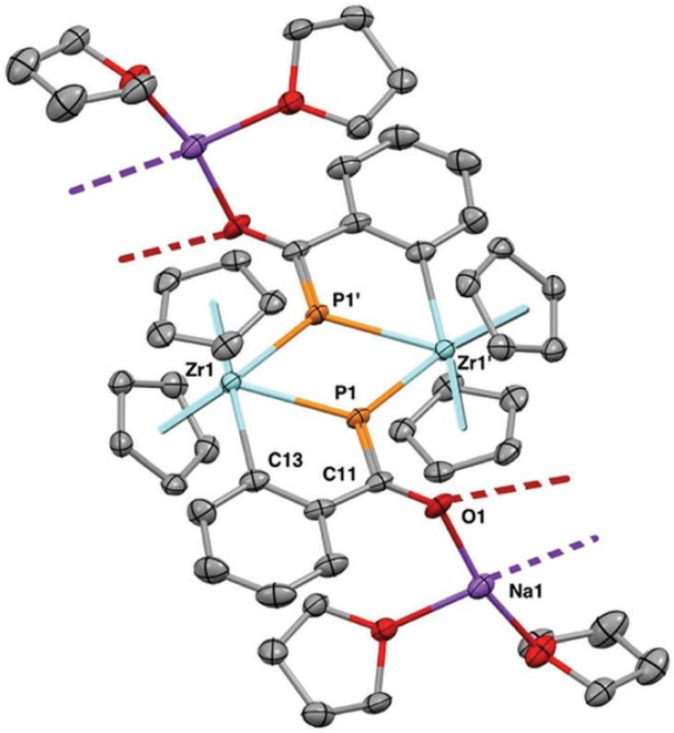

Figure 2.5: ORTEP diagram of **2.1** (ellipsoids set at 50% probability; hydrogen atoms, co-crystallized THF, and second independent coordination polymer chain omitted for clarity). Selected bond distances [Å] and angles [deg]: P1–Zr1: 2.6151(14); P1–Zr1': 2.7010(14); P1–P1': 2.548(2); P1–C11: 1.743(5); Zr1–C13: 2.406(5); O1–C11: 1.276(6); P1–Zr1–C13: 71.04(14); Zr1–P1–Zr1': 122.75(5); Zr1–P1–C11: 109.37(19); Zr1'–P1–C11: 127.22(19); P1–C11–O1: 125.6(4).

Within a single dimer, the two [$Cp_2Zr\{\kappa$-*C*,κ_2-*P*-$C_6H_4C(ONa)P\}$] units are related by an inversion center and are essentially co-planar about the plane defined by Zr1-P1-C11. The C=P distance of 1.743(5) Å within **2.1** is similar to other *P*-zirconophosphaalkenes, however the typical widening of the Zr-P-C angle, common to this type of complex, is not observed due to the cyclic nature of the phosphaalkene in **2.1**.[18–20]

Compound **2.1** could be synthesized in bulk by mixing a THF solution of Na[OCP] and zirconium-benzyne complex overnight. It should be noted that compound **2.1** is highly

sensitive to water, immediately turning from bright red to orange upon exposure to air which is coupled with a strong scent of phosphane. As such, the synthesis of **2.1** is carried out on a Schlenk line followed by evaporation of both THF and trimethylphosphine under vacuum once the precipitation of **2.1** is complete. The crude solid is then transferred to a glove box where impurities are extracted into THF and the bright red **2.1** isolated in 43% yield via filtration after additional THF washing and drying under vacuum. The extremely dark red, nearly black filtrate can be evaporated to a dark solid, though this solid has yet to be identified.

Given the insolubility of **2.1** in all of the common and compatible solvents typically used in air-free conditions, we found it difficult to perform additional purification or characterization on the material. However, we managed to obtain a solid-state ^{31}P MAS NMR spectrum of **2.1** which contained a single resonance at 50 ppm along with spinning sidebands as shown in **Figure 2.6**.

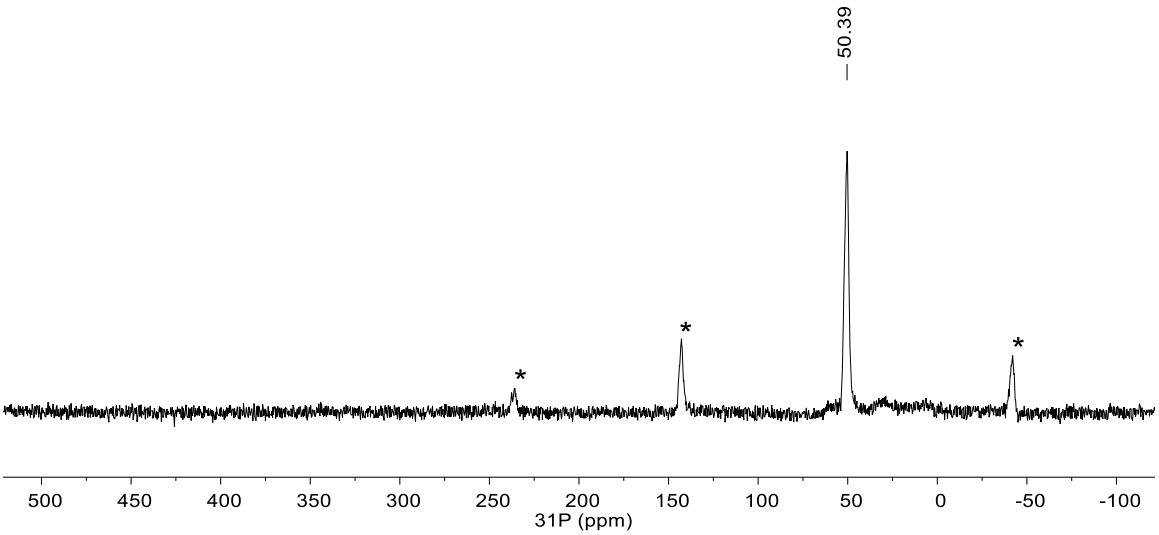

Figure 2.6: ^{31}P MAS NMR (324 MHz) spectrum of **2.1** at 30 kHz spinning rate, spinning sidebands marked.

Section 2.2.3: Isolation of Soluble Dimeric Complex Through Disruption of Coordination Polymer

The first steps towards utilizing compound **2.1** in further studies relied on obtaining a more soluble analog that otherwise maintained the bonding within the complex. We expected that the bridging Na-O interactions which were responsible for assembly of the coordination polymer could be disrupted through reaction of **2.1** with trimethylsilyl chloride (TMS-Cl).

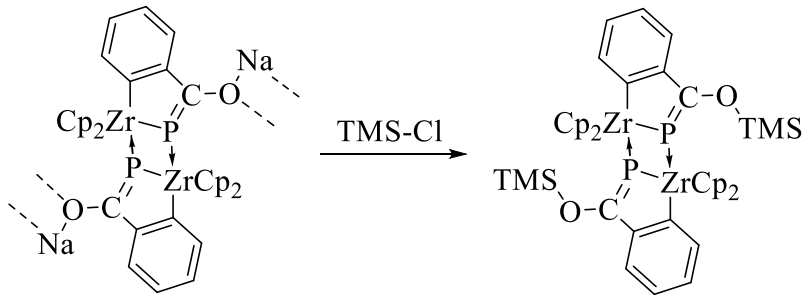

2.1 **2.2**

Scheme 2.9: Synthesis of **2.2** upon reaction of **2.1** with TMS-Cl.

Addition of TMS-Cl to a suspension of **2.1** in THF, shown in **Scheme 2.9**, resulted in a cloudy orange solution after 30 minutes. After removal of NaCl through filtration and evaporation of residual volatiles, compound **2.2** was obtained in 96% yield. Analysis by ^{31}P NMR showed a single resonance at 194 ppm and a single product by ^{1}H NMR as shown in **Figure 2.7** and **Figure 2.8**. The yield of crude **2.2** corroborates the purity of **2.1** used in this synthesis.

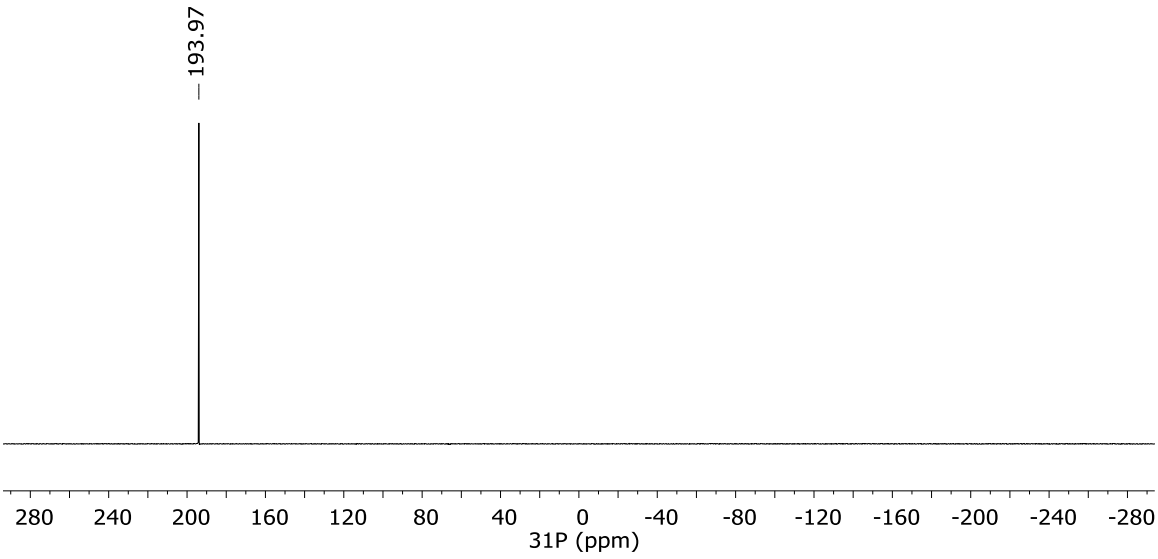

Figure 2.7: ^{13}P NMR (202 MHz, $CDCl_3$) spectrum of **2.2**.

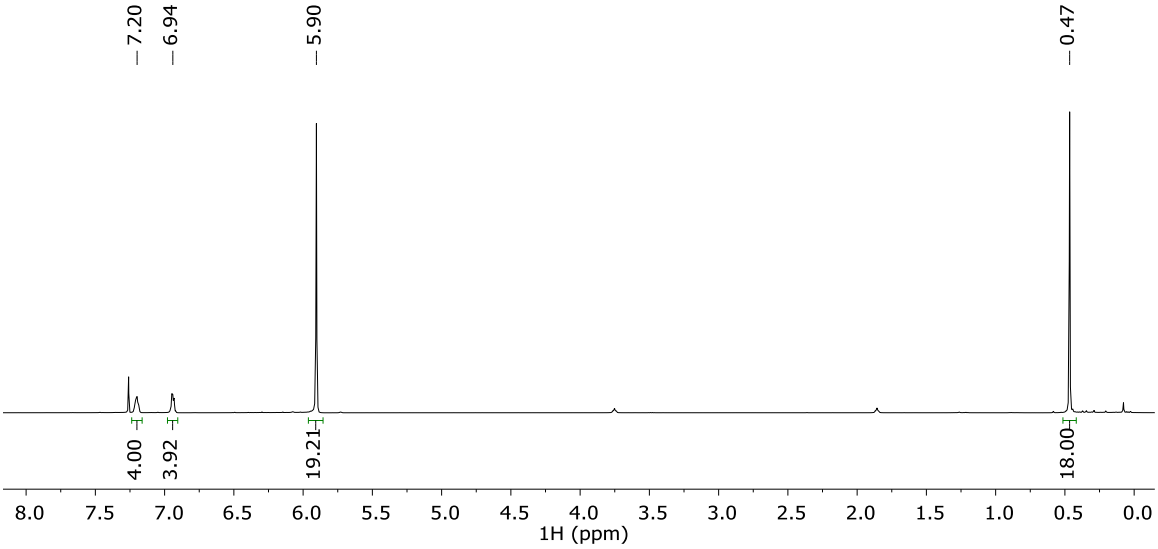

Figure 2.8: ^{1}H NMR (500 MHz, $CDCl_3$) spectrum of **2.2**.

Analytically pure single crystals of **2.2** were readily obtained by recrystallization from benzene solution. The structure of **2.2** only differs from **2.1** based on the exchange of Na^+ for Me_3Si^+ and removal of corresponding Na-O interactions and coordinated THF, shown in **Figure 2.9**.

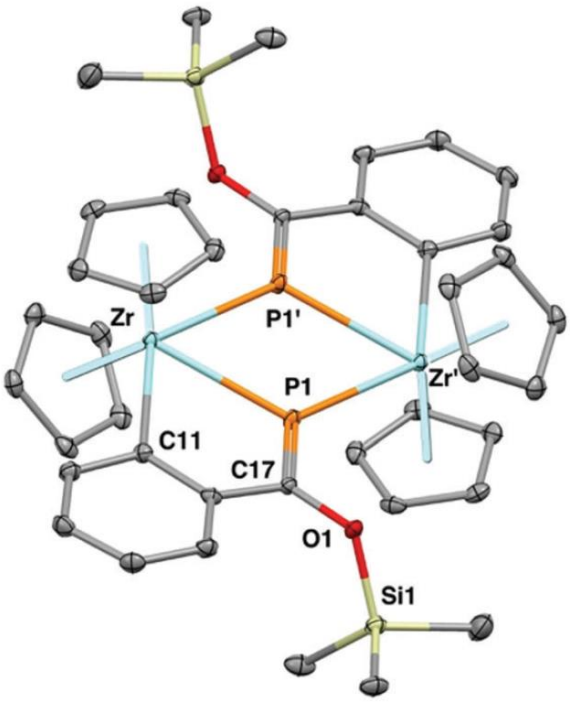

Figure 2.9: ORTEP diagram of **2.2** (ellipsoids set at 50% probability; hydrogen atoms omitted for clarity). Selected bond distances [Å] and angles [deg]: Zr1–P1: 2.6721(6); Zr1'–P1: 2.7608(6); Zr1–C11: 2.3873(19); P1–C17: 1.7046(19); O1–C17: 1.372(2); P1–Zr1–P1': 59.276(19); P1–Zr1–C11: 71.22(5); Zr1–P1–Zr1': 120.723(19); Zr1–P1–C17: 105.83(7); Zr1'–P1–C17: 131.39(7); P1–C17–O1: 124.03(14).

There were, however, a few noticeable changes when comparing the structures of **2.1** and **2.2** more closely. First, **2.2** adopts a much less planar geometry, with the phosphorus atoms lying noticeably out of plane, as shown by the reduced sum of angles incorporating P1 as the central atom (359.3° for **2.1** and 357.9° for **2.2**). Additionally, the P=C distance in **2.2** is distinctly shorter (1.743(5) Å for **2.1** and 1.7046(19) Å for **2.2**) than **2.1** as well as displaying a substantially longer C-O distance (1.276(6) Å for **2.1** and 1.372(2) Å for **2.2**). The bond lengths suggest that the oxygen atom in **2.1** could be donating more electron density into the π-system, resulting in partial C=O character and a weakened

C=P bond. A similar effect was observed in metallophosphaalkenes that incorporated a *trans*-nitrogen instead of oxygen.[21] Furthermore, the resonance displayed in **Scheme 2.10** can also be utilized to explain the greater shielding on phosphorus between **2.1** and **2.2** (^{31}P NMR, δ = 50 ppm and 194 ppm, respectively).

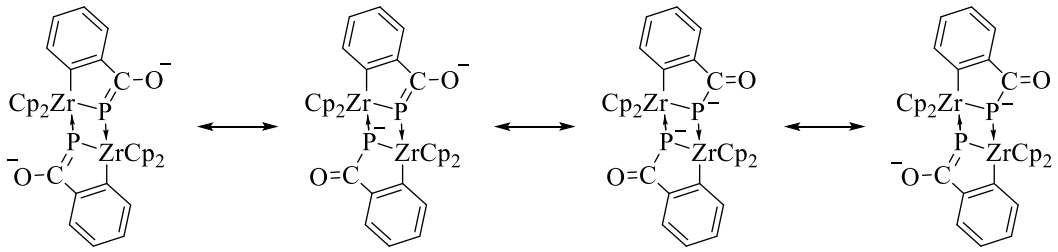

Scheme 2.10: Resonance structures of **2.1**.

We also attempted to isolate a complex containing an electron-deficient group on oxygen, such as an aryl borane (Ar_2B). The most available candidate for this reaction was dimesitylboron fluoride, which was added to a pressure tube with 1 equivalent of **2.1** and THF. The red slurry was then rapidly stirred at 80 °C overnight (**Scheme 2.11**).

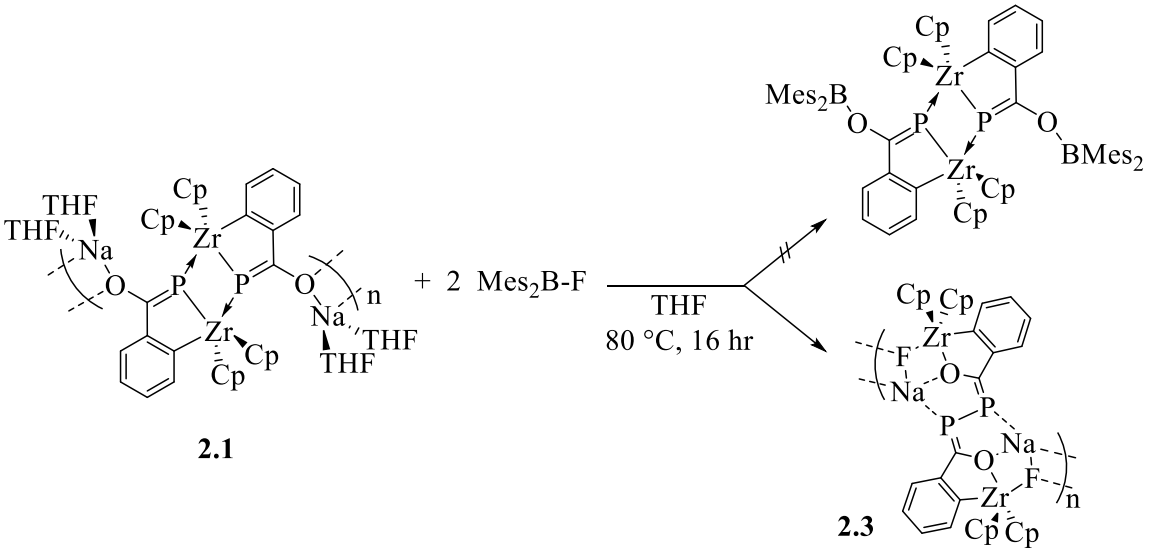

Scheme 2.11: Reaction of **2.1** and Mes_2BF to give **2.3**.

After a few hours, it was visually apparent that considerably less of **2.1** was suspended in the solution. After heating was finished, the solution was filtered under inert

atmosphere and concentrated under vacuum until saturated. A small portion of this saturated filtrate produced red single crystals suitable for X-ray diffraction after a few days of storage at -35 °C. The structure obtained for this material, shown in **Figure 2.10**, was not a simple substitution of a sodium counter-ion for borane group. Instead, a complete reassembly of the bonding within **2.1**, inclusion of a fluoride ion, and formation of another coordination polymer through Na-F interactions occurred. Furthermore, borane functionality was absent within this crystalline product.

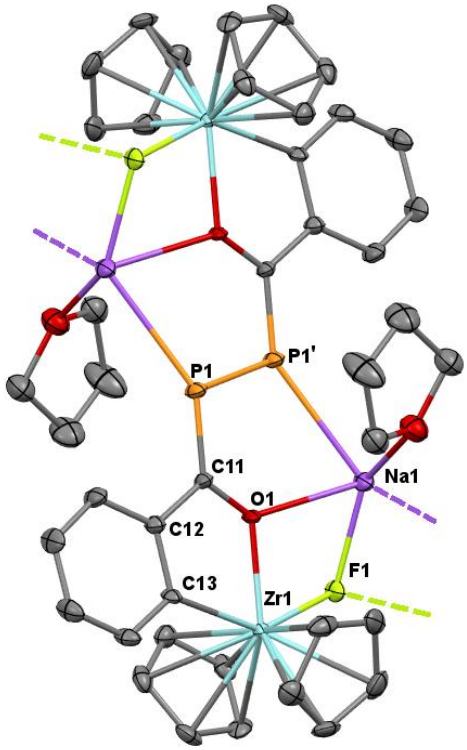

Figure 2.10: ORTEP diagram of **2.3** (ellipsoids set at 50% probability; hydrogen atoms omitted for clarity). Selected bond distances [Å] and angles [deg]: P1-P1': 2.154(1); P1-C11: 1.730(4); C11-O1: 1.319(4); Zr1-O1: 2.182(2); Zr1-F1: 2.121(2); P1'-P1-C11: 101.2(1); P1'-P1-Na1': 103.11(5); Na1'-P1-C11: 148.5(1).

The C-P distances in **2.1**, **2.2**, and **2.3** remain similar (1.743(5), 1.7046(19), and 1.730(4) Å, respectively), indicating the C=P double bond was largely maintained. The P-P distance in **2.3** (2.154(1) Å) is directly between what is expected for simple diphosphenes (Mes*P=PMes*, 2.034 Å)[22] or diphosphines (Mes_2P-$PMes_2$, 2.259 Å).[23] The sum of angles around P1(352.8°) indicates a mostly planar geometry.

The solubility of **2.3**, combined with availability of compatible solvents, resulted in only obtaining heteroatom NMR spectra. In THF, **2.3** gives a single ^{31}P resonance at 55.9 ppm and a ^{19}F resonance at -127.94 ppm.

Section 2.2.4: Mechanistic Insights into the Stepwise Hydrolysis of Zirconophosphaalkene Complexes

As mentioned previously, compound **2.1** is very sensitive towards hydrolysis upon exposure to ambient conditions. Removal of **2.1** from an inert atmosphere caused an immediate color change from bright red to orange and produced a strong scent of phosphane. Compound **2.2** was found to be less sensitive, though it would still decompose upon exposure to moist air within a few minutes. Although organometallic compounds are typically air and water sensitive, we discovered that adding a stoichiometric amount (3 equivalents per phosphorus atom) of water to either **2.1** or **2.2** produced a single product by ^{31}P NMR (δ = -108 ppm, *t*, $^{1}J_{PH}$ 219.7 Hz). Adding an anhydrous solution of hydrogen chloride in dioxane to a suspension of **2.1** in dichloromethane-d_2 provided the same phosphorus-containing major product as well as dichlorozirconocene and THF as the only other products by ^{1}H NMR spectroscopy, as shown in **Figure 2.11** and **Figure 2.12**.

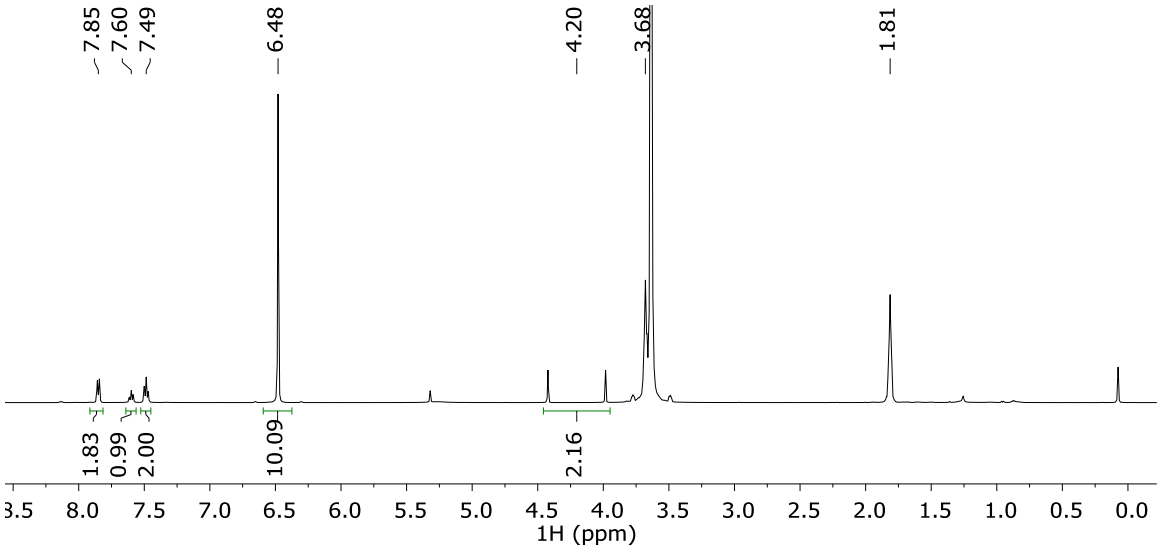

Figure 2.11: ^{1}H NMR (500 MHz, CH_2Cl_2) spectrum of reaction of **2.1** and anhydrous HCl.

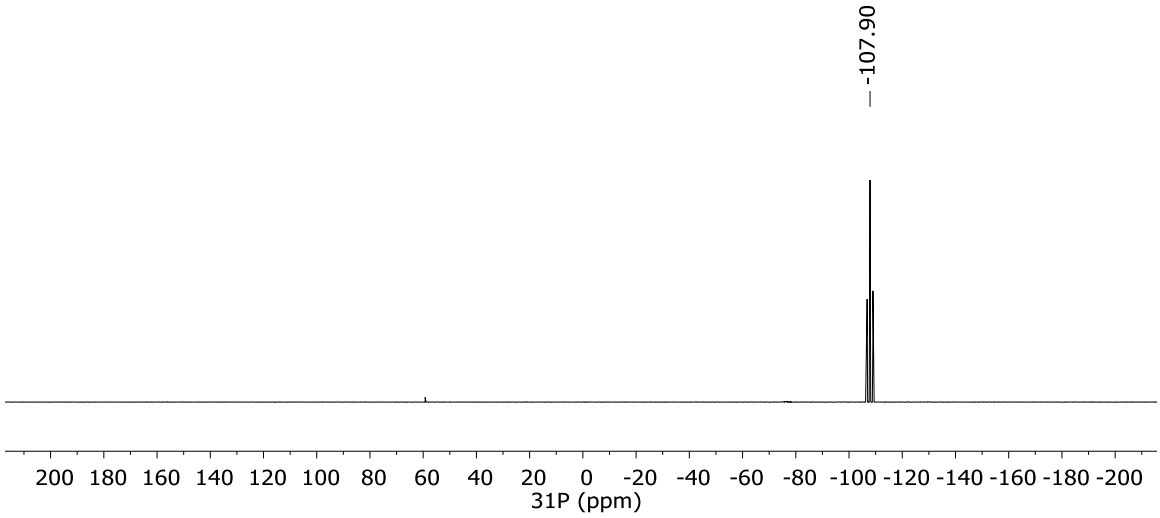

Figure 2.12: ^{31}P NMR (202 MHz, CH_2Cl_2) spectrum of reaction of **2.1** and anhydrous HCl.

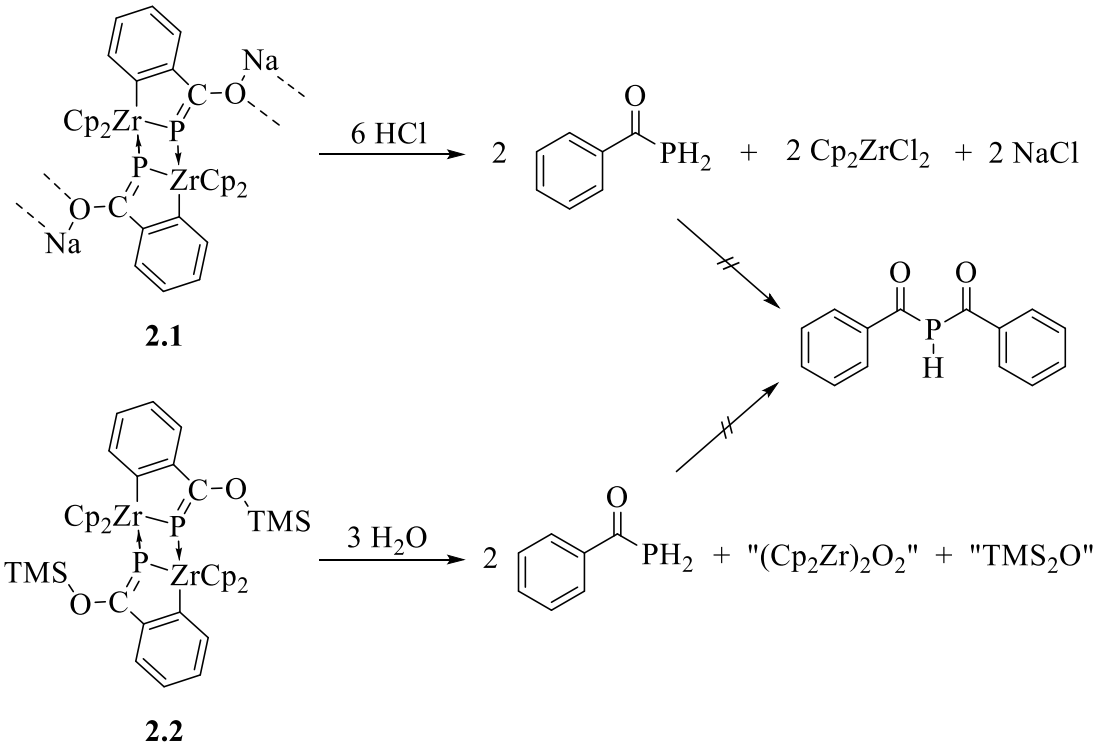

Scheme 2.12: Protonation reactions of **2.1** and **2.2** to yield benzoylphosphine.

The product of the reaction shown in **Scheme 2.12** was identified as benzoylphosphine ($PhC(O)PH_2$) which had been previously reported from the reaction between KPH_2·(18-crown-6) and benzoate esters (PhC(O)OR, R = Me, Et, ^{i}Pr, ^{t}Bu, Ph) and subsequent protonation from PhC(O)P{K}H.[24] Benzoylphosphine, as formed by this route, undergoes rapid self-condensation (6 hours at room temperature) to form dibenzoylphosphine (PhC(O)PHC(O)Ph) and PH_3. Interestingly, production of benzoylphosphine *via* the protonation of **2.1** or **2.2** does not result in a rapid self-condensation, but instead the solutions of benzoylphosphine, provided in **Scheme 2.12**, remain free of the condensation products indefinitely. Benzoylphosphine is still susceptible to additional hydrolysis, which was observed over months on a sample sealed with a Young-type valve ($t_{½} \approx 35$ days), however this results only in observed production of PH_3 and not a combination of dibenzoylphosphine and PH_3 as shown in **Figure 2.13**. Attempts

to isolate benzoylphosphine by concentrating these solutions under vacuum did not succeed, instead a number of impurities were detected by NMR spectroscopy including dibenzoylphosphine.

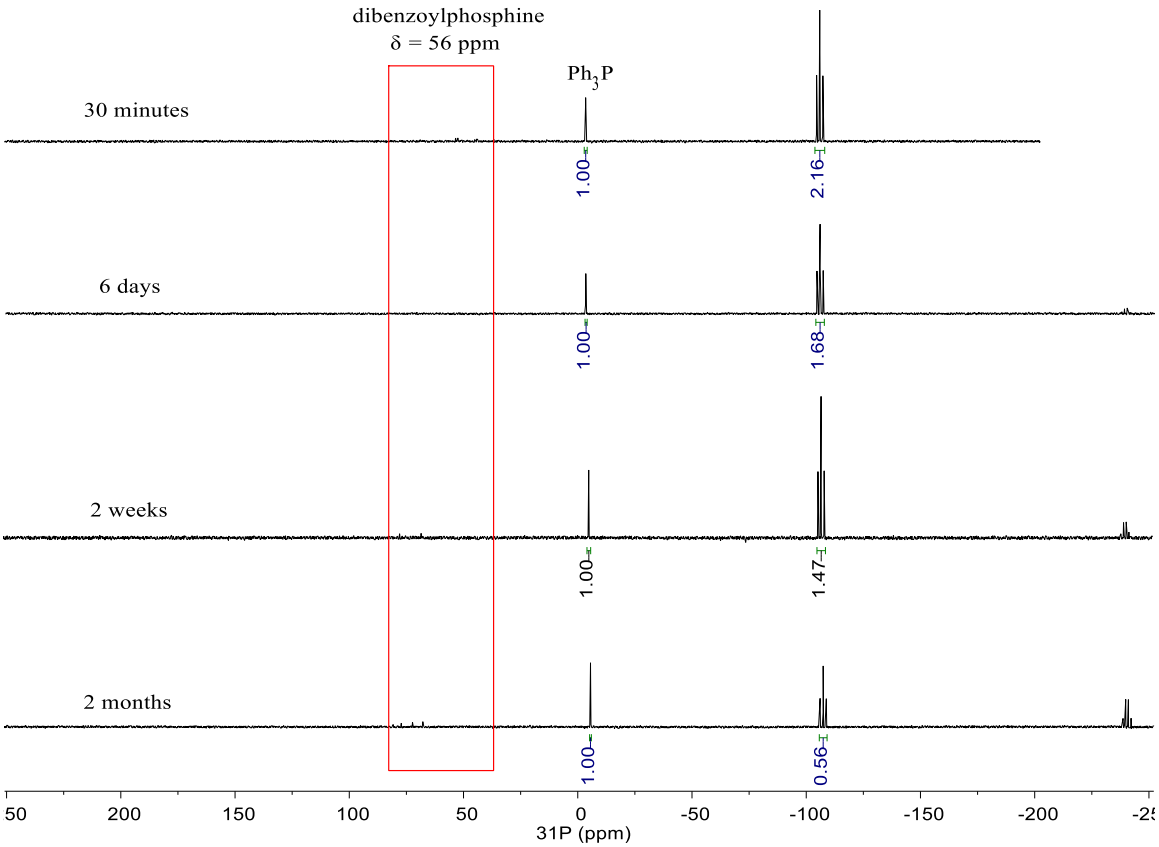

Figure 2.13: ^{31}P NMR (162 MHz, CH_2Cl_2) spectra of sealed tube containing benzoylphosphine reaction mixture. Ph_3P used as internal standard.

The mechanism whereby this set of protonation reactions was occurring was examined. As mentioned previously, **2.1** and **2.2** were highly susceptible to hydrolysis with moist air, yet produced very clean reactions when exposed to water or even stronger acids (similar results achieved with HBF_4 etherate) under inert atmosphere. We set out to show if this reaction could be controlled upon stepwise addition of water. Additionally, we attempted to track the site of reactivity upon addition of each equivalent of water by using a combination of

H_2O and D_2O as shown in **Scheme 2.13**. By examining regions containing resonances attributed to aryl, cyclopentadienyl, phosphino, and silyl groups, we were able to map out likely pathways whereby this reaction was occurring. Furthermore, the spectra after stepwise hydrolysis were nearly identical to the spectra obtained after the hydrolysis was accomplished in one step, aside from any H/D substitutions in benzoylphosphine.

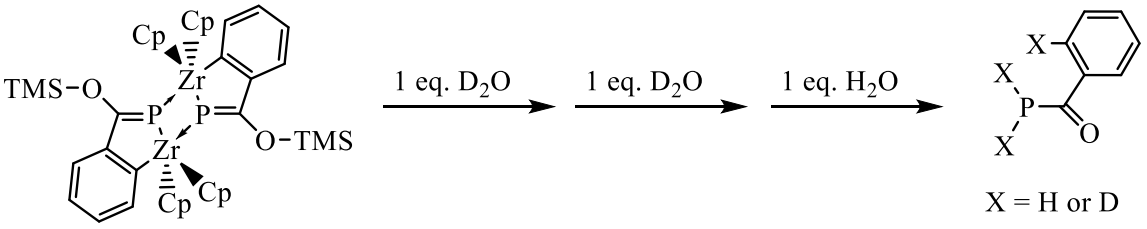

2.2

Scheme 2.13: Stepwise hydrolysis of **2.2** by stepwise addition of D_2O and H_2O.

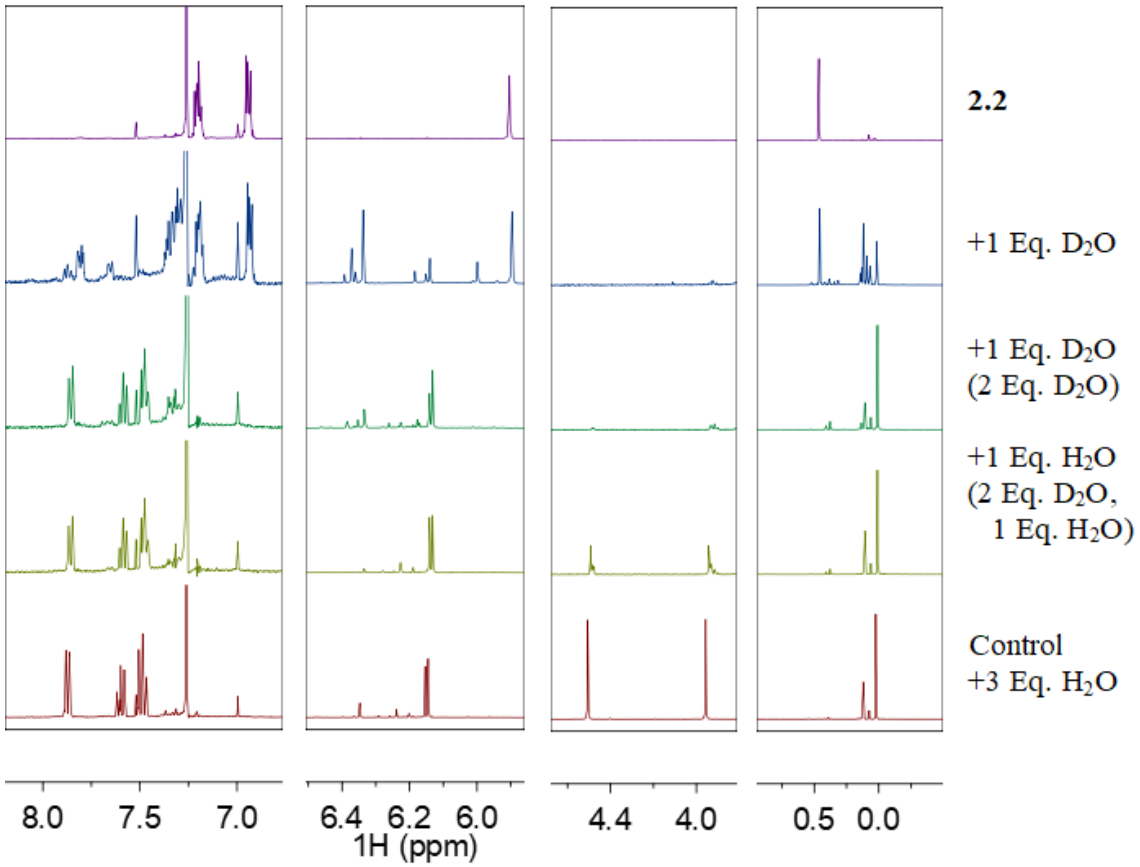

Figure 2.14: ^{1}H NMR (400 MHz, $CDCl_3$) spectra for stepwise hydrolysis of **2.2** with a combination of H_2O and D_2O

Examining this pathway was of interest to assess the potential to isolate one or more intermediate products which might be useful in further derivatization. With this goal in mind, we were able to establish a few primary findings. First, when **2.2** was reacted stepwise with two equivalents D_2O and then one equivalent H_2O, the *ortho*-CH doublet at 7.86 ppm in the ^{1}H NMR spectrum integrated to exactly 1H. This provided evidence that the Zr-C bond was hydrolyzed exclusively by D_2O. Additionally, the region corresponding to aryl resonances was relatively unchanged after only one equivalent of D_2O was added signaling that the Zr-C bond was primarily broken upon addition of the second equivalent of D_2O. However, a mixture of PD_2, PHD, and PH_2 substituted products (as evidenced by

a 1:2:3:2:1 pentet, 1:1:1 triplet, and singlet in $^{31}P\{^{1}H\}$ NMR spectrum) was present in the final solution, so the reaction had proceeded through a complex mixture of intermediates. As shown in **Scheme 2.14**, we propose two primary pathways for the stepwise hydrolysis of **2.2**, however the potential of other unknown intermediates, numerous regioisomers, as well as potentially asymmetric reactions renders this a result of little practical use unless a greater degree of control for a single pathway can be established.

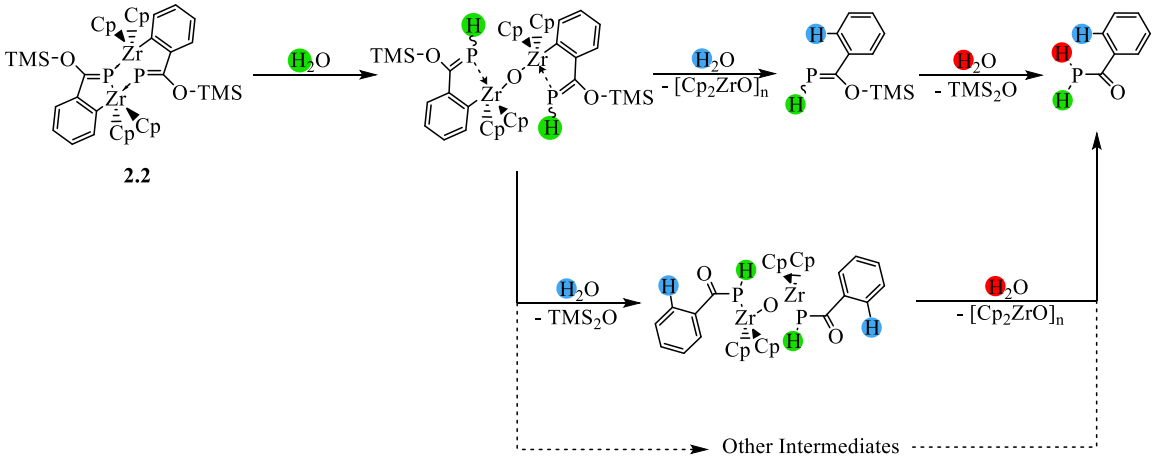

Scheme 2.14: Simplified pathway for the stepwise hydrolysis of **2.2**.

Section 2.3: Conclusions and Future Directions

The initial direction that this project started with, the reaction of Na[OCP] with benzyne, gave unanticipated but exciting results. A challenge to our original approach is that Na[OCP] undergoes side reactions with all of the aryne-forming chemicals that we tested. The method of using arynes in synthetic chemistry is typically done via trapping reactions seeing as the reactive intermediate is non-isolable. Therefore, unless all of the side reactions with Na[OCP] can be negated, it is likely that they will take precedent over the intended reaction seeing as aryne formation should be approached slowly in order to minimize self-reaction. The benzyne precursor 2-trimethylsilylphenyl triflate remains the most likely candidate for success here only due to its relatively slow, though still

noticeable, reactivity towards Na[OCP]. However, much of the focus on this reaction is specifically driven by comparison towards Heinicke's 2-lithiobenzazaphosphole.[25] We primarily sought to approach the 2-metallobenzoxaphosphole given reports of the associated 2-lithiobenzazaphosphole chemistry coupled to our previous work with luminescent benzoxaphospholes[2,5] in an effort to broaden its functionality. This driving force was lessened by the recent discovery, as discussed in **Chapter 3**, by Heinicke and our group that shows previously reported benzazaphospholes can share this luminescent behavior.

The reactivity of Na[OCP] towards metal complexes and subsequent studies of these new complexes is still an open field of research. First, our work involving borane substitution onto **2.1** is incomplete and deserves further study. We must not only determine the fate of the missing dimesitylboryl group when synthesizing **2.3**, but also determine how best to incorporate a borane into the structure of **2.1** without the observed rearrangement. To this end, we have begun examining the reaction of a dialkylbromoborane with **2.1** which should allow for substitution under milder conditions. Next, it would be beneficial to study whether the insertion chemistry we observed is maintained over other metal-aryne complexes. To this end, we have synthesized nickel[26] and ruthenium[27] complexes incorporating an aryne ligand, however their reactivity toward Na[OCP] remains undeveloped. In a similar fashion, we are not limited towards aryne ligands as the field of zirconium-alkyne chemistry is much more developed. Primarily, we can theorize a similar reaction to the synthesis of **2.1** occurring based on **Scheme 2.15**, where a zirconocene-alkyne complex is trapped by a stabilizing ligand followed by insertion of Na[OCP]. This

procedure has been used in previous studies to form asymmetric zirconacyclopentadiene complexes from two different alkynes.[28,29]

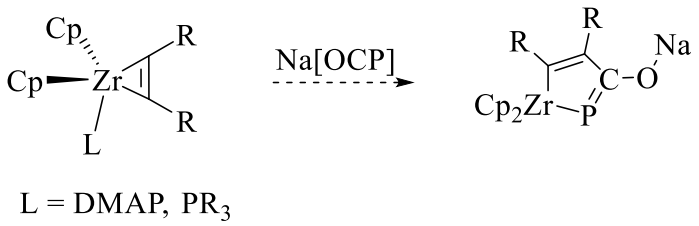

L = DMAP, PR_3

Scheme 2.15: Proposed reaction between Na[OCP] and zirconacyclopropene complex.

The broader goal for this project, however, is to utilize the complexes that we have developed towards the synthesis of functional phosphorus-containing molecules and materials. The chemistry of similar zirconacyclopentadienes, formed from fully organic alkynes, has long been utilized towards the formation of heteroles upon reaction with a main-group dihalide as given by the work of Fagan and Nugent, shown in **Scheme 2.16**.[30–32]

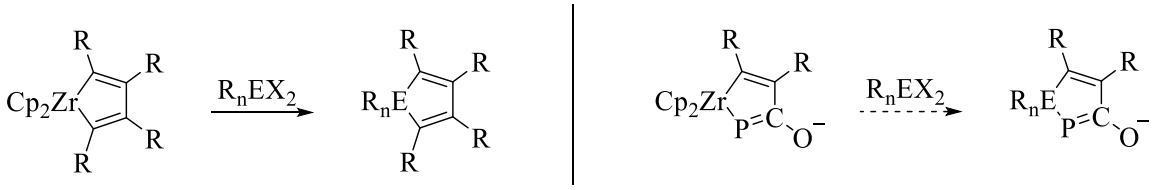

Scheme 2.16: (left) Typical Fagan-Nugent type synthesis of heteroles. (right) Proposed reaction for synthesis of 2-phosphaheteroles.

A similar heterole to that proposed in **Scheme 2.16**, a series of 1,3,4-azadiphospholides, was reported by Grützmacher from the reaction of Na[OCP] and 2-chloropyridenes and was shown to exhibit excellent optical tunability. The reactivity presented here could be used in a similar way through functionalized arynes. Of note, not only can the parent lithioarene, used to form the zirconium-aryne complex, be

functionalized, but also known are a zirconium-benzdiyne complex and a zirconium-phosphabenzyne complex which offer additional routes of tunability.[33,34]

Section 2.4: Experimental

General Considerations: All reactions were performed under an atmosphere of rigorously dry and oxygen-free nitrogen using either an MBraun glove box or standard Schlenk line techniques. Unless otherwise stated, all chemicals were purchased from commercial sources and used without further purification. Tetrahydrofuran was purified using an MBraun solvent purification system. Benzene was distilled over sodium benzophenone ketyl prior to use. Chloroform-d and dichloromethane-d_2 were dried over alumina or 3 Å molecular sieves and degassed prior to use. $[Cp_2Zr(C_6H_4)(PMe_3)]$[15] and Na[OCP][14] were prepared following literature procedures. Solution NMR spectra were recorded on a Bruker AVANCE III 500 or Varian Inova 400 spectrometers and chemical shifts referenced to residual solvent signal (^{1}H and ^{13}C) or to 85% H_3PO_4 (^{31}P). Unless otherwise stated, ^{13}C and ^{31}P NMR spectra were ^{1}H-decoupled. Solid-state ^{31}P MAS NMR spectrum was recorded on a Bruker AVANCE III 800 spectrometer using a 2.5 mm rotor with a spinning rate of 30 kHz and chemical shift (δ) referenced to Na_2HPO_4 as an external standard (2.3 ppm).[35] Elemental Analysis was performed by Robertson Microlit Laboratories (Ledgewood, NJ).

Reaction of Na[OCP] with Zr-Benzyne Complex (2.1): To a solution of Na[OCP]·$Dioxane_{2.5}$ (1.70 g, 5.6 mmol) in 50 mL THF was added a solution of $[Cp_2Zr(C_6H_4)(PMe_3)]$ (2.11 g, 5.6 mmol) in 5 mL THF. The resulting dark red solution was stirred at room temperature for 24 hours. During this time, **2.1** precipitated from solution and was collected by filtration through a fine porosity filter funnel. The precipitate

was washed with additional THF and dried under reduced pressure to give a bright red insoluble solid (1.26 g, 43%). Single crystals were obtained by carefully layering a solution of Na[OCP] in THF on top of a solution of [$Cp_2Zr(C_6H_4)(PMe_3)$] in THF in a thin glass tube and allowing to sit undisturbed for 24 hours. ^{31}P MAS NMR (324 MHz): δ 50.6.

Disruption of Coordination Polymer with TMS-Cl (2.2): To a suspension of **2.1** (0.47 g, 0.45 mmol) in 25 mL THF was added trimethylchlorosilane (0.12 mL, 0.95 mmol) which slowly formed a cloudy red-orange solution upon stirring for 30 minutes. Removal of volatiles under reduced pressure produced a bright orange powder. Crude product was dissolved in 50 mL THF, filtered, and filtrate evaporated under reduced pressure to afford a bright orange powder (0.37 g, 96%). Analytically pure single crystals were produced through recrystallization from benzene. ^{1}H NMR ($CDCl_3$, 500 MHz): δ 0.47 (s, 18H), 5.90 (s, 20H), 6.93-6.95 (m, 4H), 7.19-7.22 (m, 4H). ^{13}C{^{1}H} NMR ($CDCl_3$, 126 MHz): δ 1.77 (s), 105.53 (s), 119.66 (t, J_{PC} = 6.55 Hz), 122.14 (s), 124.09 (s), 141.46 (s), 152.18 (t, J_{PC} = 5.43 Hz), 186.16 (t, J_{PC} = 6.26 Hz), 209.10 (d, J_{PC} = 21.02 Hz). ^{31}P{^{1}H} NMR ($CDCl_3$, 202 MHz): δ 193.97. Anal. Calcd. for $C_{40}H_{46}O_2P_2Zr_2$: C, 55.91; H, 5.40. Found: C, 55.79; H, 5.28.

Rearrangement of Coordination Polymer (2.3): In a pressure tube, **2.1** (0.49 g, 0.43 mmol) and Mes_2BF (0.23 g, 0.86 mmol) were combined with 25 mL dry THF. This bright red slurry slowly turned into a dark red-purple solution upon heating at 80 °C overnight. Volatiles were removed under vacuum and resulting dark purple solid washed with 5 mL toluene, 3x 2 mL hexanes, then dried under vacuum, 0.188 g, 47%. ^{31}P{^{1}H} NMR (THF, 202 MHz): δ 55.85. ^{19}F NMR (THF, 471 MHz): δ -127.94.

Hydrolysis Reactions Yielding Benzoylphosphine:

A) To a suspension of **2.1** (36 mg, 0.034 mmol) in 1 mL dichloromethane-d_2 was added a solution of HCl in Dioxane (0.21 mmol). After mixing, the reaction mixture was filtered to yield a bright yellow solution containing benzoylphosphine and Cp_2ZrCl_2. ^{1}H NMR (CD_2Cl_2, 500 MHz): δ 4.20 (d, $^1J_{PH}$ = 219.6 Hz, 2H), 6.48 (Cp_2ZrCl_2, s, 10H), 7.49 (t, J = 7.6 Hz, 2H), 7.60 (t, J = 7.5 Hz, 1H), 7.85 (d, J = 7.7 Hz, 2H). ^{13}C{^{1}H} NMR (CD_2Cl_2, 126 MHz): δ 116.65 (Cp_2ZrCl_2), 127.97 (d, J_{PC} = 5.04 Hz), 129.29, 134.31, 140.50 (d, J_{PC} = 27.47 Hz), 211.93 (d, J_{PC} = 30.10 Hz). ^{31}P NMR ^{1}H Coupled (CD_2Cl_2, 202 MHz): δ -107.90 (t, $^1J_{PH}$ = 219.7 Hz).

B) To a suspension of **2.2** (29 mg, 0.034 mmol) in 1 mL CD_2Cl_2 was added H_2O (2 μL, 0.1 mmol). The bright orange suspension slowly turned to a clear, light orange solution and after 30 minutes was analyzed by multinuclear NMR. Spectra show complete conversion of **2.2** to benzoylphosphine as well as unidentified byproducts containing zirconocene or trimethylsilyl functionality**.** ^{1}H NMR (CD_2Cl_2, 500 MHz): δ 4.22 (d, J = 219.7 Hz, 2H), 7.50 (t, J = 7.6 Hz, 2H), 7.61 (t, J = 7.4 Hz, 1H), 7.86 (d, J = 7.6 Hz, 2H). ^{13}C{^{1}H} NMR (CD_2Cl_2, 126 MHz): δ 127.98 (d, J_{PC} = 5.07 Hz), 129.31, 134.33, 140.51 (d, J_{PC} = 27.40), 212.02, (d, J_{PC} = 30.13). ^{31}P NMR ^{1}H Coupled (CD_2Cl_2, 202 MHz): δ -107.74 (t, J_{PH} = 219.7 Hz).

Section 2.5: References

(1) Kieser, J. M.; Gilliard, R. J.; Rheingold, A. L.; Grützmacher, H.; Protasiewicz, J. D. Insertion of Sodium Phosphaethynolate, Na[OCP], into a Zirconium-Benzyne Complex. *Chem. Commun.* **2017**, *53*, 5110–5112.

(2) Washington, M. P.; Gudimetla, V. B.; Laughlin, F. L.; Deligonul, N.; He, S.; Payton,

J. L.; Simpson, M. C.; Protasiewicz, J. D. Phosphorus Can Also Be a “Photocopy.” *J. Am. Chem. Soc.* **2010**, *132*, 4566–4567.

(3) Shi, F.; Waldo, J. P.; Chen, Y.; Larock, R. C. Benzyne Click Chemistry: Synthesis of Benzotriazoles from Benzynes and Azides. *Org. Lett.* **2008**, *10*, 2409–2412.

(4) Wu, S.; Rheingold, A. L.; Protasiewicz, J. D. Luminescent Materials Containing Multiple Benzoxaphosphole Units. *Chem. Commun.* **2014**, *50*, 11036–11038.

(5) Simpson, M. C.; Protasiewicz, J. D. Phosphorus as a Carbon Copy and as a Photocopy: New Conjugated Materials Featuring Multiply Bonded Phosphorus. *Pure Appl. Chem.* **2013**, *85*, 801–815.

(6) Heinicke, J.; Steinhauser, K.; Peulecke, N.; Spannenberg, A.; Mayer, P.; Karaghiosoff, K. Metalated 1,3-Azaphospholes: Structure and Reactivity of 2-Lithio-1-Methy1-1,3-Benzazaphosphole, an Isolable -P=C(Li)-NR Heterocycle. *Organometallics* **2002**, *21*, 912–919.

(7) Hart, H. Arynes and Heteroarynes. In *Supplement C2: The Chemistry of Triple-Bonded Functional Groups*; John Wiley & Sons, Ltd: Chichester, UK, 2004; pp 1017–1134.

(8) Urnéžius, E.; Protasiewicz, J. D. Synthesis and Structural Characterization of New Hindered Aryl Phosphorus Centers (Aryl = 2,6-Dimesitylphenyl). *Main Gr. Chem.* **1996**, *1*, 369–372.

(9) Wright, V. A.; Patrick, B. O.; Schneider, C.; Gates, D. P. Phosphorus Copies of PPV: π-Conjugated Polymers and Molecules Composed of Alternating Phenylene and Phosphaalkene Moieties. *J. Am. Chem. Soc.* **2006**, *128*, 8836–8844.

(10) Gilliard, R. J.; Heift, D.; Benko, Z.; Keiser, J. M.; Rheingold, A. L.; Grützmacher,

H.; Protasiewicz, J. D. An Isolable Magnesium Diphosphaethynolate Complex. *Dalt. Trans.* **2018**, *47*, 666–669.

(11) Becker, G.; Heckmann, G.; Hübler, K.; Schwarz, W. Alkylidinphosphane Und -arsane. II. Über Die Oxydation Des Lithoxy-methylidinphosphans P≡C-O-Li Mit Schwefeldioxid Und Iod. *Z. Anorg. Alleg. Chem.* **1995**, *621*, 34–46.

(12) Becker, G.; Schwarz, W.; Seidler, N.; Westerhausen, M. Acyl- Und Alkylidenphosphane. XXXIII. Lithoxy-methylidenphosphan · DME Und -methylidinphosphan · 2 DME — Synthese Und Struktur. *Z. Anorg. Alleg. Chem.* **1992**, *612*, 72–82.

(13) Westerhausen, M.; Schneiderbauer, S.; Piotrowski, H.; Suter, M.; Nöth, H. Synthesis of Alkaline Earth Metal Bis(2-Phosphaethynolates). *J. Organometalic Chem.* **2002**, *643–644*, 189–193.

(14) Puschmann, F. F.; Stein, D.; Heift, D.; Hendriksen, C.; Gal, Z. A.; Grützmacher, H.-F.; Grützmacher, H. Phosphination of Carbon Monoxide: A Simple Synthesis of Sodium Phosphaethynolate (NaOCP). *Angew. Chem. Int. Ed.* **2011**, *50*, 8420–8423.

(15) Buchwald, S. L.; Watson, B. T.; Huffman, J. C. The Trimethylphosphine Adduct of the Zirconocene-Benzyne Complex: Synthesis, Reactions, and X-Ray Crystal Structure. *J. Am. Chem. Soc.* **1986**, *108*, 7411–7413.

(16) Binger, P.; Biedenbach, B.; Mynott, R.; Regitz, M. Synthese von Bis(Cyclopentadienyl)-1-Metalla-3-Phosphaindenen (M = Titan, Zirkonium). *Chem. Ber.* **1988**, *121*, 1455–1456.

(17) Ma, X.-B.; Regitz, M. Organophosphorus Compounds; 99. An Efficient One-Pot Synthesis of 1,1-Bis(H5-Cyclopentadienyl)-1-Zircona-3-Phosphaindenes. *Synthesis*

1995, *1995*, 667–670.

(18) d'Arbeloff-Wilson, S. E.; Hitchcock, P. B.; Nixon, J. F.; Kawaguchi, H.; Tatsumi, K. [2+2] Cyclo-Addition Reactions of Bis-Pentamethylcyclopentadienyl Zirconium Metal Complexes Containing Terminal Chalcogenide Ligands with the Phospha-Alkyne PCtBu. Syntheses, Crystal and Molecular Structures of the Four Complexes. *J. Organomet. Chem.* **2003**, *672*, 1–10.

(19) Weber, L. Metallophosphaalkenes—from Exotics to Versatile Building Blocks in Preparative Chemistry. *Angew. Chem. Int. Ed.* **1996**, *35*, 271–288.

(20) Weber, L. Recent Developments in the Chemistry of Metallophosphaalkenes. *Coord. Chem. Rev.* **2005**, *249*, 741–763.

(21) Weber, L.; Kleinebekel, S.; Rühlicke, A.; Stammler, H. Syntheses and Structures of C-Monoamino-P-Ferriophosphaalkenes. *Eur. J. Inorg. Chem* **2000**, *1*, 1185–1191.

(22) Yoshifuji, M.; Shima, I.; Inamoto, N.; Hirotsu, K.; Higuchi, T. Synthesis and Structure of Bis(2,4,6-Tri-Tert-Butylphenyl)Diphosphene: Isolation of a True "Phosphobenzene." *J. Am. Chem. Soc.* **1981**, *103*, 4587–4589.

(23) Baxter, S. G.; Cowley, A. H.; Davis, R. E.; Riley, P. E. Crystal Structure and Low-Temperature 1H NMR Spectrum of Tetramesityldiphosphine. Evidence for the Anti-Conformational Preference in Tetraaryldiphosphines. *J. Am. Chem. Soc.* **1981**, *103*, 1699–1702.

(24) Liotta, C. L.; MeLaughlin, M. L.; O'Brien, B. A. The Synthesis and Reactions of Potassium Benzoylphosphide, Benzoylphosphine, and Benzoylmethylphosphine. *Tetrahedron Lett.* **1984**, *25*, 1249–1252.

(25) Heinicke, J.; Steinhauser, K.; Peulecke, N.; Spannenberg, A.; Mayer, P.;

Karaghiosoff, K. Metalated 1,3-Azaphospholes: Structure and Reactivity of 2-Lithio-1-Methyl-1,3-Benzazaphosphole, an Isolable −PC(Li)−NR Heterocycle. *Organometallics* **2002**, *21*, 912–919.

(26) Retbøll, M.; Edwards, A. J.; Rae, A. D.; Willis, A. C.; Bennett, M. A.; Wenger, E. Preparation of Benzyne Complexes of Group 10 Metals by Intramolecular Suzuki Coupling of Ortho-Metalated Phenylboronic Esters: Molecular Structure of the First Benzyne-Palladium(0) Complex. *J. Am. Chem. Soc.* **2002**, *124*, 8348–8360.

(27) Hartwig, J. F.; Bergman, R. G.; Andersen, R. A. Reactions with Arenes, Alkenes, and Heteroatom-Containing Organic Compounds. *J. Am. Chem. Soc.* **1991**, *113*, 3404–3418.

(28) Takahashi, T.; Swanson, D. R.; Negishi, E. Zirconacyclopropanes and Zirconacyclopropenes. Their Synthesis, Characterization, and Reactions. *Chem. Lett.* **1987**, *16*, 623–626.

(29) Van Wagenen, B. C.; Livinghouse, T. On the Generation of Stabilized Low-Valent Metallocene Derivatives. The Direct Synthesis and Reductive Coupling Reactions of 1-Methylthioalkyne-Zirconocene Complexes. *Tetrahedron Lett.* **1989**, *30*, 3495–3498.

(30) Fagan, P. J.; Nugent, W. A. Synthesis of Main Group Heterocycles by Metallacycle Transfer from Zirconium. *J. Am. Chem. Soc.* **1988**, *110*, 2310–2312.

(31) Fagan, P. J.; Nugent, W. A.; Calabrese, J. C. Metallacycle Transfer from Zirconium to Main Group Elements: A Versatile Synthesis of Heterocycles. *J. Am. Chem. Soc.* **1994**, *116*, 1880–1889.

(32) Yan, X.; Xi, C. Conversion of Zirconacyclopentadienes into Metalloles: Fagan-

Nugent Reaction and Beyond. *Acc. Chem. Res.* **2015**, *48*, 935–946.

(33) Buchwald, S. L.; Lucas, E. A.; Dewan, J. C. Synthesis, Structure, and Reactions of a Zirconocene-Benzdiyne Complex. *J. Am. Chem. Soc.* **1987**, *109*, 4396–4397.

(34) Rosa, P.; Le Floch, P.; Ricard, L.; Mathey, F. Synthesis, Structure, and Reactivity of η 2 -Phosphabenzyne−Zirconocene Dimers. *J. Am. Chem. Soc.* **1997**, *119*, 9417–9423.

(35) Turner, G. L.; Smith, K. A.; Kirkpatrick, R. J.; Oldfieldt, E. Structure and Cation Effects on Phosphorus-31 NMR Chemical Shifts and Chemical-Shift Anisotropies of Orthophosphates. *J. Magn. Reson.* **1986**, *70*, 408–415.

Chapter 3: Emission Quenching of a Luminescent Benzazaphosphole via Reactions with Isolable *N*-Heterocyclic Carbenes

Section 3.1: Introduction

Our primary focus on the study of 1,3-benzoxaphospholes was driven by their luminescent behavior. Until this point, the similar 1,3-benzazaphosphole (BAP) was not known to exhibit any luminescence. To this end, our group had prepared the first luminescent benzazaphosphole which incorporated a carbazole moiety into the structure in order to obtain the desired emission.[1] The synthesis for BAPs is slightly different than is standard for BOPs, namely the metal catalyzed phosphorylation, as shown within **Scheme 3.1**.[2]

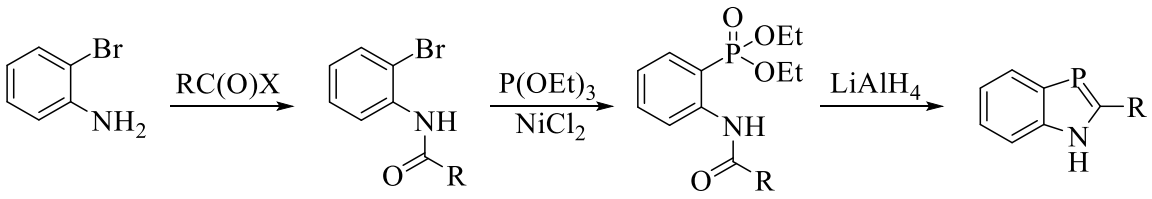

Scheme 3.1: Synthesis of 1,3-benzazaphospholes.[2]

We recently received a private communication from Professor Joachim Heinicke detailing the observation of luminescent behavior in a BAP not reported to be luminescent, which suggested new opportunities for study. Based on this, we began a collaboration to study these properties, primarily involving the thiophenyl and bithiophenyl substituted BAPs. We also began to develop new chemistry of these materials, though this work will be presented in a future report.

Section 3.2: Results and Discussion

Section 3.2.1: Reaction of 2-(thiophen-2-yl)-1,3-benzazaphosphole with 1,3-bis(2,6-diisopropylphenyl)imidazole-2-ylidene

Our interest in studying the reactivity of 1,3-benzazaphospholes (BAPs) with isolable carbenes was prompted by two separate observations. As mentioned previously, we had begun quantifying the luminescence of a few BAPs as well as studying their chemistry. Coinciding with this study was the continuation of a mentorship program involving a high school level student playing an active role in our research project. In order to continue this student's work from a previous project in which they had synthesized *N*-heterocyclic carbenes, as well as integrate this student into our current efforts, we began to study the reaction of 2-(thiophen-2-yl)-1,3-benzazaphosphole (Th-BAP) with 1,3-bis(2,6-diisopropylphenyl)imidazol-2-ylidene (IPr) as shown in **Scheme 3.2**.

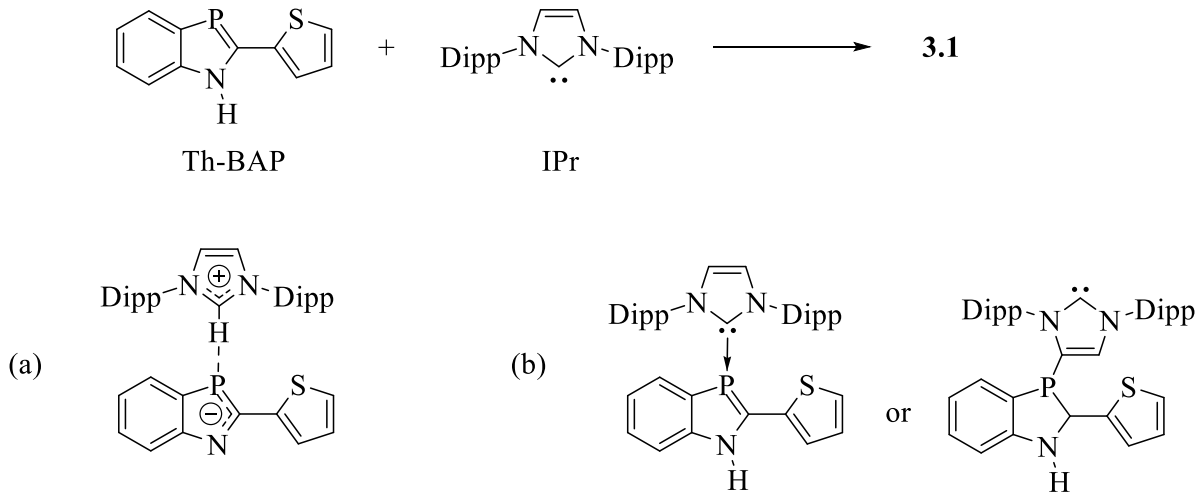

Scheme 3.2: Reaction of Th-BAP and IPr to give **3.1**. (lower) potential structures of **3.1**.

At the start, we realized that the multiple functional groups within Th-BAP offered multiple sites of potential reactivity, the two most likely being either the phosphaalkene or amine functionalities. Given IPr can act as a strong base, proton transfer between the BAP

and carbene seemed possible (**Scheme 3.2 (a)**), and this was shown to be the case in the similar reaction between IMes and Ph-BAP.[3] Also, we envisioned the possibility for a product similar to those obtained by Gates between NHCs and acyclic phosphaalkenes (**Scheme 3.2 (b)**).[4]

Scheme 3.3 reveals that the strong blue emission of Th-BAP was almost completely quenched upon addition of IPr. Furthermore, we observed that this phenomenon was concentration dependent (dilute solutions returned the observed emission) and chemically reversible (addition of BH_3·THF immediately returned the observed emission).

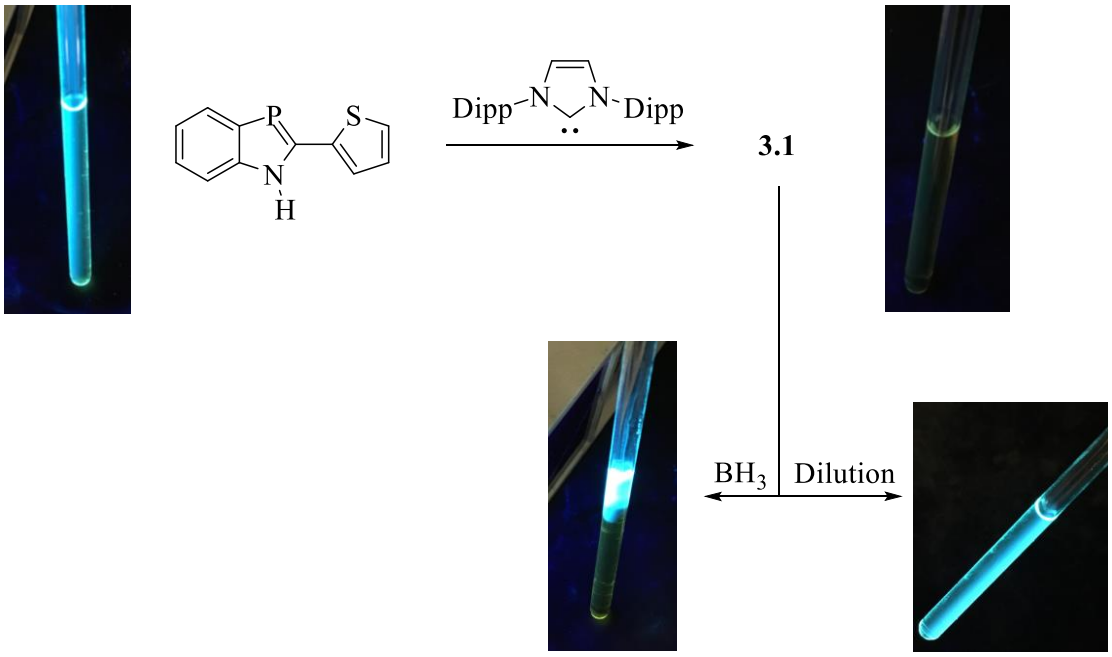

Scheme 3.3: Qualitative emission quenching of **3.1**, pictures obtained by co-author.

Identification of the structure for compound **3.1** was inconclusive, however. ^{31}P NMR analysis showed only a slight change in chemical shift between 69 ppm for a concentrated solution and 73 ppm when diluted, suggesting that the C=P bond within the BAP was relatively unchanged. Furthermore, when we attempted to obtain a UV-visible absorbance spectrum of **3.1**, we found that it was essentially the same as for Th-BAP due

to the reversibility at dilute concentrations. While X-ray crystallographic methods were needed to conclusively identify **3.1**, crystalline samples of **3.1** were plagued by significant disorder within the Th-BAP unit having multiple rotamers within the crystal unit.

Our difficulty in identifying the structure of **3.1** provided impetus toward examining similar systems in the hope of generalizing reactivity over a range of compounds. To this end, we began examining both different fluorophores and different carbenes. The study resulting from our work with other fluorophores is contained within **Chapter 4**, and has provided us a roadmap on how to analyze these systems. One of the methods we employed to study solution behavior at higher concentrations is diffusion ordered spectroscopy (DOSY). This analysis allows us to examine both the nature of an analyte in solution (are we observing the diffusion of separate parts or a single compound, for example) as well as provide an accurate determination of molecular weight. In the case of compound **3.1**, we found that the chemical shifts corresponding to either Th-BAP or IPr fragments diffused in solution at equal rates (as shown in **Figure 3.1**). Furthermore, the calculated mass for **3.1** using this method was within 1% of the expected value ($MW_{3.1}$ = 606, MW_{cal} = 614).

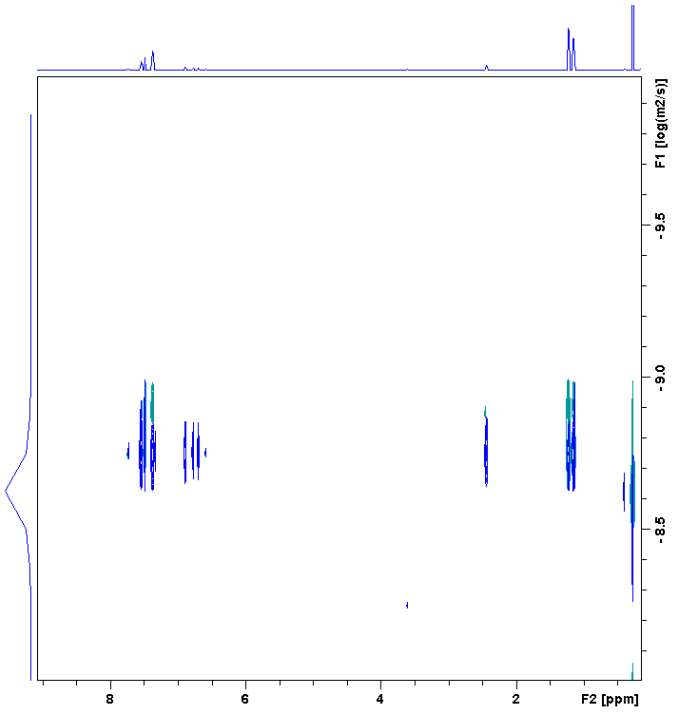

Figure 3.1: 2D ^{1}H DOSY-NMR spectrum of Th-BAP-IPr adduct (**3.1**) (THF-d_8, 298 K, 50 mM, tetrakis(trimethylsilyl)silane added as internal standard).

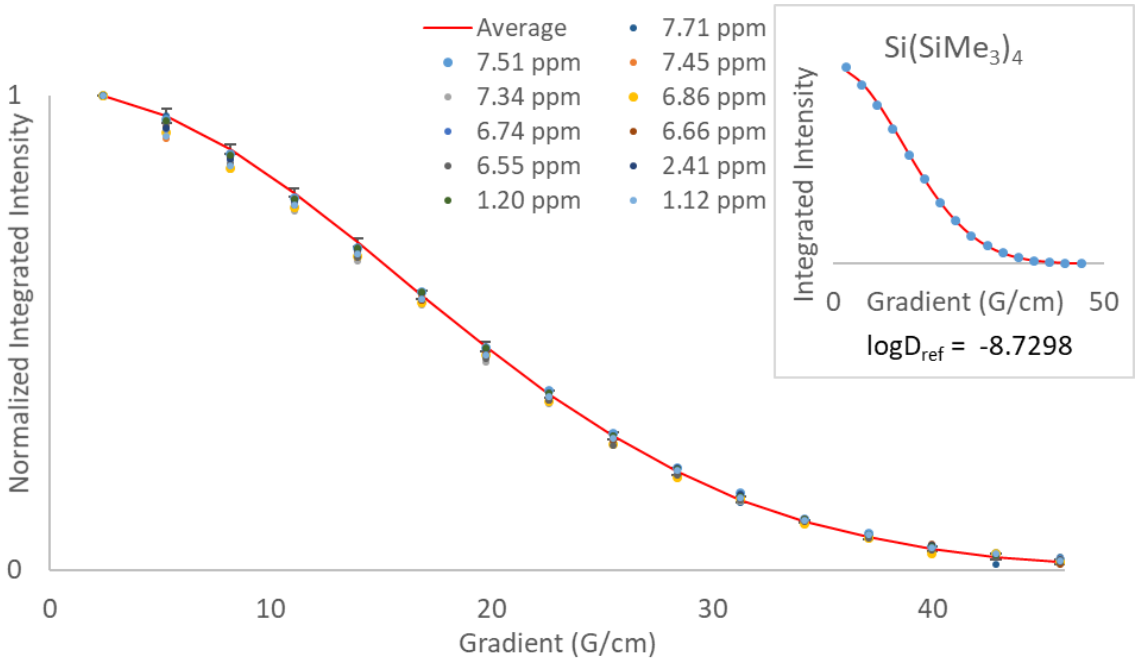

Figure 3.2: Calculated relaxation curve fits and molecular weights for **3.1** from ^{1}H DOSY NMR.

Our initial examination of **3.1** provided more questions than answers, however in driving us to study similar systems we were able to broaden these results to more widely available fluorophores as well as assemble the methods necessary for completing our examination of **3.1**.

Section 3.2.2: Reaction of 2-(thiophen-2-yl)-1,3-benzazaphosphole with ^{Et}CAAC, a Cyclic (alkyl)(amino)carbene

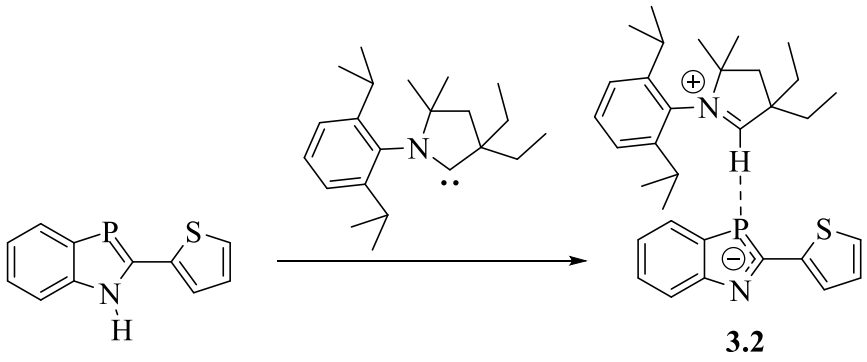

3.2

Scheme 3.4: Reaction of Th-BAP and ^{Et}CAAC to give **3.2**.

Given our observations of compound **3.1**, we were interested to study a similar reaction with Th-BAP, though with a different isolable carbene. Cyclic (alkyl)(amino)carbenes are a significantly more nucleophilic and electrophilic type of carbene when compared to the Arduengo type imidazole-2-ylidenes, and have been shown to activate E-H bonds such as ammonia.[5–7] However, unlike observing expected reactivity where the carbene inserts into the E-H bond, the reaction of ^{Et}CAAC with Th-BAP, shown in **Scheme 3.4**, produces NMR spectra inconsistent with an E-H insertion, primarily due to lack of the new C-H resonance around 5-6 ppm, as shown in **Figure 3.3**.

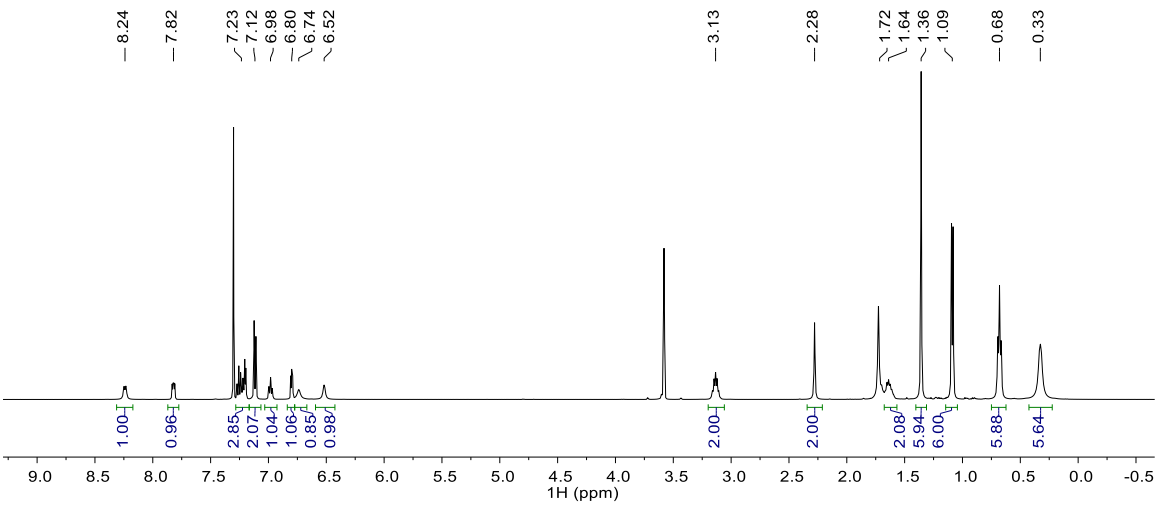

Figure 3.3: ^{1}H NMR (THF-d_8, 500 MHz) spectrum of **3.2**.

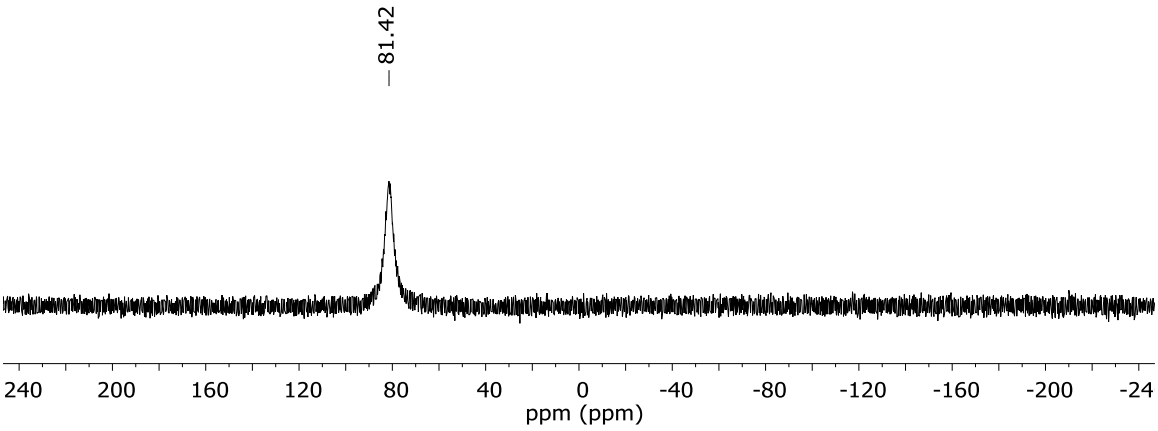

Figure 3.4: ^{31}P{^{1}H} NMR (THF-d_8, 202 MHz) spectrum of **3.2**.

Additionally, the ^{31}P NMR spectrum gives a single, extremely broad signal at 81.42 ppm (FWHM ≈ 900 Hz), as shown in **Figure 3.4**. As with **3.1**, compound **3.2** was easily recrystallized from benzene however the recovered crystals were too disordered for analysis by X-ray diffraction. We later were able to crystallize compound **3.4**, which confirms our suspicions that compound **3.2** is the product of ^{Et}CAAC acting as a base and the resulting salt was obtained.

Section 3.2.3: Comparison of Carbene Reactivity Towards 2-tert-butyl-1,3-benzazaphosphole

Rather than changing the nature of the fluorophore entirely away from a BAP moiety in order to study these reactions crystallographically, we also began looking into non-luminescent BAPs as a means to obtain crystallographic data on effectively the same reaction products. As shown in **Scheme 3.5**, we chose to examine the reactivity of 2-*tert*-butyl-1,3-benzazaphosphole (^{t}Bu-BAP) with both IPr and ^{Et}CAAC as analogs of **3.1** and **3.2**.

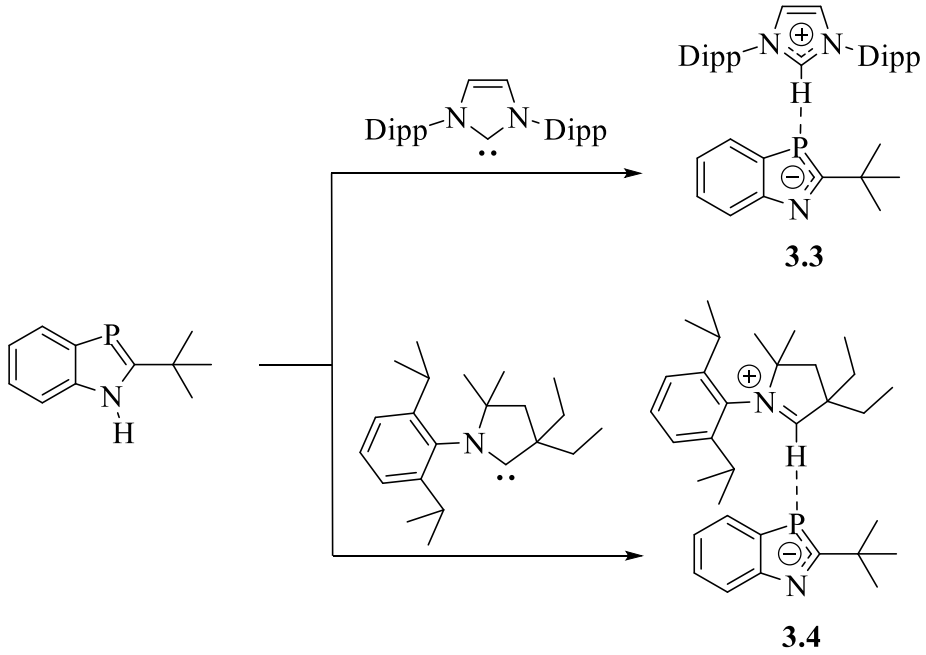

Scheme 3.5: Reaction between ^{t}Bu-BAP and either IPr or ^{Et}CAAC to give **3.3** and **3.4**.

^{t}Bu-BAP and IPr were first dissolved in THF, then recrystallized from a 1:6 THF/hexanes mixture. From this, we were able to obtain colorless rods that were suitable for X-ray diffraction. The structure was not disordered and provided our first look at a BAP-carbene adduct as shown in **Figure 3.5**.

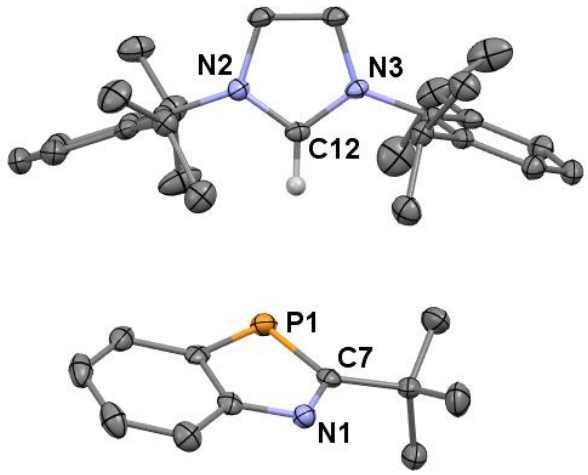

Figure 3.5: ORTEP diagram of **3.3** (ellipsoids set at 50% probability, non-hydrogen bonded hydrogen atoms omitted for clairity). Selected bond distances (Å) and angles (deg): C12-P1: 3.593(2); C12-N2: 1.331(3); C12-N3: 1.334(2); P1-C7: 1.770(2); C7-N1: 1.339(2); N2-C12-N3: 108.2(3); C12-P1-C7-N1: 110.8(1).

Based on the structure obtained for compound **3.3**, we could best describe it, and potentially **3.1**, as a hydrogen bonding salt obtained from the reaction in which IPr acted as a Brønsted base towards the N-H group of the benzazaphosphole, similar to product in **Scheme 3.2 (a)**. The proton transfer is confirmed by analyzing the structural parameters of the imidizolium fragment, particularly the N2-C12-N3 angle. In **3.3**, this angle was reported as 108.2(3)°, which is in line with other reported imidazolium hydrogen bonding complexes derived from NHCs.[3,8,9] Compound **3.3** was prepared concurrently with the work discussed in **Chapter 4**, and is structurally similar to compound **4.4**. The most striking differences between these two compounds are the differences in intermolecular distance (C···P = 3.593 Å in **3.3** and C···N = 3.083 Å in **4.4**) and the offset angle of the imidazolium from the plane of the fluorophore (N-C-P···C = 110.8° for **3.3** and N-C-N···C = 121.6° for **4.4**). The increase in intermolecular distance could be explained, at least in

part, by the change to a larger heteroatom. The shift from a co-planar arrangement between imidazolium and benzazaphospholide rings is even more pronounced in **3.3**. The structure of **3.3** could best be compared to the adduct of 2-phenylbenzazaphospholide and 1,3-bis(2,4,6-trimethylphenyl)imidazolium, however that structure exhibits a C···N interaction instead of the C···P interaction observed in **3.3**.[10] As such, the intermolecular distance is significantly shorter (3.144 Å). Finally, it should be noted that **3.3** exhibits a weakened C=P bond, given by the significant increase in C-P distance between ^{t}Bu-BAP and **3.3** (1.711 Å and 1.770 Å, respectively).[11]

Based on the success of crystallizing **3.3**, we attempted a similar reaction between ^{t}Bu-BAP and ^{Et}CAAC. Unlike **3.2**, ^{t}Bu-BAP and ^{Et}CAAC were mixed in THF and then diluted with hexanes to induce precipitation. This provided an interesting result as the THF solution turned from dark purple to colorless when diluted to a 1:1 ratio with hexanes. Furthermore, no precipitation was observed at 1:8 THF/hexanes so the solvent was removed which promptly returned the red color as the solution was concentrated. Additionally, when **3.4** was recrystallized from benzene, the solution once again provided a substantial color change, becoming a deep blue when heated then giving way to a dark purple after standing at room temperature. Given these observations, **3.4** may provide interesting solvatochromism in a future study. Recrystallization of **3.4** from benzene provided large red blocks which were sufficient quality for X-ray diffraction, shown in **Figure 3.6**.

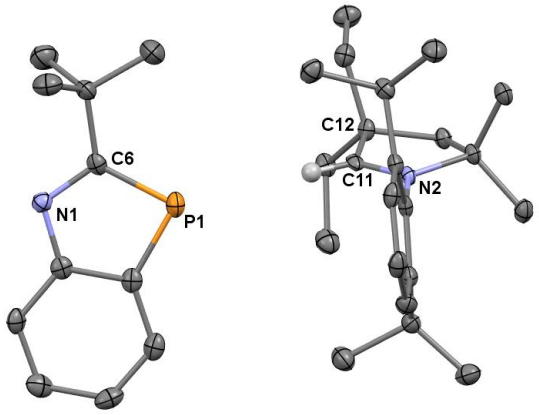

Figure 3.6: ORTEP diagram of **3.4** (ellipsoids set at 50% probability, non-hydrogen bonded hydrogen atoms omitted for clairity). Selected bond distances (Å) and angles (deg): C11-P1: 3.689(3); C6-P1: 1.761(2); C6-N1: 1.344(3); C11-N2: 1.278(3); N1-C6-P1-C11: 179.5(1); C6-P1-C11-N2: 121.7(3).

Similar to **3.3**, the structure we obtained for compound **3.4** contrasts with results obtained in **Chapter 4**. Specifically, **3.4** was the product of a reaction in which ^{Et}CAAC acted similarly to IPr and simply deprotonated the N-H group of the benzazaphosphole instead of undergoing N-H insertion. Other than incorporating a different carbene salt, the structures of **3.3** and **3.4** are comparable. Both display weakened C=P bonds and significantly longer intermolecular distances (C-P distance of 1.770 and 1.761 Å and P⋯C distance of 3.593 and 3.689 Å, respectively). The results obtained for **3.4** were instrumental in explaining the NMR spectra of **3.2**. Given that we have now observed two different reactions between ^{Et}CAAC and structurally similar NH-containing fluorophores, the second one discussed in **Chapter 4**, completing our study on compound **3.2** may provide some interesting and unexpected results.

Section 3.3: Conclusion and Future Directions

The results discussed in both **Chapter 3** and **Chapter 4** are intertwined as are the future steps we intend to make in continuing this study. Our immediate task is to use the methods and conclusions that we developed in completing our work in **Chapter 4** in order to finish our initial study of the reactions between Th-BAP and carbenes. This includes both collecting full NMR analyses, including DOSY and concentration dependence studies, as well as a similar set of absorbance and emission spectra as obtained for **4.1**-**4.4**.

Additionally, we originally began this series of experiments based on the discovery of the luminescence of BAPs and our interest to study them in conjunction with our work on BOPs. As evidenced in **Section 2.1**, the chemistry of BAPs and BOPs does not entirely overlap, therefore we intend to utilize the chemistry of luminescent BAPs to supplement our work on BOPs, particularly in accessing materials we have otherwise been unable to obtain (such as polymeric BOPs).

Finally, some of the early reactions with **3.1** involved introducing Lewis acids, such as boranes, to bind with free carbene in solution and return the luminescence of the parent fluorophore. This potential use in sensing was otherwise unexplored for the most part and should be examined to determine the breadth or selectivity that we can introduce, particularly if the carbene is customized to sense a specific analyte.

Section 3.4: Experimental

General Considerations: All manipulations were performed under an atmosphere of nitrogen using either an MBraun glove box or standard Schlenk line techniques. Unless otherwise stated, all chemicals were purchased from commercial sources and used without further purification. Samples of Th-BAP and ^{t}Bu-BAP were provided by Prof. Joachim

Heinicke. Tetrahydrofuran and hexanes were purified using an MBraun solvent purification system. Benzene was distilled over sodium benzophenone. THF-d_8 was distilled over sodium. IPr and ^{Et}CAAC were prepared following literature procedures and recrystallized from toluene or pentane, respectively.[12,13] NMR spectra were recorded on a Bruker AVANCE III 500 MHz spectrometer and chemical shifts referenced to residual solvent signal.

Reaction of Th-BAP and ^{Et}CAAC (3.2): A solution of ^{Et}CAAC (0.227 g, 0.724 mmol) in 2 mL benzene was added to a solution of Th-BAP (0.158 g, .0726 mmol) in 5 mL benzene giving an immediate color change from yellow to red. After sitting at RT for 2 days, an orange solid had precipitated from the reaction mixture. The entire contents of the reaction mixture were added to a pressure tube, heated to dissolve the orange solid, and then slowly cooled. After a few days, red rods had crystallized from this mixture along with a red oil. The oil continued to crystallize over several days sitting undisturbed. Crystals were then washed with benzene, hexanes, and dried under vacuum. ^{1}H NMR (THF-d_8, 500 MHz): δ 8.24 (d, *J* = 8.04 Hz, 1H), 7.83-7.81 (m, 1H), 7.27-7.20 (m, 3H), 7.12 (d, *J* = 7.69 Hz, 2H), 6.98 (t, *J* = 7.20 Hz, 1H), 7.81-7.79 (m, 1H), 6.74 (br s, 1H), 6.52 (br s, 1H), 3.13 (sep, *J* = 6.60 Hz, 2H), 2.28 (s, 2H), 1.78-1.68 (m, 2H), 1.68-1.58 (m, 2H), 1.36 (s, 6H), 1.09 (d, *J* = 6.67 Hz, 6H), 0.68 (t, *J* = 7.22 Hz, 6H), 0.33 (br s, 6H). ^{31}P{^{1}H} NMR (THF-d_8, 202 MHz): δ 81.42 (br).

Reaction of ^{t}Bu-BAP and IPr (3.3): ^{t}Bu-BAP (31 mg, 0.16 mmol) and IPr (62 mg, 0.16 mmol) were combined with 1 mL THF in a pressure tube. This solution was diluted with 6 mL hexanes, heated until clear, and then slowly cooled. Colorless rods obtained after one day which were suitable for X-ray diffraction.

Reaction of ^{t}Bu-BAP and ^{Et}CAAC (3.4): ^{t}Bu-BAP (41 mg, 0.22 mmol) and ^{Et}CAAC (66 mg, 0.21 mmol) were combined with 1 mL THF to give a dark purple solution. Addition of 1 mL hexanes to this solution lightened color significantly and addition of another 1 mL hexanes gave a colorless solution. After diluting the solution to 1:10 THF:hexanes, no precipitation observed and solution was evaporated to a burgundy solid under vacuum. Solid transferred to a pressure tube with 3 mL benzene, red/brown suspension heated until clear, and then cooled slowly. Red rods suitable for X-ray diffraction formed slowly over 4 days.

Section 3.5: References

(1) Wu, S.; Rheingold, A. L.; Golen, J. A.; Grimm, A. B.; Protasiewicz, J. D. Synthesis of a Luminescent Azaphosphole. *Eur. J. Inorg. Chem.* **2016**, *2016*, 768–773.

(2) Bansal, R. K.; Gupta, N.; Heinicke, J.; Nikonov, G. N.; Saguitova, F.; Sharma, D. C. 1H-1,3-Benzazaphospholes: The Organometallic Route and a New Three-Step Synthesis with Reductive Ring Closure. *Synthesis* **1999**, No. 2, 264–269.

(3) Pi, C.; Yu, X.; Zheng, W. Imidazolium 1,3-Benzazaphospholide Ion Pairs with Strong C-H···N Hydrogen Bonds - Synthesis, Structures, and Reactivity. *Eur. J. Inorg. Chem.* **2015**, *2015*, 1804–1810.

(4) Majhi, P. K.; Chow, K. C. F.; Hsieh, T. H. H.; Bowes, E. G.; Schnakenburg, G.; Kennepohl, P.; Streubel, R.; Gates, D. P. Even the Normal Is Abnormal: N-Heterocyclic Carbene C 2 Binding to a Phosphaalkene without Breaking the P=C π-Bond. *Chem. Commun.* **2016**, *52*, 998–1001.

(5) Frey, G. D.; Lavallo, V.; Donnadieu, B.; Schoeller, W. W.; Bertrand, G. Facile Splitting of Hydrogen at a Single Carbon Center. *Science* **2007**, *316*, 439–441.

(6) Melaimi, M.; Jazzar, R.; Soleilhavoup, M.; Bertrand, G. Cyclic (Alkyl)(Amino)Carbenes (CAACs): Recent Developments. *Angew. Chem. Int. Ed.* **2017**, *56*, 10046–10068.

(7) Paul, U. S. D.; Radius, U. Ligand versus Complex: C−F and C−H Bond Activation of Polyfluoroaromatics at a Cyclic (Alkyl)(Amino)Carbene. *Chem. - Eur. J.* **2017**, *23*, 3993–4009.

(8) Arduengo, Anthony J., I.; Gamper, S. F.; Tamm, M.; Calabrese, J. C.; Davidson, F.; Craig, H. A. A Bis(Carbene)—Proton Complex: Structure of a C—H—C Hydrogen Bond. *J. Am. Chem. Soc.* **1995**, *117*, 572–573.

(9) Cowan, J. A.; Clyburne, J. A. C.; Davidson, M. G.; Harris, R. L. W.; Howard, J. A. K.; Küpper, P.; Leech, M. A.; Richards, S. P. On the Interaction between N-Heterocyclic Carbenes and Organic Acids: Structural Authentication of the First N-H ... C Hydrogen Bond and Remarkably Short C-H ... O Interactions. *Angew. Chem. Int. Ed.* **2002**, *41*, 1432–1434.

(10) Quan, Z.-J.; Wang, X.-C. The 2-Phosphaethynolate Anion: Convenient Synthesis and the Reactivity. *Org. Chem. Front.* **2014**, *1*, 1128–1131.

(11) Surana, A.; Singh, S.; Bansal, R. K.; Peulecke, N.; Spannenberg, A.; Heinicke, J. Metalated 1,3-Azaphospholes: Synthesis of Lithium-1,3-Benzazaphospholides and Reactivity towards Organoelement and Organometal Halides. *J. Organometalic Chem.* **2002**, *646*, 113–124.

(12) Arduengo, A. J.; Krafczyk, R.; Schmutzler, R.; Craig, H. A.; Goerlich, J. R.; Marshall, W. J.; Unverzagt, M. Imidazolylidenes, Imidazolinylidenes and Imidazolidines. *Tetrahedron* **1999**, *55*, 14523–14534.

(13) Mahoney, J. K.; Martin, D.; Moore, C. E.; Rheingold, A. L.; Bertrand, G. Bottleable (Amino)(Carboxy) Radicals Derived from Cyclic (Alkyl)(Amino) Carbenes. *J. Am. Chem. Soc.* **2013**, *135*, 18766–18769.

Chapter 4: Three Ways Isolable Carbenes Can Modulate Emission of NH-Containing Fluorophores

Section 4.1: Introduction

Please note, a majority of the results discussed in **Chapter 4** represent this author's contributions to a previously published work.[1]

Based on the initial results in **Chapter 3**, we began to study the reactivity and photophysical impact of carbenes on simple NH-containing fluorophores. These reactions were developed as models for Th-BAP where phosphorus would be replaced by nitrogen (similar to 2-phenylbenzimidazole (Ph-BIM)) or if the second heteroatom was removed altogether (similar to carbazole). These fluorophores presented a slightly different steric profile around the N-H group, with carbazole being less bulky due to its biphenyl moiety being unable to approach the N-H group. Furthermore, the N-H for carbazole and Ph-BIM presented a slightly different acidity, p*K*a = 11.9 and 19.9, respectively.[2,3]

Reactions involving N-H bonds and isolable carbenes, in the case of this work IPr or ^{Et}CAAC, have been reported by multiple researchers. In the case of IPr and similar imidazolium based carbenes, a hydrogen bonding complex either through a proton-transfer or between the neutral molecules is known. Arduengo studied the hydrogen bonding complex between carbenes and their conjugate acids and provided evidence that certain structural properties, namely the N-C-N angle (107.6 and 106.6° for imidazolium units and 102.8 and 101.2° for imidazolylidene units) within the imidazolium heterocycle are particularly diagnostic toward determining the nature of the carbene within these complexes as either the free carbene or imidazolium salt.[4] As well, Clyburne and Davidson studied the reaction between diphenylamine and 1,3-bis(2,4,6-trimethylphenyl)imidazole-

2-ylidene (IMes) which is structurally similar to what we proposed to study.[5] In this adduct, IMes is bound to diphenylamine through C···H-N hydrogen bonding with the carbene still in its neutral form given a small N-C-N angle (101.7°) and similar ^{13}C NMR chemical shift to the unreacted carbene (219.7 ppm). Neither of these earlier studies, however, incorporate luminescent materials into the reactions. Other N-H and O-H containing molecules have also been shown to react with carbenes to form similar hydrogen bonding complexes.[6–14] It is also important to note that such hydrogen bonding to carbazole, though not with carbenes, has been shown to reduce its observed emission.[15–19] This effect could be the result of an energy transfer or excited state proton transfer (ESPT) process.[20,21] Also of importance for Ph-BIM luminescence is that the freely rotating phenyl group be co-planar to the imidazole ring.[22]

Cyclic (alkyl)(amino)carbenes have also been studied for their reactivity towards E-H bonds. These more reactive carbenes have the added benefit of activating particularly unreactive molecules such as H_2 or ammonia.[23] A common mode of reactivity between these substrates and CAACs is insertion into the E-H bond.[24] Of particular interest to this study is the reaction of CAACs with imidazole and benzimidazole, inserting into the N-H bond of each.[25] One downside of CAACs being able to activate less reactive bonds is that the resulting compounds tend to be very stable and non-labile. This, of course, is in contrast to the weak interactions of the hydrogen bonding complexes associated with IPr for instance. However, this report shows that the N-H insertion reaction can be reversible and the publication of this work coincided with a similar report by Bertrand.[26]

Section 4.2: Results and Discussion

As discussed in **Section 3.2**, we had discovered that addition of IPr to a luminescent solution of 2-(thiophen-2-yl)-1,3-benzazaphosphole (Th-BAP) resulted in a substantial decrease in emission intensity. In parallel to our work modifying the parent benzazaphosphole in order to characterize the product crystallographically, as discussed in **Section 3.2.3**, we sought to explore which of the functional groups contained within the benzazaphosphole moiety might be responsible for the observed emission quenching. To this end, we tested similar reactions with carbazole and 2-phenylbenzimidazole (Ph-BIM) which represent simple fluorophores wherein functional groups of the benzazaphosphole had either been altered or removed.

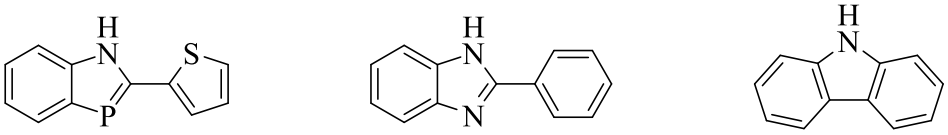

Th-BAP Ph-BIM carbazole

Figure 4.1: Representative fluorophores used in this study

Section 4.2.1: Reaction of Carbazole with IPr, an Imidazole-2-ylidene

The first reaction studied was between carbazole and IPr. It was immediately observed that a 1:1 mixture of these compounds in either benzene or THF resulted in a substantial drop in emission intensity. After further tests, we found that compound **4.1,** as shown in **Scheme 4.1**, could be isolated from a benzene solution as an analytically pure white solid in nearly quantitative yield upon removal of volatiles. The reaction was equally successful in THF, however trace amounts of solvent remained even after storage for days under vacuum. Remarkably, the solid was found to be stable when stored open to air.

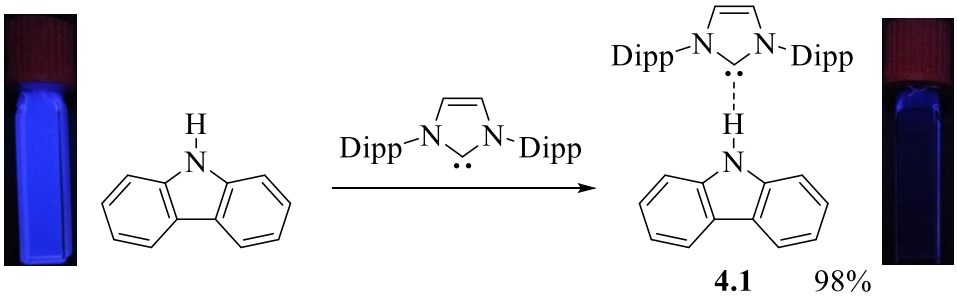

Scheme 4.1: Synthesis of carbazole-IPr adduct (**4.1**). Cuvettes of carbazole (left) and **4.1** (right) under 365 nm irradiation at 50 mM in THF.

Compound **4.1** was structurally characterized after recrystallization from acetonitrile, though later NMR studies provided evidence for significant H/D exchange with MeCN-d_3 and further analyses avoided this solvent when possible. The reactivity between IPr and certain deuterated solvents has been previously reported.[27] The results provided from single crystal X-ray diffraction revealed **4.1** to be an unusual hydrogen bonded carbene complex with a short C···N intermolecular distance of 2.972(3) Å and a C···H-N distance of 2.07(3) Å as shown in **Figure 4.2**.

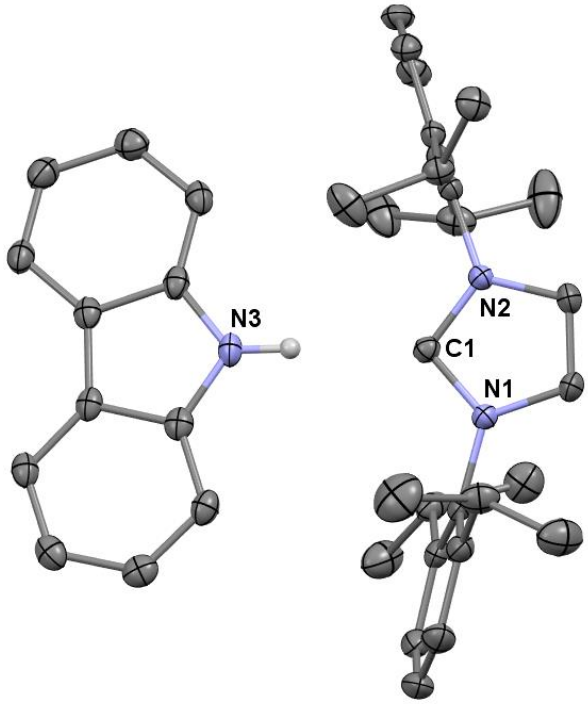

Figure 4.2: ORTEP diagram of **4.1**, obtained by co-author (ellipsoids set at 50% probability; non-hydrogen bonded hydrogen atoms omitted for clarity). Selected bond distances (Å) and angles (deg): C1-N3: 2.972(3); C1-N1: 1.363(2); C1-N2: 1.361(2); N1-C1-N2: 102.21(15).

As discussed in **Section 4.1**, this does not represent an unknown bonding motif for NHCs, however there are few examples reported and none that incorporate additional photophysical observations. Furthermore, the crystal structure provides evidence that the carbene fragment in compound **4.1** remains deprotonated due to the small N-C-N angle of 102.21(2)°. This angle is a key indicator between imidazolium and imidazolylidene structures as shown in similar hydrogen bonded carbene complexes by Arduengo. These earlier structures described the complexes obtained from a mixture of 1,3-bis(trimethylphenyl)imidazole-2-ylidene, IMes, and its conjugate acid containing either hexafluorophosphate or triflate counterion, providing a pair of free-carbene N-C-N angles

(102.8(4) and 101.2(5)°) and imidazolium N-C-N angles (107.6(4) and 106.6(6)°).[4] Additionally, a similar adduct between IMes and diphenylamine has been studied by Clyburn and Davidson which has similar structural properties to compound **4.1**, displaying an intermolecular C···N distance of 3.196(2)Å and an N-C-N angle of 101.7(1)° for the IMes fragment.[5] As well, this IMes-diphenylamine adduct was reported to retain its distinctive ^{13}C NMR resonance at 219.7 ppm in THF-d_8 which was similarly observed for compound **4.1** as a weak, broadened signal at 215.0 ppm in THF-d_8.

While discovery of a rarely reported hydrogen-bonded carbene complex was important in advancing our knowledge in this field, it was the qualitative emission quenching that we observed which drew our attention to this reaction. Accordingly, compound **4.1** was subjected to a series of photophysical analyses in order to quantitatively probe the extent of luminescence quenching. However, our initial UV-visible absorption and fluorescence emission spectra were essentially a sum of the individual IPr and carbazole components as shown in **Figure 4.3**.

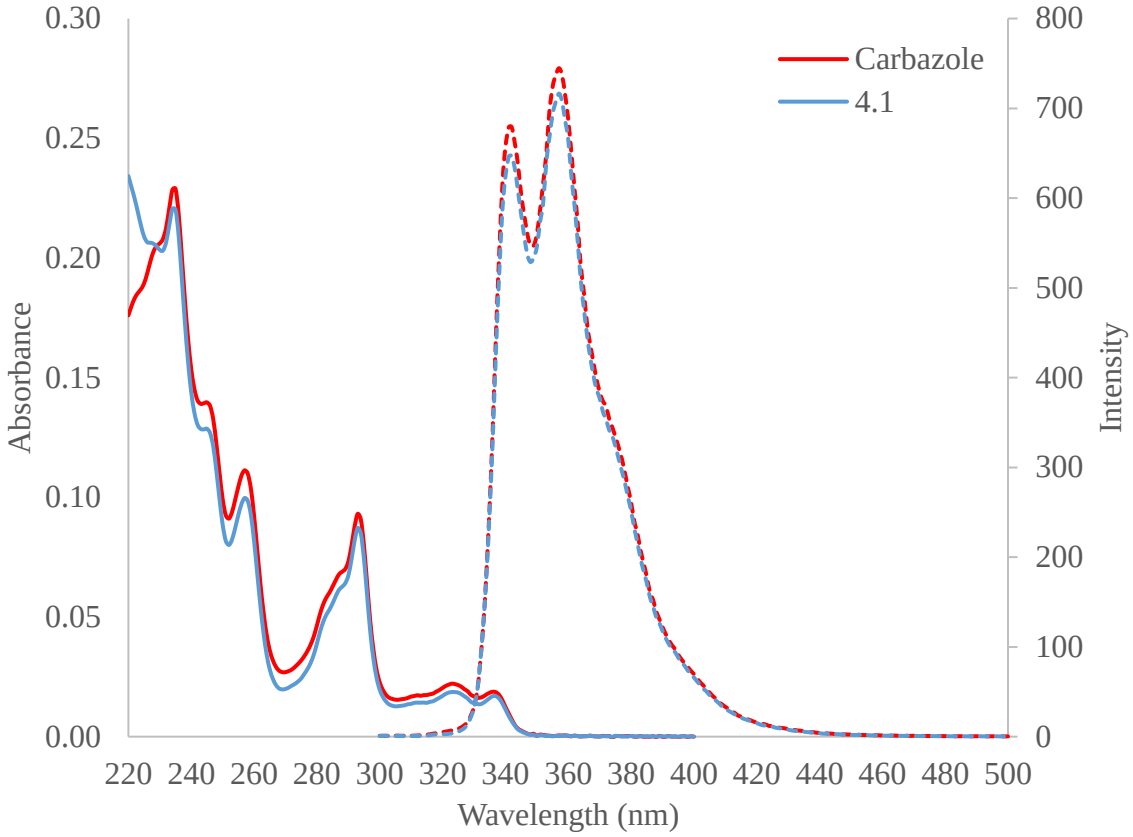

Figure 4.3: Photophysical characterization of **4.1** and carbazole (absorption spectra = solid lines, emission spectra = dashed lines). Conditions: λ_{ex} = 290 nm, THF, RT, [carbazole] and [**4.1**] = 5 μM

We later determined that this was a result of compound **4.1** dissociating into its free constituent pieces at relatively high concentrations, and attempting to study this complex at the required μM concentrations would not be possible. We attempted to shift the equilibrium towards compound **4.1** through addition of excess free carbene, up to a 100-fold excess, however the emission spectra remained unchanged as shown in **Figure 4.4**. Furthermore, the dissociation observed with compound **4.1** did not depend on solvent (THF, benzene or MeCN) or show significant variance across a range of concentrations 50-5 μM in THF, as spectra provided in **Appendix B** show.

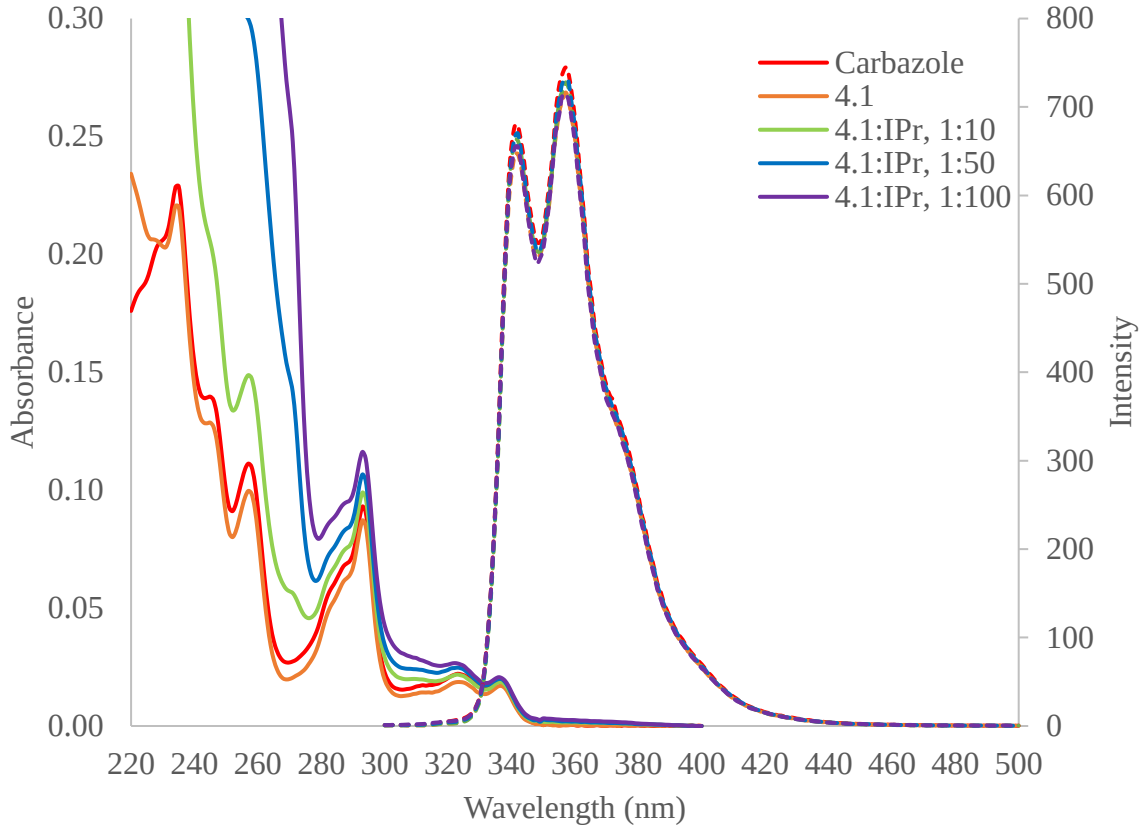

Figure 4.4: Photophysical characterization of **4.1** with excess free carbene (absorption spectra = solid lines, emission spectra = dashed lines). Conditions: λ_{ex} = 290 nm, THF, RT, [carbazole] and [**4.1**] = 5 μM

Provided with an inconsistent description of compound **4.1** between the solid and solution phases, we searched for an additional solution-phase analyses wherein we might obtain evidence for the intact complex in solution. The higher concentrations employed by NMR spectroscopy became our primary focus. We had previously performed a complete set of NMR experiments in order to fully assign both ^{1}H and ^{13}C chemical shifts, as provided in **Figure 4.5**, and noticed a significant downfield shift of the N-H proton which could be attributed to hydrogen-bonding.

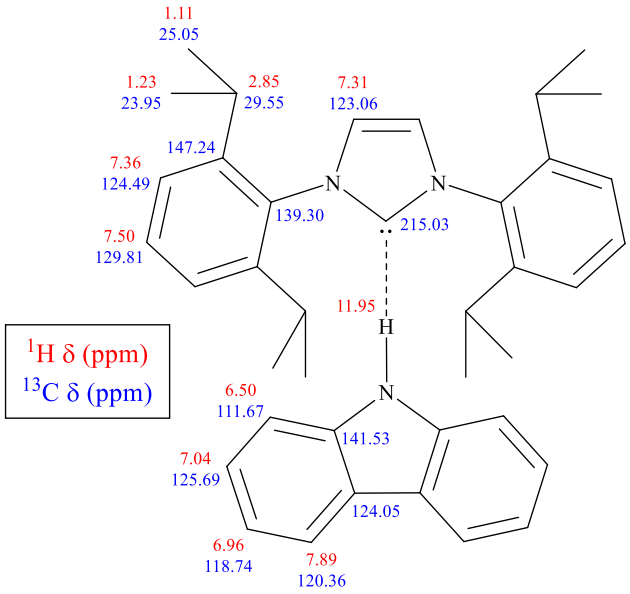

Figure 4.5: ^{1}H and ^{13}C NMR assignments for carbazole-IPr adduct (**4.1**).

We subsequently analyzed a series of solutions across a range of concentrations from 50-0.5 mM in benzene-d_6 hoping to observe a concentration dependence on the N-H chemical shift. This effect was immediately observed with a $\Delta\delta$ = +4.30 ppm between 1 and 50 mM, moreover we were able to track changes in almost all of the other signals as provided in **Figure 4.6**. This concentration dependence is well studied for a rapid equilibrium on the NMR timescale, and was fit to a non-linear least-squares analysis of a monomer-dimer equilibrium model in order to obtain association constants.[28,29] The association constants provided by analyzing the changes in each chemical shift, as shown in **Figure 4.7**, were calculated, average K_d = 105 ± 3 M^{-1}, and could be correlated to a $\Delta G \approx$ -2.8 kcal mol^{-1}. A similar hydrogen bond strength of -2.9 kcal mol^{-1} has been previously reported for the O···H-N hydrogen bonded complex of benzophenone and carbazole, which also displayed emission quenching at 77K and partial quenching at room temperature.[30]

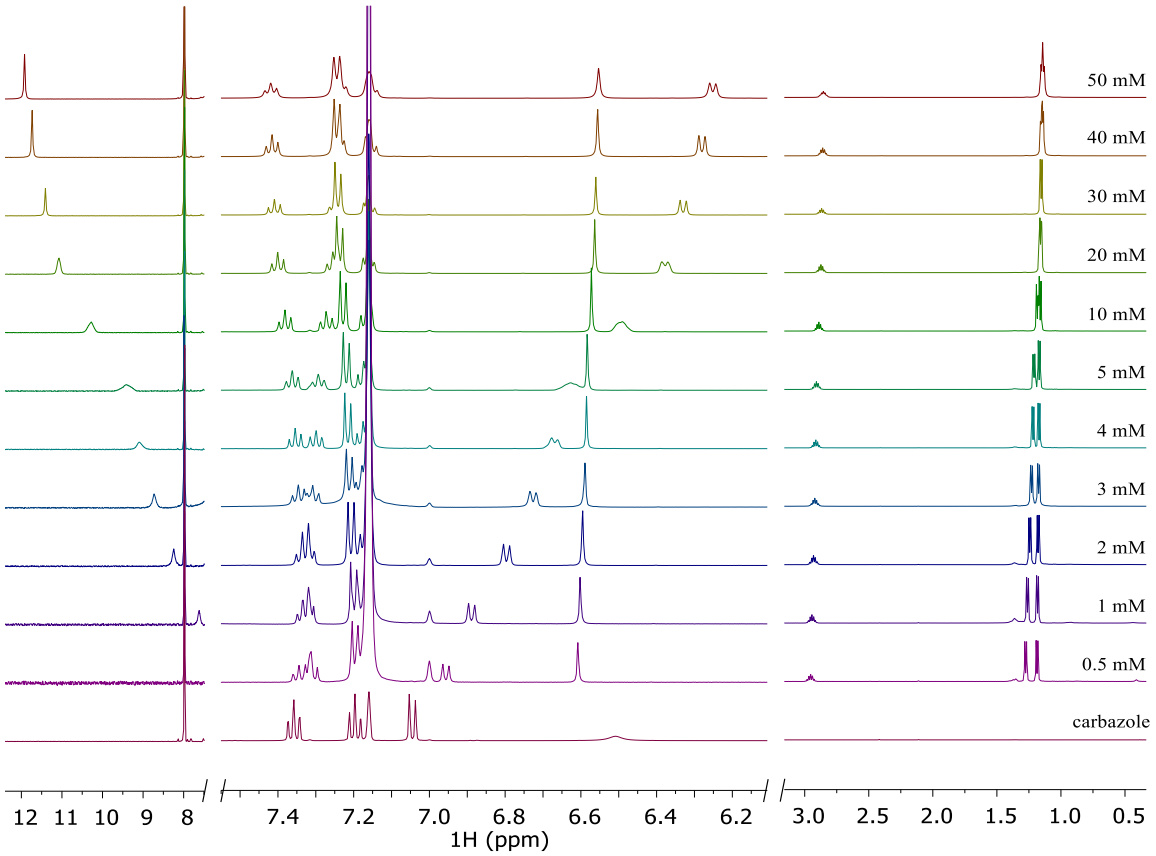

Figure 4.6: Concentration effect on the equilibrium of **4.1** as determined by ^{1}H NMR over a range of concentrations 50-0.5 mM (500 MHz, C_6D_6, 298K). Spectrum of carbazole provided for reference and vertical magnification adjusted to account for weaker signals.

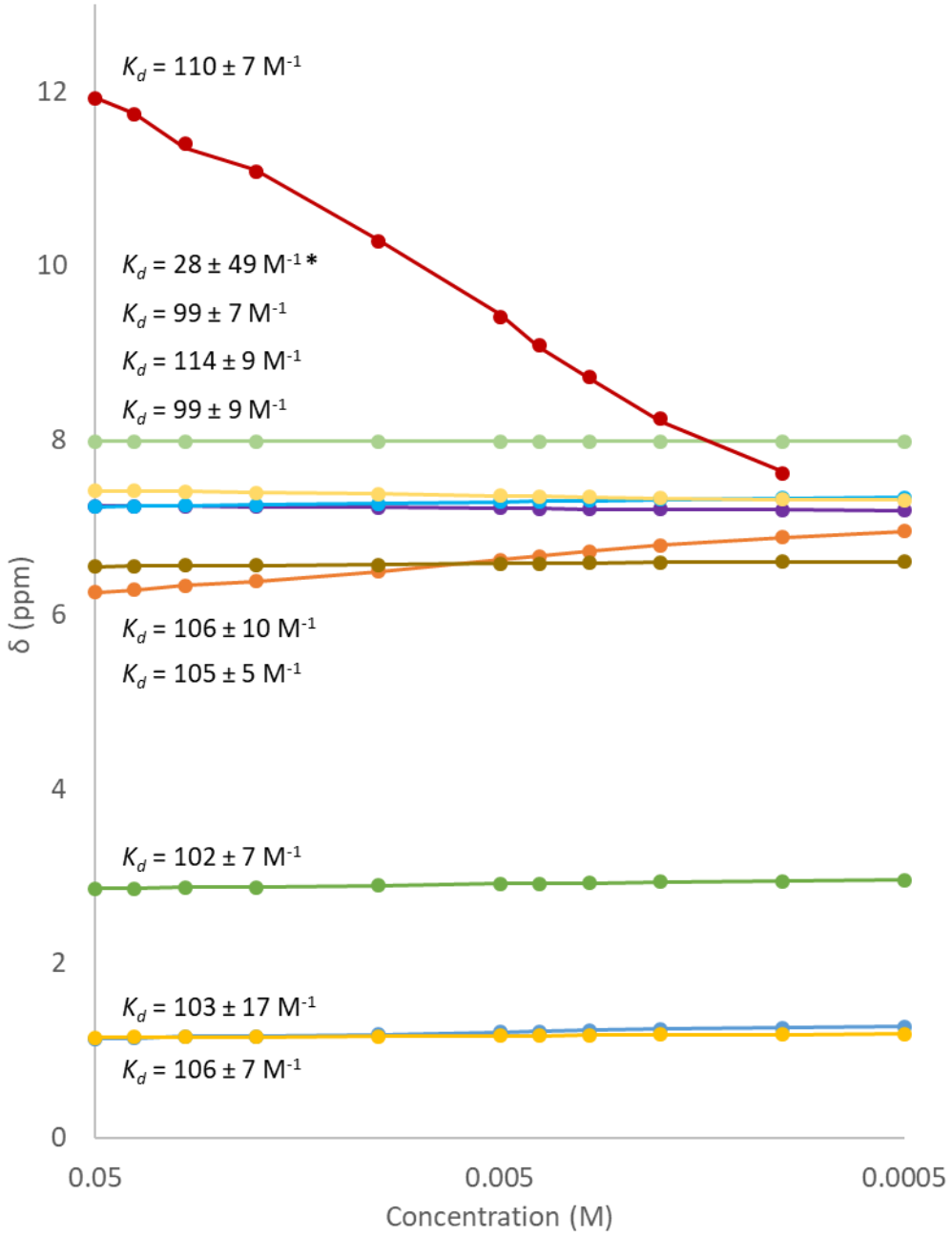

Figure 4.7: Plot of ^{1}H resonance over concentration range of **4.1** in C_6D_6. Association constants fit using a non-linear least-squares analysis.[28] Marked value (*) excluded due to minimal change in chemical shift ($\Delta\delta < 0.05$ ppm).

With quantitative data showing the relatively weak hydrogen bonding interaction between IPr and carbazole, we continued to study the solution-phase behavior of this

complex by NMR techniques. One experiment that is not widely utilized, but offers unique and important information for the type of interaction we were examining is known as diffusion ordered spectroscopy (DOSY). This pseudo-2D NMR experiment requires a set of spectra, typically ^{1}H though not exclusively, to be obtained through a spin echo pulse sequence. However, unique to this experiment is the application of a gradient pulse along the Z-axis of the sample, effectively encoding the Z-coordinate for each molecule. After some diffusion time, a second gradient pulse is applied to decode the current positions and any attenuation of the echo signal can be attributed to diffusion of the analyte within the sample over the diffusion time. Based on the following equation, a diffusion coefficient can be determined based on variable gradient strength.[31,32]

$$I = I_0 e^{-D\gamma^2 g^2 \delta^2 (\Delta - \delta/3)}$$

Equation 4.1: Intensity change by DOSY NMR. I = observed intensity, I_0 = reference intensity, D = diffusion coefficient, γ = gyromagnetic ratio, g = gradient strength, δ = length of gradient, Δ = diffusion time.

Additionally, the diffusion coefficient can be used to calculate accurate molecular weights, ± 9%, through the use of external calibration curves, assuming a known standard is present within the sample.[33] Performing this analysis on compound **4.1** at 75 mM in THF-d_8, which is near the upper limit for this technique, revealed that the chemical shifts attributed to either carbazole or IPr fragments were diffusing in solution at slightly different rates and not as a single species as shown in **Figure 4.8** and **Figure 4.9**. However, the calculated molecular weights were also significantly larger than those of the free compounds, $MW_{Carbazole}$ = 167 vs. MW_{cal} = 307 and MW_{IPr} = 389 vs. MW_{cal} = 500, providing additional evidence for the rapid equilibrium of **4.1** and its constituent parts.

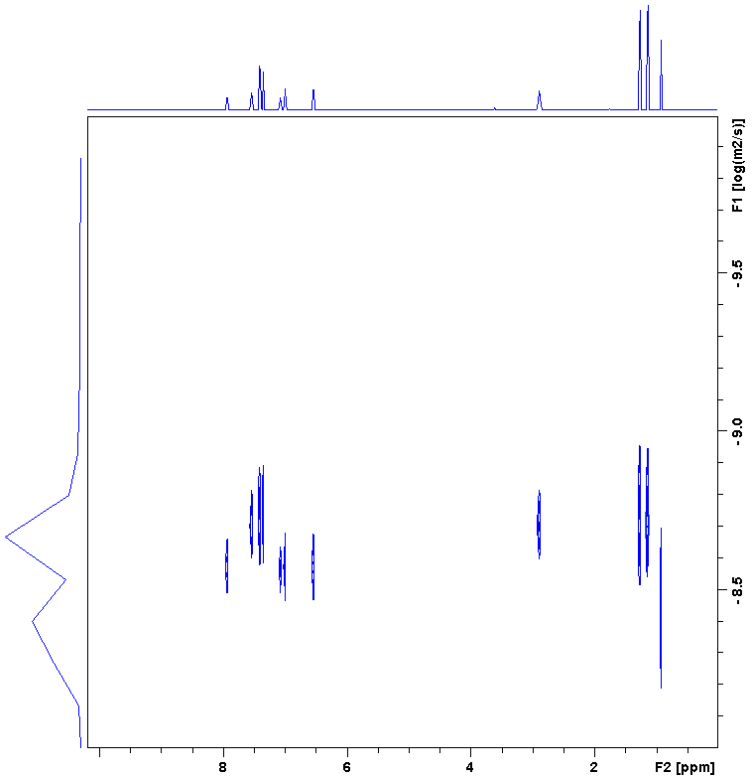

Figure 4.8: 2D ^{1}H DOSY-NMR spectrum of carbazole-IPr adduct (**4.1**) (THF-d_8, 298 K, 75 mM, tetramethylbutane added as internal standard).

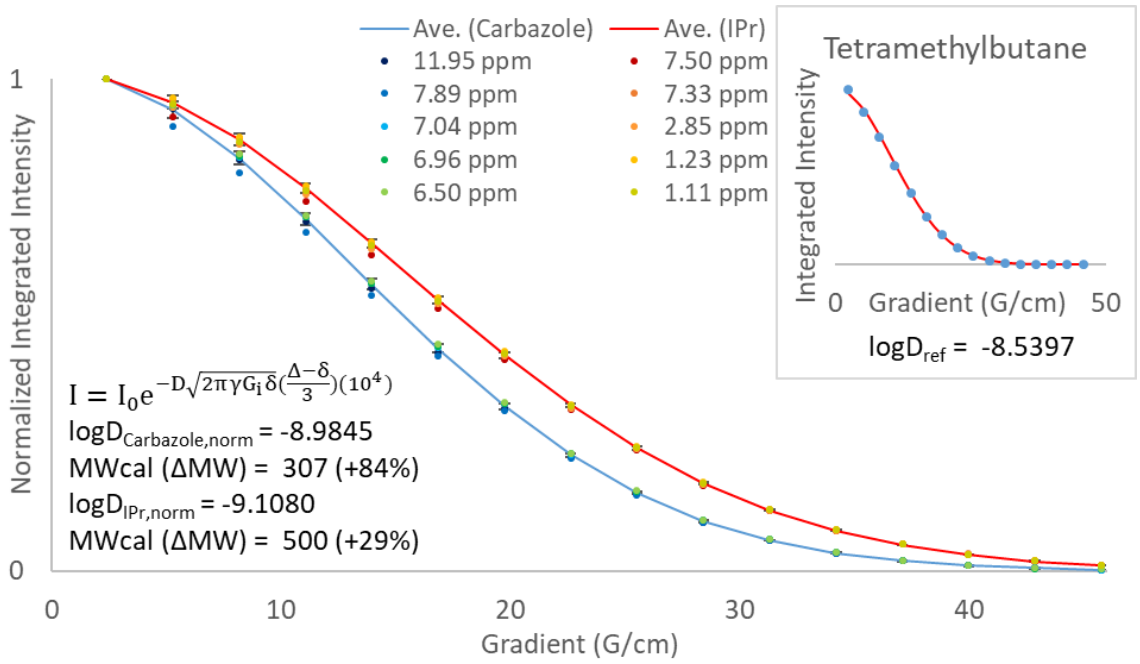

Figure 4.9: Calculated relaxation curve fits and molecular weights for **4.1** from ^{1}H DOSY NMR. Separate diffusion rates are observed for the chemical shifts assigned to carbazole and IPr fragments in **4.1**, each significantly different from the individual components, indicating that **4.1** is in rapid equilibrium in solution, even at elevated concentration.

Section 4.2.2: Reaction of Carbazole with ^{Et}CAAC, a Cyclic (alkyl)(amino) carbene

Given our results studying the reaction of carbazole and IPr, we proceeded to investigate the effect that a change in carbene could provide, specifically a cyclic (alkyl)(amino)carbene due to their enhanced reactivity as discussed in **Section 4.1**. Qualitatively, addition of ^{Et}CAAC to a solution of carbazole in THF did not produce a visible effect on the emission intensity as shown in **Scheme 4.2**. After removal of volatiles under vacuum and washing the resulting white solid with pentane, we were able to isolate an analytically pure solid in 86% yield.

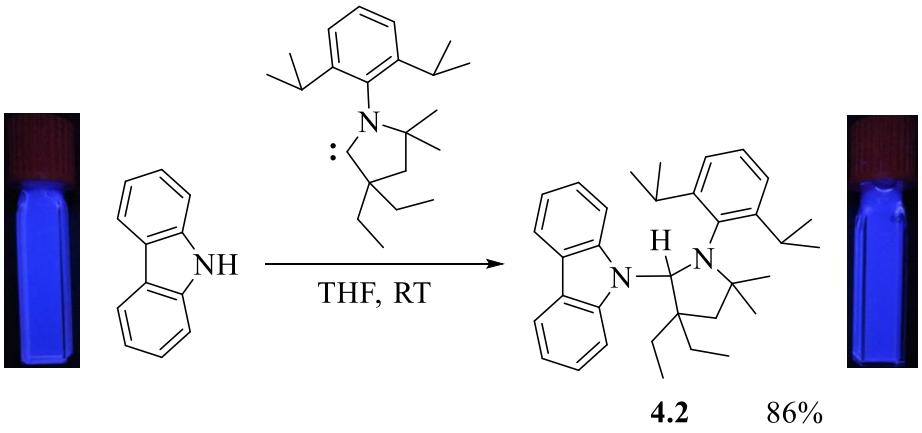

Scheme 4.2: Insertion of ^{Et}CAAC into the N-H bond of carbazole to produce **4.2**.

Cuvettes of carbazole (left) and **4.2** (right) under 365 nm irradiation at 50 mM in THF.

Recrystallization from 8:1 hexanes:toluene provided single crystals suitable for X-ray diffraction, resulting structure provided in **Figure 4.10**, which confirmed the expected N-H insertion shown in **Scheme 4.2**. As expected, considering the formal C-N σ-bond formation, we discovered that compound **4.2** was also stable as a solid when stored open to air. NMR spectra provided strong evidence for intact complex in solution, due to both appearance of the new C-H as a sharp singlet at 6.40 ppm and a large amount of NOE signals between carbazole and both the diisopropylphenyl and ethyl groups on the carbene fragment. Furthermore, one of the isopropyl groups was locked spatially above the carbazole ring, resulting in a large upfield shift of the ^{1}H NMR signal to -0.75 ppm. The remainder of the NMR assignments revealed **4.2** to be a very rigid structure, displaying a complex set of inequivalent signals, as shown in **Figure 4.11**, which were then fully assigned, as provided in **Figure 4.12**, after multidimensional NMR experiments.

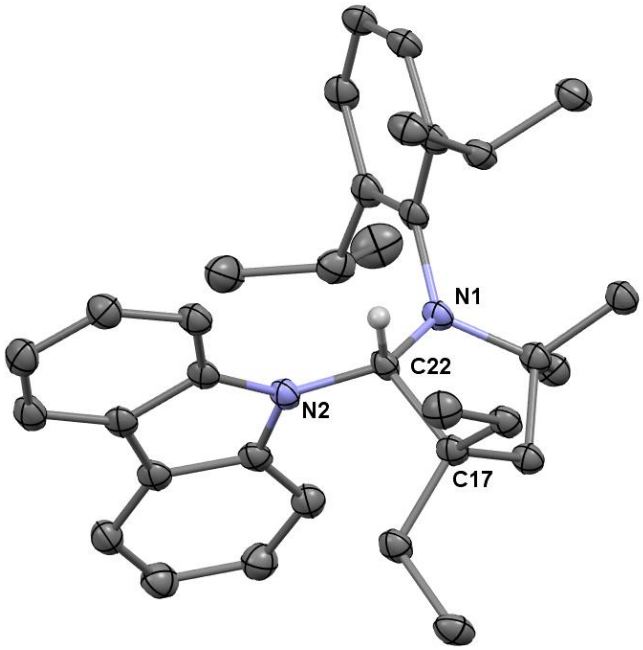

Figure 4.10: ORTEP diagram of **4.2**, obtained by co-author (ellipsoids set at 50% probability; hydrogen atoms omitted for clarity). Selected bond distances (Å) and angles (deg):C22-N1: 1.452(2); C22-N2: 1.485(2); C22-C17: 1.568(2); C17-C22-N1: 106.3(1); N1-C22-N2: 112.9(1); N2-C22-C17: 115.3(1).

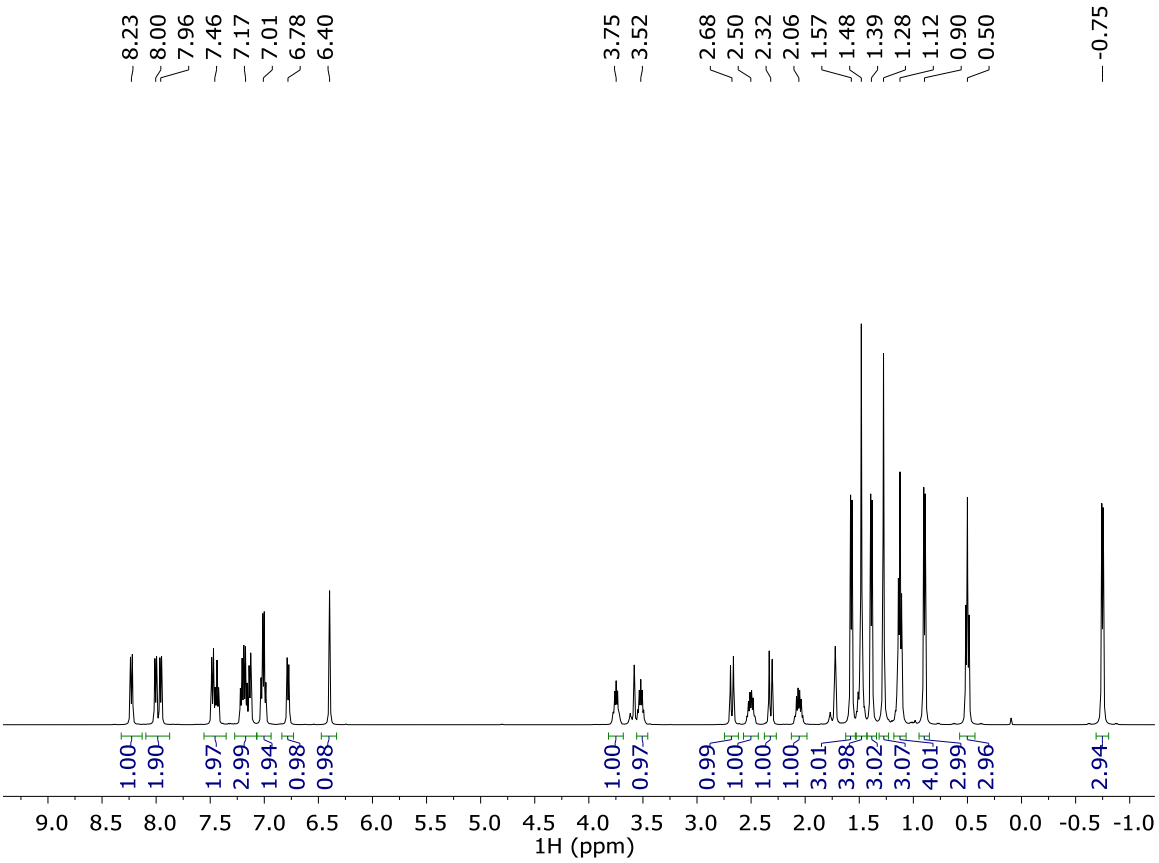

Figure 4.11: ^{1}H NMR (500 MHz, THF-d_8) spectrum of compound **4.2**.

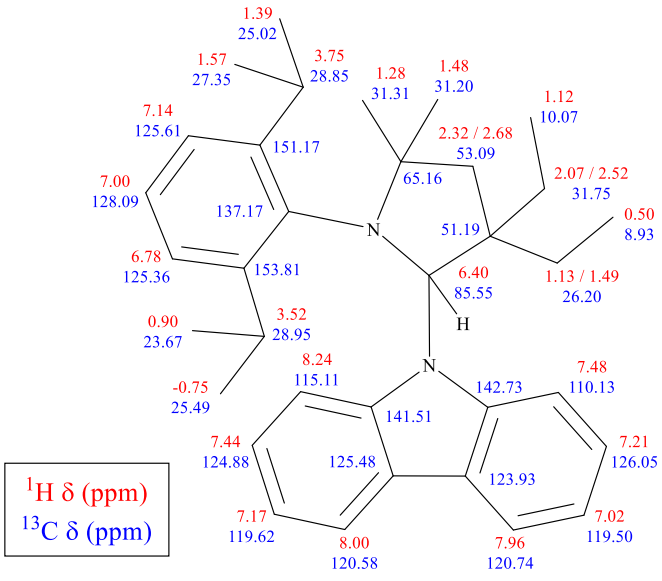

Figure 4.12: ^{1}H and ^{13}C NMR assignments for compound **4.2**.

The photophysical properties of **4.2** were analyzed in the same manner as for

compound **4.1**. Compound **4.2** displayed a slight change in the emission spectrum as well as a decrease in emission intensity as shown in **Figure 4.13**. These effects, though, are common for *N*-alkyl substituted carbazole,[34,35] and further tests showed that the properties of **4.2** were not solvent dependent or effected by additional free carbene. The lack of significant emission quenching or a noticeable reversibility into the free components was not surprising given the type of reaction observed and this was further confirmed by observing all chemical shifts attributed to compound **4.2** diffusing at a single rate by DOSY NMR.

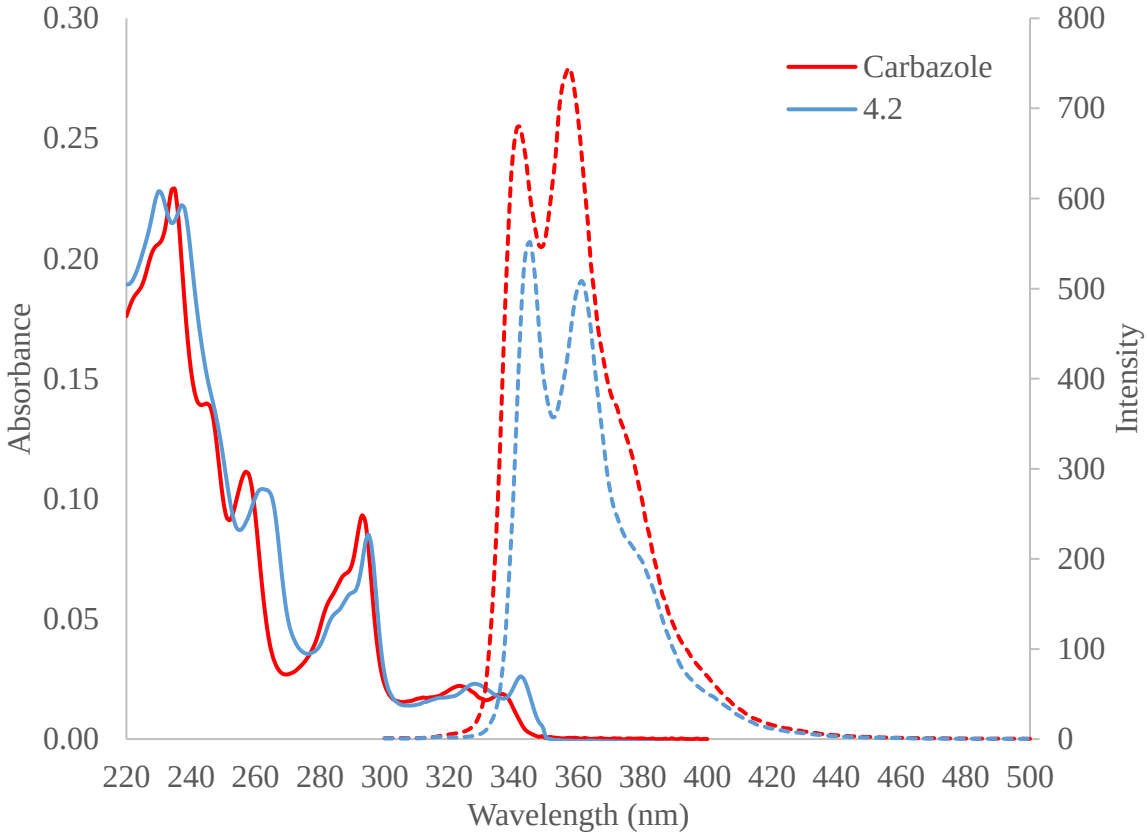

Figure 4.13: Photophysical characterization of **4.2** and carbazole (absorption spectra = solid lines, emission spectra = dashed lines). Conditions: λ_{ex} = 290 nm, THF, RT, [carbazole] and [**4.2**] = 5 μM

Section 4.2.3: Reaction of 2-phenylimidazole with ^{Et}CAAC, a Cyclic (alkyl)(amino)carbene

The comparison between reactions involving IPr and ^{Et}CAAC on carbazole to produce compounds **4.1** and **4.2** was expected based on the currently known reactivity involving these carbenes on N-H containing molecules.[23–25] Furthermore, our observations on the emission of these products, particularly at high concentrations, also agrees with the reported luminescence of both hydrogen-bonded carbazole and *N*-alkylcarbazole.[15,17–19,30,34–36] However, the use of isolable carbenes remains an unexplored avenue towards modulating the emission of metal-free systems. With this in mind, we proceeded to study if the results we obtained from reactions with carbazole would be transferrable to another NH-containing fluorophore, 2-phenylbenzimidazole (Ph-BIM), or if we could introduce additional tunability by altering the fluorophore. The two main differences between carbazole and Ph-BIM are fairly simple: Ph-BIM is noticeably more acidic than carbazole (pK_a values of 11.9 and 19.9 in DMSO, respectively)[2,3] and Ph-BIM is not restricted to a rigid planar geometry due to the free rotation of the phenyl-substituent.

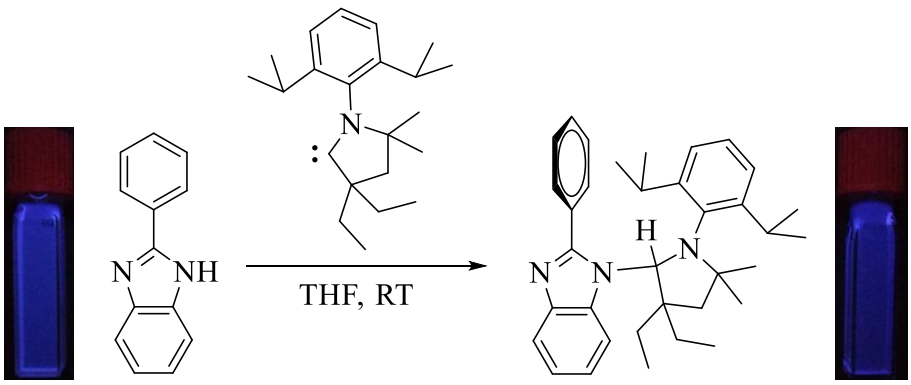

4.3 43%

Scheme 4.3: Insertion of ^{Et}CAAC into the N-H bond of Ph-BIM to produce **4.3**. Cuvettes of Ph-BIM (left) and **4.3** (right) under 365 nm irradiation at 50 mM in THF.

As show in **Scheme 4.3**, the combination of Ph-BIM and ^{Et}CAAC in THF produces analytically pure **4.3** in 43% yield after removal of volatiles and recrystallization from 1:2 THF:hexanes. This colorless solid was found to be non-emissive under UV irradiation and also substantially more sensitive towards ambient air and water than compound **4.2**, partially decomposing when stored open in moist air for days. Analysis by single crystal X-ray diffraction, as given in **Figure 4.14**, shows a similar structure as seen between the reaction of carbazole and ^{Et}CAAC, though the newly formed C-N bond (1.501(2) Å) is significantly longer than what was seen in **4.2** (1.485(2) Å) and also similarly longer than the known structures of the product from the reaction of a less-hindered ^{Me}CAAC with imidazole and benzimidazole (1.485(2) and 1.480(2) Å, respectively).[25]

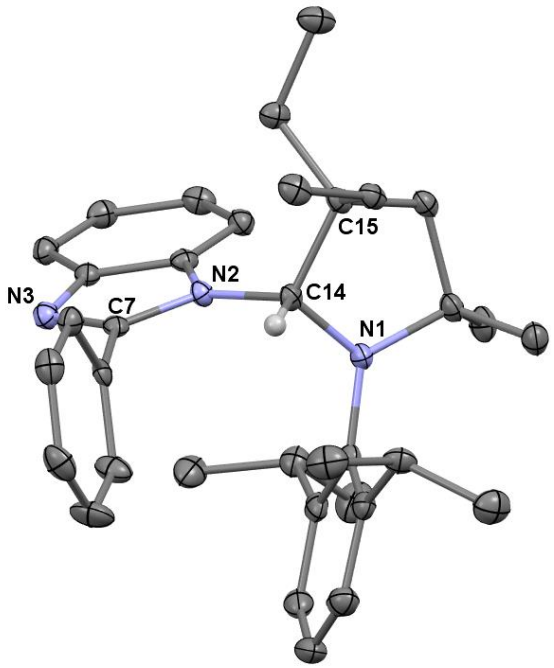

Figure 4.14: ORTEP diagram of **4.3** (ellipsoids set at 50% probability; hydrogen atoms omitted for clarity). Selected bond distances (Å) and angles (deg): C14-N1: 1.438(2); C14-N2: 1.501(2); C14-C15: 1.561(2); C7-N2:1.382(2); C7-N3: 1.315(2); N1-C14-C15: 106.4(1); N1-C14-N2: 112.8(1); C15-C14-N2: 115.4(1).

The most likely cause of this increased distance is due to the added strain imposed by the additional phenyl group, which is forced into a perpendicular geometry compared the benzimidazole plane (N2-C7-C8-C13 = -88.4°). Notably, previous reports have studied the importance on this dihedral angle remaining nearly 0° in order for Ph-BIM to exhibit a high luminescence quantum yield.[37] As with compound **4.2**, the NMR spectra of **4.3** showed similar diagnostic chemical shifts attributed to the newly formed C-H (sharp singlet at 5.59 ppm) and a similarly ring-shielded isopropyl group appearing at -0.45 ppm in the ^{1}H NMR spectrum as provided in **Figure 4.15**. However, while the complexity of the spectra were similar to compound **4.2** and indicative that **4.3** was equally sterically locked, the 2D NOESY spectrum (**Figure 4.16**) contained both NOE as well as EXSY signals from which two distinct rotamers about the new C-N bond could be assigned (**Figure 4.17**).

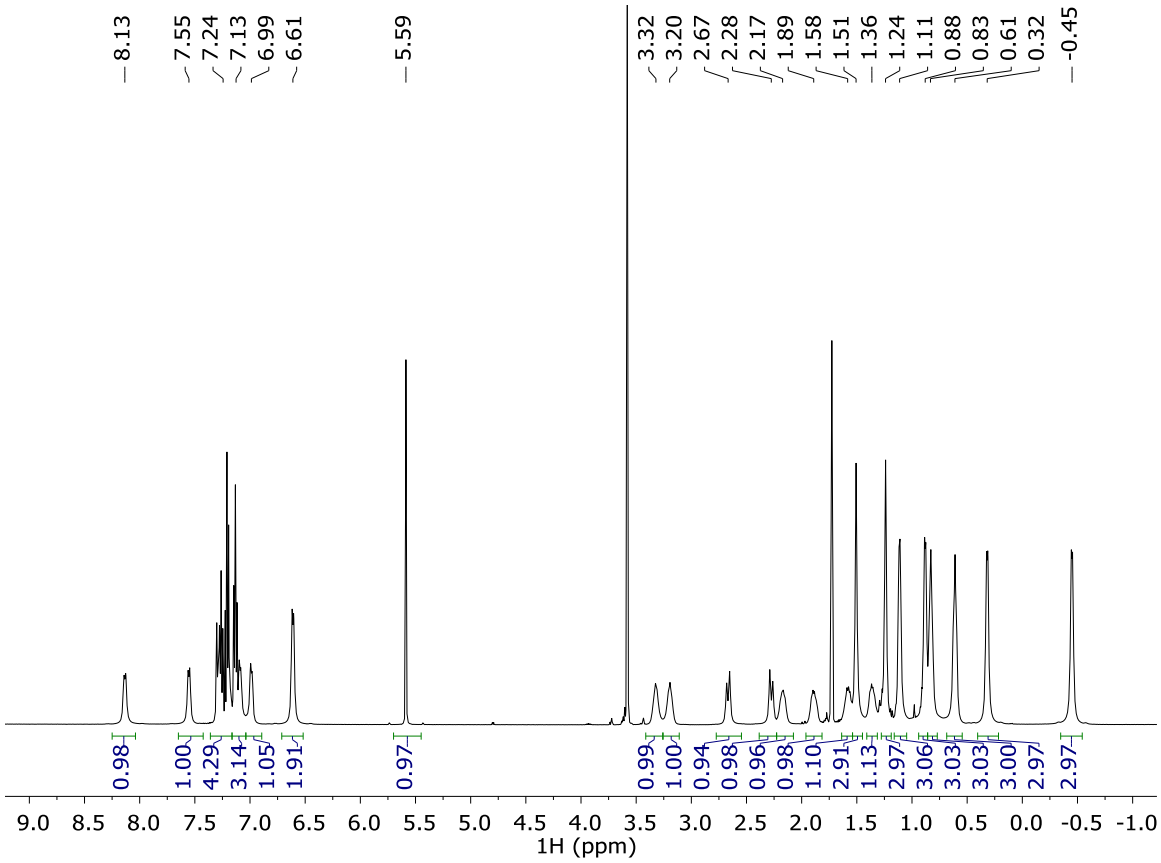

Figure 4.15: ^{1}H NMR (500 MHz, THF-d_8) spectrum of compound **4.3**.

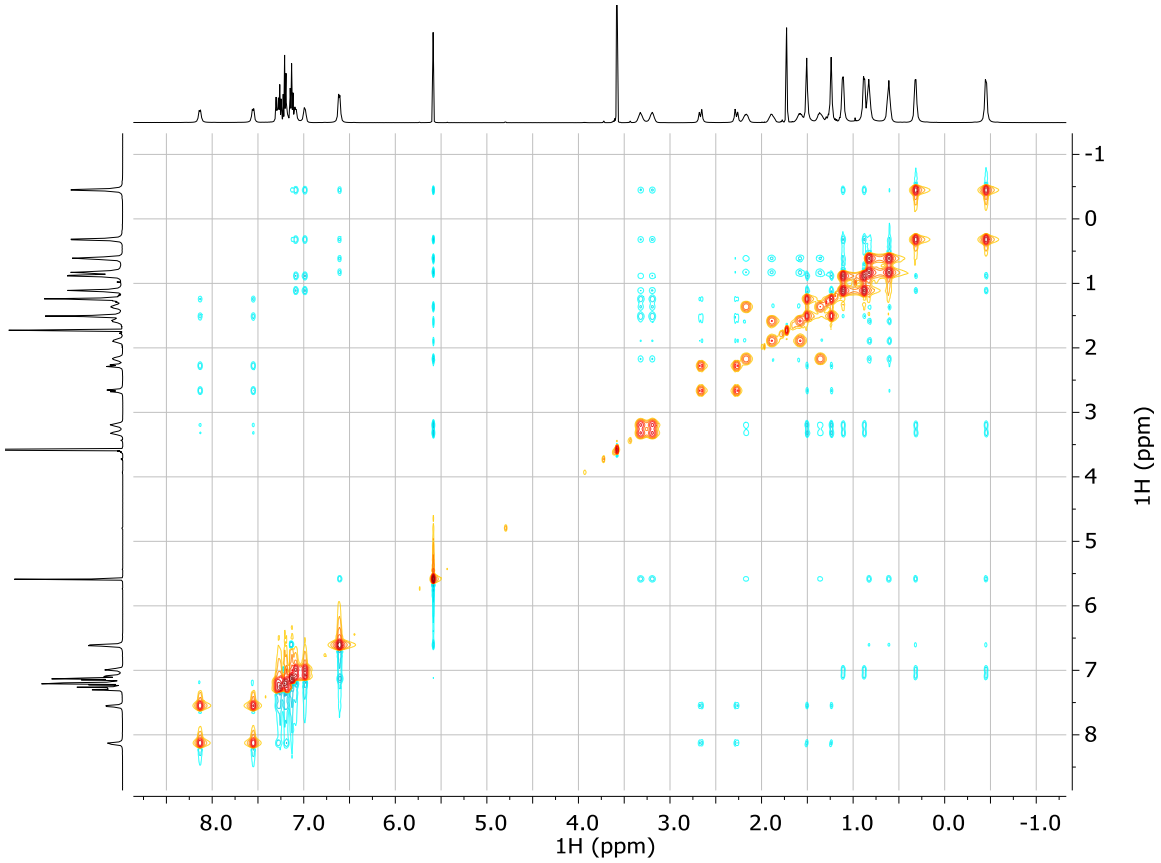

Figure 4.16: ^{1}H-^{1}H NOESY NMR (500 MHz, THF-d_8) spectrum of **4.3**. Two distinct rotomers centered on the new C-N bond can be observed and assigned in **4.3** (meaning the exchange rate between rotomers is slow enough to be observable on the NMR timescale, mixing time = 0.9 s). This yields a spectrum with through space proton (NOESY, blue) and exchangeable proton (EXSY, off-diagonal red) signals.

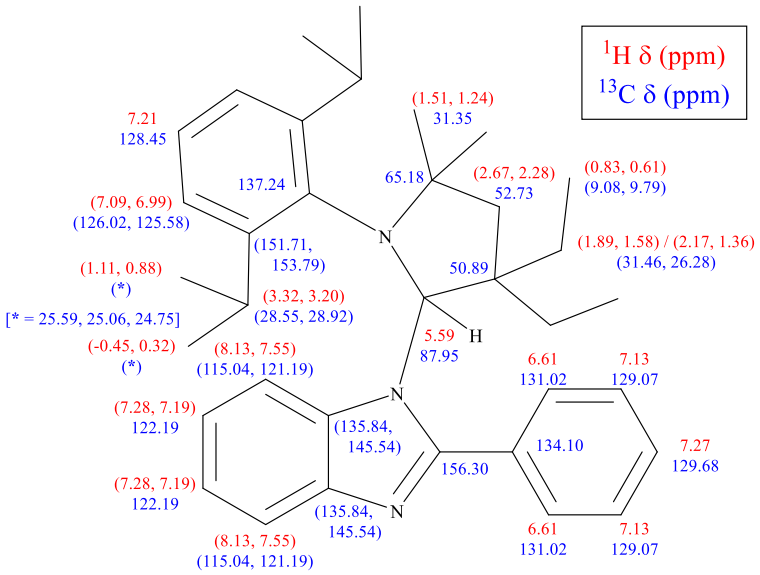

Figure 4.17: ^{1}H and ^{13}C NMR assignments for compound **4.3**. Signals showing EXSY signals were paired. Carbon signals marked with ***** could not be accurately assigned to a specific methyl group due to overlap and distorted HSQC cross peaks.

Compound **4.3** also exhibited photophysical properties which contrasted those we had obtained for compound **4.2**. Instead of collecting absorbance and emission spectra corresponding to an *N*-alkylbenzimidazole, we once again obtained data which was consistent with the sum of isolated fluorophore and carbene spectra as shown in **Figure 4.18**. While obtaining such a result from the weakly bound hydrogen bonding complex **4.1** was less surprising, observing such reversibility from a formally sigma-bonded complex under such mild conditions was exciting. Additionally, the incorporation of excess carbene to solutions of **4.3** produced a sharp decrease in emission intensity along with a corresponding loss of original absorbance profile starting at a ratio of **4.3**:^{Et}CAAC equal to 1:35 and reaching a minimum at a ratio of 1:70 as shown in **Figure 4.19**.

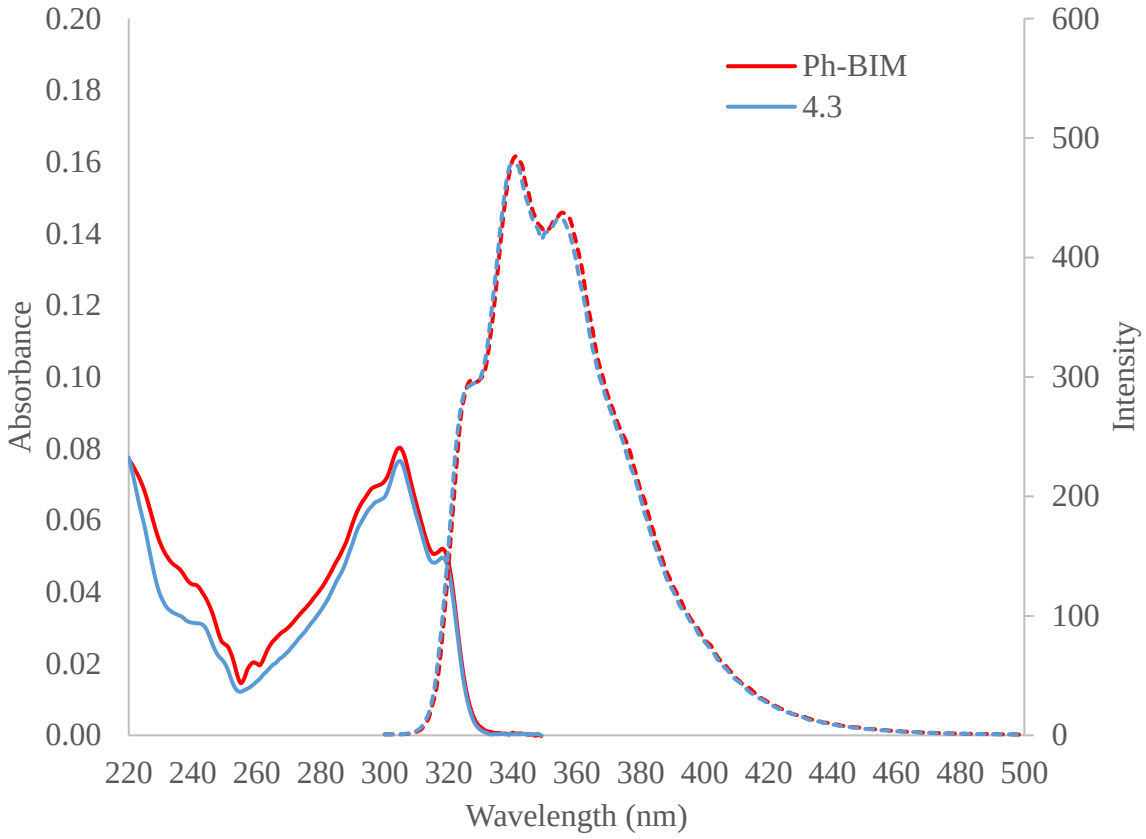

Figure 4.18: Photophysical characterization of **4.3** and Ph-BIM (absorption spectra = solid lines, emission spectra = dashed lines). Conditions: λ_{ex} = 290 nm, THF, RT, [Ph-BIM] and [**4.3**] = 3 μM

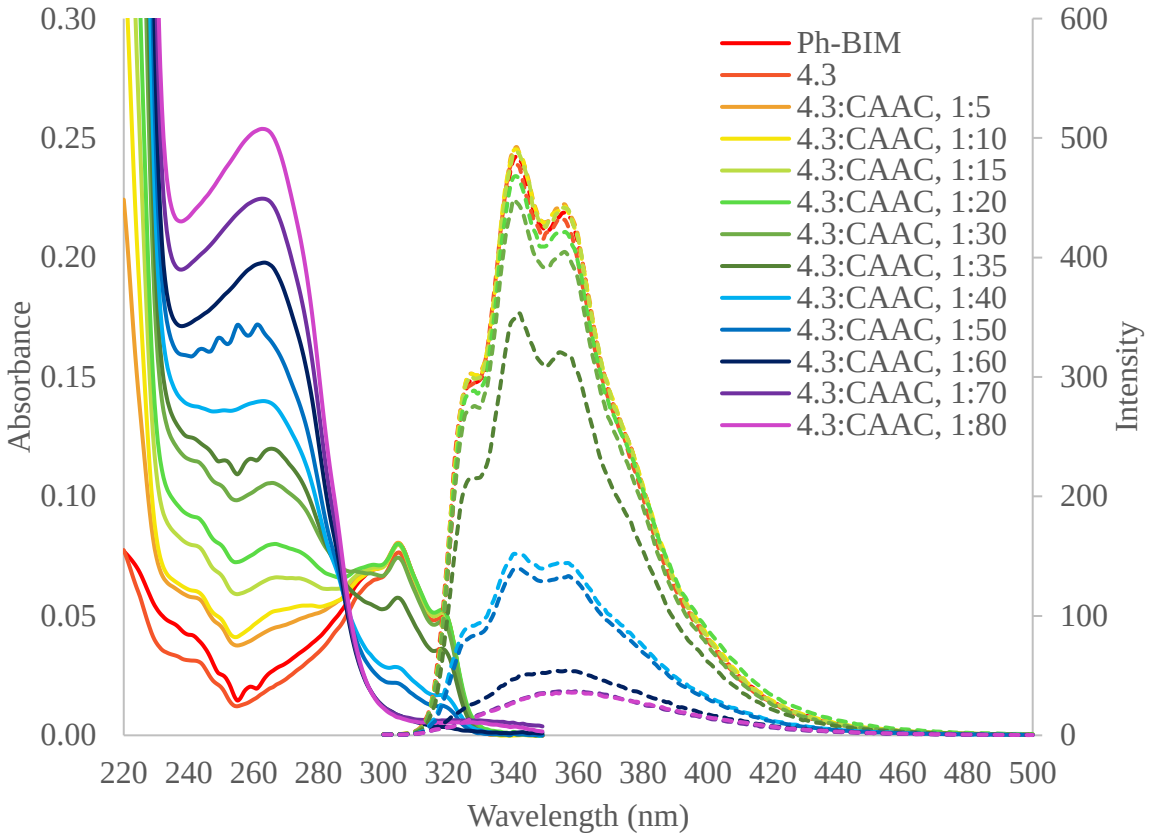

Figure 4.19: Photophysical characterization of **4.3** with excess ^{Et}CAAC (absorption spectra = solid lines, emission spectra = dashed lines). Conditions: λ_{ex} = 290 nm, THF, RT, [Ph-BIM] and [**4.3**] = 3 μM

Based on our current set of data, solutions of **4.3** presented a partial equilibrium with the starting Ph-BIM and ^{Et}CAAC. While extremely dilute solutions were best described as a mixture of starting components, more concentrated NMR spectra clearly indicated the distinct chemical shifts attributed to **4.3**. However, the exchange signals observed in the NOESY spectrum could also be attributed to this equilibrium. ^{1}H DOSY NMR was once again used to provide a vital look at the solution behavior of **4.3**, shown in **Figure 4.20** providing an equal diffusion constant for all chemical shifts attributed to **4.3** as well as a calculated molecular weight almost identical to the expected value (MW_{cal} = 503, $MW_{\mathbf{4.3}}$ = 508), suggesting that concentrated solutions are best described as intact **4.3**.

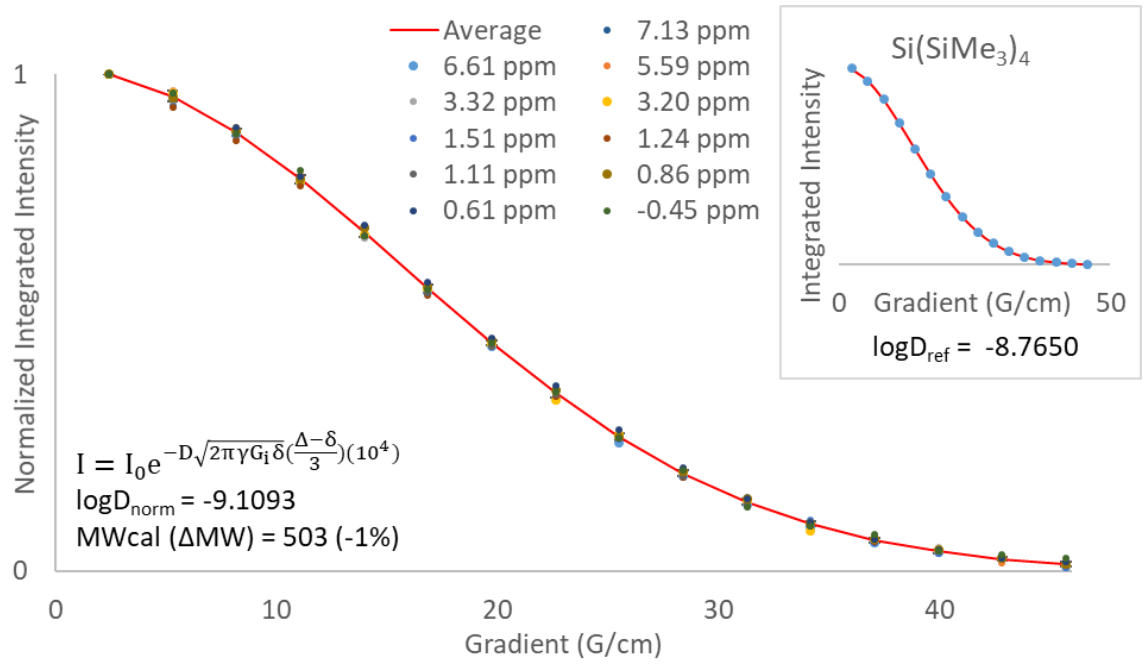

Figure 4.20: Calculated relaxation curve fits from ^{1}H DOSY NMR and calculated molecular weight for **4.3** (THF-d$_8$, 298 K, 50 mM, (Me$_3$Si)$_4$Si added as internal standard).

In order to form a more complete picture of the potential equilibrium between **4.3** and a mixture of Ph-BIM and ^{Et}CAAC, we probed a known reaction wherein formation of free ^{Et}CAAC obtained by dissolving **4.3** could be trapped by a secondary reactant. The most convenient reaction to display this behavior was to monitor formation of **4.2** from a mixture of **4.3** and carbazole, shown in **Scheme 4.4**, relying on our observations of **4.2** showing no significant contribution to the corresponding reverse reaction.

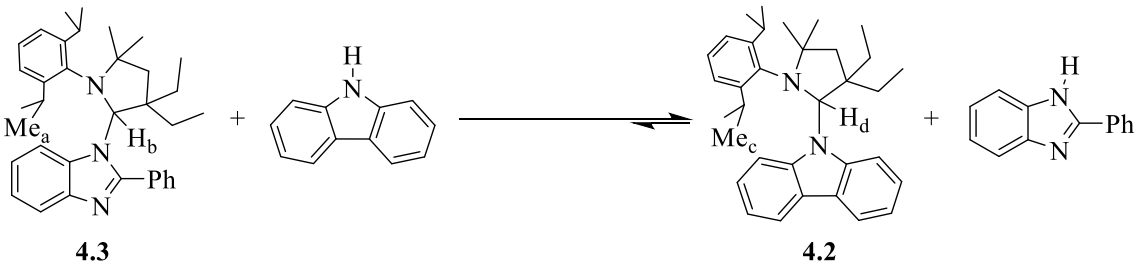

Scheme 4.4: Reaction of **4.3** and carbazole to form **4.2** via *in situ* release of ^{Et}CAAC.

Accordingly, **4.3** was combined with carbazole in THF-d_8 at 50 mM, and analyzed by ^{1}H NMR after 15 minutes. The spectrum showed a nearly complete conversion to compound **4.2** and free Ph-BIM, however there was a trace amount of **4.3** present as well (**Figure 4.21**).

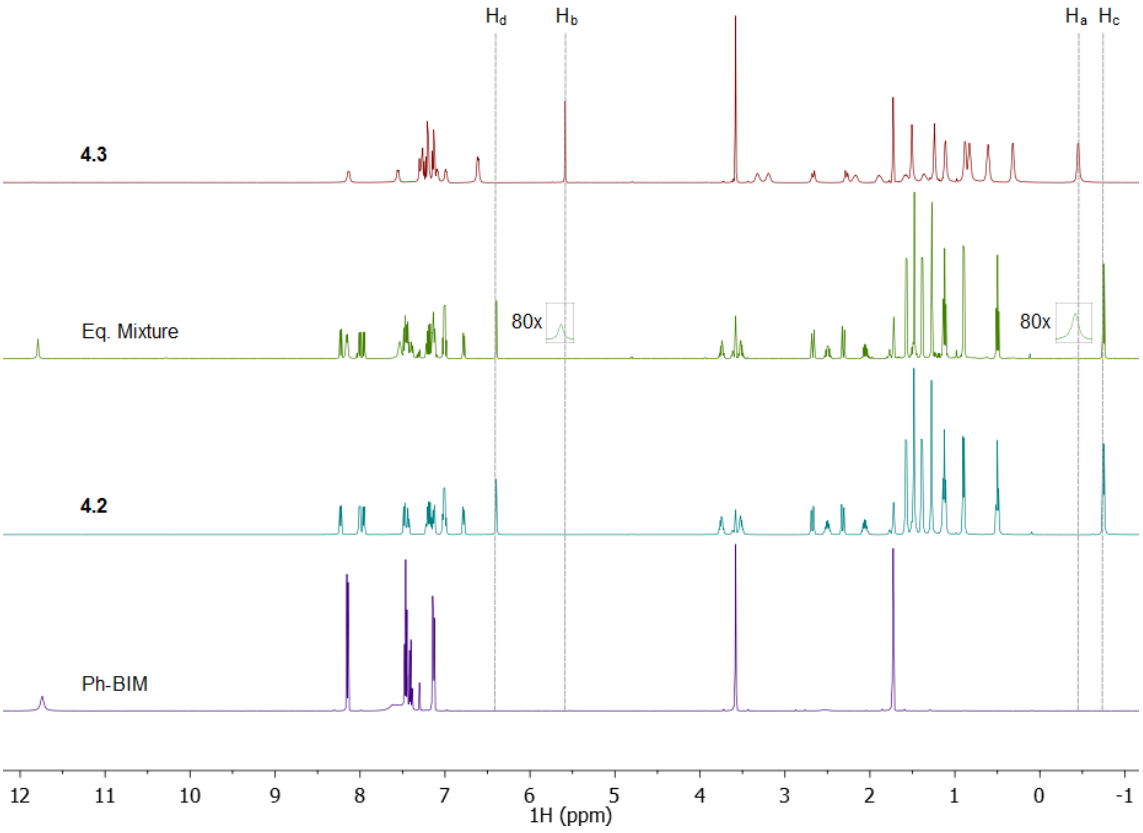

Figure 4.21: ^{1}H NMR spectrum (500 MHz, 50 mM in THF-d_8, 298 K) of a combination of **4.3** and carbazole after 15 minutes. Spectra of **4.3**, **4.2**, and Ph-BIM provided for reference.

In order to probe whether this trace amount of **4.3** was due to a slight stoichiometric excess or the release of ^{Et}CAAC from **4.2**, we performed the reverse reaction wherein **4.2** was combined with Ph-BIM in THF-d_8 at 50mM, given by **Scheme 4.5**. The ^{1}H NMR spectrum taken after 15 minutes closely resembled that of the prior reaction, displaying predominantly **4.2** and Ph-BIM, but also trace amount of **4.3** as shown in **Figure 4.22**.

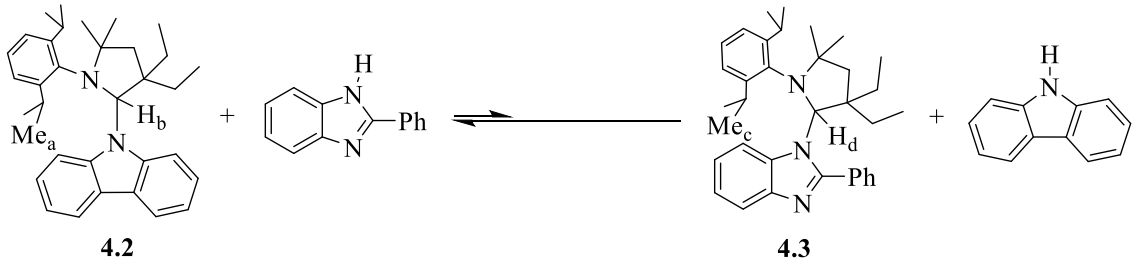

Scheme 4.5: Reaction of **4.2** and Ph-BIM to form **4.3** via *in situ* release of ^{Et}CAAC.

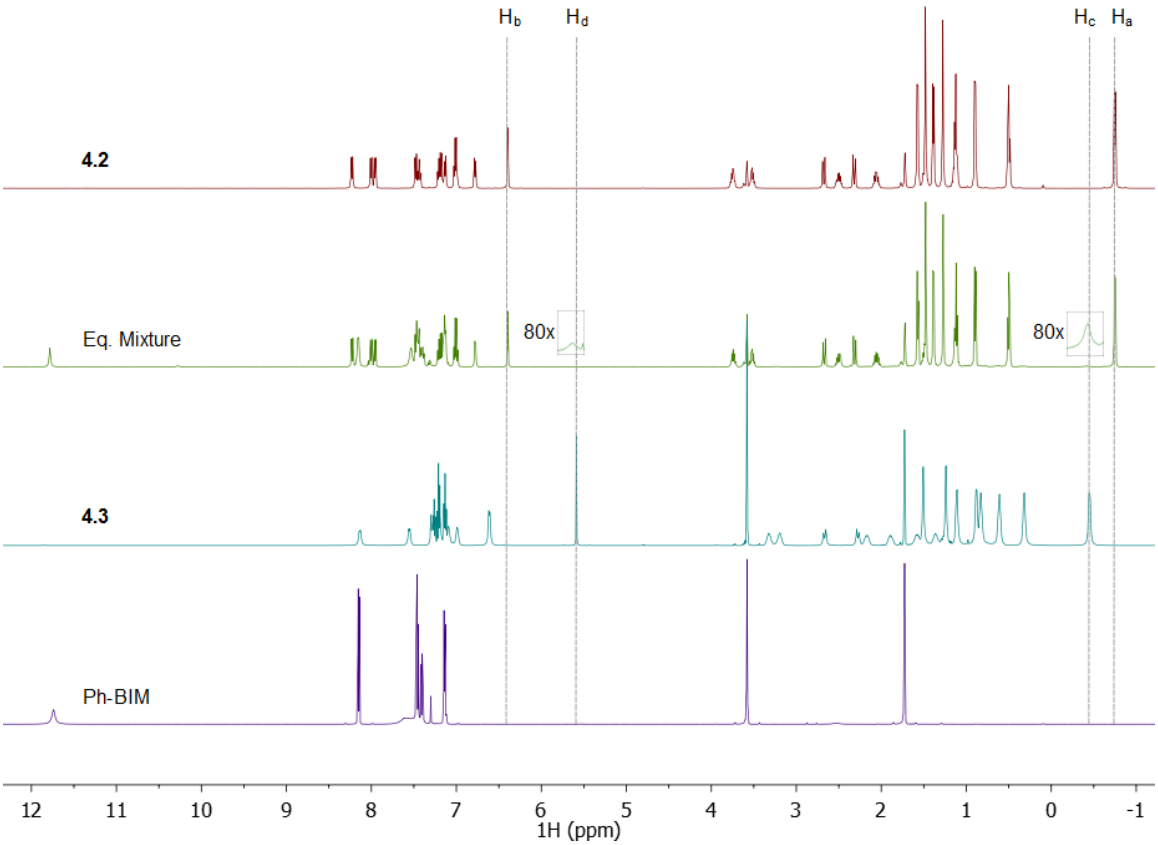

Figure 4.22: ^{1}H NMR spectrum (500 MHz, 50 mM in THF-d_8, 298 K) of a combination of **4.2** and Ph-BIM after 15 minutes. Spectra of **4.2**, **4.3**, and Ph-BIM provided for reference.

In order to quantify the equilibrium reactions we had observed, the most distinct and isolated signals corresponding to **4.2** and **4.3**, namely the newly formed C-H and strongly ring-shielded methyl group, were integrated and equilibrium constants calculated

based on the ratios of each component, assuming [**4.3**] = [carbazole] and [**4.2**] = [Ph-BIM]. The constants derived from each dataset, $K_{eq} \approx 450$ for reaction of **4.3** and carbazole and $K_{eq} \approx 1/560$ for reaction of **4.2** and Ph-BIM, correlated well and signaled that we were indeed observing the equilibria shown in both **Scheme 4.4** and **Scheme 4.5**. Coincidentally, a report detailing similar equilibria was published by the Bertrand group at the same time as our report on these results.[26] In their report, this reductive elimination of an N-H group from a CAAC was studied in depth, focusing on the steric profile around the carbene center and showing that the elimination was only achievable when using bulky CAACs. Likewise, the results shown in **Figure 4.21** and **Figure 4.22** show the same reliance on steric bulk around the carbene, however in our case we approach this by adjusting the size of the N-H containing species.

Section 4.2.4: Reaction of 2-phenylimidazole with IPr, an Imidazole-2-ylidene

In order to finish this initial survey on the reactivity between carbenes and N-H containing fluorophores and the resulting photophysical impacts, we studied the reaction between IPr and Ph-BIM, shown in **Scheme 4.6**. Based on the results obtained for compound **4.1**, namely the crystallographic data and lack of significant NOE interaction between IPr and carbazole, the small change in steric profile of Ph-BIM was not expected to impact this reaction as significantly as in **4.3**. However, the difference in acidity between Ph-BIM and carbazole (pK_a values of 11.9 and 19.9 in DMSO, respectively)[2,3] remained a potential avenue for a change in reactivity. Qualitatively, a mixture of IPr and Ph-BIM in THF resulted in a substantial decrease in emission intensity upon irradiation at 365 nm as shown in **Scheme 4.6**. This solution was then concentrated to dryness *in vacuo* to give an analytically pure white solid, **4.4**, in quantitative yield.

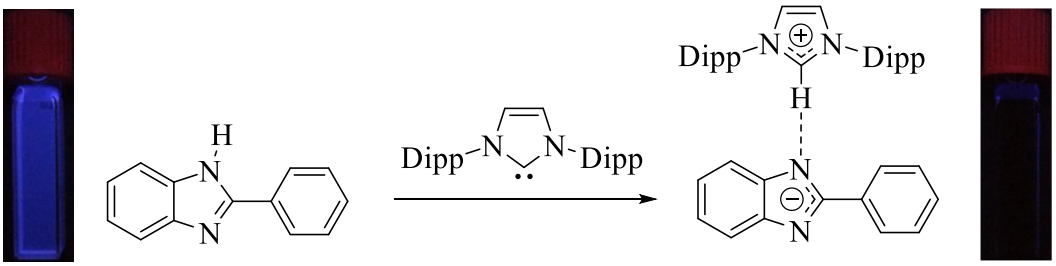

Scheme 4.6: Reaction of Ph-BIM and IPr (**4.4**). Cuvettes of Ph-BIM (left) and **4.4** (right) under 365 nm irradiation at 50 mM in THF.

Compound **4.4** was recrystallized from a 1:2 mixture of THF and hexanes to provide crystals suitable for X-ray diffraction, revealing a hydrogen-bonded salt wherein IPr had acted as a Brønsted base. Furthermore, the crystal structure presented **4.4** as forming an extended coordination polymer connected by hydrogen bonding between the carbene carbon and N-H group of Ph-BIM as well as the backbone C-H of the carbene and the second Nitrogen atom in Ph-BIM (**Figure 4.23**).

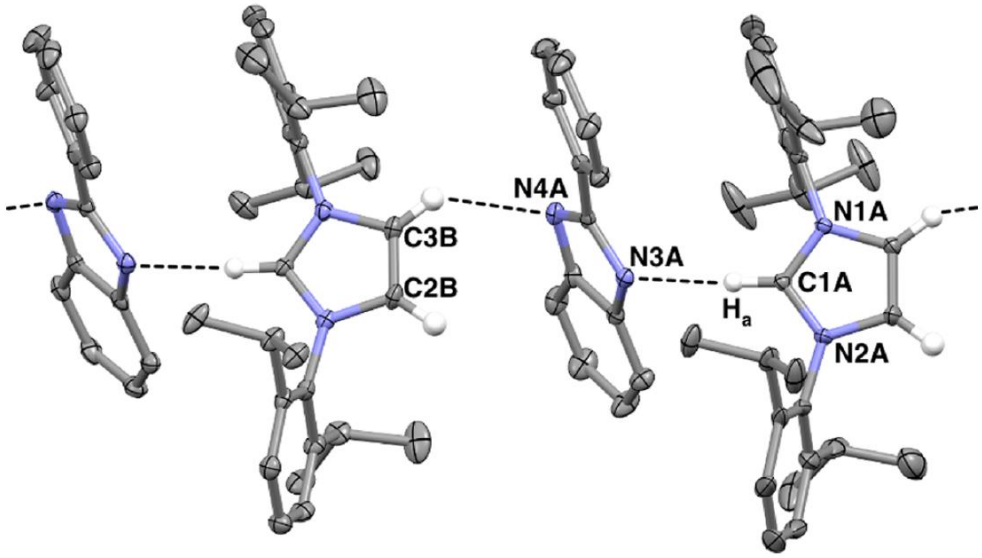

Figure 4.23: ORTEP diagram showing two of the six independently solved units of **4.4** (ellipsoids set at 50% probability; non-hydrogen bonded hydrogen atoms and remaining

four independent units within supercell omitted for clarity). Selected bond distances (Å) and angles (deg): C1A-N3A: 3.100(5); C3B-N4A: 3.137(6); N1A-C1A-N2A: 107.9(3).

Each of the six independently solved units within the extended structure of **4.4** were nearly identical, giving an average C1-N3 distance of 3.083 Å, which represents the primary hydrogen bonding interaction we expected, and an average C3-N4 distance of 3.126 Å, representing the second hydrogen bonding interaction which completes the coordination polymer. Additionally, characterization of the IPr fragment as its protonated imidazolium salt was accomplished by examining the N1-C1-N2 angle, where an average of 107.8° is very comparable to structurally similar imidazolium hydrogen bonding complexes by Arduengo (107.8(4) and 106.6(6)° for imidazolium-NHC complexes),[4] Clyburne and Davidson (107.3(2)° for imidazolium-aryl oxide complex),[5] and Pi and Zheng (108.4(2)° for an imidazolium-benzazaphospholide complex).[38]

Much like what we observed with compound **4.1**, the reactivity shown in **Scheme 4.6** can be attributed to the basicity of the carbene (p*K*a (DMSO) = 24.0)[39] however the accompanying emission quenching of Ph-BIM once again makes this system unique. As with the previously studied compounds, we first sought to analyze the photophysical properties of **4.4**. Similar to **4.1**, this weakly bound complex displays only the sum of Ph-BIM and IPr absorbance and emission spectra at μM concentrations, shown in **Figure 4.24**, a product of the reversible proton-transfer and dissociation into free Ph-BIM and IPr.

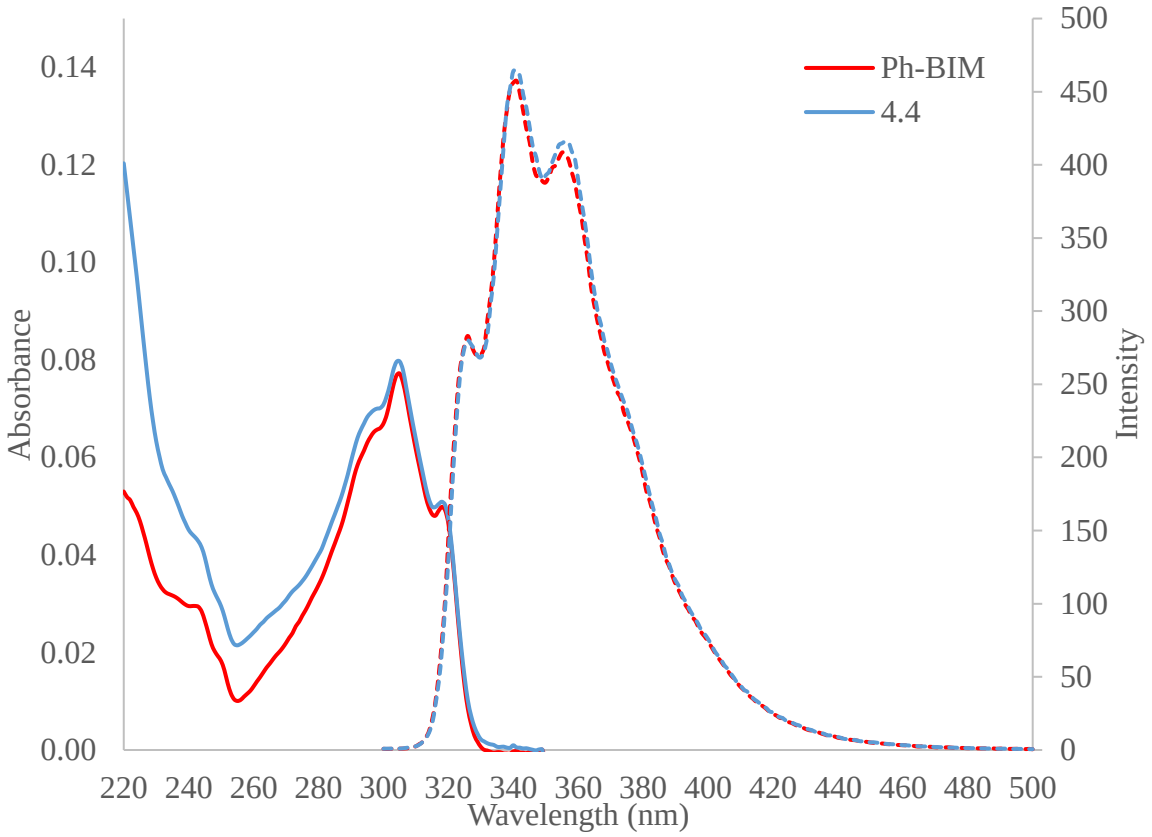

Figure 4.24: Photophysical characterization of **4.4** and Ph-BIM (absorption spectra = solid lines, emission spectra = dashed lines). Conditions: λ_{ex} = 290 nm, THF, RT, [Ph-BIM] and [**4.4**] = 3 μM

Additional photophysical characterization resulted in spectra displaying no significant change in either absorbance or emission profile, both upon change of solvent (THF, MeCN, benzene) or addition of excess IPr (up a ratio of **4.4**:IPr of 1:100 in THF). These results were consistent with the reversibility observed in **4.1**, therefore similar NMR techniques were utilized to obtain solution-state analysis of the intact complex **4.4**.

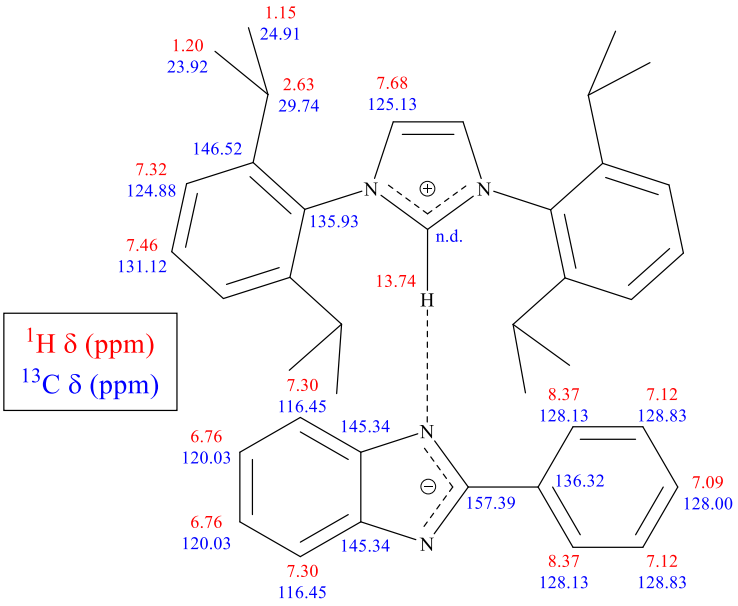

Figure 4.25: ^{1}H and ^{13}C NMR assignments for **4.4**. The carbon atom participating in hydrogen bonding was not located by ^{13}C NMR.

As with compound **4.1**, the ^{1}H NMR spectrum of **4.4** is consistent with a highly symmetric structure, assignments presented in **Figure 4.25**, and displays no significant NOE interaction between Ph-BIM and IPr fragments. Once again, ^{1}H DOSY NMR was vital in determining the solution behavior of **4.4** at these concentrations, either as free Ph-BIM and IPr, an intact ion pair, or something in-between. At 75 mM in THF-d_8, we can observe all chemical shifts attributed to **4.4** diffusing at equal rates (**Figure 4.26**). As well, the calculated molecular weight, MW_{cal} = 669 and $MW_{\mathbf{4.4}}$ = 583, indicates that **4.4** is a single contact ion pair and not a higher-order oligomer at this concentration.

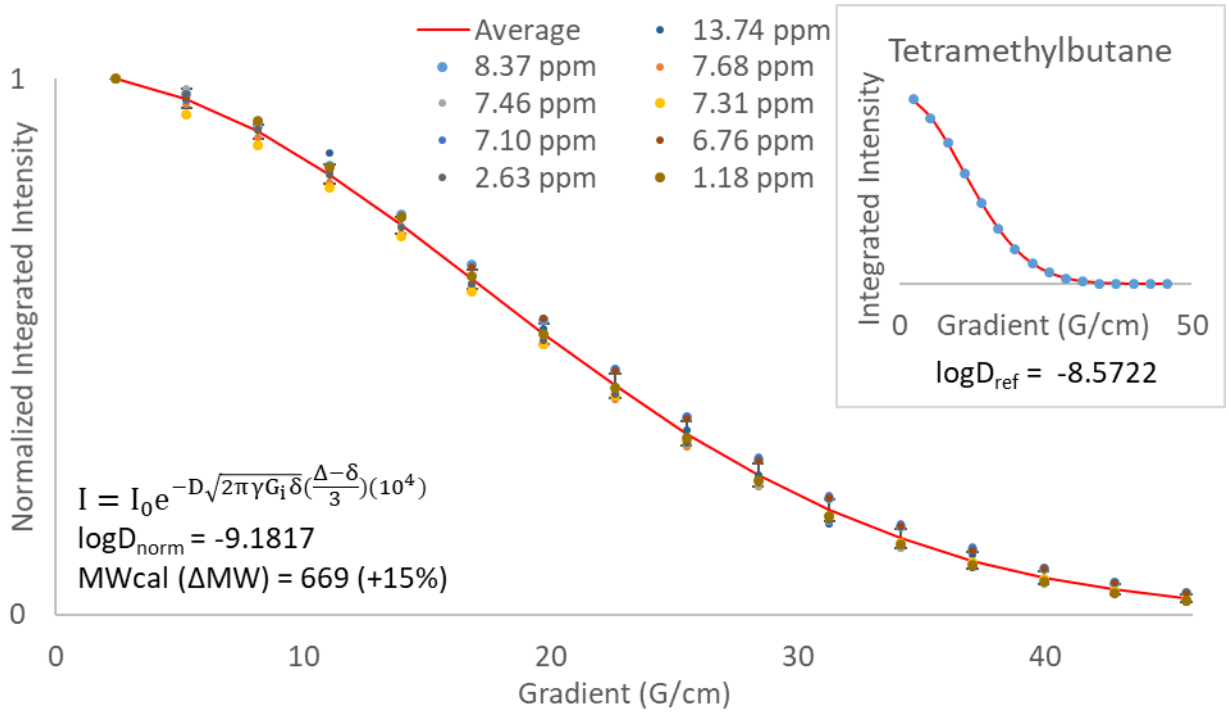

Figure 4.26: Calculated relaxation curve fits from ^{1}H DOSY NMR and calculated molecular weight for **4.4** (THF-d_8, 298 K, 75 mM, tetramethylbutane added as internal standard).

While we observed that **4.4** diffused in THF as a single ion pair, we were also aware that the ^{1}H NMR chemical shifts displayed a similar concentration dependence as we had investigated in **4.1**. To finish our analysis of compound **4.4**, we analyzed a similar set of dilutions of **4.4** in THF-d_8, ranging from 50-0.5 mM, and tracked each chemical shift that remained unobstructed throughout the range of concentrations (**Figure 4.27**). By analyzing this data in the same manner as **4.1**, we were able to obtain a set of association constants for **4.4**, average K_d = 49.9 ± 4.3 M^{-1}, corresponding to a $\Delta G \approx$ -2.3 kcal mol^{-1}. While this result suggests that **4.4** is more labile than **4.1**, in contrast to the results obtained by DOSY NMR analysis, the change in solvent between benzene and THF in these studies is known to have an effect on hydrogen bond strength.[40]

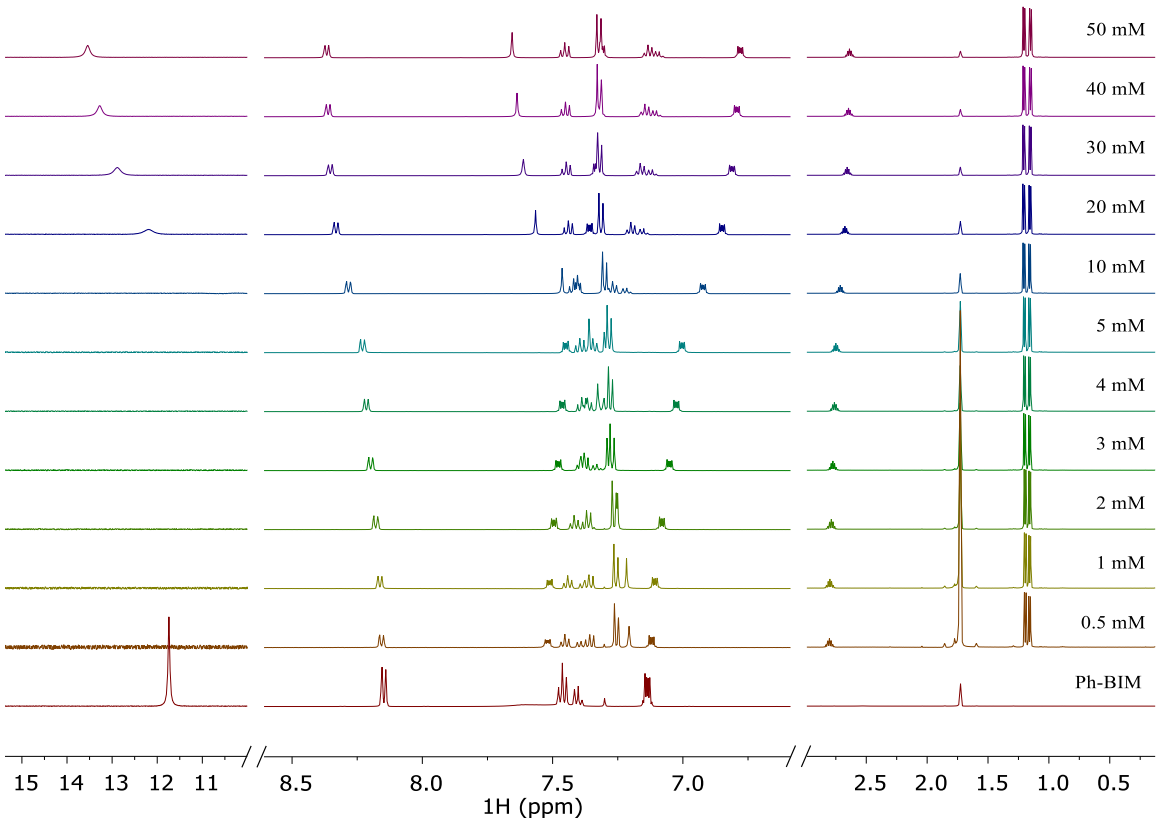

Figure 4.27: Concentration effect on the equilibrium of **4.4** as determined by ^{1}H NMR over a range of concentrations 50-0.5 mM (500 MHz, THF-d_8, 298K). Spectrum of Ph-BIM provided for reference and vertical magnification adjusted to account for weaker signals.

Section 4.3: Conclusions and Future Directions

The primary goal for the work detailed in this chapter was undertaken in an effort to understand or generalize the reactivity and photophysical effect observed from the reaction between 2-(thiophen-2-yl)-1,3-benzazaphosphole (Th-BAP) and IPr. To this end, we have successfully shown that the primary mode of reactivity and associated emission quenching is based around the carbene interacting with the N-H group of each fluorophore, summarized in **Scheme 4.7**. More importantly, our results show the high degree of

tunability that can be introduced to this type of system, even when only studying a handful of complexes. However, this tunability is not only limited to the electronic and steric properties of the NHC, but can be included in the N-H containing group as well. This was a particularly important point of contrast when comparing the reversibility of **4.2** and **4.3** as well as the proton transfer, or lack thereof, in **4.1** and **4.4**. Both of these major differences in reactivity were attributed to minor changes in the steric or electronic properties of the N-H containing molecule.

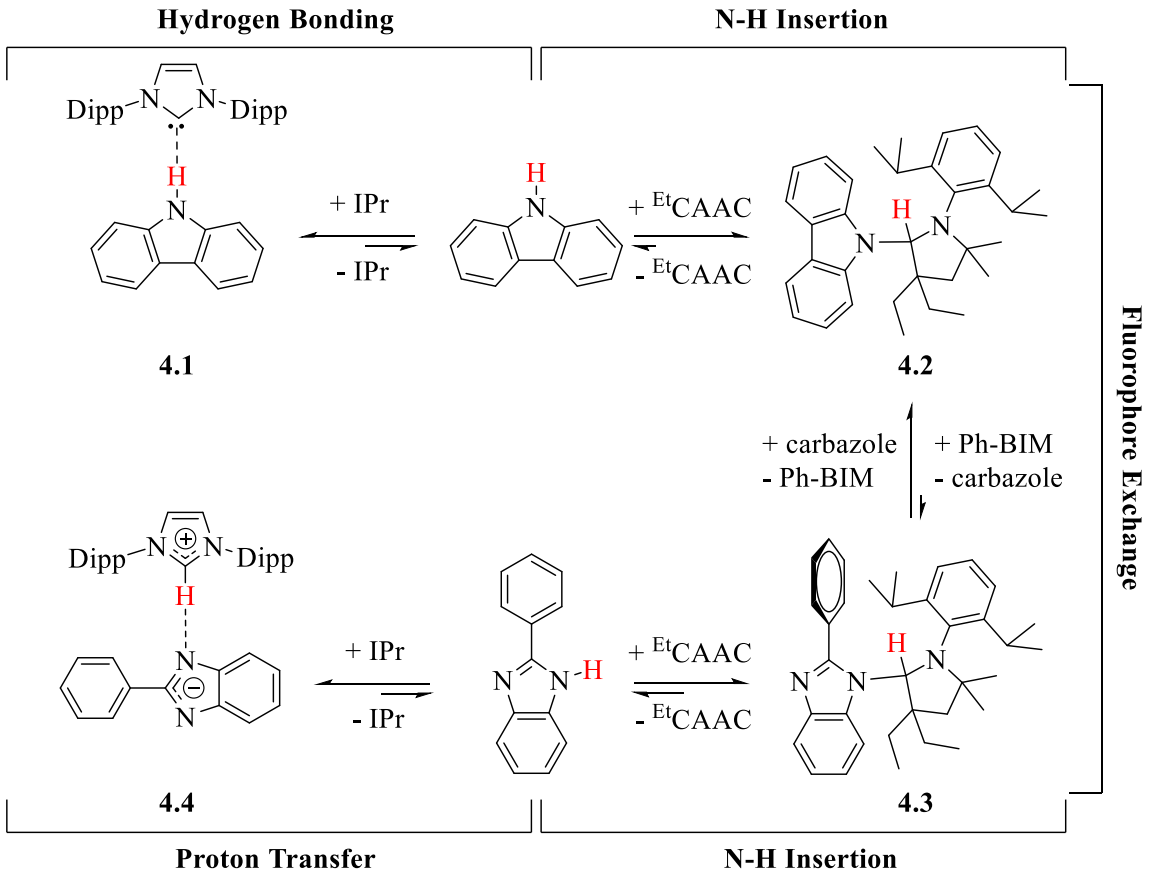

Scheme 4.7: Summary of reactivity studied in **Chapter 4** involving N-H containing fluorophores, carbazole and Ph-BIM, and isolable carbenes, IPr and ^{Et}CAAC.

Although much of the emission quenching that we observed in the reaction mixtures, and what originally drew us to study these reactions, was not quantifiable at reduced concentrations, we were able to assemble a set of analyses wherein the solution behavior of each intact complex was studied and verified. Not only did this provide a blueprint on how to study similar complexes in future work, it also afforded evidence to quantify the strength of the interactions we were studying.

The future of this project is extremely broad, given the aforementioned tunability of both fluorophore and carbene playing an important role in the observed reactivity. Primarily, the methods employed to study the various products obtained in this project, and their equilibria, will be utilized to finish our previous study on Th-BAP, as discussed in **Chapter 3**. Additionally, though we have obtained a great deal of data to show the various reactivity and reversibility differences between the reactions studied, the underlying mechanism behind the observed emission quenching is not explained. As such, we have engaged in an ongoing collaboration with Prof. Dunietz at Kent State University in order to explore this phenomenon computationally via TD-DFT calculations.

One area of future interest involves our analysis of **4.2** and **4.3**. Putting aside their use as a source of ^{Et}CAAC upon dilution, our interest was drawn to the congested structure of each, wherein the isopropyl group on the carbene was thrust into very close proximity of the fluorophore. Our aim is to employ a heavy atom, such as bromine, in place of this isopropyl group and thereby increase the emission quenching observed for the complex through the heavy atom effect. This project will be detailed in **Chapter 5**.

One consequence of temporarily shifting our study from Th-BAP, as discussed in **Chapter 3**, to fully organic fluorophores, discussed in this chapter, is the accessibility of

carbazole or benzimidazole derivatives. As such, extending this work to include oligomers or polymers of carbazole, for instance, is far more trivial than first attempting to develop new polymerization techniques for benzazaphospholes, particularly when the synthesis of a related poly-benzoxaphosphole has thus far escaped our efforts. To this end, a bis-carbazole-IPr hydrogen bonding adduct has already been produced by a co-author, with the intention to extend this study toward larger oligomers as well as introducing a dicarbene, as summarized in **Scheme 4.8**.

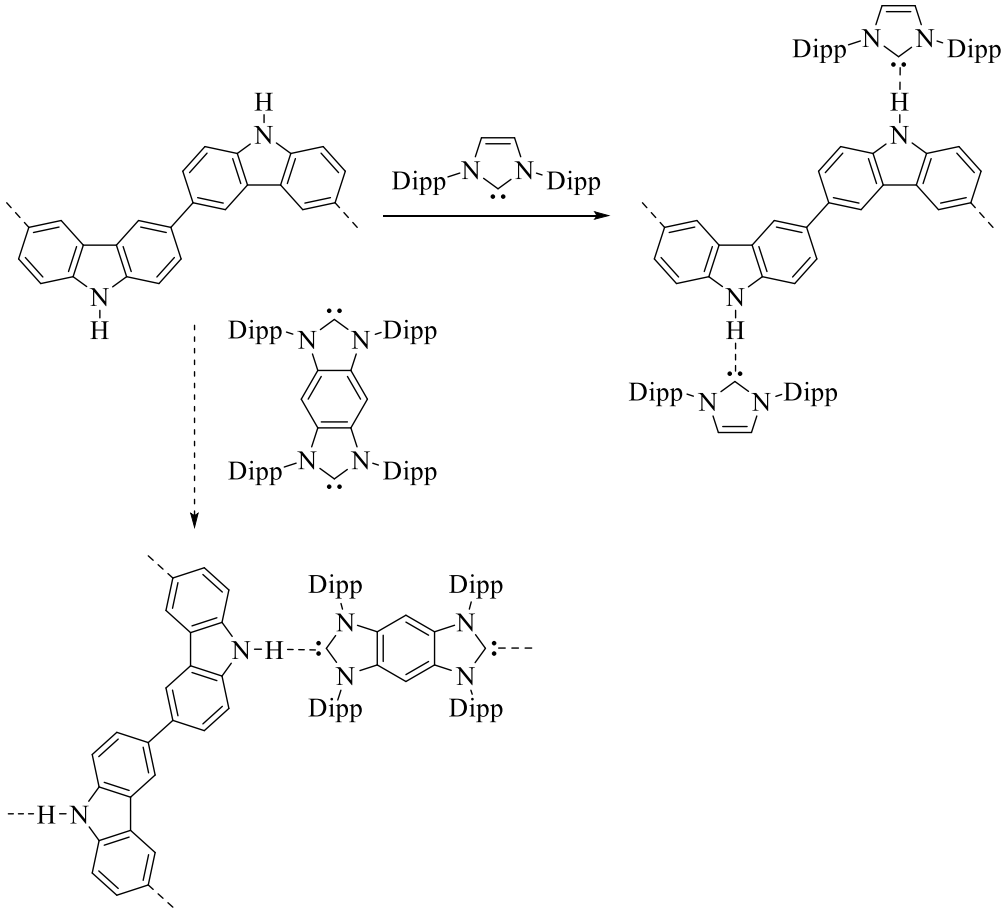

Scheme 4.8: Proposed reactions involving carbazole oligomers and IPr or similar dicarbenes.

Finally, although much of our work thus far has focused on N-H containing fluorophores, we envision that these results could be utilized towards similar reactions involving other E-H groups. The two most obvious and interesting systems to study would be comparative studies involving fluorene and 2-phenylindene, where we substitute the N-H group of carbazole and Ph-BIM with a methylene. The acidities of these fluorophores (p*K*a (DMSO) of 22.6 and 19.4, respectively)[41] are similar to carbazole, and the potential for rare C-H···C hydrogen bonding makes these systems worthy of investigation. Additionally, difluoromethyl groups have been known to participate in hydrogen bonding and have the added benefit of being utilized for biochemical applications.[42–44] Reactions of carbenes with appropriate -CF_2H substituted fluorophores provide yet another potentially important field to explore.

Section 4.4: Experimental

General Considerations: All manipulations were performed under an atmosphere of nitrogen using either an MBraun glove box or standard Schlenk line techniques. Unless otherwise stated, all chemicals were purchased from commercial sources and used without further purification. Tetrahydrofuran, toluene, and hexanes were purified using an MBraun solvent purification system. Pentane was distilled over sodium benzophenone. Acetonitrile was distilled over CaH_2. THF-d_8 and C_6D_6 were distilled over sodium. Carbazole was recrystallized from toluene. IPr and ^{Et}CAAC were prepared following literature procedures and recrystallized from toluene or pentane, respectively.[45,46] Elemental analyses were performed by Robertson Microlit Laboratories, Ledgewood, New Jersey. NMR spectra were recorded on a Bruker AVANCE III 500 MHz spectrometer and chemical shifts referenced to residual solvent signal. Absorbance spectra were recorded on Cary 5000

spectrophotometer and corrected for solvent background absorbance and instrument drift. Emission spectra were recorded on Cary Eclipse spectrophotometer. All spectra were recorded at room temperature using 1 cm path length quartz cuvettes with solutions prepared under inert atmosphere.

Carbazole-IPr Adduct (4.1): A flame dried round bottom flask was charged with IPr (0.537 g, 1.38 mmol), carbazole (0.231 g, 1.38 mmol), and 20 mL benzene. The reaction was stirred for 15 minutes at room temperature followed by removal of volatiles *in vacuo* to give an analytically pure white solid (0.754 g, 98%). Recrystallization from MeCN provided single crystals suitable for X-ray diffraction. ^{1}H NMR (THF-d_8, 500 MHz): δ 11.95 (s, 1H), 7.89 (d, J = 7.7 Hz, 2H), (7.50 (t, J = 7.8 Hz, 2H), 7.36 (d, J = 7.8 Hz, 4H), 7.31 (s, 2H), 7.04 (t, J = 7.5 Hz, 2H), 6.96 (t, J = 7.4 Hz, 2H), 6.50 (d, J = 8.0 Hz, 2H), 2.85 (hept, J = 6.9 Hz, 4H), 1.23 (d, J = 6.9 Hz, 12H), 1.11 (d, J = 6.9 Hz, 12H). ^{13}C{^{1}H} NMR (THF-d_8, 126 MHz): δ 215.03, 147.24, 141.53, 139.30, 129.81, 125.69, 124.49, 124.05, 123.06, 120.36, 118.74, 111.67, 29.55, 25.05, 23.95. Anal. Calcd. for $C_{39}H_{45}N_3$: C, 84.28; H, 8.16; N, 7.56. Found: C, 83.87; H, 8.14; N, 7.51.

Carbazole-^{Et}CAAC Insertion (4.2): A flame dried round bottom flask was charged with ^{Et}CAAC (0.516 g, 1.65 mmol), carbazole (0.275 g, 1.65 mmol), and 20 mL THF. Solution stirred for 30 minutes before volatiles were removed *in vacuo* and crude solid washed 3x with pentane to give an analytically pure white solid (0.679 g, 86%). Recrystallization from 8:1 hexanes/toluene provided single crystals suitable for X-ray diffraction. ^{1}H NMR (THF-d_8, 500 MHz): δ 8.23 (d, J = 8.3 Hz, 1H), 7.98 (m, 2H), 7.46 (m, 2H), 7.17 (m, 3H), 7.01 (m, 2H), 6.78 (d, J = 7.57 Hz, 1H), 6.40 (s, 1H), 3.75 (hept, J = 6.4 Hz, 1H), 3.52 (hept, J = 6.6 Hz, 1H), 2.68 (d, J = 13.7 Hz, 1H), 2.56-2.44 (m, 1H), 2.32 (d, J = 13.7 Hz, 1H),

2.11-2.00 (m, 1H), 1.57 (d, *J* = 6.7 Hz, 3H), 1.53-1.44 (m, 4H), 1.39 (d, *J* = 6.5 Hz, 3H), 1.28 (s, 3H), 1.18-1.07 (m, 4H), 0.90 (d, *J* = 6.8 Hz, 3H), 0.50 (t, *J* = 7.4 Hz, 3H), -0.75 (d, *J* = 6.6 Hz, 3H). $^{13}C\{^{1}H\}$ NMR (THF-d_8, 126 MHz): *δ* 153.81, 151.17, 142.73, 141.51, 137.17, 128.09, 126.05, 125.61, 125.48, 125.36, 124.88, 123.93, 120.74, 120.58, 119.62, 119.50, 115.11, 110.13, 85.55, 65.16, 53.09, 51.19, 31.75, 31.31, 31.20, 28.95, 28.85, 27.35, 26.20, 25.49, 25.02, 23.67, 10.07, 8.93. Anal. Calcd. for $C_{34}H_{44}N_2$: C, 84.95; H, 9.23; N, 5.83. Found: C, 85.21; H, 8.95; N, 5.84.

2-Phenylbenzimidazole-^{Et}CAAC Insertion (4.3): A flame dried round bottom flask was charged with ^{Et}CAAC (0.66 g, 2.10mmol), 2-phenylbenzimidazole (0.40 g, 2.06 mmol), and 50 mL THF. The reaction was stirred for 30 minutes at room temperature followed by removal of volatiles *in vacuo*. Recrystallization from 1:2 THF/hexanes provided colorless analytically pure single crystals (0.45 g, 43%) that were suitable for X-ray diffraction. ^{1}H NMR (500 MHz, THF-d_8) δ 8.13 (d, *J* = 7.1 Hz, 1H), 7.55 (d, *J* = 7.1 Hz, 1H), 7.32 – 7.16 (m, 4H), 7.16-7.06 (m, 3H), 6.99 (d, *J* = 6.9 Hz, 1H), 6.61 (d, *J* = 6.7 Hz, 2H), 5.59 (s, 1H), 3.39 – 3.26 (m, 1H), 3.25 – 3.14 (m, 1H), 2.67 (d, *J* = 13.7 Hz, 1H), 2.28 (d, *J* = 13.7 Hz, 1H), 2.23-2.10 (m, 1H), 1.96-1.82 (m, 1H), 1.66 – 1.54 (m, 1H), 1.51 (s, 3H), 1.43-1.31 (m, 1H), 1.24 (s, 3H), 1.15 – 1.05 (m, 3H), 0.94 – 0.86 (m, 3H), 0.83 (t, *J* = 7.3 Hz, 3H), 0.61 (t, *J* = 7.3 Hz, 3H), 0.32 (d, *J* = 6.8 Hz, 3H), -0.45 (d, *J* = 6.7 Hz, 3H). $^{13}C\{^{1}H\}$ NMR (THF-d_8, 126 MHz): *δ* 156.30, 153.79, 151.71, 145.54, 137.24, 135.84, 134.10, 131.02, 129.68, 129.07, 128.45, 126.02, 125.58, 122.19, 121.19, 115.04, 87.95, 65.18, 52.73, 50.89, 31.46, 31.35, 28.92, 28.55, 26.28, 25.59, 25.07, 24.75, 9.79, 9.08. Anal. Calcd. for $C_{35}H_{45}N_3$: C, 82.79; H, 8.93; N, 8.28. Found: C, 82.41; H, 8.67; N, 8.26.

2-Phenylbenzimidazole-IPr Adduct (4.4): A flame dried round bottom flask was charged with IPr (1.00 g, 2.58 mmol), 2-phenylbenzimidazole (0.50 g, 2.58 mmol), and 50 mL THF. The reaction was stirred for 15 minutes at room temperature followed by removal of volatiles *in vacuo* to give an analytically pure white solid (quantitative). Recrystallization from 1:2 THF/hexanes provided single crystals suitable for X-ray diffraction. ^{1}H NMR (THF-d_8, 500 MHz): δ 13.74 (s, 1H), 8.37 (d, J = 7.3 Hz, 2H), 7.68 (s, 2H), 7.46 (t, J = 7.8 Hz, 2H), 7.34-7.27 (m, 6H), 7.15-7.05 (m, 3H), 6.79-6.73 (m, 2H), 2.63 (hept, J = 6.6, 4H), 1.20 (d, J = 6.9, 12H), 1.15 (d, J = 6.9, 12H). ^{13}C{^{1}H} NMR (THF-d_8, 126 MHz): δ 157.39, 146.52, 145.34, 136.32, 135.93, 131.12, 128.83, 128.13, 128.00, 125.13, 124.88, 120.03, 116.45, 29.74, 24.91, 23.92. Anal. Calcd. for $C_{40}H_{46}N_4$: C, 82.43; H, 7.96; N, 9.61. Found: C, 82.46; H, 8.06; N, 9.57.

Section 4.5: References

(1) Kieser, J. M.; Kinney, Z. J.; Gaffen, J. R.; Evariste, S.; Harrison, A. M.; Rheingold, A. L.; Protasiewicz, J. D. Three Ways Isolable Carbenes Can Modulate Emission of NH-Containing Fluorophores. *J. Am. Chem. Soc.* **2019**, *141*, 12055–12063.

(2) Bordwell, F. G.; Drucker, G. E.; Fried, H. E. Acidities of Carbon and Nitrogen Acids: The Aromaticity of the Cyclopentadienyl Anion. *J. Org. Chem.* **1981**, *46*, 632–635.

(3) Walba, H.; Isensee, R. W. Acidity Constants of Some Arylimidazoles and Their Cations. *J. Org. Chem.* **1961**, *26*, 2789–2791.

(4) Arduengo, Anthony J., I.; Gamper, S. F.; Tamm, M.; Calabrese, J. C.; Davidson, F.; Craig, H. A. A Bis(Carbene)—Proton Complex: Structure of a C—H—C Hydrogen Bond. *J. Am. Chem. Soc.* **1995**, *117*, 572–573.

(5) Cowan, J. A.; Clyburne, J. A. C.; Davidson, M. G.; Harris, R. L. W.; Howard, J. A. K.; Küpper, P.; Leech, M. A.; Richards, S. P. On the Interaction between N-Heterocyclic Carbenes and Organic Acids: Structural Authentication of the First N-H ... C Hydrogen Bond and Remarkably Short C-H ... O Interactions. *Angew. Chem. Int. Ed.* **2002**, *41*, 1432–1434.

(6) Shih, W. C.; Wang, C. H.; Chang, Y. T.; Yap, G. P. A.; Ong, T. G. Synthesis and Structure of an Amino-Linked N-Heterocyclic Carbene and the Reactivity of Its Aluminum Adduct. *Organometallics* **2009**, *28*, 1060–1067.

(7) Movassaghi, M.; Schmidt, M. A. N-Heterocyclic Carbene-Catalyzed Amidation of Unactivated Esters with Amino Alcohols. *Org. Lett.* **2005**, *7*, 2453–2456.

(8) Li, C. Y.; Kuo, Y. Y.; Tsai, J. H.; Yap, G. P. A.; Ong, T. G. Amine-Linked N-Heterocyclic Carbenes: The Importance of an Pendant Free-Amine Auxiliary in Assisting the Catalytic Reaction. *Chem. - Asian J.* **2011**, *6*, 1520–1524.

(9) Raut, A. H.; Karir, G.; Viswanathan, K. S. Matrix Isolation Infrared and Ab Initio Study of the Interaction of N-Heterocyclic Carbene with Water and Methanol: A Case Study of a Strong Hydrogen Bond. *J. Phys. Chem. A* **2016**, *120*, 9390–9400.

(10) Hollóczki, O. Unveiling the Peculiar Hydrogen Bonding Behavior of Solvated N-Heterocyclic Carbenes. *Phys. Chem. Chem. Phys.* **2016**, *18*, 126–140.

(11) Del Bene, J. E.; Alkorta, I.; Elguero, J. Hydrogen-Bonded Complexes with Carbenes as Electron-Pair Donors. *Chem. Phys. Lett.* **2017**, *675*, 46–50.

(12) Standard, J. M. Effects of Solvation and Hydrogen Bond Formation on Singlet and Triplet Alkyl or Aryl Carbenes. *J. Phys. Chem. A* **2017**, *121*, 381–393.

(13) Giffin, N. A.; Makramalla, M.; Hendsbee, A. D.; Robertson, K. N.; Sherren, C.; Pye,

C. C.; Masuda, J. D.; Clyburne, J. A. C. Anhydrous TEMPO-H: Reactions of a Good Hydrogen Atom Donor with Low-Valent Carbon Centres. *Org. Biomol. Chem.* **2011**, *9*, 3672–3680.

(14) Schmidt, M. A.; Müller, P.; Movassaghi, M. On the Interactions of N,N′-Bismesitylimidazolin-2-Yl and Alcohols. *Tetrahedron Lett.* **2008**, *49*, 4316–4318.

(15) Alkorta, I.; Rozas, I.; Elguero, J. Non-Conventional Hydrogen Bonds. *Chem. Soc. Rev.* **1998**, *27*, 163–170.

(16) Brown, A. B.; Gibson, T. L.; Baum, J. C.; Ren, T.; Smith, T. M. Fluorescence-Enhancement Sensing of Ammonia and Hydrazines via Disruption of the Internal Hydrogen Bond in a Carbazolopyridinophane. *Sensors Actuators, B Chem.* **2005**, *110*, 8–12.

(17) El-Bayoumi, M. A.; Kasha, M. Energy Transfer in Hydrogen-Bonded *N* -Heterocyclic Complexes and Their Possible Role as Energy Sinks. *J. Chem. Phys.* **1961**, *34*, 2181–2182.

(18) Emsley, J. Very Strong Hydrogen Bonding. *Chem. Soc. Rev.* **1968**, *9*, 91–124.

(19) Martin, M. M.; Ware, W. R. Fluorescence Quenching of Carbazole by Pyridine and Substituted Pyridines. Radiationless Processes in the Carbazole-Amine Hydrogen Bonded Complex. *J. Phys. Chem.* **1978**, *82*, 2770–2776.

(20) Tanaka, F.; Kato, M.; Mataga, N. Electronic Energy Transfers in Intermolecular Hydrogen Bonded Systems: Sensitization of Quinoline Phosphorescence in the Carbazole—Quinoline System. *Zeitschrift für Phys. Chemie* **1970**, *70*, 104–112.

(21) Mataga, N.; Tanaka, F.; Kato, M. Electronic Energy Relaxation Processes in the Intermolecular Hydrogen-Bonded Systems. *Acta Phys. Pol.* **1968**, *34*, 733–745.

(22) Catalán, J.; Mena, E.; Fabero, F.; Amat-Guerri, F. The Role of the Torsion of the Phenyl Moiety in the Mechanism of Stimulated Ultraviolet Light Generation in 2-Phenylbenzazoles. *J. Chem. Phys.* **1992**, *96*, 2005–2016.

(23) Frey, G. D.; Lavallo, V.; Donnadieu, B.; Schoeller, W. W.; Bertrand, G. Facile Splitting of Hydrogen at a Single Carbon Center. *Science* **2007**, *316*, 439–441.

(24) Melaimi, M.; Jazzar, R.; Soleilhavoup, M.; Bertrand, G. Cyclic (Alkyl)(Amino)Carbenes (CAACs): Recent Developments. *Angew. Chem. Int. Ed.* **2017**, *56*, 10046–10068.

(25) Paul, U. S. D.; Radius, U. Ligand versus Complex: C−F and C−H Bond Activation of Polyfluoroaromatics at a Cyclic (Alkyl)(Amino)Carbene. *Chem. - Eur. J.* **2017**, *23*, 3993–4009.

(26) Tolentino, D. R.; Neale, S. E.; Isaac, C. J.; Macgregor, S. A.; Whittlesey, M. K.; Jazzar, R.; Bertrand, G. Reductive Elimination at Carbon under Steric Control. *J. Am. Chem. Soc.* **2019**, 8–11.

(27) Perez, F.; Ren, Y.; Boddaert, T.; Rodriguez, J.; Coquerel, Y. A Stable N-Heterocyclic Carbene Organocatalyst for Hydrogen/Deuterium Exchange Reactions between Pseudoacids and Deuterated Chloroform. *J. Org. Chem.* **2015**, *80*, 1092–1097.

(28) Chu, M.; Scioneaux, A. N.; Hartley, C. S. Solution-Phase Dimerization of an Oblong Shape-Persistent Macrocycle. *J. Org. Chem.* **2014**, *79*, 9009–9017.

(29) Martin, R. B. Comparisons of Indefinite Self-Association Models. *Chem. Rev.* **2002**, *96*, 3043–3064.

(30) Spencer, T. S.; O'Donnell, C. M. Energy Transfer in a Hydrogen-Bonded

Carbazole–Benzophenone Complex. *J. Am. Chem. Soc.* **1972**, *94*, 4846–4849.

(31) Stejskal, E. O.; Tanner, J. E. Spin Diffusion Measurements: Spin Echoes in the Presence of a Time-Dependent Field Gradient. *J. Chem. Phys.* **1965**, *42*, 288–292.

(32) Johnson, C. S. Diffusion Ordered Nuclear Magnetic Resonance Spectroscopy: Principles and Applications. *Prog. Nucl. Magn. Reson. Spectrosc.* **1999**, *34*, 203–256.

(33) Neufeld, R.; Stalke, D. Accurate Molecular Weight Determination of Small Molecules via DOSY-NMR by Using External Calibration Curves with Normalized Diffusion Coefficients. *Chem. Sci.* **2015**, *6*, 3354–3364.

(34) Romero-Ale, E. E.; Olives, A. I.; Martín, M. A.; Del Castillo, B.; López-Alvarado, P.; Menéndez, J. C. Environmental Effects on the Fluorescence Behaviour of Carbazole Derivatization Reagents. *Luminescence* **2005**, *20*, 162–169.

(35) Schroeder, W. A.; Wilcox, P. E.; Trueblood, K. N.; Dekker, A. O. Ultraviolet and Visible Absorption Spectra in Ethyl Alcohol. *Anal. Chem.* **1951**, *23*, 1740–1747.

(36) Brown, A. B.; Gibson, T. L.; Baum, J. C.; Ren, T.; Smith, T. M. Fluorescence-Enhancement Sensing of Ammonia and Hydrazines via Disruption of the Internal Hydrogen Bond in a Carbazolopyridinophane. *Sensors Actuators, B Chem.* **2005**, *110*, 8–12.

(37) Catalán, J.; De Paz, J. L. G.; del Valle, J. C.; Kasha, M. Inter-Ring Torsional Modulation in Molecular Lasers. Ultraviolet Lasing via Amplified Spontaneous Emission Spectroscopy of Phenylimidazoles. *J. Phys. Chem. A* **1997**, *101*, 5284–5291.

(38) Pi, C.; Yu, X.; Zheng, W. Imidazolium 1,3-Benzazaphospholide Ion Pairs with

Strong C-H···N Hydrogen Bonds - Synthesis, Structures, and Reactivity. *Eur. J. Inorg. Chem.* **2015**, *2015*, 1804–1810.

(39) Magill, A. M.; Cavell, K. J.; Yates, B. F. Basicity of Nucleophilic Carbenes in Aqueous and Nonaqueous Solvents - Theoretical Predictions. *J. Am. Chem. Soc.* **2004**, *126*, 8717–8724.

(40) Cook, J. L.; Hunter, C. A.; Low, C. M. R.; Perez-Velasco, A.; Vinter, J. G. Solvent Effects on Hydrogen Bonding. *Angew. Chem. Int. Ed.* **2007**, *46*, 3706–3709.

(41) Bordwell, Frederick, G. Equilibrium Acidities in Dimethyl Sulfoxide Solution. *Acc. Chem. Res.* **1988**, *21*, 456–463.

(42) Sessler, C. D.; Rahm, M.; Becker, S.; Goldberg, J. M.; Wang, F.; Lippard, S. J. CF2H, a Hydrogen Bond Donor. *J. Am. Chem. Soc.* **2017**, *139*, 9325–9332.

(43) Gillis, E. P.; Eastman, K. J.; Hill, M. D.; Donnelly, D. J.; Meanwell, N. A. Applications of Fluorine in Medicinal Chemistry. *J. Med. Chem.* **2015**, *58*, 8315–8359.

(44) Zafrani, Y.; Yeffet, D.; Sod-Moriah, G.; Berliner, A.; Amir, D.; Marciano, D.; Gershonov, E.; Saphier, S. Difluoromethyl Bioisostere: Examining the "Lipophilic Hydrogen Bond Donor" Concept. *J. Med. Chem.* **2017**, *60*, 797–804.

(45) Arduengo, Anthony J., I.; Krafczyk, R.; Schmutzler, R.; Craig, H. A.; Goerlich, J. R.; Marshall, W. J.; Unverzagt, M. Imidazolylidenes, Imidazolinylidenes and Imidazolidines. *Tetrahedron* **1999**, *55*, 14523–14534.

(46) Mahoney, J. K.; Martin, D.; Moore, C. E.; Rheingold, A. L.; Bertrand, G. Bottleable (Amino)(Carboxy) Radicals Derived from Cyclic (Alkyl)(Amino) Carbenes. *J. Am. Chem. Soc.* **2013**, *135*, 18766–18769.

Chapter 5: Development of Modified *N*-Heterocyclic Carbenes with Enhanced Luminescence Quenching Ability

Section 5.1: Introduction

As mentioned in **Chapter 4**, compounds **4.2** and **4.3** inspired us to further explore tuning the photophysical properties of these compounds by developing modified carbenes. Specifically, the close proximity of a methyl group on the diisopropylphenyl substituent in **4.2** or **4.3** and the π-system of the parent fluorophore, 3.343 Å for **4.2** (as shown in **Figure 5.1**) and 3.211 Å for **4.3**, suggested that if we could position a heavy atom, such as bromine, at this location we could increase the rate of intersystem crossing into the triplet manifold through the heavy atom effect.[1–3] This has been shown to follow an exponential dependence on distance, suggesting the geometry afforded by **4.2** and **4.3** could help us exploit such an effect.[4] Indeed, substituting bromine atoms in place of isopropyl groups in **4.2** and optimizing the resulting structure at the GFN2-xTB level[5,6] results in a small intramolecular distance, 3.162 Å, between the bromine atom and plane of the carbazole.

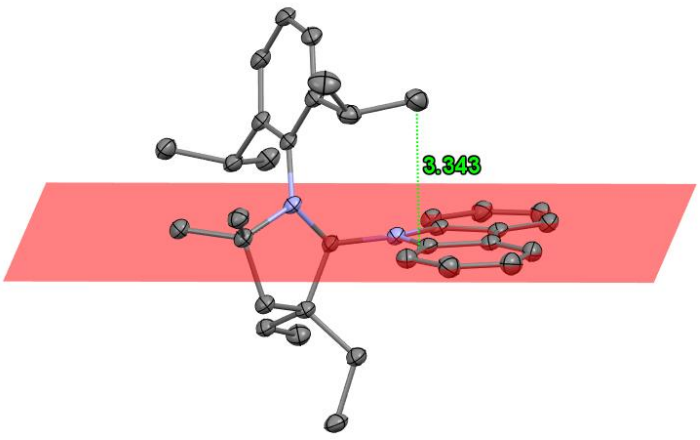

Figure 5.1: ORTEP diagram of **4.2**, detailing short intramolecular distance between Dipp group and the plane defined by carbazole unit.

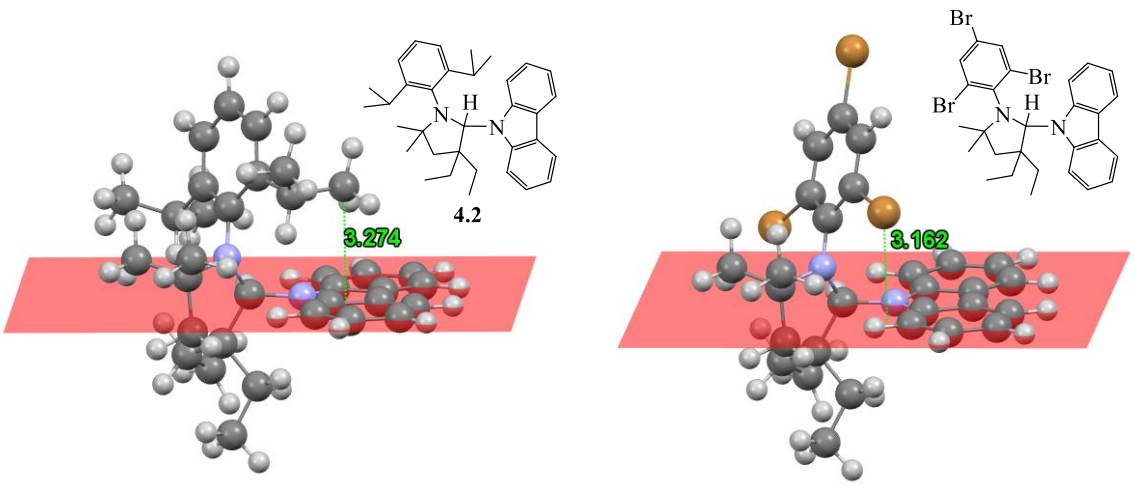

Figure 5.2: Optimized geometries (GFN2-xTB) of **4.2** and proposed structurally similar product from reaction of carbazole with bromine-substituted CAAC.

For carbazole, this has been previously reported through intermolecular interactions with bromine or iodine-containing compounds.[7,8] However, if the non-radiative decay rate is sufficiently small, increased phosphorescence emission will be observed along with the loss of fluorescence emission. Such an instance was observed for bromoalkyl-substituted carbazole derivatives which displayed room-temperature phosphorescence in the solid state.[9] As well, this design strategy has been utilized toward the development of other organic phosphors.[10,11] Regardless if we observe increased emission quenching or a shift instead to phosphorescence, the development of a carbene that could enhance the intersystem crossing rate would not only be beneficial toward advancing our work but also impact luminescent metal-complexes incorporating carbene ligands.

While synthesis of NHCs allows for a large variation to steric and electronic properties, inclusion of halogens into the carbene structure is comparatively unexplored. **Scheme 5.1** summarizes some halogen-containing carbenes or carbene complexes.[12–17]

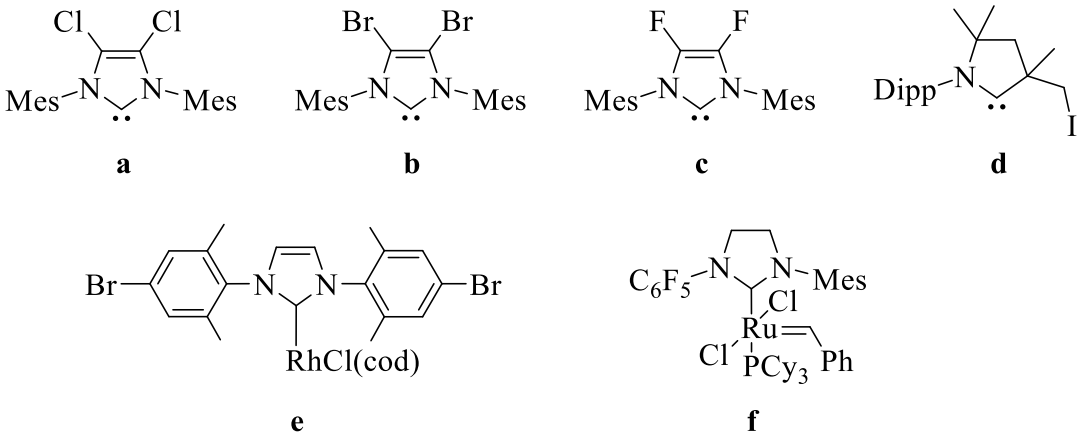

Scheme 5.1: Representative carbene and carbene complexes incorporating halogen atoms.

Chlorination of the carbene backbone to afford **a** was described in early work by Arduengo through the reaction of, for example, 1,3-bis(2,4,6-trimethylphenyl)imidazole-2-ylidene (IMes) and carbontetrachloride.[12] Unlike the starting carbene, the addition of chlorines withdraw enough electron density away from the carbene center to make the product air-stable. Likewise, bromination of the backbone can occur through reaction of IMes and carbon tetrabromide to afford **b**.[13] As expected, addition of an electronegative atom at this position again produces a more air-stable carbene, though less so than chlorine substitution as the product was observed to decompose over a week in moist air. Fluorination in a similar form to the previous reactions was not as successful, though the substitution was possible on a carbene complex. The backbone of IMes could be deprotonated while coordinated to Mn(I), fluorinated via *N*-fluorobenzenesulfonamide, and isolated as the triflate salt of **c** after workup with triflic acid.[14] These examples, however represent a halogen atom positioned in a remote location on the carbene relative to where we would expect our fluorophore to be bound. Given the ease of synthesis, we attempted a reaction between Ph-BIM and a brominated IPr (IPrBr, an analog of compound

b in **Scheme 5.1**),[13] however crystallographic analysis only provided us a structure for the imidazolium bromide salt, [IPrBrH][Br] as shown in **Scheme 5.2(b)**. This presents a secondary problem with substitution on the backbone of these carbenes, the halogen can be non-innocent in our reactions.

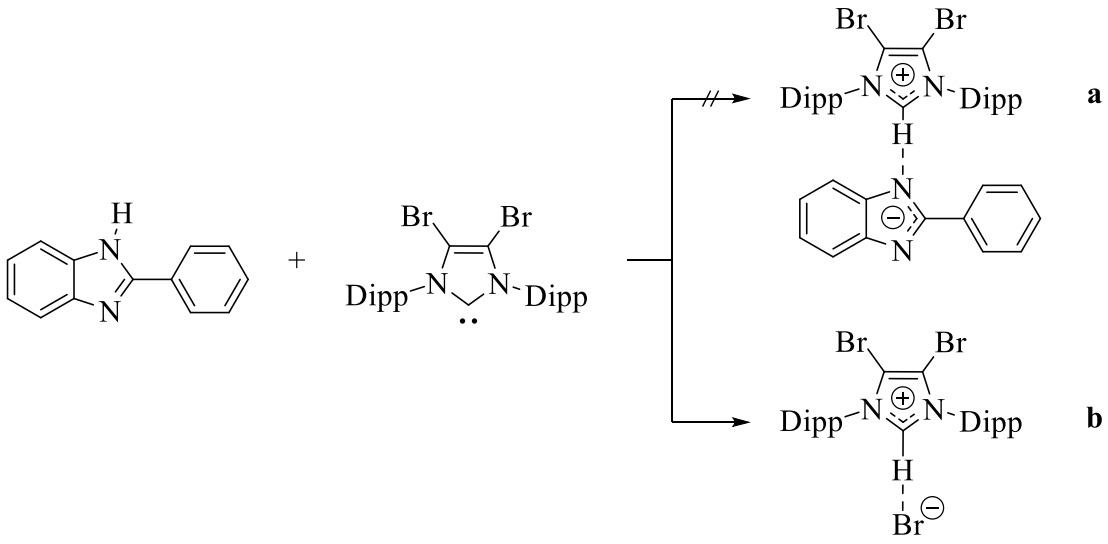

Scheme 5.2: Reaction between brominated carbene, IPrBr, and 2-phenylbenzimidazole.

Therefore our target carbene shifted towards examples which would both position the halogen closer to the fluorophore, such as at the 2- or 6- position on the *N*-substituted aryl group, as well as provide for a more inert C-X bond. Examples of this type of substitution can be found in rhodium (**e**) or ruthenium (**f**) complexes in **Scheme 5.1**, however these examples either included bromine as a remote substituent or only included fluorine at the position we were most interested in.[15,16] Bertrand also showed a very similar example for the type of substitution we were interested in with hemilabile CAACs, however the alkyliodide substituted free carbene shown in **Scheme 5.1(d)**, specifically, decomposed within hours.[17] We therefore projected a series of reactions whereby adjustment of the starting aniline used in the typical synthetic pathways for NHCs could

afford us a carbene incorporating 2,4,6-tribromophenyl groups in place of the usual 2,6-diisopropyl groups, as shown in **Scheme 5.3**.

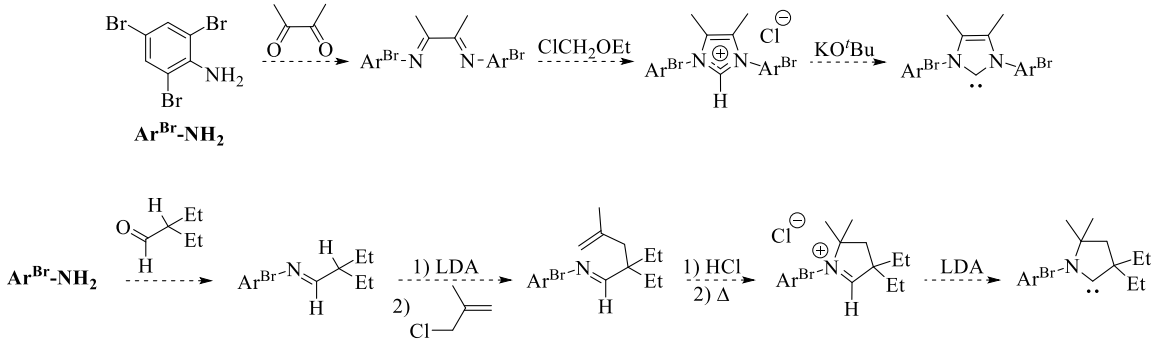

Scheme 5.3: Proposed synthetic pathways toward production of two types of brominated carbenes.

Section 5.2: Results and Discussion

Section 5.2.1: Condensation Reactions to Produce Diimines Utilizing Halogenated Anilines

Our first target continued with a focus on imidazolylidene type carbenes. The multistep synthesis for making these carbenes is well studied, simple, and scalable to the hundred gram scale or greater. Therefore, we attempted to modify the synthesis of IPr[12] by using 2,4,6-tribromoaniline instead of 2,6-diisopropylaniline. As well, 2,3-butanedione was used in place of glyoxal to ultimately give a carbene with C-Me instead of C-H functionality on the backbone. Unfortunately, the reduced nucleophilicity of the halogenated aniline had a detrimental effect on the initial condensation reaction with butanedione, as shown in **Scheme 5.4**, and we were only able to isolate the pure diimine in 15% yield after attempting the reaction with multiple solvents, catalysts, and other conditions.

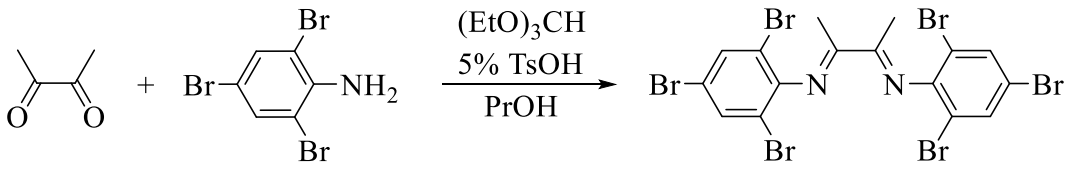

5.1

Scheme 5.4: Condensation reaction of 2,3-butanedione and 2,4,6-tribromoaniline.

Furthermore, the next step of this synthesis, reaction with either chloromethylethyl ether (as shown in **Scheme 5.3**(top)) or formaldehyde to form the imidazolium salt, would also be greatly affected by the changes to the electronics on each nitrogen atom. We did attempt to solve this problem by templating this reaction with zinc chloride, similar to reported procedure to form an extremely bulky carbene salt,[18] however this was not successful.

Section 5.2.2: Metal Catalyzed Heterometathesis as Method to Produce Carbene Precursors from Halogenated Anilines

Based on the difficulty of performing this condensation reaction effectively, we shifted our focus temporarily to a brominated CAAC instead of imidazolylidene. Although the synthesis of each class of carbene starts with a condensation reaction to form an imine, the synthesis of a CAAC salt does not require additional reactivity on nitrogen other than a final step where an iminium is used in a proton-transfer with a terminal alkene, as shown in **Scheme 5.3**(bottom).[19] Therefore, our modification of starting aniline would not be as detrimental in the overall reaction pathway. However, the difficulty in performing the initial condensation between bromine-substituted aniline and 2-ethylbutyraldehyde remained, and we have found this reaction more difficult when synthesizing CAAC salts than for imidazolium salts.

We then discovered that a synthesis for imines, specifically from electron poor anilines, had already been developed. However, unlike the typical condensation reaction, the imine was formed via catalyzed heterometathesis using a silica supported vanadium, molybdenum, tantalum, or titanium catalyst.[20–22] Contrasting the more well-known C=C metathesis reactions, the heterometathesis provided in **Scheme 5.5** produces a C=N bond from an *N*-sulfinylamine and either aldehyde or ketone coupled with a loss of SO_2.

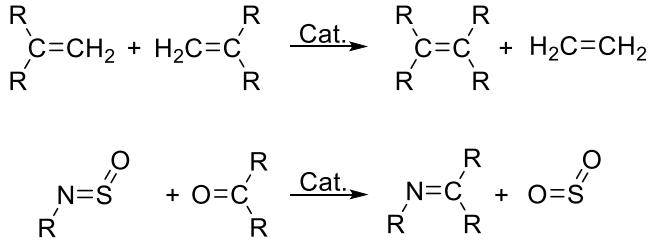

Scheme 5.5: Simple metathesis and heterometathesis reactions.

The supported vanadium catalyst offered the simplest path to entry as we were able to purchase the vanadium oxychloride pre-catalyst directly. The supported titanium complex, obtained through a multi-step synthesis, was shown to be much more active than vanadium (5 min vs 12 hour reactions), however the vanadium catalyzed metathesis was sufficient for our initial reactions moving forward.

Instead of directly using tribromoaniline, we first had to synthesize the *N*-sulfinyl derivative for use in this reaction. As shown in **Scheme 5.6**, the reaction using this aniline derivative, obtained from a standard bromination procedure, is simple and remains relatively unchanged from earlier reports.[23,24]

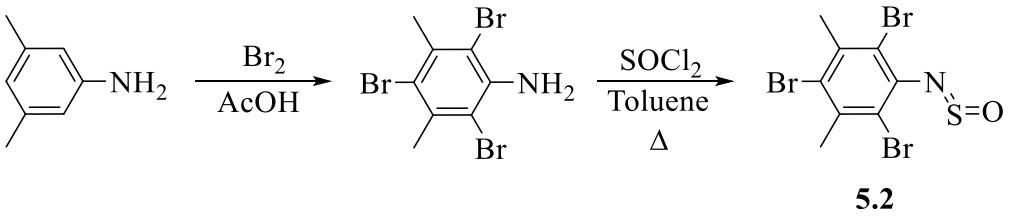

5.2

Scheme 5.6: Synthesis of *N*-sulfinyl-2,4,6-tribromo-3,5-dimethylaniline (**5.2**).

Once the proper reagents and catalyst were readied, the reaction to form imine **5.3**, as shown in **Scheme 5.7**, proceeds as reported.[25] Once the *N*-sulfinylaniline and aldehyde have been added to a slurry of the supported catalyst in either toluene or heptane, the reaction was refluxed for 2-3 days to complete the heterometathesis. Note, however, that failure to add the aldehyde quickly can result in a reaction between *N*-sulfinylamine and the metal-imido complex that is formed *in situ*, giving a sulfurdiimine.

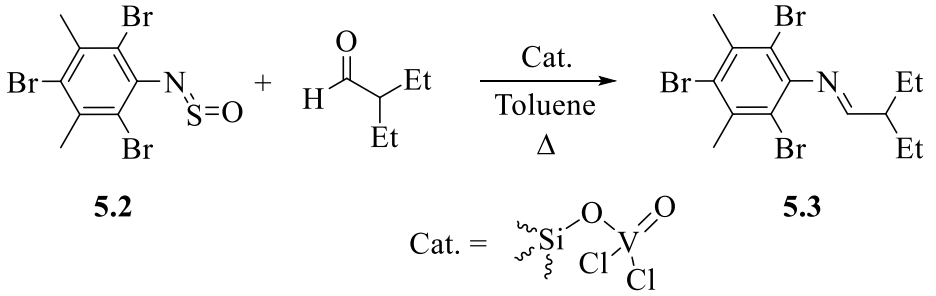

5.2 **5.3**

Scheme 5.7: Heterometathesis reaction to form imine **5.3**.

Section 5.2.3: Toward a Halogen-substituted Cyclic (alkyl)(amino)carbene Salt

While the reaction to form our desired imine had succeeded, we did encounter additional difficulties due to **5.3** showing a much greater sensitivity toward hydrolysis, reforming our starting aniline, than we had encountered with other imines typically used in the synthesis of carbenes. As mentioned previously, the imines used to form IPr and also CAAC salts can be synthesized on a large scale and stored for years without decomposition. However, **5.3** decomposed within days to 2,4,6-tribromo-3,5-dimethylaniline.

Furthermore, our attempts to purify it via column chromatography were not completely successful. We did find that adequate purity could be obtained by concentrating the reaction filtrate containing **5.3** and eluting through a short column of neutral alumina with 6:1 pentane:ether. This technique still resulted in a small concentration of impurities in the eluent, as shown in **Figure 5.3**, however the purity obtained was sufficient for proceeding with further steps.

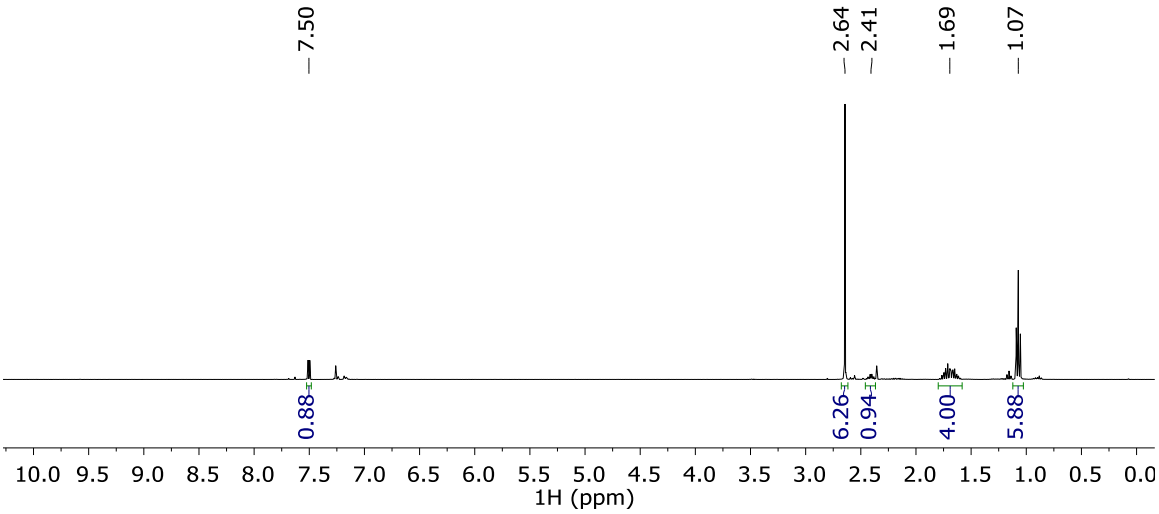

Figure 5.3: ^{1}H NMR (400 MHz, $CDCl_3$) spectrum of **5.3**.

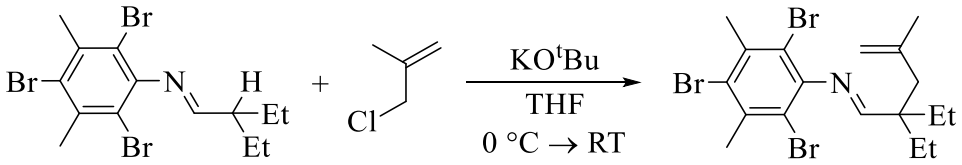

5.3 **5.4**

Scheme 5.8: Alkylation of **5.3** with 3-chloro-2-methylpropene to give **5.4**.

Based on a modified procedure for synthesizing the ^{Et}CAAC salt,[26] we attempted to alkylate **5.3** as given in **Scheme 5.8**. This represented a significant problem not discussed previously due to potential side reactions had our starting aniline been 2,4,6-tribromoaniline. We initially attempted the procedure with this aniline, however the strong base required by the reaction in **Scheme 5.8**, in our hands ^{n}BuLi is typically used for this

step, could result in lithiation of the arene ring and subsequent elimination of LiBr to form an unstable aryne. Addition of methyl groups at the 3- and 5- positions presumably limits the possibility of this type of side reaction, and we later found that weaker bases, such as KO^{t}Bu, were able to deprotonate **5.3** effectively. Addition of **5.3** to a solution of KO^{t}Bu and 3-chloro-2-methylpropene in THF gave a 2:1 mixture of **5.4**:**5.3** as shown in **Figure 5.4**.

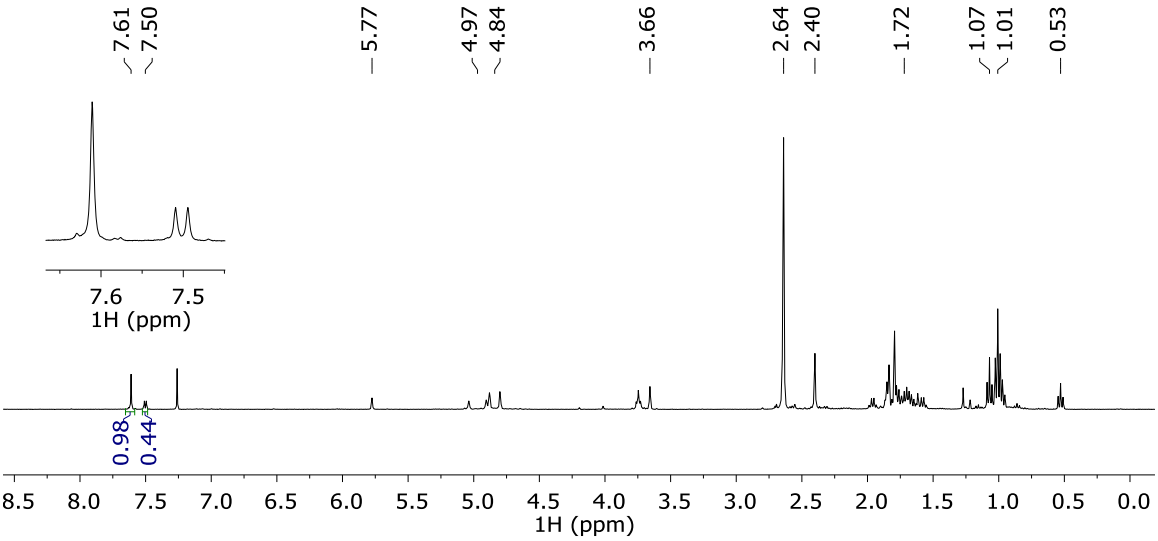

Figure 5.4: ^{1}H NMR (400 MHz, $CDCl_3$) spectrum of crude reaction mixture of **5.4**.

Attempts to purify **5.4** in a similar manner to **5.3** only resulted in substantial decomposition to produce the starting aniline, so the mixture was used immediately without further purification if **5.4** was present as a large percentage of the mixture.

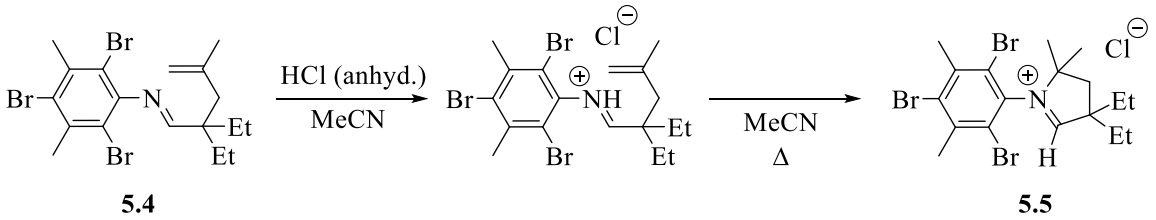

5.4 **5.5**

Scheme 5.9: Synthesis of brominated CAAC salt (**5.5**).

We had determined from earlier results involving the synthesis of the ^{Et}CAAC salt that washing with THF provided a pure product. Based on this, we proposed that an impure sample of **5.4** could be used for the synthesis of **5.5** provided this purification step was equally effective. Synthesis of the CAAC salt followed the reactions shown in **Scheme 5.9**, again modified from the synthesis of the ^{Et}CAAC salt.[26] First, the imine was protonated by an anhydrous solution of HCl and then the resulting iminium was cyclized. Compound **5.5** was isolated as a pure gray solid after washing with THF, NMR analysis provided in **Figure 5.5** and **Figure 5.6**, though the yield was low.

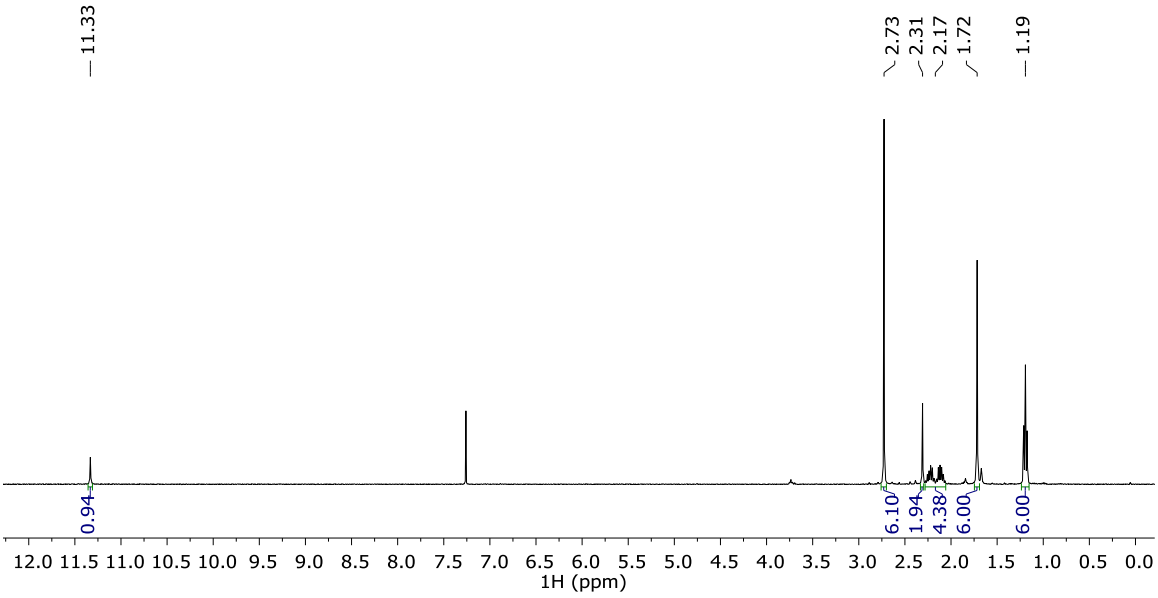

Figure 5.5: ^{1}H NMR (400 MHz, $CDCl_3$) spectrum of **5.5.**

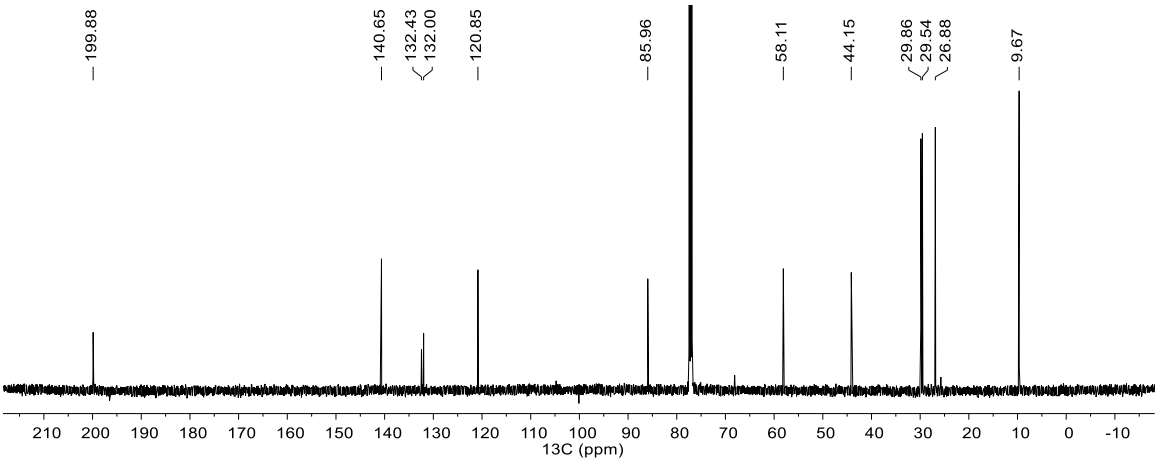

Figure 5.6: ^{13}C NMR (126 MHz, $CDCl_3$) spectrum of **5.5.**

One method we have yet to fully explore is to reorganize the order of the overall reaction scheme to make **5.5**. CAACs have also been synthesized from similar, though slightly different procedures.[27] The strong bases used **Scheme 5.8**, typically ^{n}BuLi or LDA, require significant training to handle safely, therefore the alkylation with 3-chloro-2-methylpropene could first be carried out on the starting aldehyde using NaOH. Condensation of this substituted aldehyde with an aniline provides an imine that can be used per the usual synthetic route.

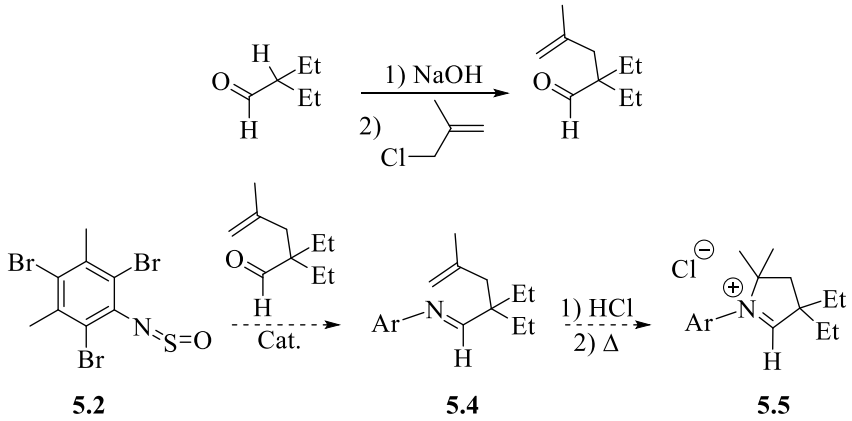

Scheme 5.10: Reorganized synthetic pathway towards formation of **5.5**.

Using a similar plan, given by **Scheme 5.10**, we could theoretically perform the heterometathesis reactions immediately prior to the reaction in **Scheme 5.9** and bypass impurities which we found difficult to separate once the imine had been formed. However, the effect of adding a terminal alkene to the aldehyde has not yet been examined for compatibility with this catalyst system.

Section 5.3: Conclusions and Future Directions

The results shown in **Chapter 5** show that the first stage of this project has reached a critical point: we have isolated a suitable brominated carbene salt. Progressing from here involves both continuing to refine our synthesis of **5.5** as well as determining its reactivity. We chose to maintain the diethyl- substitution so as to have a better comparison to our results in **Chapter 4**, given we can obtain similar products to **4.2** and **4.3**. However, removal of the isopropyl groups will also yield a less bulky carbene center and therefore we could potentially find that deprotonation of **5.5** results in a non-isolable carbene. We can easily employ larger aldehydes in the reactions we have already developed in order to isolate a CAAC salt with more steric bulk added by the alkyl substituents, making up for the loss of the isopropyl groups. Additionally, it has been shown that extremely small, otherwise non-isolable CAACs can be generated *in situ*.[28] Using a similar approach, we could react **5.5** directly with *N*-lithiocarbazole to form a product similar to **4.2**.

Section 5.4: Experimental

General Considerations: Unless otherwise stated, all chemicals were purchased from commercial sources and used without further purification. Tetrahydrofuran and toluene were purified using an MBraun solvent purification system. 10V-SiO25 catalyst was prepared according to literature procedure.[20] 2,4,6-tribromo-3,5-dimethylaniline was

prepared from a standard bromination procedure. NMR spectra were recorded on a Bruker AVANCE III 500 MHz or Varian Inova 400 MHz spectrometers and chemical shifts referenced to residual solvent signal.

Synthesis of *N*,*N*'-bis(2,4,6-tribromophenyl)butane-2,3-diimine (5.1): To a 100 mL flask was added 2,4,6-tribromoaniline (16.5 g, 50 mmol), 1-propanol (60 mL), 2,3-butanedione (2.2 mL, 25.1 mmol), triethylorthoformate (16 mL, 111 mmol), and *p*-toluenesulfonic acid (0.21 g, 1.1 mmol). The slurry was stirred rapidly for 6 days. Precipitate from reaction was filtered and washed with 3x 20 mL 1-propanol then dried under vacuum, 4.84 g. Recrystallization from 1-propanol gave yellow rods, 2.62 g, 15%. ^{1}H NMR ($CDCl_3$, 400 MHz): δ 7.73 (s, 4H), 2.14 (s, 6H). ^{13}C NMR ($CDCl_3$, 126 MHz): δ 171.70, 146.87, 134.44, 116.75, 113.27, 17.28.

Synthesis of *N*-sulfinyl-2,4,6-tribromo-3,5-dimethylaniline (5.2): Thionyl chloride (15 mL, 119 mmol) was added to a solution of 2,4,6-tribromo-3,5-dimethylaniline (7.368 g, 20.6 mmol) in 100 mL benzene (or toluene). Reaction was then refluxed for 2 days. Upon cooling, volatiles were removed via rotary evaporation to give a yellow solid which was further dried under high-vacuum, 8.08 g, 97%. ^{1}H NMR ($CDCl_3$, 500 MHz): δ 2.67 (s, 6H). ^{13}C NMR ($CDCl_3$, 126 MHz): δ 139.58, 138.33, 125.36, 114.23, 26.09.

Synthesis of 5.3 via vanadium catalyzed heterometathesis: *N*-sulfinyl-2,4,6-tribromo-3,5-dimethylaniline (6.418 g, 15.9 mmol) was added over a counterstream of argon to a slurry of 10V-SiO25 catalyst (1.26 g) in 100 mL dry toluene. Directly after, 2-ethylbutyraldehyde (2.05 mL, 16.7 mmol) was added via syringe and the resulting dark suspension was refluxed under argon for 3 days. After cooling, the catalyst was removed by filtration through celite and filtrate concentrated to a brown oil. This oil was passed

through a short column of neutral alumina (6:1 pentane:ether as eluent) and first band collected. Concentrating this fraction gave a red-orange oil, 4.5 g, 64%. ^{1}H NMR ($CDCl_3$, 400 MHz): δ 7.50 (d, *J* = 6.01 Hz, 1H), 2.64 (s, 6H), 2.44-2.37 (m, 1H), 1.78-1.60 (m, 4H), 1.07 (t, *J* = 7.47 Hz, 6H).

Synthesis of 3,3-diethyl-5-methylhex-5-en-2-one: Tetrabutylammonium bromide (0.94 g, 11 mol%) was added to 200 mL toluene followed by 2-ethylbutyraldehyde (2.58 g, 25.8 mmol) and slow addition of NaOH (40 g in 50 mL water). After stirring for 5 minutes, 3-chloro-2-methylpropene (5.18 g, 57.2 mmol) was added and reaction stirred rapidly overnight. After, organic layer was separated and aqueous layer extracted with additional toluene. Combined organics dried over sodium sulfate and concentrated to yellow oil under rotary evaporation. This was purified by fractional vacuum distillation (25 °C, 0.02 mmHg) discarding fraction that distilled at < 0 °C. Distillate was then loaded into pressure tube and heated at 175 °C for 16 hours, 5.07 g. ^{1}H NMR ($CDCl_3$, 400 MHz): 9.50 (s, 1H), 4.82 (s, 1H), 4.69 (s, 1H), 2.26 (s, 2H), 1.68-1.41 (m, 7H), 0.79 (t, *J* = 7.54 Hz, 6H).

Deprotonation and alkylation of 5.3 to give 5.4: A solution of KO^{t}Bu (0.153 g, 1.36 mmol) in dry THF (15 mL) was cooled to 0 °C prior to addition of 3-chloro-2-methylpropene (1.0 mL, 10.2 mmol) via syringe. After, a solution of **5.3** (0.556 g, 1.26 mmol) in 5 mL dry THF was added dropwise via syringe resulting in a transition from colorless to yellow to ruby. The solution warmed slowly and stirred under argon for overnight. After, the now yellow-orange solution was concentrated to a very thick orange oil and used without further purification. Reaction progress assessed by ^{1}H NMR imine resonance (δ = 7.50 (d, *J* = 6.01 Hz, 1H) for **5.3** and δ = 7.61 (s, 1H) for **5.4**).

Synthesis of brominated ^{Et}CAAC salt (5.5): Crude **5.4** (approx. 0.8 mmol) was added to 10 mL dry MeCN and stirred vigorously to produce a suspension which was cooled to 0 °C. Anhydrous HCl (0.7 mL, 4.35 M in dioxane, 3 mmol) was added dropwise to this and the resulting tan slurry warmed to RT and stirred an additional 1 hour. After stirring, the mixture was transferred to a nitrogen filled pressure tube, sealed, and heated at 80 °C overnight. The resulting dark brown solution was concentrated to a sticky, black solid which was washed with 10 mL THF and dried under vacuum to give a gray powder, 0.20 g. ^{1}H NMR ($CDCl_3$, 400 MHz): 11.33 (s, 1H), 2.73 (s, 6H), 2.31 (s, 2H), 2.28-2.06 (m, 4H), 1.72 (s, 6H), 1.19 (t, J = 7.49 Hz, 6H). ^{13}C NMR ($CDCl_3$, 126 MHz): 199.88, 140.65, 132.43, 132.00, 120.85, 85.96, 58.11, 44.15, 29.86, 29.54, 26.88, 9.67.

Section 5.5: References

(1) McGlynn, S. P.; Sunseri, R.; Christodouleas, N. External Heavy-Atom Spin-Orbital Coupling Effect. I. The Nature of the Interaction. *J. Chem. Phys.* **1962**, *37*, 1818–1824.

(2) El-Sayed, M. A. The Triplet State: Its Radiative and Nonradiative Properties. *Acc. Chem. Res.* **1968**, *1*, 8–16.

(3) Artyukhov, V. Y.; Morev, A. V.; Morozova, Y. P.; Pomogaev, V. A. Investigation of the Heavy-Atom Effect on the Spectral-Luminescent Properties of Dichloroanilines. *Russ. Phys. J.* **2002**, *45*, 1203–1207.

(4) Rae, M.; Fedorov, A.; Berberan-Santos, M. N. Fluorescence Quenching with Exponential Distance Dependence: Application to the External Heavy-Atom Effect. *J. Chem. Phys.* **2003**, *119*, 2223–2231.

(5) Grimme, S.; Bannwarth, C.; Shushkov, P. A Robust and Accurate Tight-Binding

Quantum Chemical Method for Structures, Vibrational Frequencies, and Noncovalent Interactions of Large Molecular Systems Parametrized for All Spd-Block Elements (Z = 1-86). *J. Chem. Theory Comput.* **2017**, *13*, 1989–2009.

(6) Bannwarth, C.; Ehlert, S.; Grimme, S. GFN2-XTB – an Accurate and Broadly Parametrized Self-Consistent Tight-Binding. *ChemRxiv* **2018**, http://doi.org/10.26434/chemrxiv.7246238.v1.

(7) Berlman, I. B. Empirical Study of Heavy-Atom Collisional Quenching of the Fluorescence State of Aromatic Compounds in Solution. *J. Phys. Chem.* **1973**, *77*, 562–567.

(8) Najbar, J.; Munro, I. H. External Heavy Atom Effects on the Decay of the Triplet State of Aromatic Hydrocarbons III. The Decay Functions of Fluorescence and Phosphorescence of Carbazole in the Presence of KI. *J. Lumin.* **1978**, *17*, 135–148.

(9) Sun, X.; Zhang, B.; Li, X.; Trindle, C. O.; Zhang, G. External Heavy-Atom Effect via Orbital Interactions Revealed by Single-Crystal X-Ray Diffraction. *J. Phys. Chem. A* **2016**, *120*, 5791–5797.

(10) Mukherjee, S.; Thilagar, P. Recent Advances in Purely Organic Phosphorescent Materials. *Chem. Commun.* **2015**, *51*, 10988–11003.

(11) Bolton, O.; Lee, K.; Kim, H. J.; Lin, K. Y.; Kim, J. Activating Efficient Phosphorescence from Purely Organic Materials by Crystal Design. *Nat. Chem.* **2011**, *3*, 205–210.

(12) Arduengo, Anthony J., I.; Krafczyk, R.; Schmutzler, R.; Craig, H. A.; Goerlich, J. R.; Marshall, W. J.; Unverzagt, M. Imidazolylidenes, Imidazolinylidenes and Imidazolidines. *Tetrahedron* **1999**, *55*, 14523–14534.

(13) Furfari, S. K.; Gyton, M. R.; Twycross, D.; Cole, M. L. Air Stable NHCs: A Study of Stereoelectronics and Metallorganic Catalytic Activity. *Chem. Commun.* **2015**, *51*, 74–76.

(14) Grineva, A. A.; Filippov, O. A.; Nefedov, S. E.; Lugan, N.; César, V.; Valyaev, D. A. Direct Access to IMesF and IMesF2 by Electrophilic Fluorination of Abnormal N-Heterocyclic Carbenes. *Organometallics* **2019**, *38*, 2330–2337.

(15) Wolf, S.; Plenio, H. Synthesis of (NHC)Rh(Cod)Cl and (NHC)RhCl(CO)2 Complexes - Translation of the Rh- into the Ir-Scale for the Electronic Properties of NHC Ligands. *J. Organomet. Chem.* **2009**, *694*, 1487–1492.

(16) Vougioukalakis, G. C.; Grubbs, R. H. Ruthenium-Based Olefin Metathesis Catalysts Coordinated with Unsymmetrical N-Heterocyclic Carbene Ligands: Synthesis, Structure, and Catalytic Activity. *Chem. - Eur. J.* **2008**, *14*, 7545–7556.

(17) Chu, J.; Munz, D.; Jazzar, R.; Melaimi, M.; Bertrand, G. Synthesis of Hemilabile Cyclic (Alkyl)(Amino)Carbenes (CAACs) and Applications in Organometallic Chemistry. *J. Am. Chem. Soc.* **2016**, *138*, 7884–7887.

(18) Hans, M.; Lorkowski, J.; Demonceau, A.; Delaude, L. Efficient Synthetic Protocols for the Preparation of Common N-Heterocyclic Carbene Precursors. *Beilstein J. Org. Chem.* **2015**, *11*, 2318–2325.

(19) Jazzar, R.; Bourg, J. B.; Dewhurst, R. D.; Donnadieu, B.; Bertrand, G. Intramolecular “Hydroiminiumation and -Amidiniumation” of Alkenes: A Convenient, Flexible, and Scalable Route to Cyclic Iminium and Imidazolinium Salts. *J. Org. Chem.* **2007**, *72*, 3492–3499.

(20) Zhizhko, P. A.; Zhizhin, A. A.; Zarubin, D. N.; Ustynyuk, N. A.; Lemenovskii, D.

A.; Shelimov, B. N.; Kustov, L. M.; Tkachenko, O. P.; Kirakosyan, G. A. Oxo/Imido Heterometathesis of N-Sulfinylamines and Carbonyl Compounds Catalyzed by Silica-Supported Vanadium Oxochloride. *J. Catal.* **2011**, *283*, 108–118.

(21) Zhizhko, P. A.; Zhizhin, A. A.; Belyakova, O. A.; Zubavichus, Y. V.; Kolyagin, Y. G.; Zarubin, D. N.; Ustynyuk, N. A. Oxo/Imido Heterometathesis Reactions Catalyzed by a Silica-Supported Tantalum Imido Complex. *Organometallics* **2013**, *32*, 3611–3617.

(22) Zhizhko, P. A.; Pichugov, A. V.; Bushkov, N. S.; Allouche, F.; Zhizhin, A. A.; Zarubin, D. N.; Ustynyuk, N. A. Catalytic Oxo/Imido Heterometathesis by a Well-Defined Silica-Supported Titanium Imido Complex. *Angew. Chem. Int. Ed.* **2018**, *57*, 10879–10882.

(23) Michaelis, A. Ueber Die Thionylamine. *Berichte der Dtsch. Chem. Gesellschaft* **1891**, *24*, 745–757.

(24) Anschütz, L.; Delijski, Z. M. Studien an Aromatischen Thionylaminen. *Justus Liebig's Ann. der Chemie* **1932**, *493*, 241–250.

(25) Zhizhin, A. A.; Zarubin, D. N.; Ustynyuk, N. A. An Imido-Transfer Reaction of Aldehydes with N-Sulfinylamines Using Vanadium and Molybdenum Oxochlorides as Catalysts. *Tetrahedron Lett.* **2008**, *49*, 699–702.

(26) Mahoney, J. K.; Martin, D.; Moore, C. E.; Rheingold, A. L.; Bertrand, G. Bottleable (Amino)(Carboxy) Radicals Derived from Cyclic (Alkyl)(Amino) Carbenes. *J. Am. Chem. Soc.* **2013**, *135*, 18766–18769.

(27) Mignani, G. Preparation of Precursors of Carbenes of CAAC Type and Preparing Said Carbenes Therefrom. US2010113791 (A1), 2010.

(28) Mandal, D.; Dolai, R.; Kalita, P.; Narayanan, R. S.; Kumar, R.; Sobottka, S.; Sarkar, B.; Rajaraman, G.; Chandrasekhar, V.; Jana, A. “Abnormal” Addition of NHC to a Conjugate Acid of CAAC: Formation of N -Alkyl-Substituted CAAC. *Chem. - Eur. J.* **2018**, *24*, 12722–12727.

Appendix A: NMR Spectral Data

Section A.1: General Considerations

$CDCl_3$ and CD_2Cl_2 were distilled over activated alumina and degassed by three freeze-pump-thaw cycles. THF-d_8 and C_6D_6 were distilled over sodium. MeCN-d_3 was distilled over CaH_2 and degassed by three freeze-pump-thaw cycles. NMR spectra were recorded on a Bruker AVANCE III 500 MHz or Varian Inova 400 MHz spectrometer. ^{1}H and ^{13}C chemical shifts referenced to residual solvent signal and ^{31}P chemical shifts were referenced to an external standard of 85% H_3PO_4. Solid-state ^{31}P MAS NMR spectrum was recorded on a Bruker AVANCE III 800 spectrometer using a 2.5 mm rotor with a spinning rate of 30 kHz and referenced to Na_2HPO_4 as an external standard (2.3 ppm).[1]

All 2D ^{1}H DOSY spectra were recorded on a Bruker AVANCE III 500 MHz spectrometer with a 5 mm BBO cryoprobe using a z-gradient coil with maximum nominal field strength of 48 G cm^{-1}. Spectra were acquired using standard ledgp2s pulse program with z-gradient varied linearly between 5-95% over 16 steps, collected as 16 spectra on 32 K data points, and diffusion coefficients calculated using the T1/T2 module in Topspin 4.0.3. All spectra were acquired at 298 K with sample spinning disabled, diffusion time Δ = 0.1 s, and length of gradient δ = 1.5 ms. Diffusion coefficients were corrected using tetramethylbutane ($\log D_{ref,fix}$(TMB) = -8.7749) or tetrakis(trimethylsilyl)silane ($\log D_{ref,fix}$(TTS) = -8.9773) as internal standard per the ECC-DOSY method using the calibration curve for dissipated spheres and ellipsoids.[2] Spectra for Ph-BIM, carbazole, IPr, ^{Et}CAAC, **4.1**, and **4.4** were recorded at a concentration of 75 mM with equimolar amount of TMB as an internal standard. Compounds **3.1**, **4.2**, and **4.3** were recorded at a concentration of 50 mM with equimolar amount of TTS as an internal standard.

Section A.2: NMR Spectra for Compounds Included in **Chapter 2**

Figure A.2.1: ^{31}P NMR (162 MHz, THF) of reaction between Na[OCP] and PhMgBr, followed by addition of TMS-Cl.

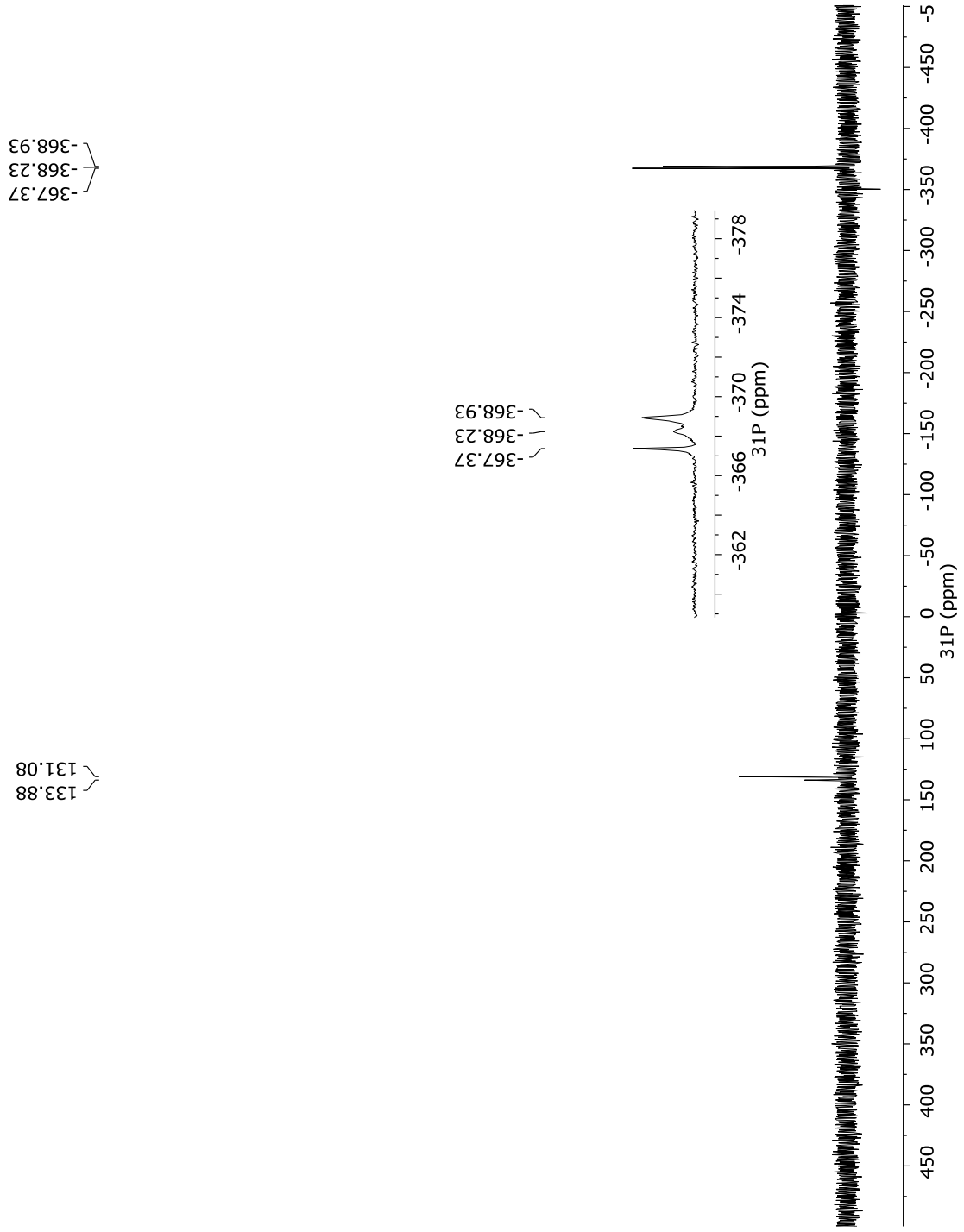

Figure A.2.2: $^{31}P\{^{1}H\}$ NMR (202 MHz, THF) spectrum of reaction between Na[OCP] and 2-trifluoromethylphenyl triflate after 10 minutes of heating.

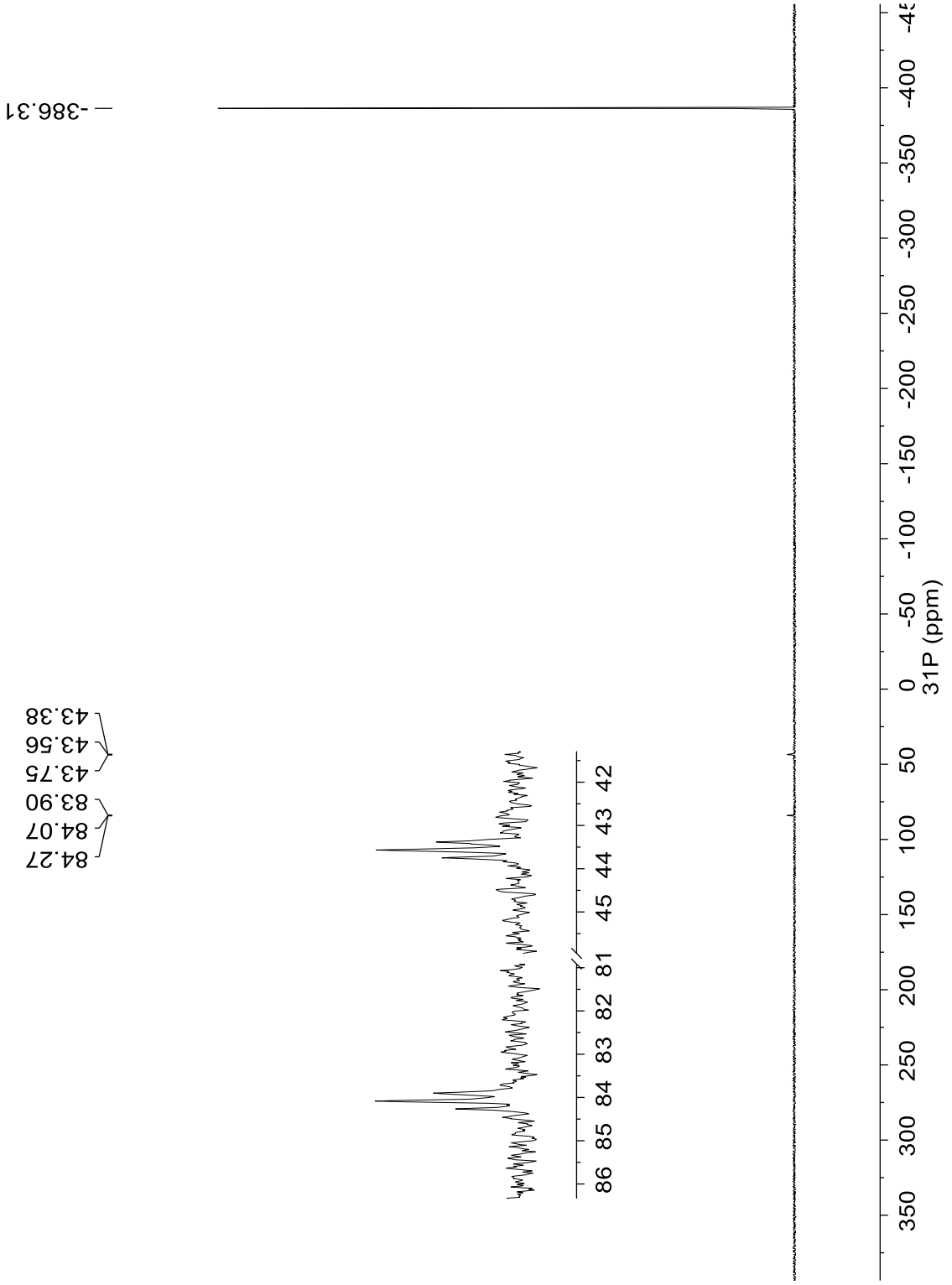

Figure A.2.3: $^{31}P\{^{1}H\}$ NMR (202 MHz, THF) spectrum of reaction between Na[OCP] and CsF. Capillary containing Na[OCP] in THF used as internal standard.

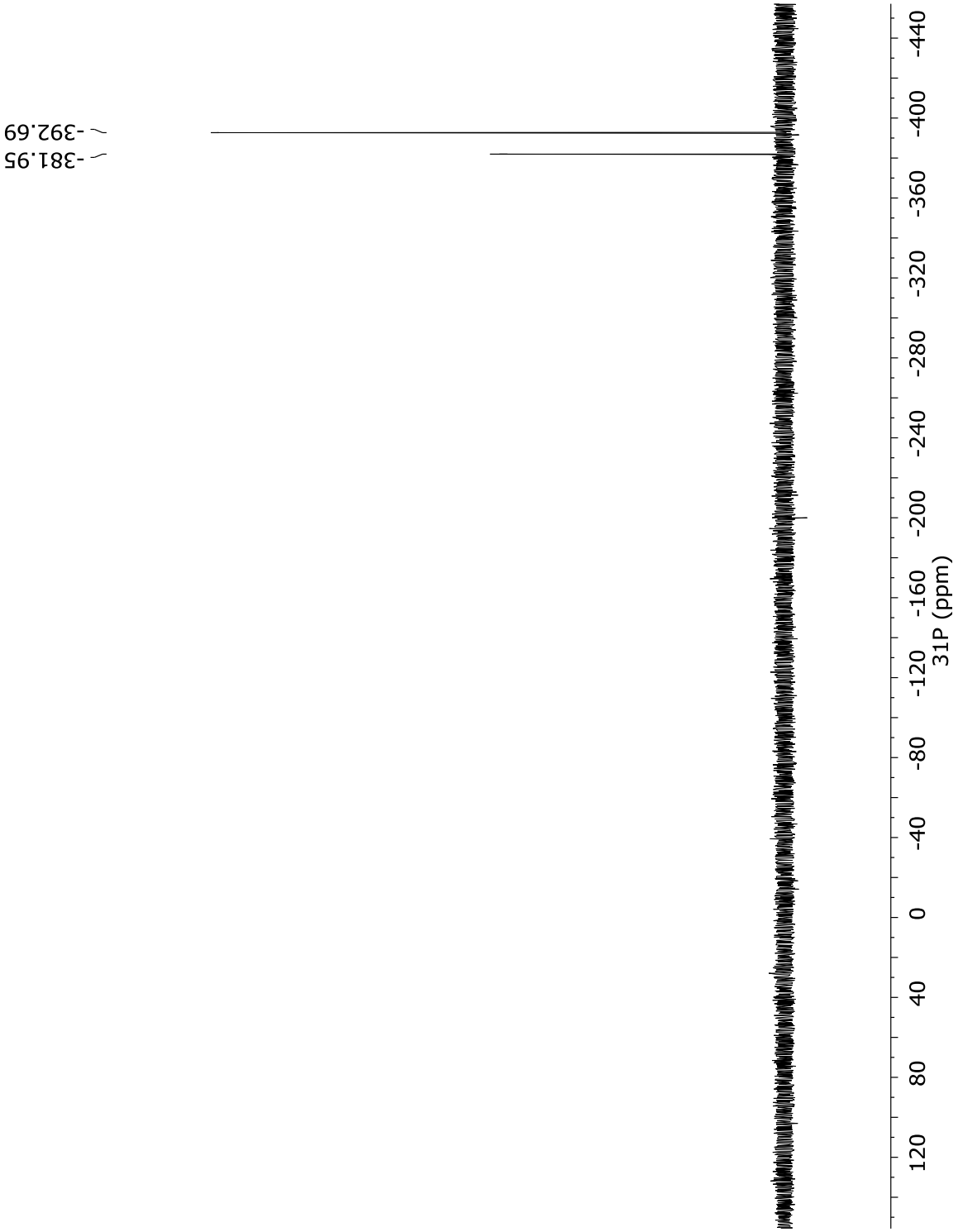

Figure A.2.4: ^{31}P MAS NMR (324 MHz) spectrum of **2.1** at 30 kHz spinning rate, spinning sidebands marked with *.

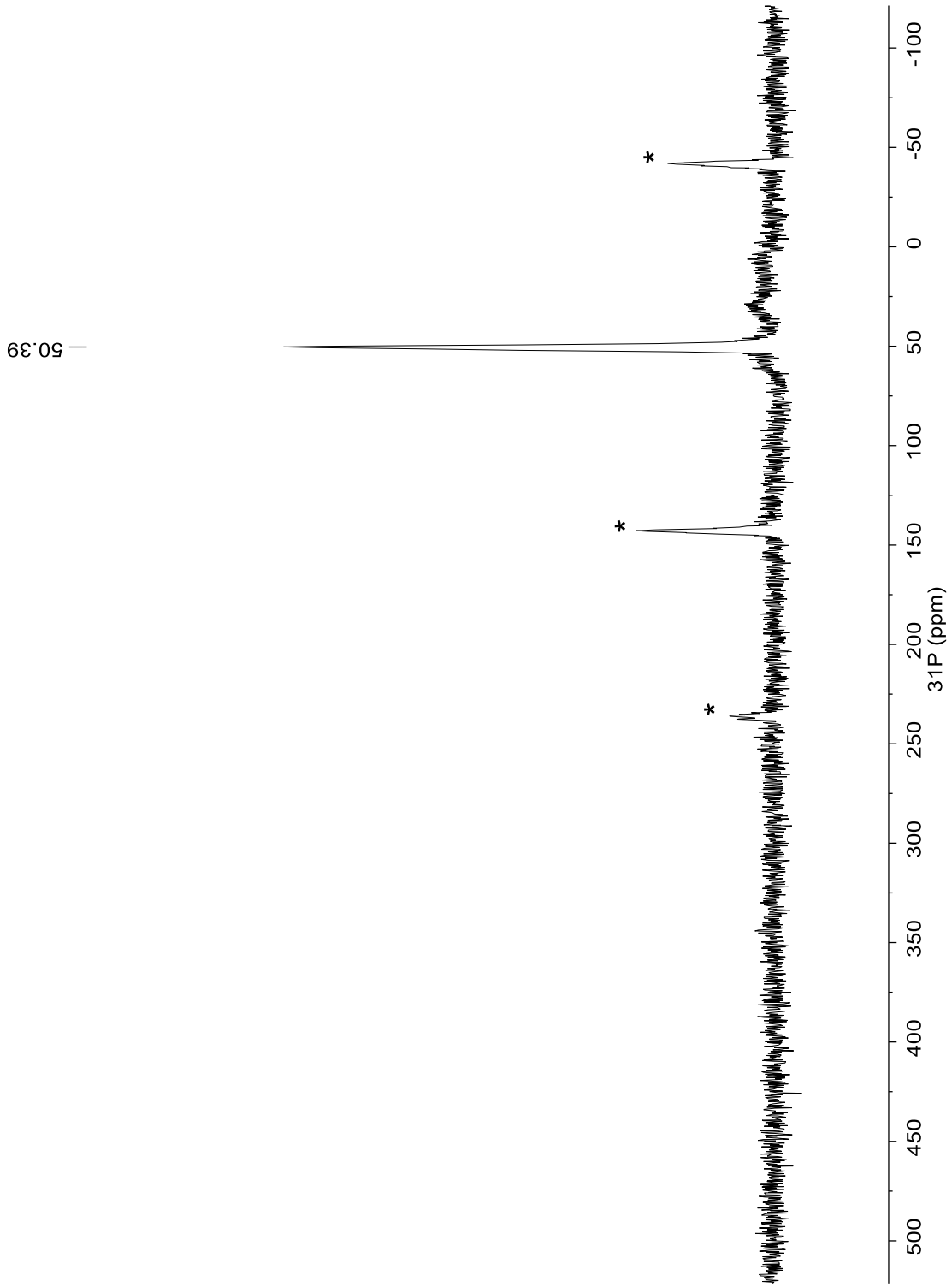

Figure A.2.5: ^{1}H NMR (500 MHz, $CDCl_3$) spectrum of **2.2**.

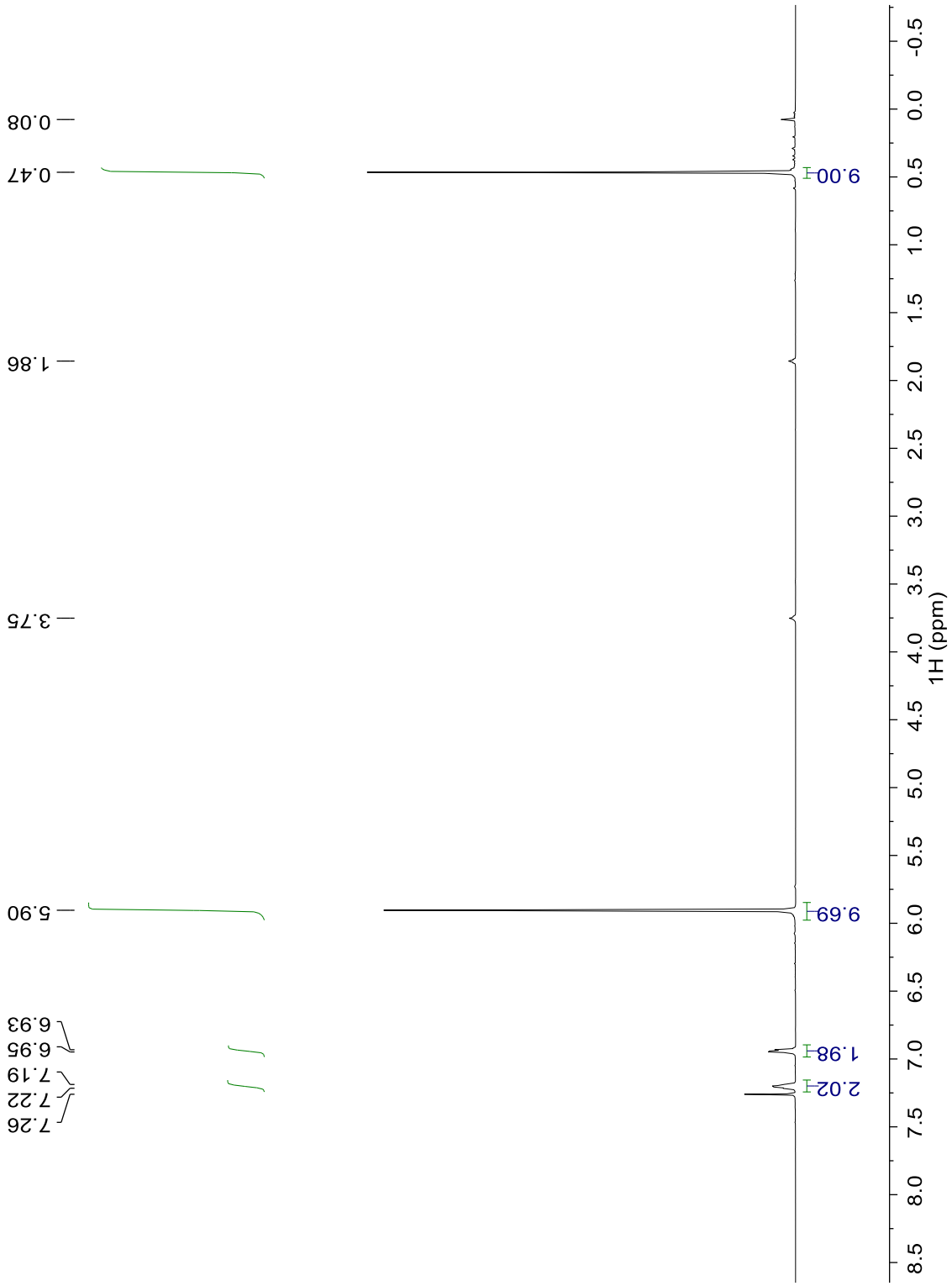

Figure A.2.6: $^{13}C\{^{1}H\}$ NMR (126 MHz, $CDCl_3$) spectrum of **2.2**.

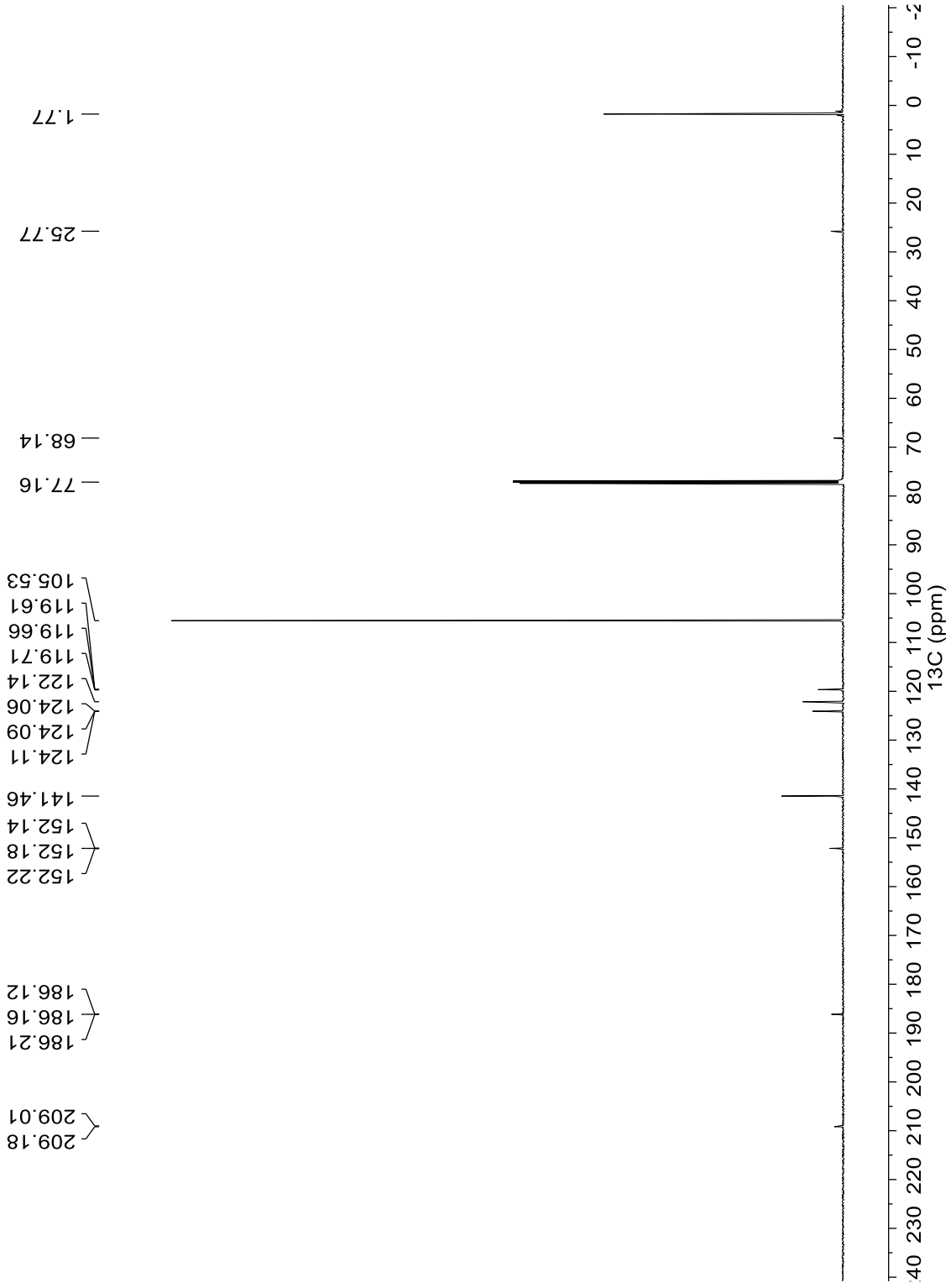

Figure A.2.7: $^{31}P\{^{1}H\}$ NMR (202 MHz, $CDCl_3$) spectrum of **2.2**.

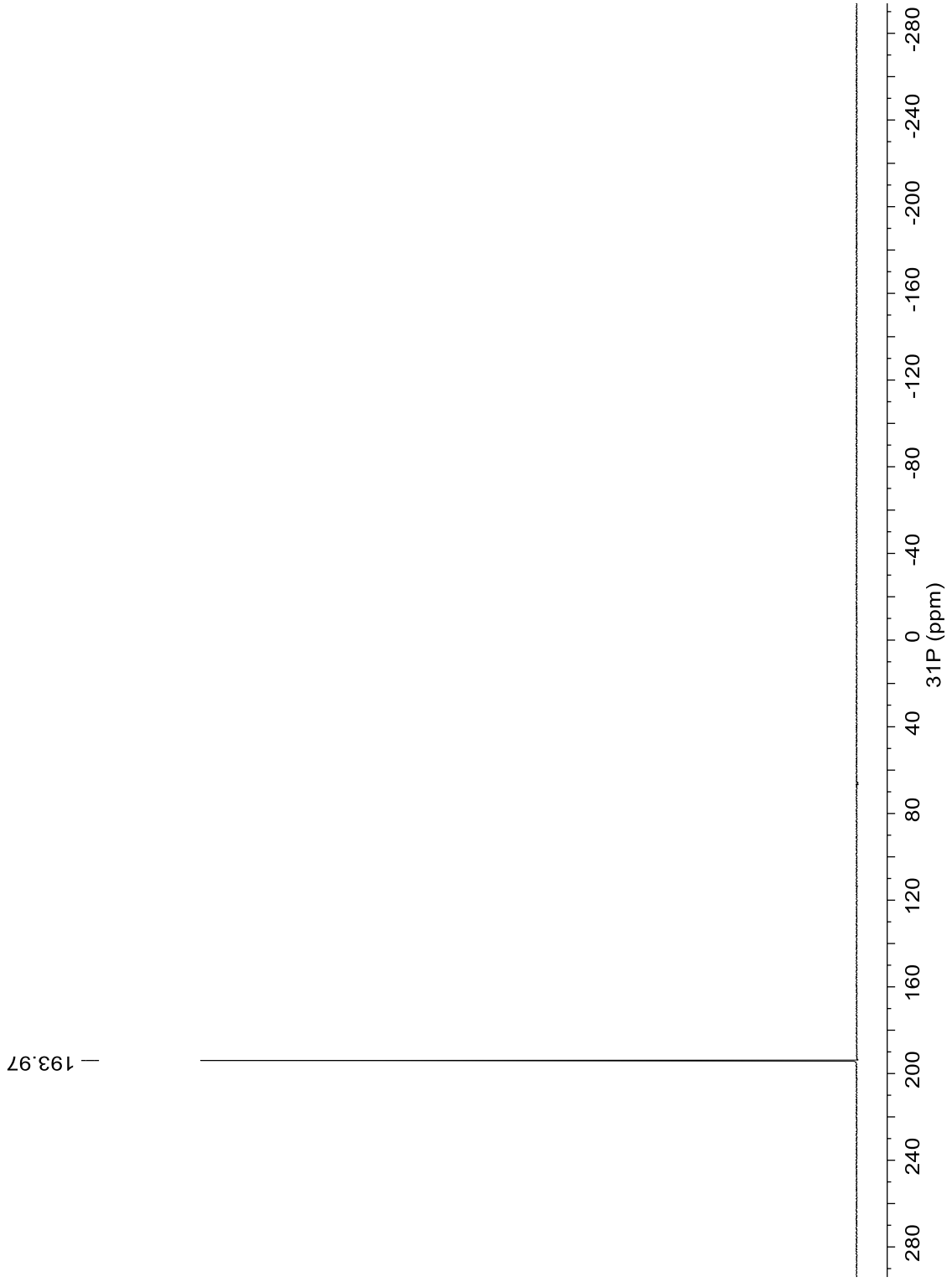

Figure A.2.8: $^{31}P\{^{1}H\}$ NMR (202 MHz, THF) spectrum of **2.3**.

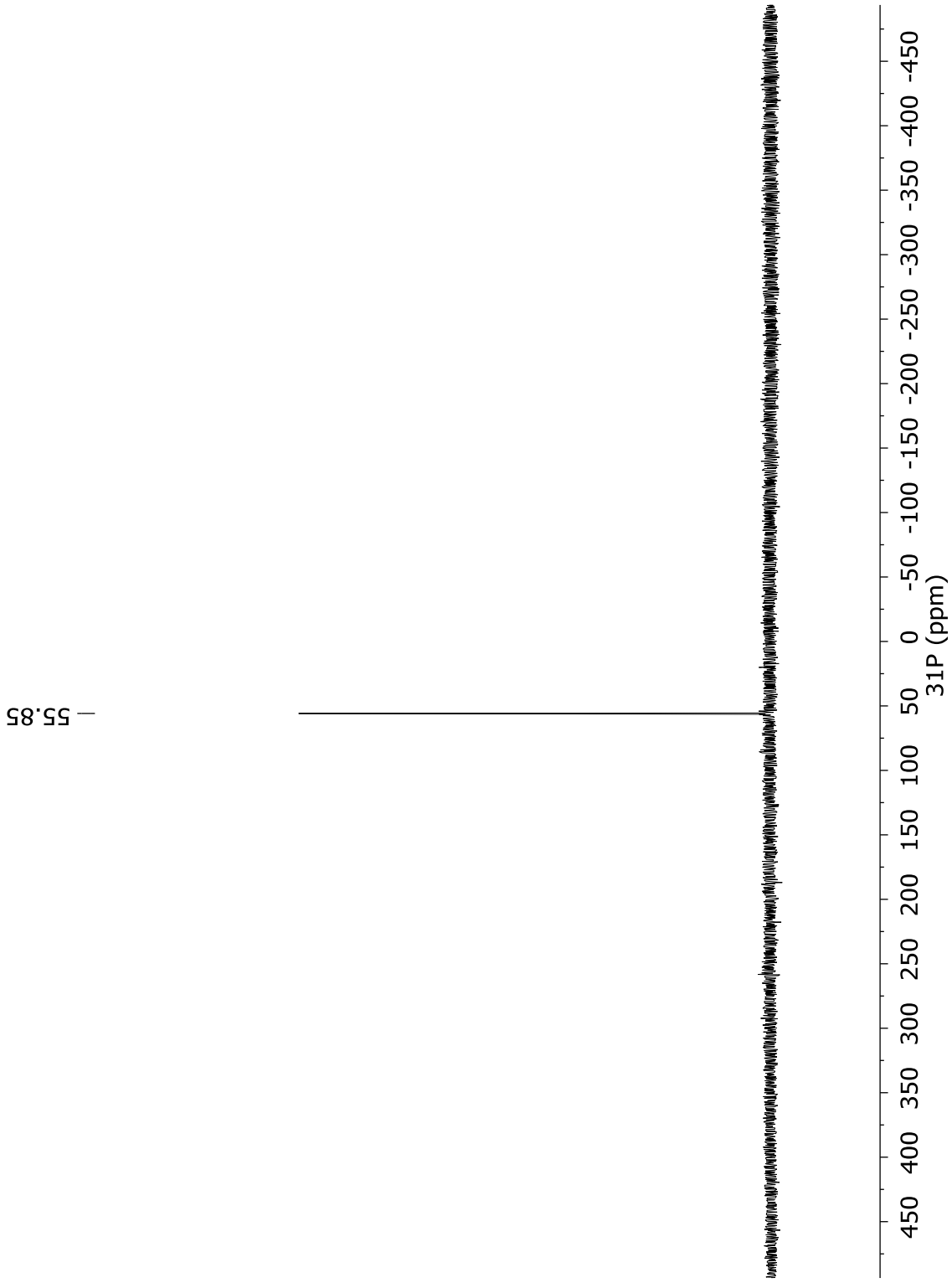

Figure A.2.9: ^{19}F NMR (471 MHz, THF) spectrum of **2.3**.

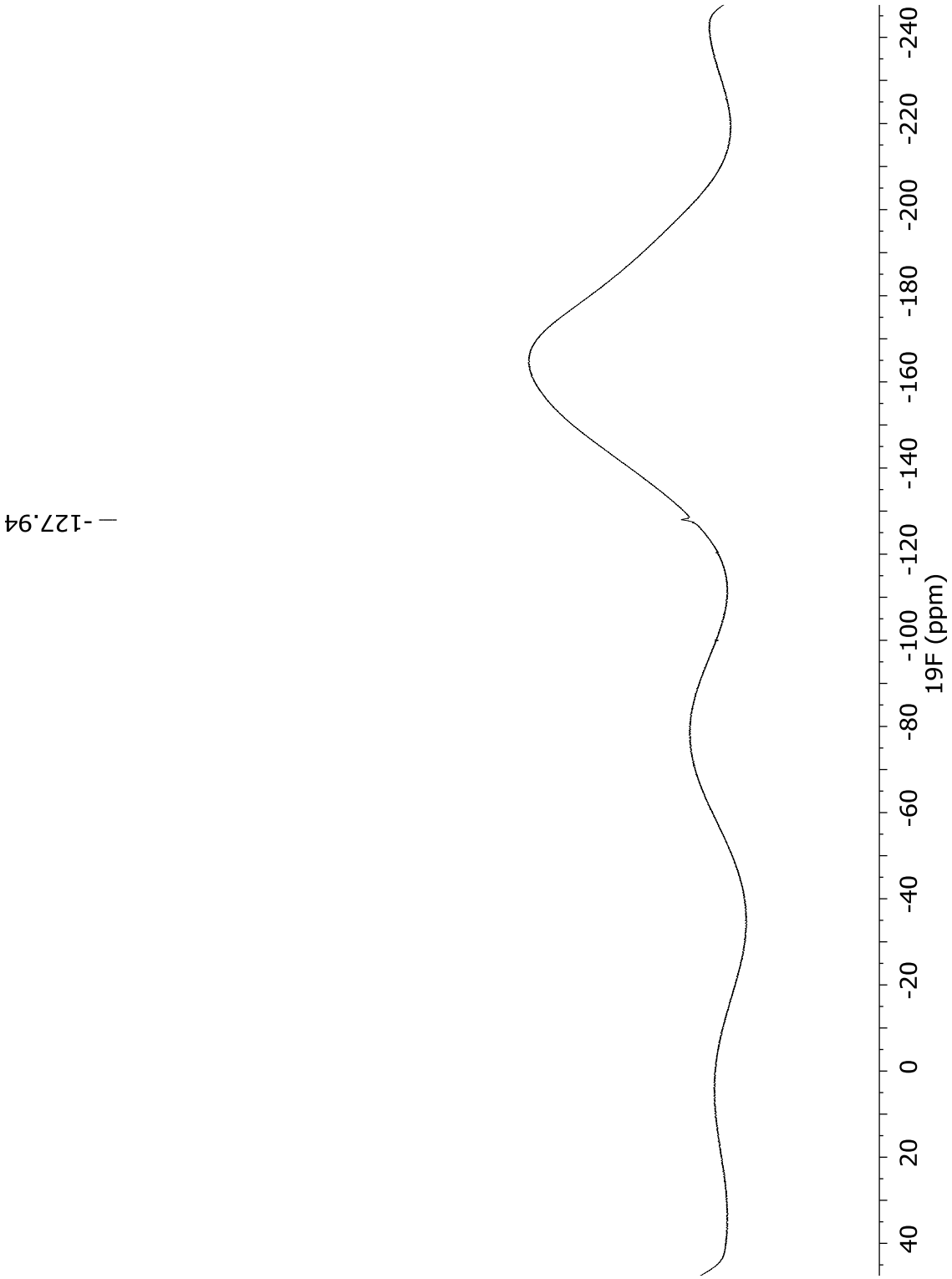

Figure A.2.10: ^{1}H NMR (500 MHz, CD_2Cl_2) spectrum of reaction mixture containing benzoylphosphine and Cp_2ZrCl_2 using procedure **A** in **Chapter 2**.

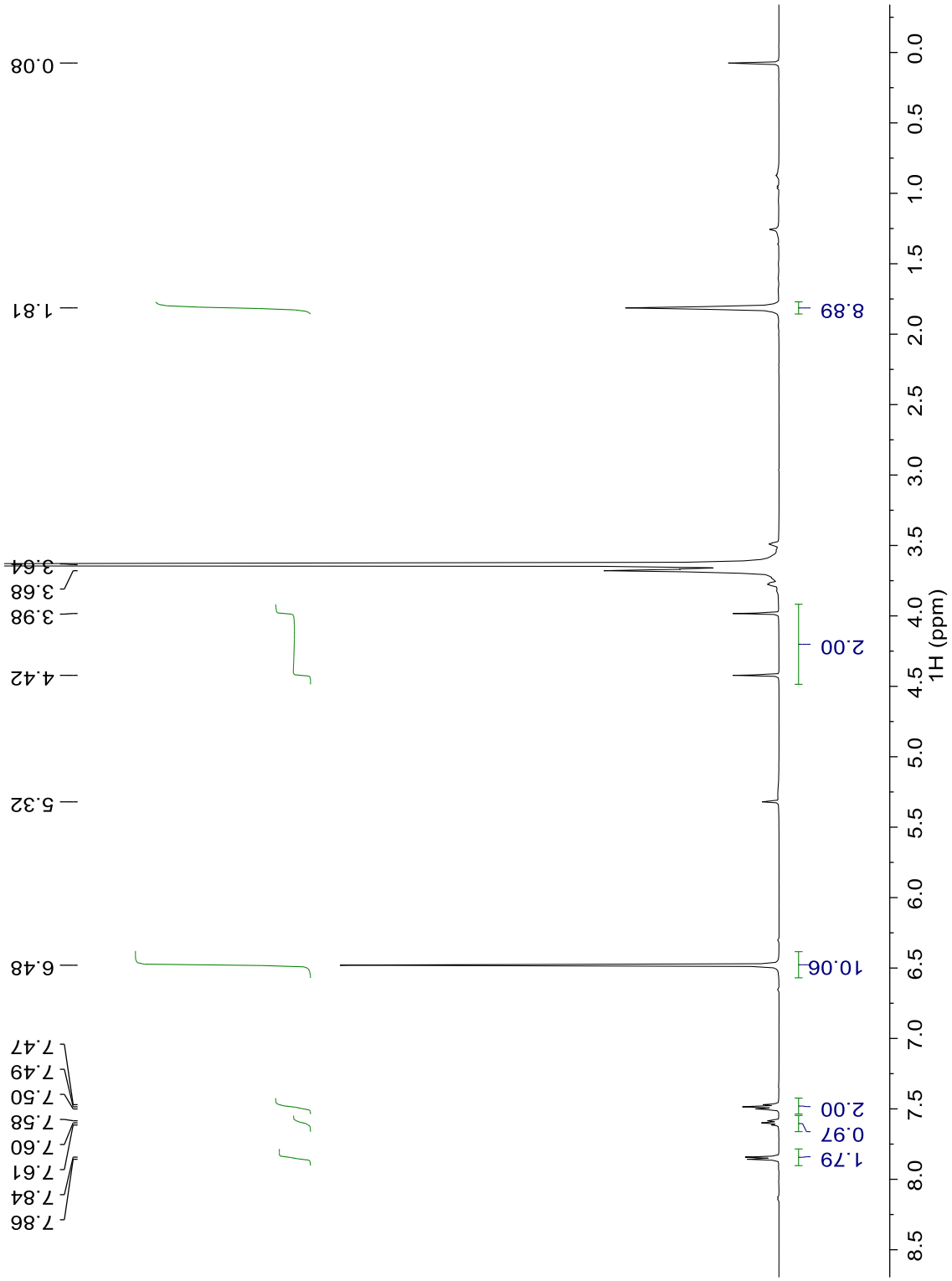

Figure A.2.11: $^{13}C\{^{1}H\}$ NMR (126 MHz, CD_2Cl_2) spectrum of reaction mixture containing benzoylphosphine and Cp_2ZrCl_2 using procedure **A** in **Chapter 2**.

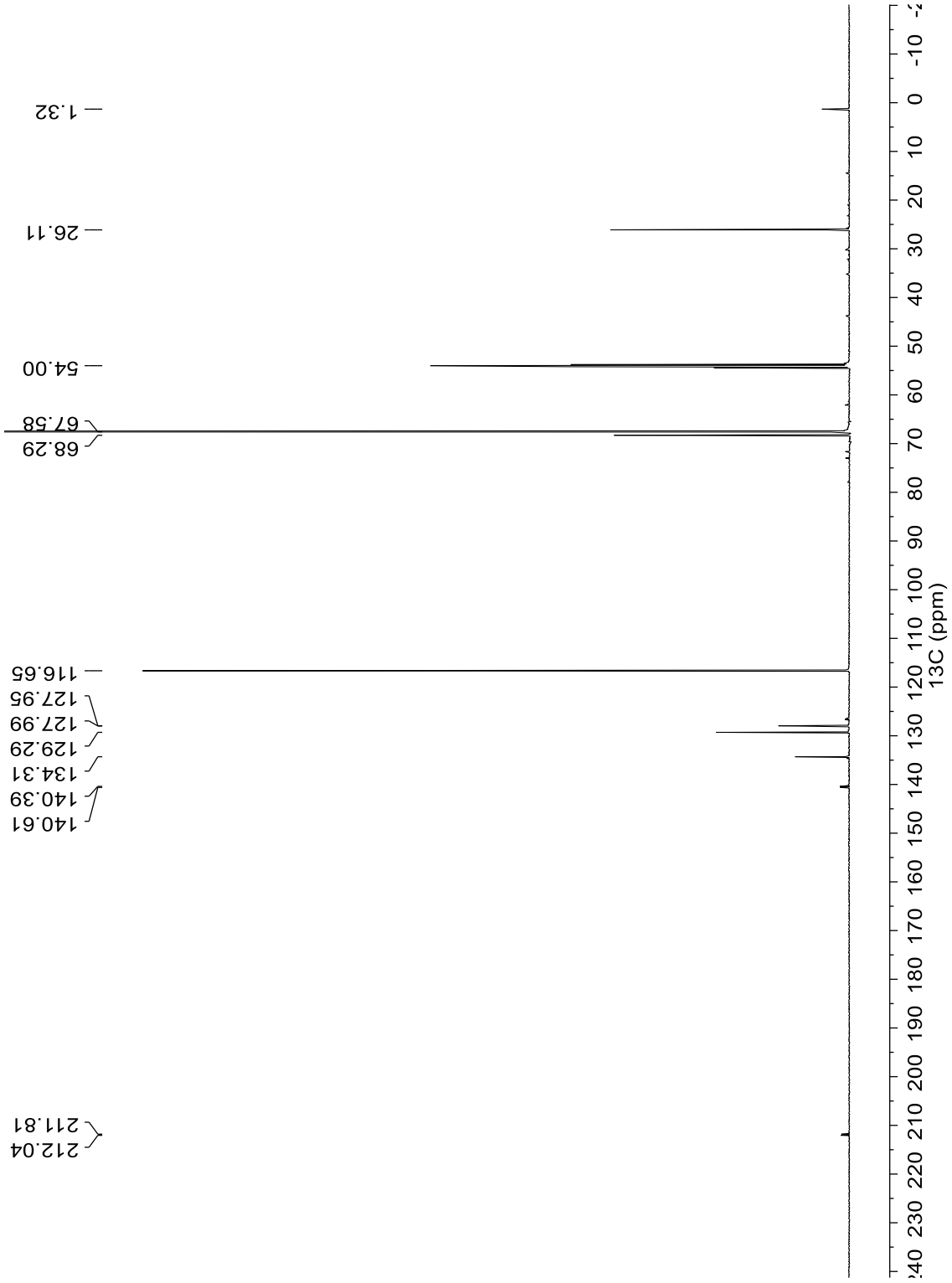

Figure A.2.12: ^{31}P NMR (202 MHz, CD_2Cl_2) spectrum of reaction mixture containing benzoylphosphine and Cp_2ZrCl_2 using procedure **A** in **Chapter 2**.

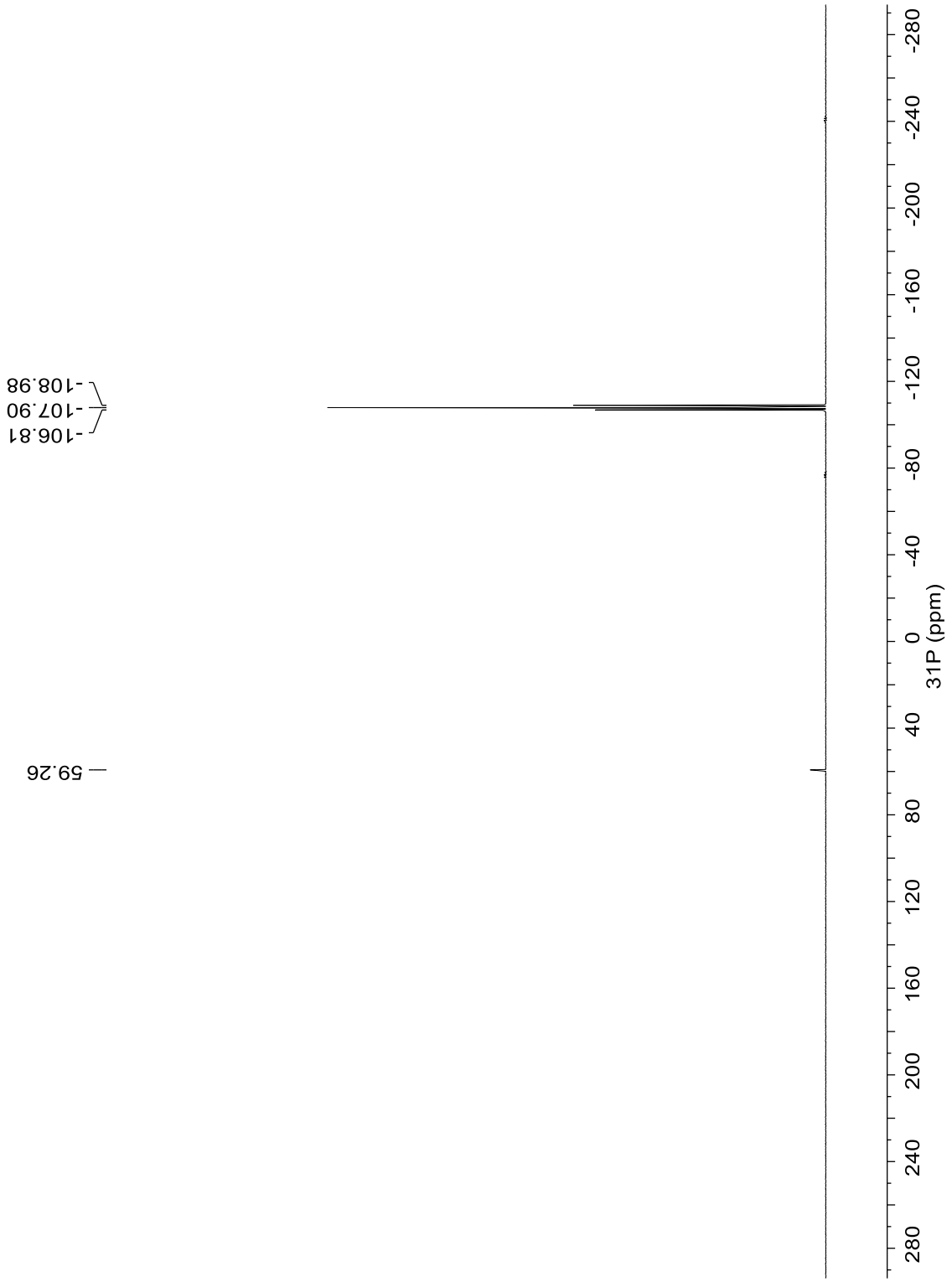

Figure A.2.13: ^{1}H NMR (500 MHz, CD_2Cl_2) spectrum of reaction mixture containing benzoylphosphine using procedure **B** in **Chapter 2**.

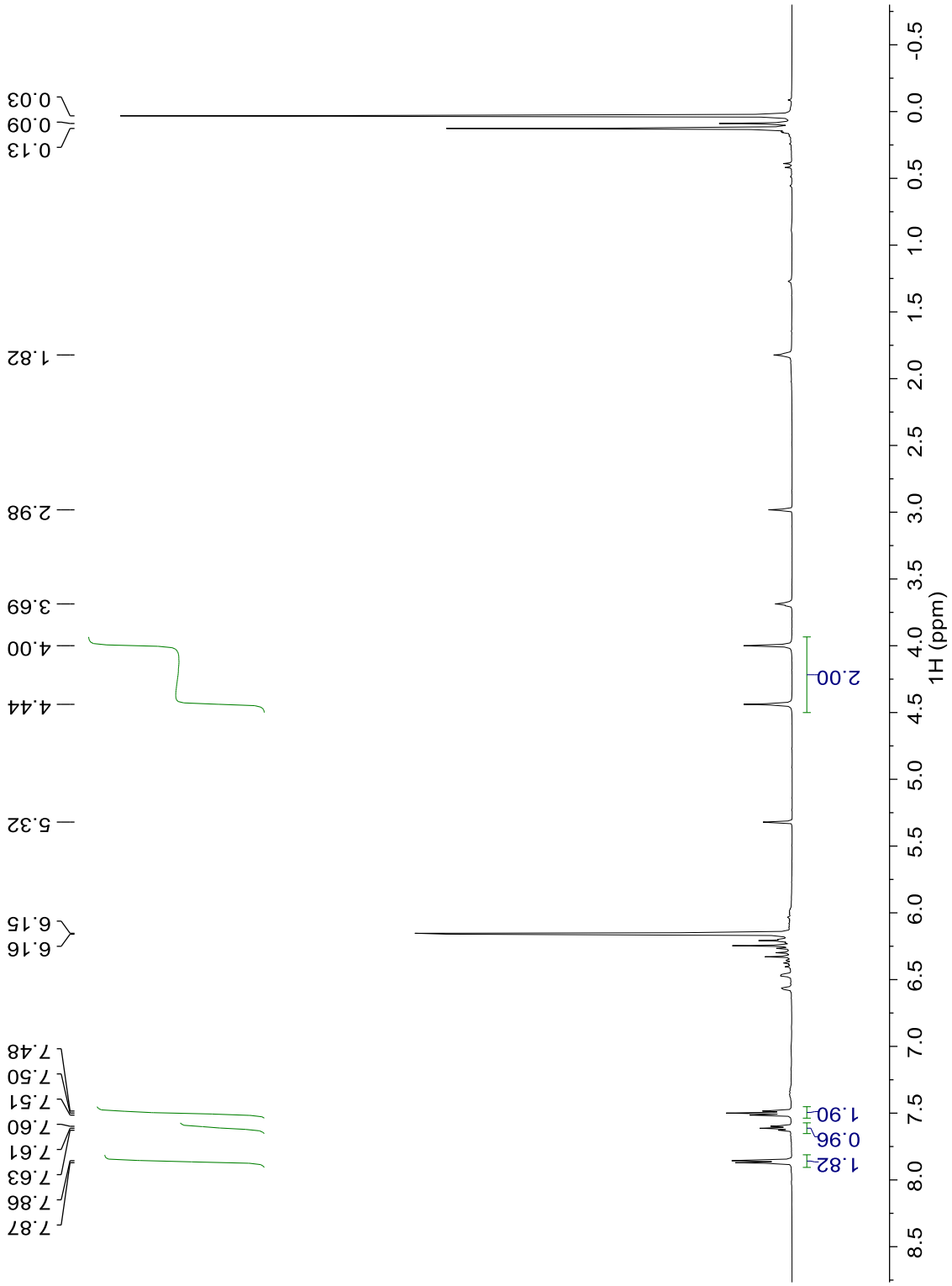

Figure A.2.14: $^{13}C\{^{1}H\}$ NMR (126 MHz, CD_2Cl_2) spectrum of reaction mixture containing benzoylphosphine using procedure **B** in **Chapter 2**.

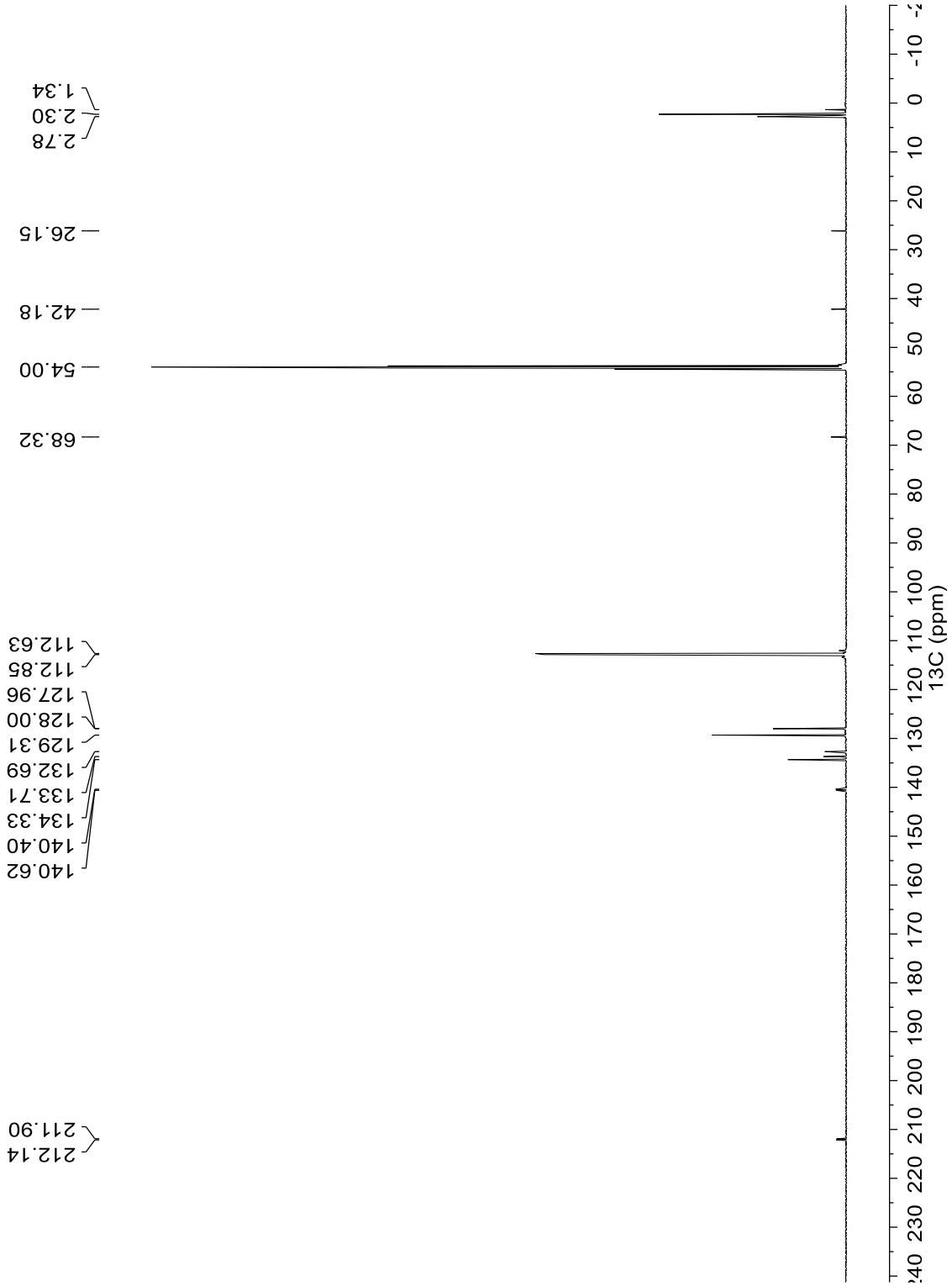

Figure A.2.15: ^{31}P NMR ^{1}H Coupled NMR (202 MHz, CD_2Cl_2) spectrum of reaction mixture containing benzoylphosphine using procedure **B** in **Chapter 2**.

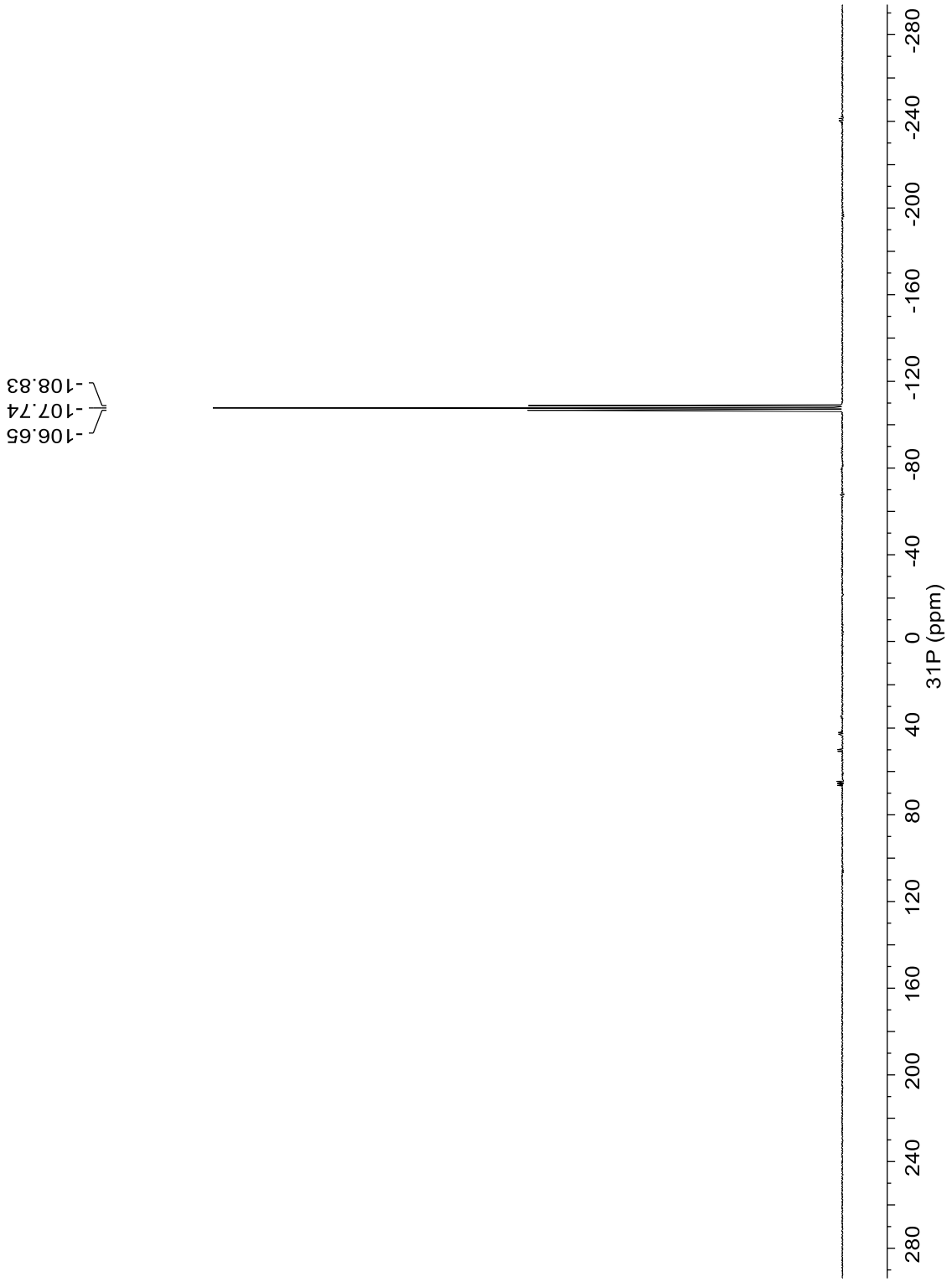

Figure A.2.16: ^{1}H NMR (500 MHz, $CDCl_3$) spectrum of benzoylphosphine after attempted isolation.

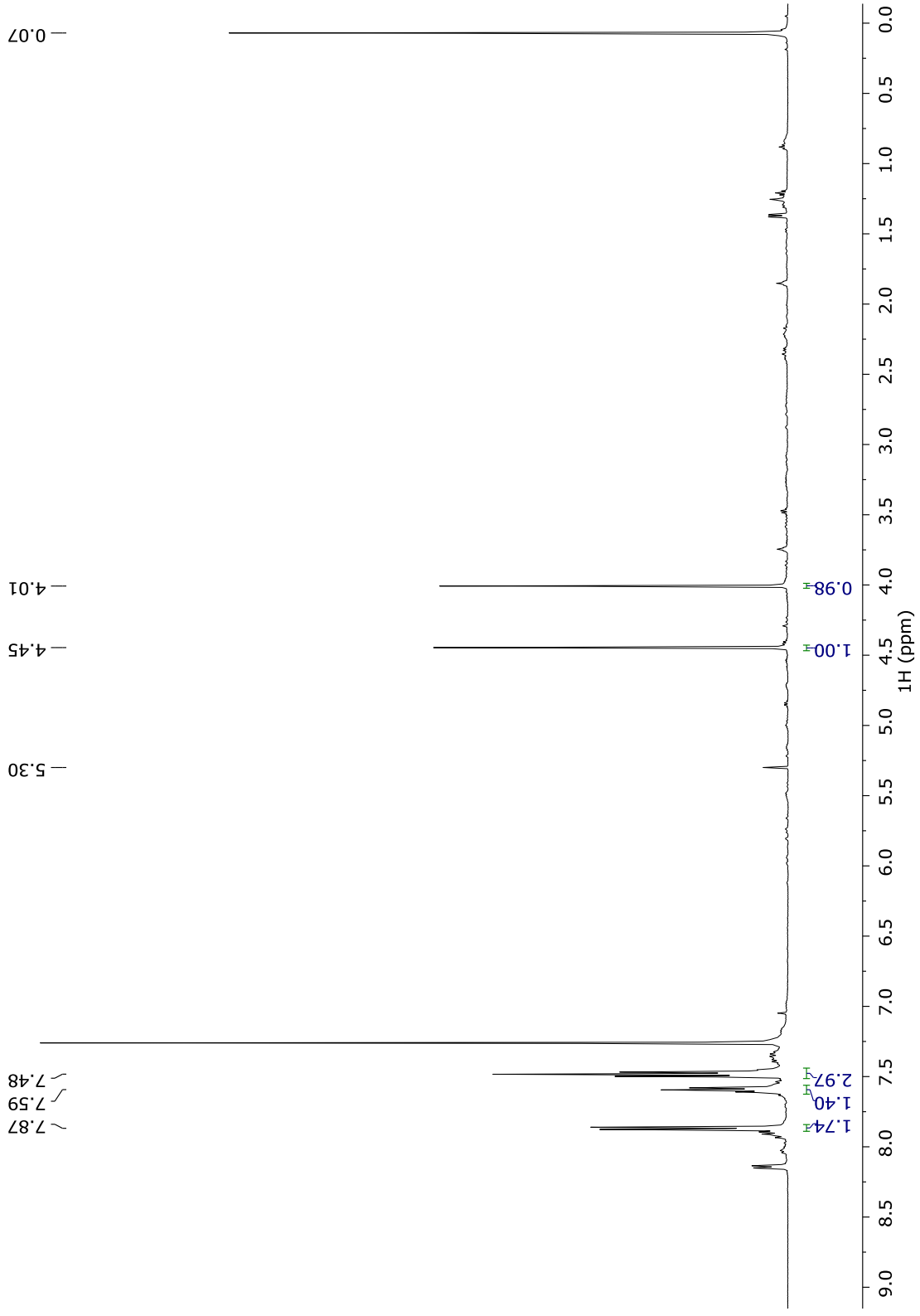

Figure A.2.17: ^{31}P NMR ^{1}H Coupled NMR (202 MHz, $CDCl_3$) benzoylphosphine after attempted isolation.

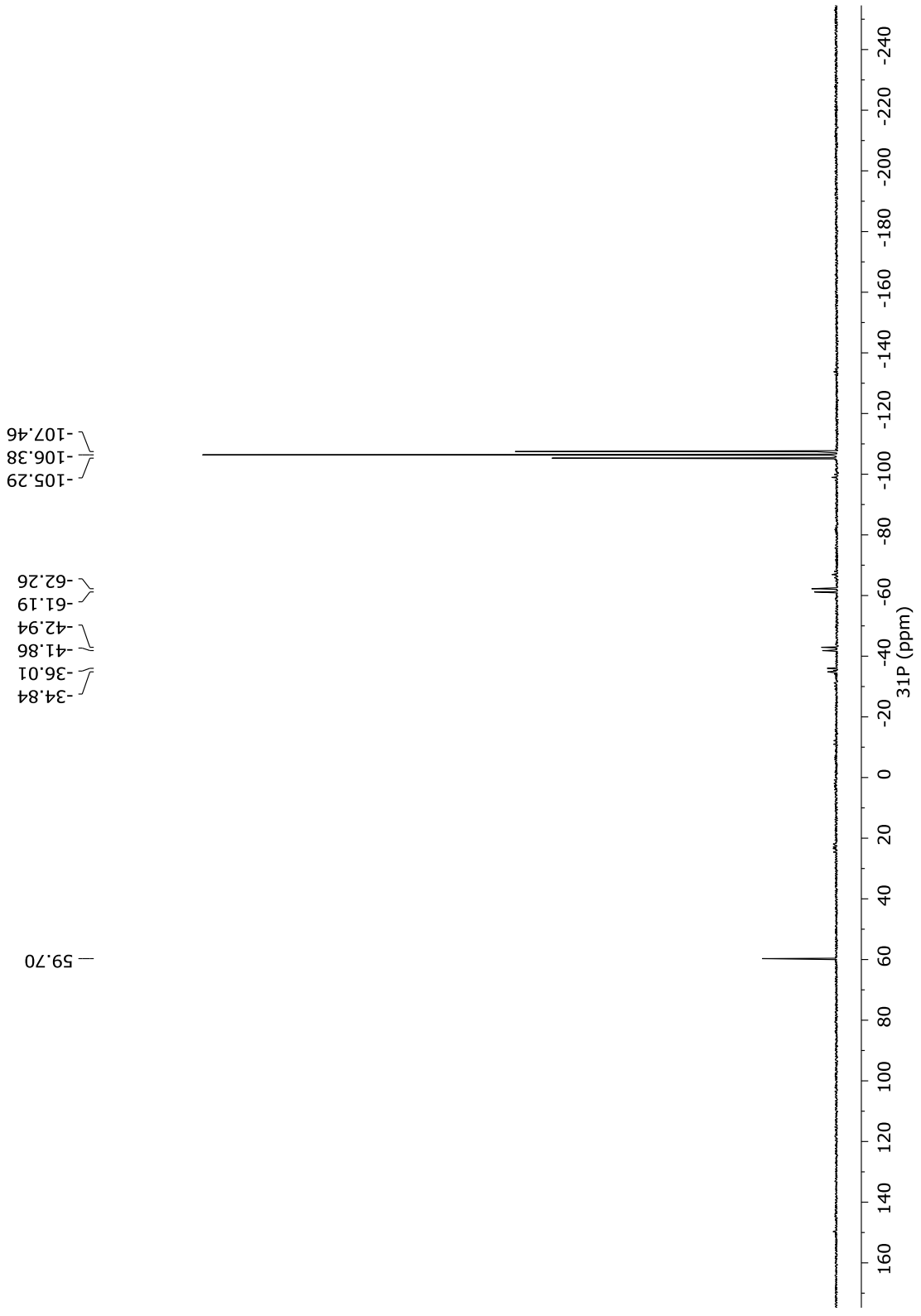

Figure A.2.18: ^{31}P NMR ^{1}H Coupled NMR (162 MHz, CH_2Cl_2) spectra of sealed tube containing reaction mixture of benzoylphosphine using procedure **B** in **Chapter 2**, sample tube stored in ambient conditions for 2 months.

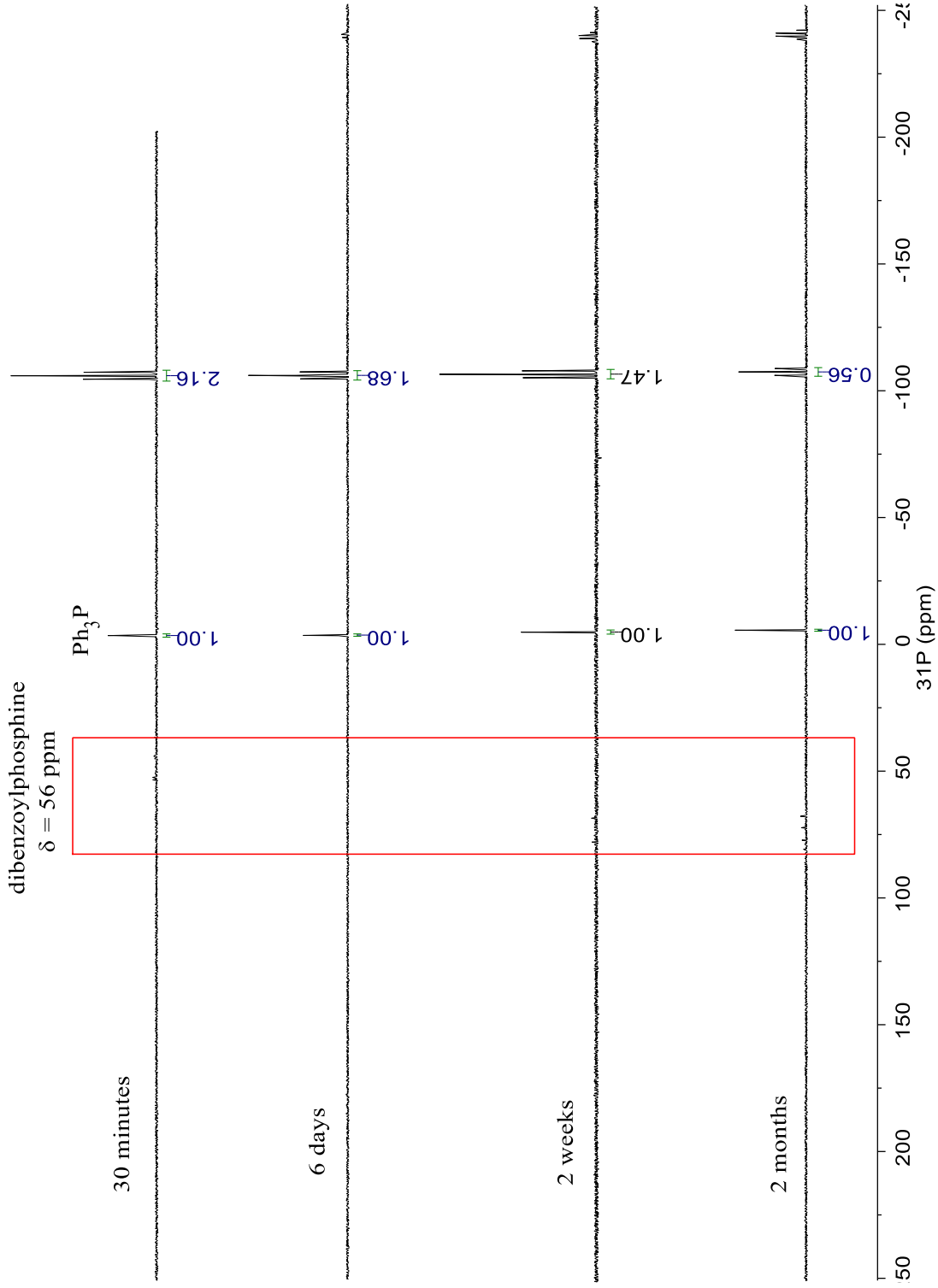

Figure A.2.19: ^{1}H NMR (400 MHz, $CDCl_3$) spectra of stepwise hydrolysis of **2.2** with combination of D_2O and H_2O.

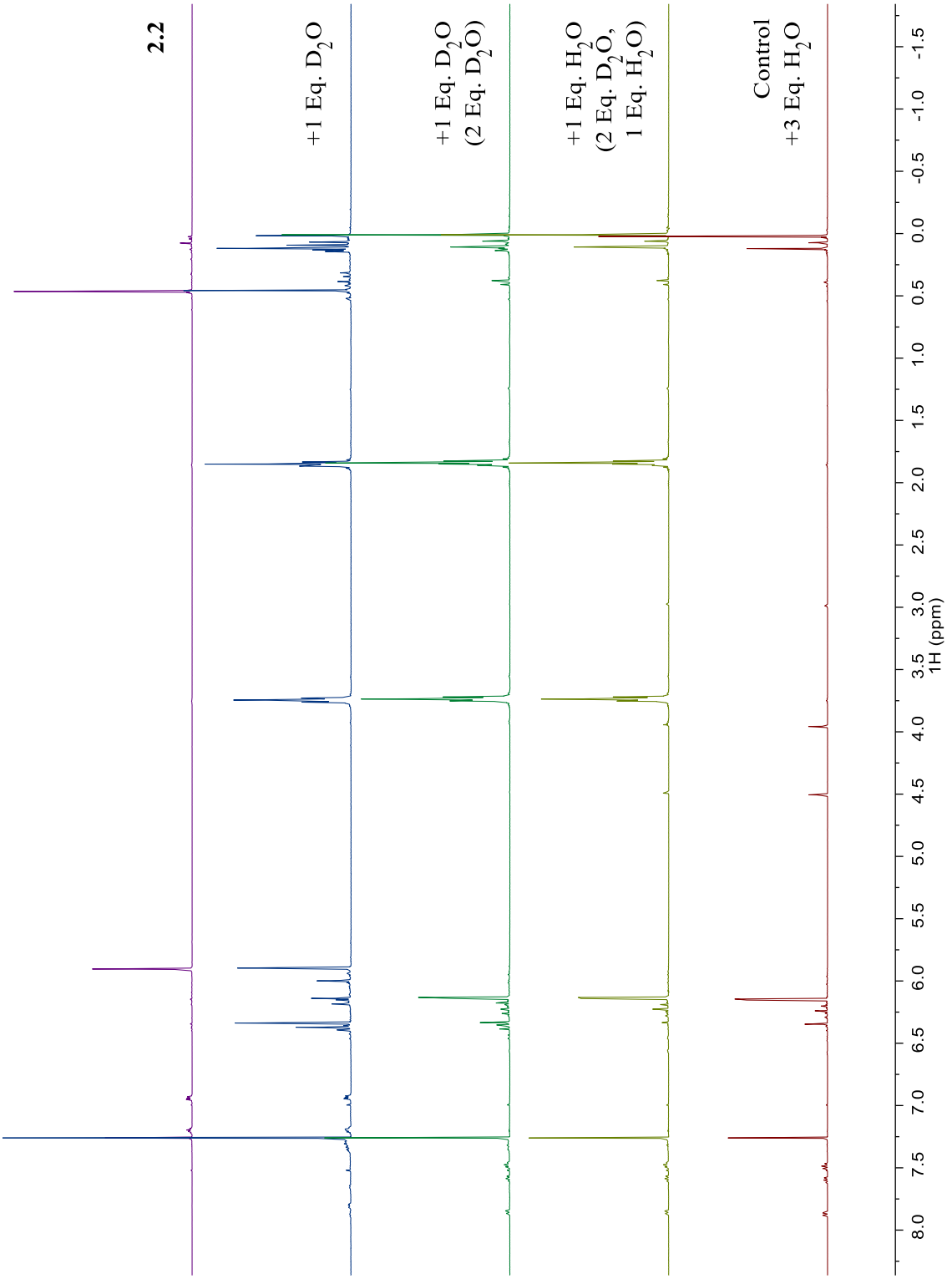

Figure A.2.20: ^{31}P NMR (162 MHz, $CDCl_3$) spectra of stepwise hydrolysis of **2.2** with combination of D_2O and H_2O.

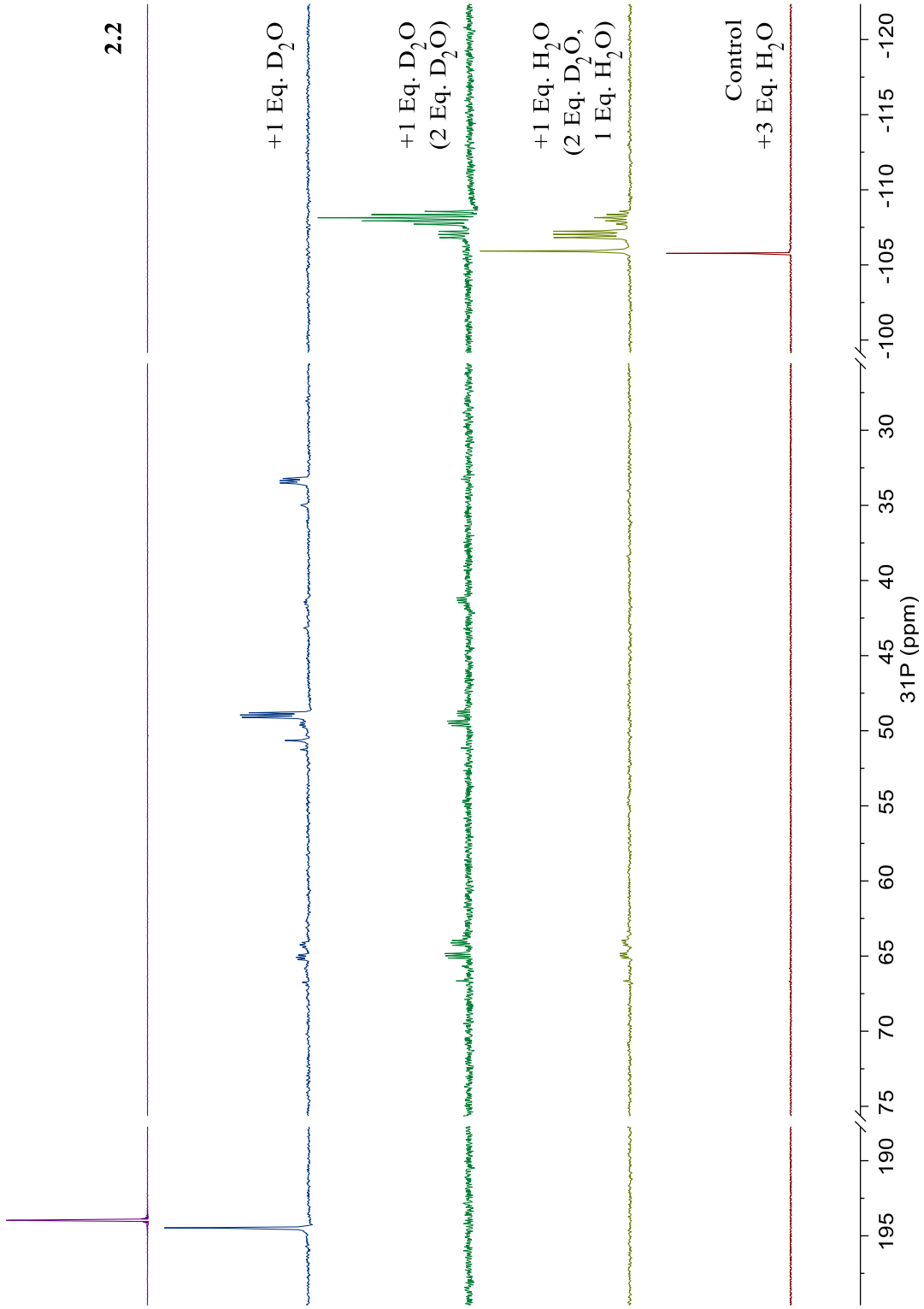

Section A.3: NMR Spectra for Compounds Included in **Chapter 3**.

Figure A.3.1: ^{1}H NMR (500 MHz, THF-d_8) spectrum of compound **3.2**.

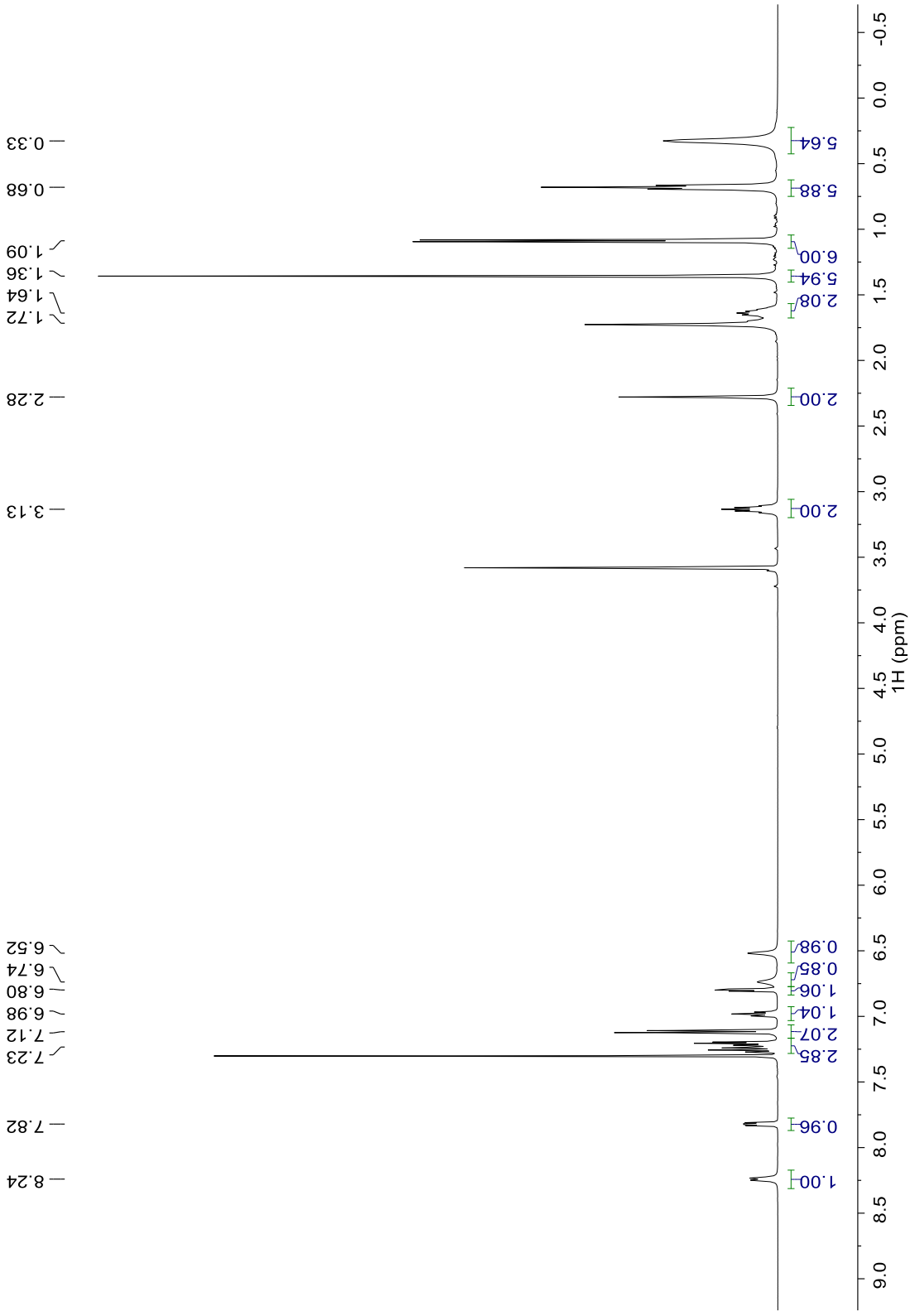

Figure A.3.2: ^{31}P NMR (202 MHz, THF-d_8) spectrum of compound **3.2**.

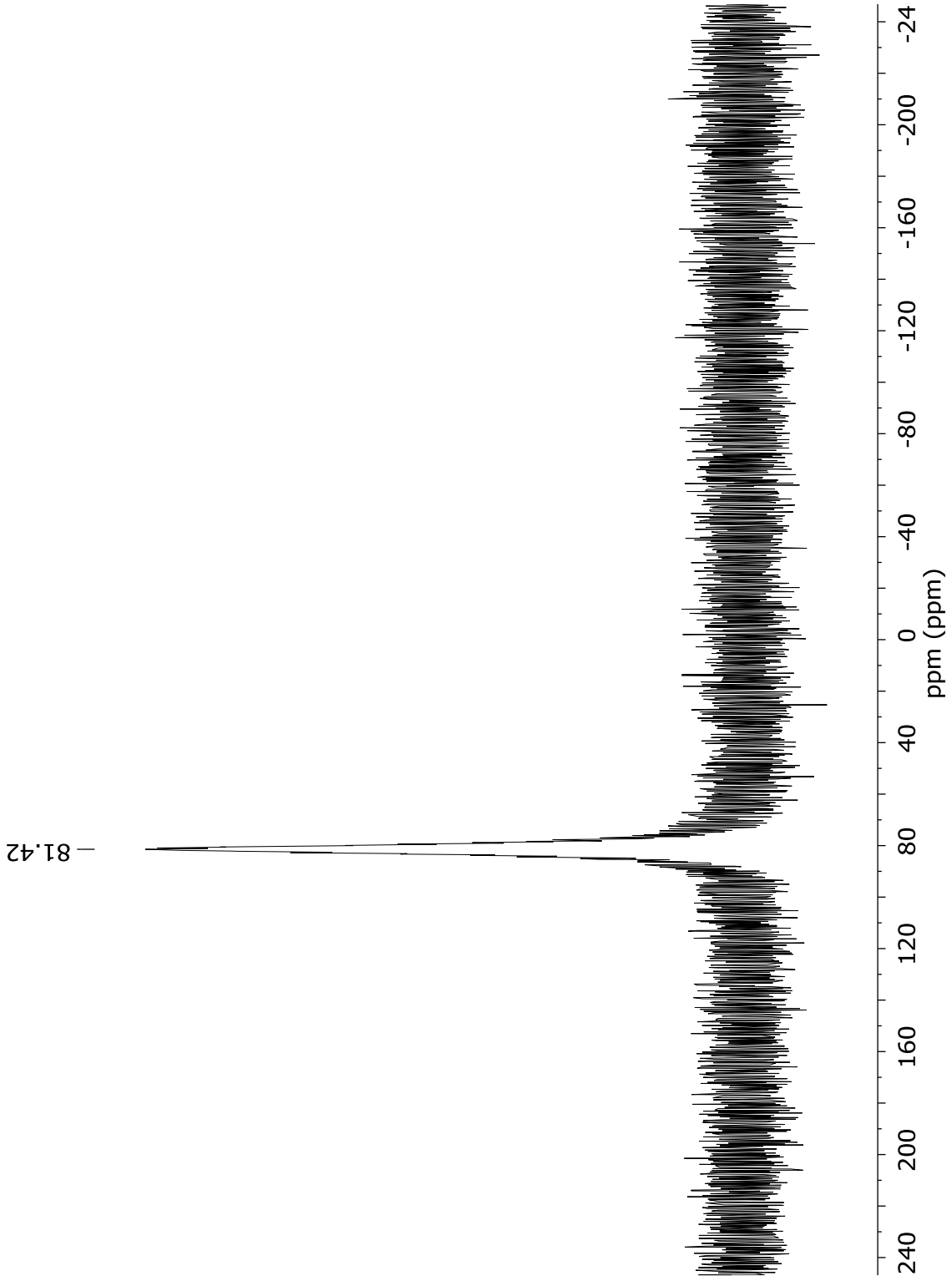

Figure A.3.3: ^{13}C NMR (126 MHz, THF-d_8) spectrum of compound **3.2**.

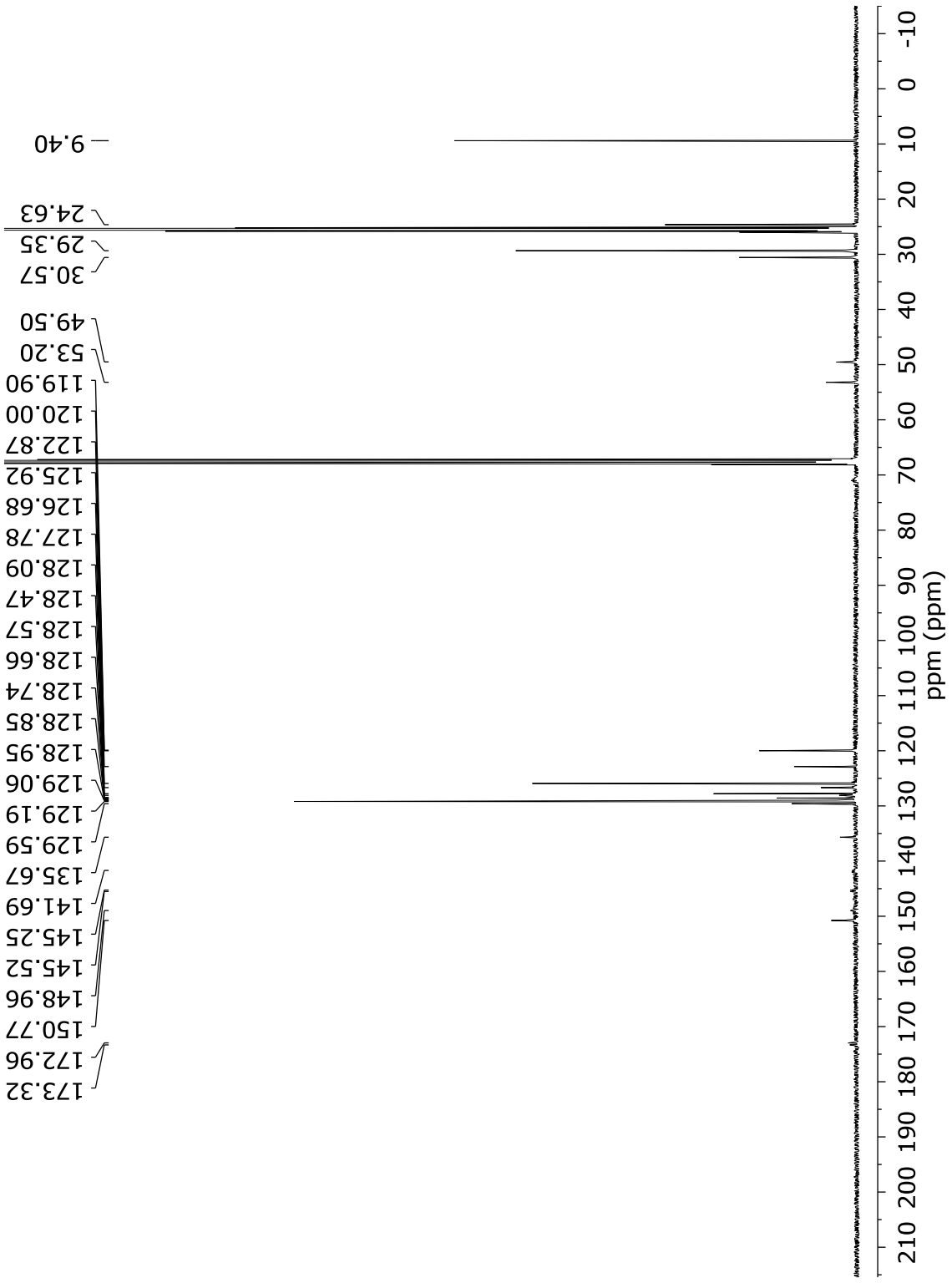

Figure A.3.4: ^{13}C APT NMR (126 MHz, THF-d_8) spectrum of compound **3.2**.

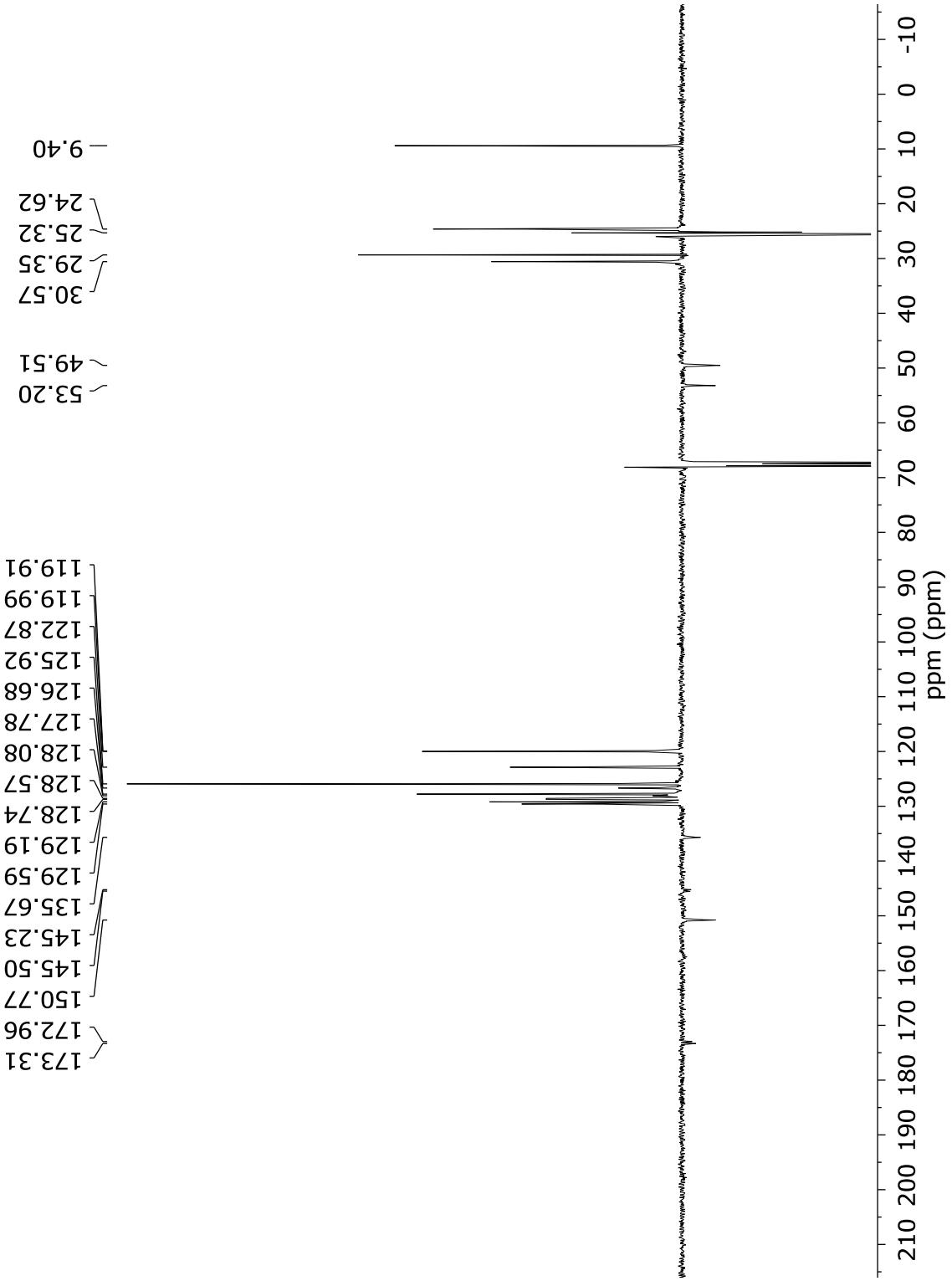

Figure A.3.5: ^{1}H-^{1}H COSY NMR (500 MHz, THF-d_8) spectrum of compound **3.2**.

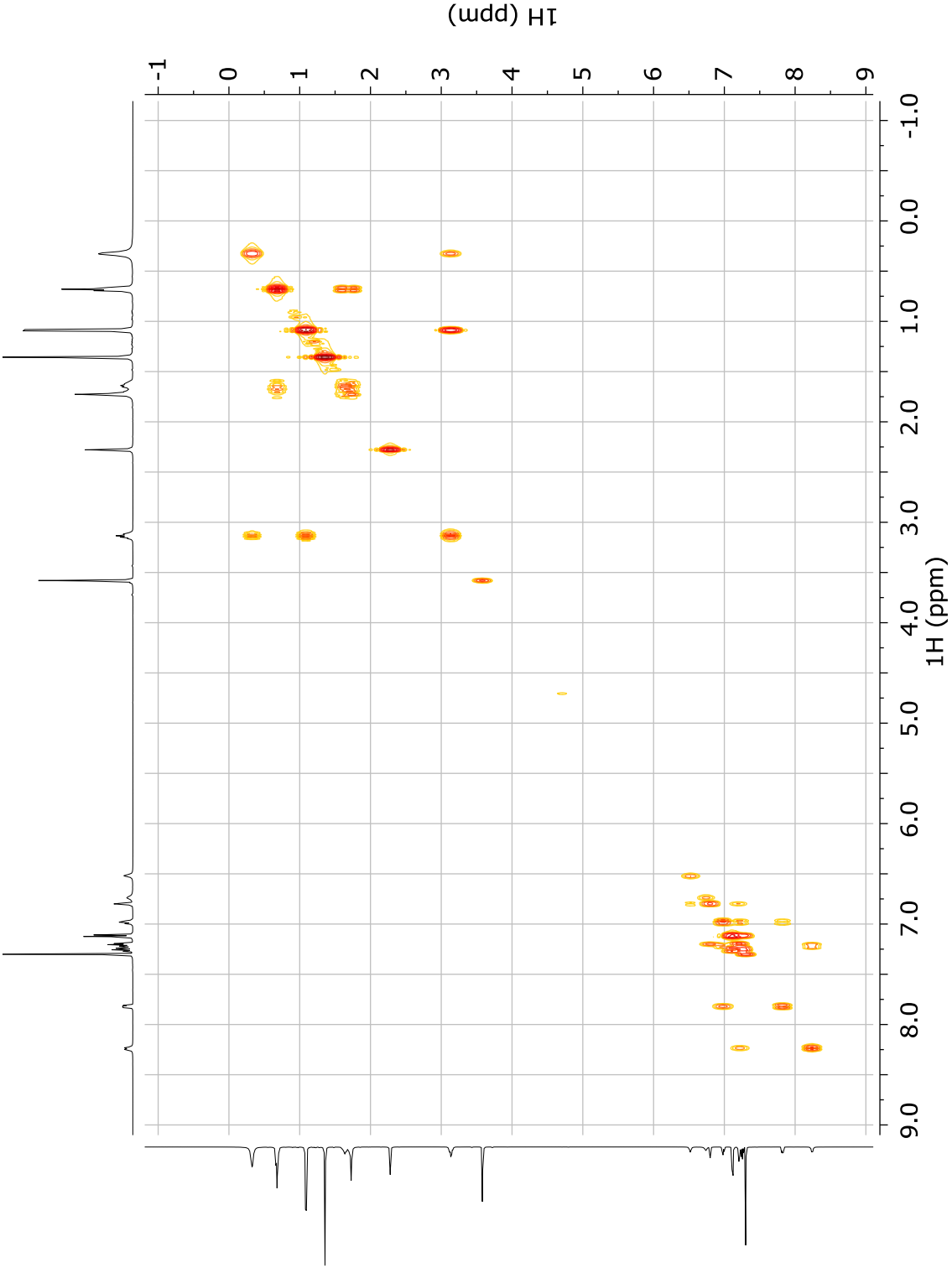

Figure A.3.6: ^{1}H-^{1}H NOESY NMR (500 MHz, THF-d_8) spectrum of compound **3.2**.

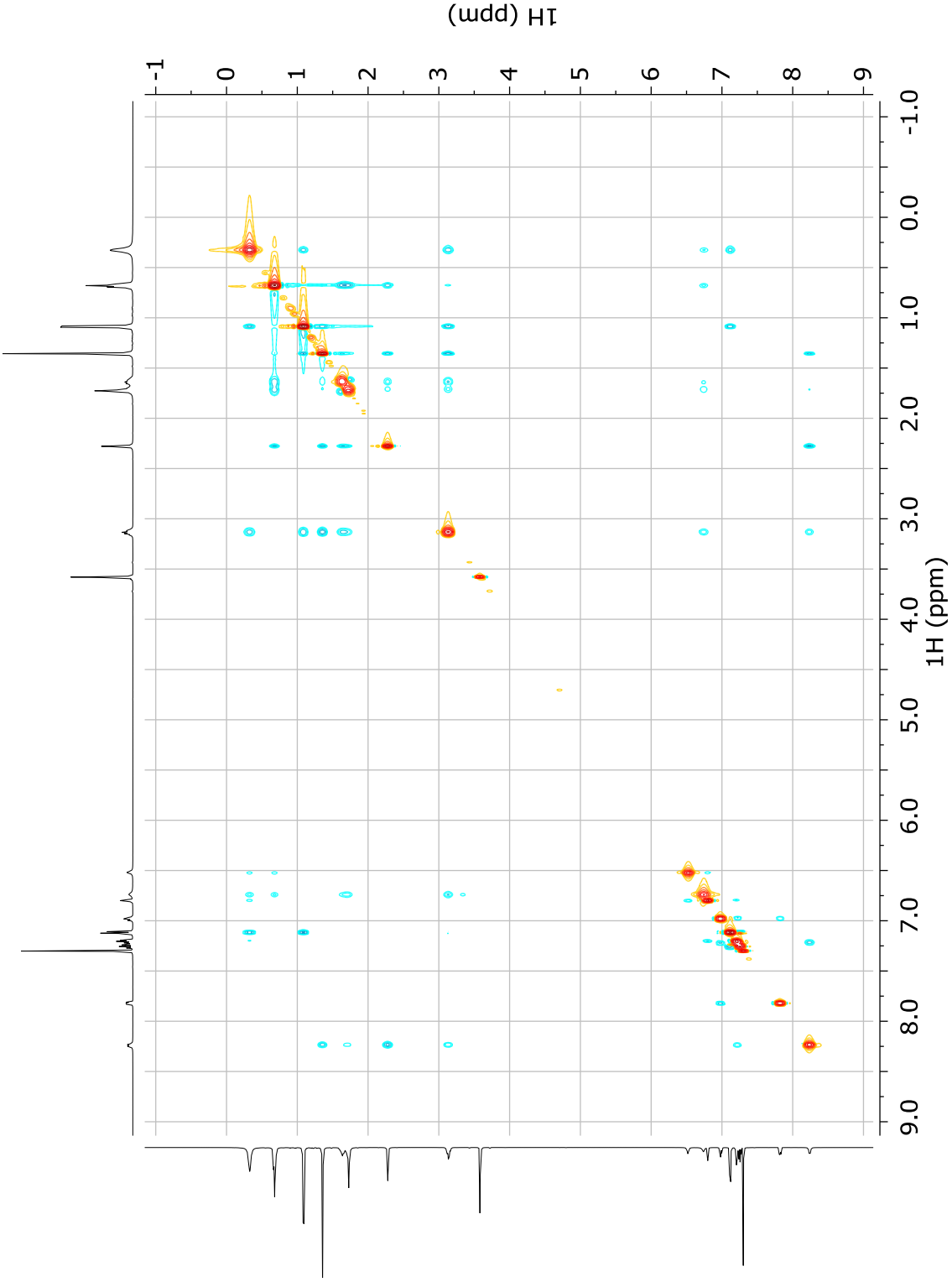

Figure A.3.7: ^{1}H-^{13}C HSQC NMR (500 MHz, THF-d_8) spectrum of compound **3.2**.

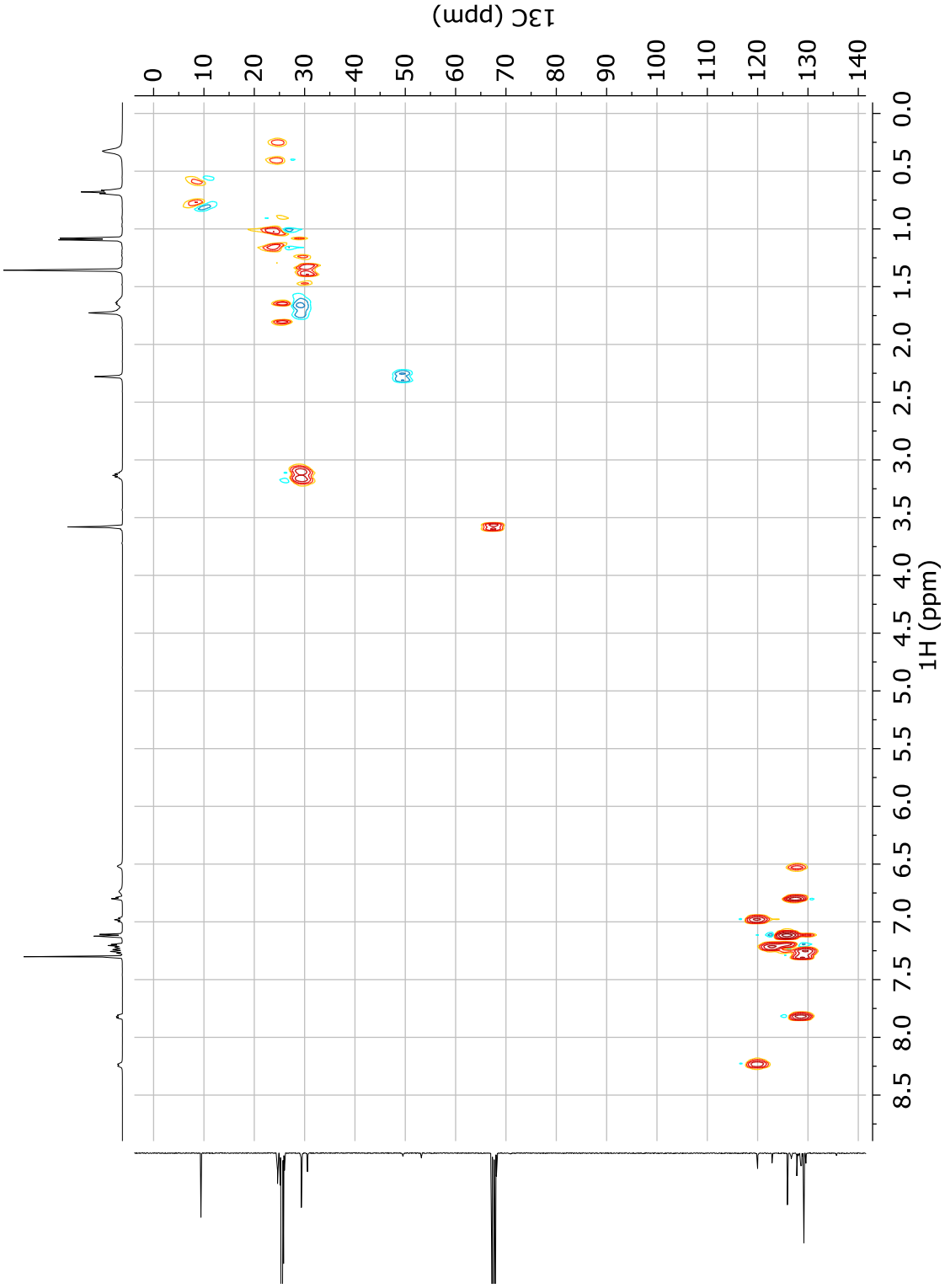

Figure A.3.8: ^{1}H-^{13}C HMBC NMR (500 MHz, THF-d_8) spectrum of compound **3.2**.

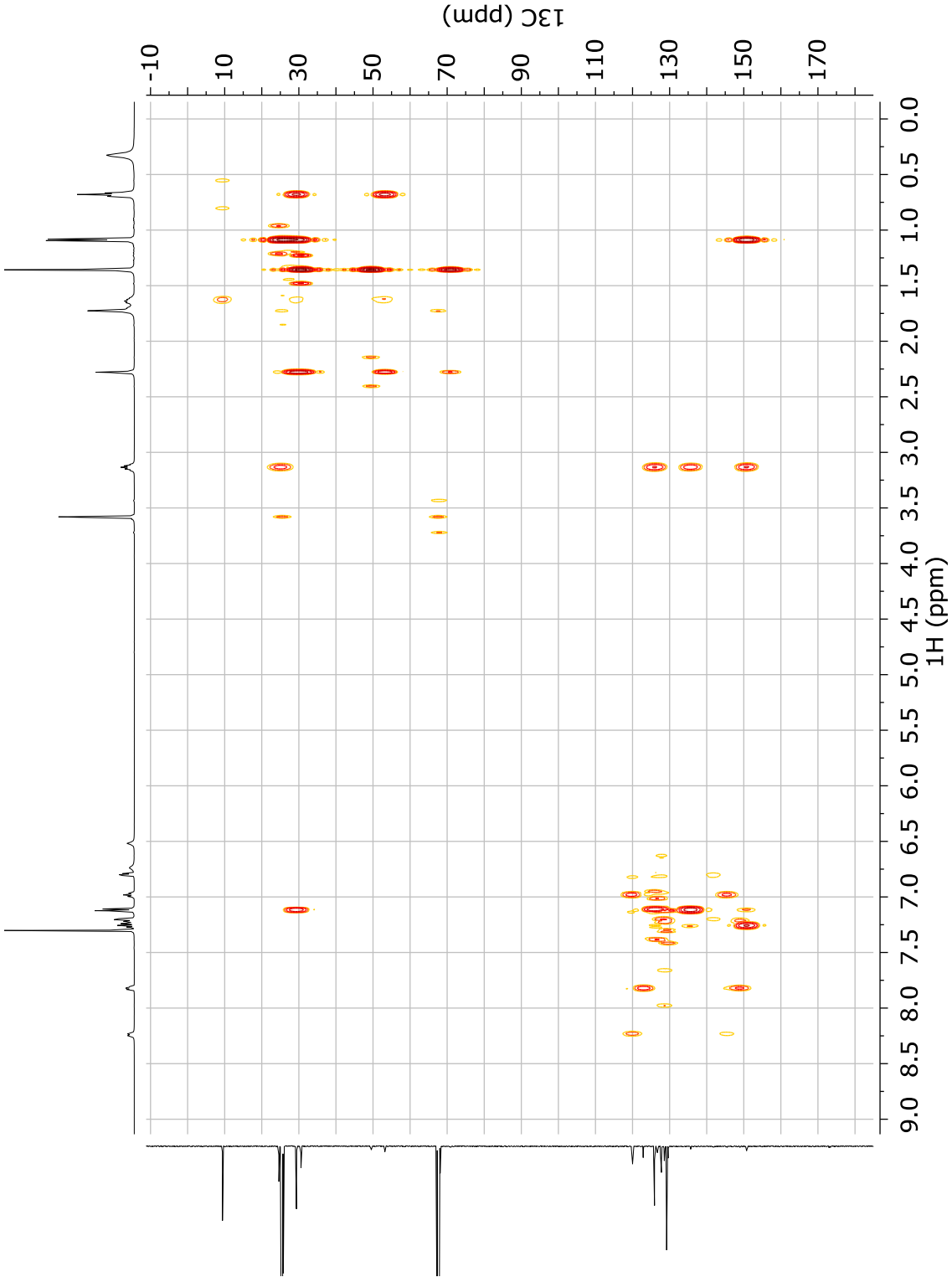

Section A.4: NMR Spectra for Compounds Included in **Chapter 4**.

Figure A.4.1: ^{1}H NMR (500 MHz, THF-d_8) spectrum of compound **4.1**.

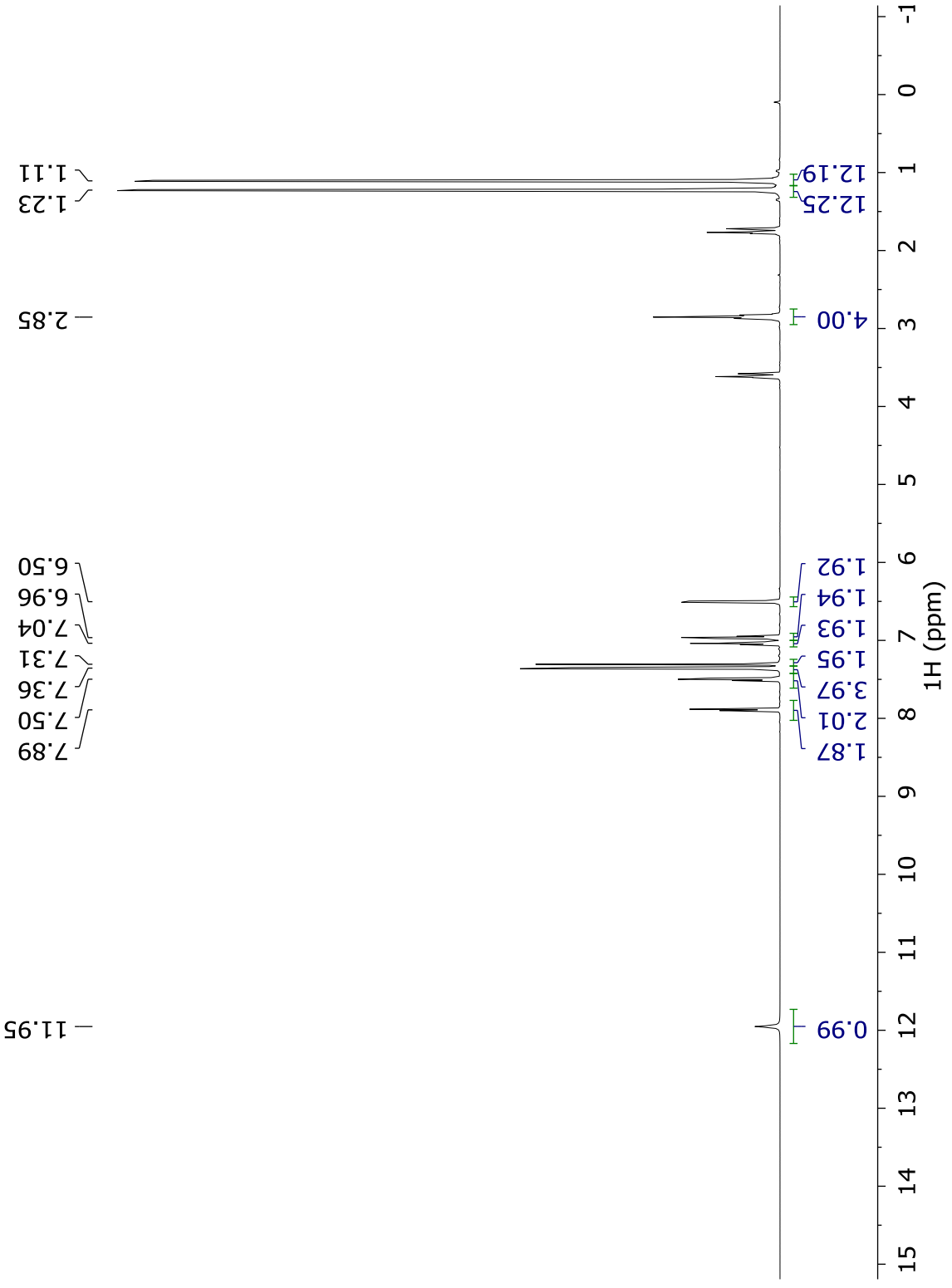

Figure A.4.2: ^{13}C {^{1}H} NMR (126 MHz, THF-d_8) spectrum of compound **4.1**.

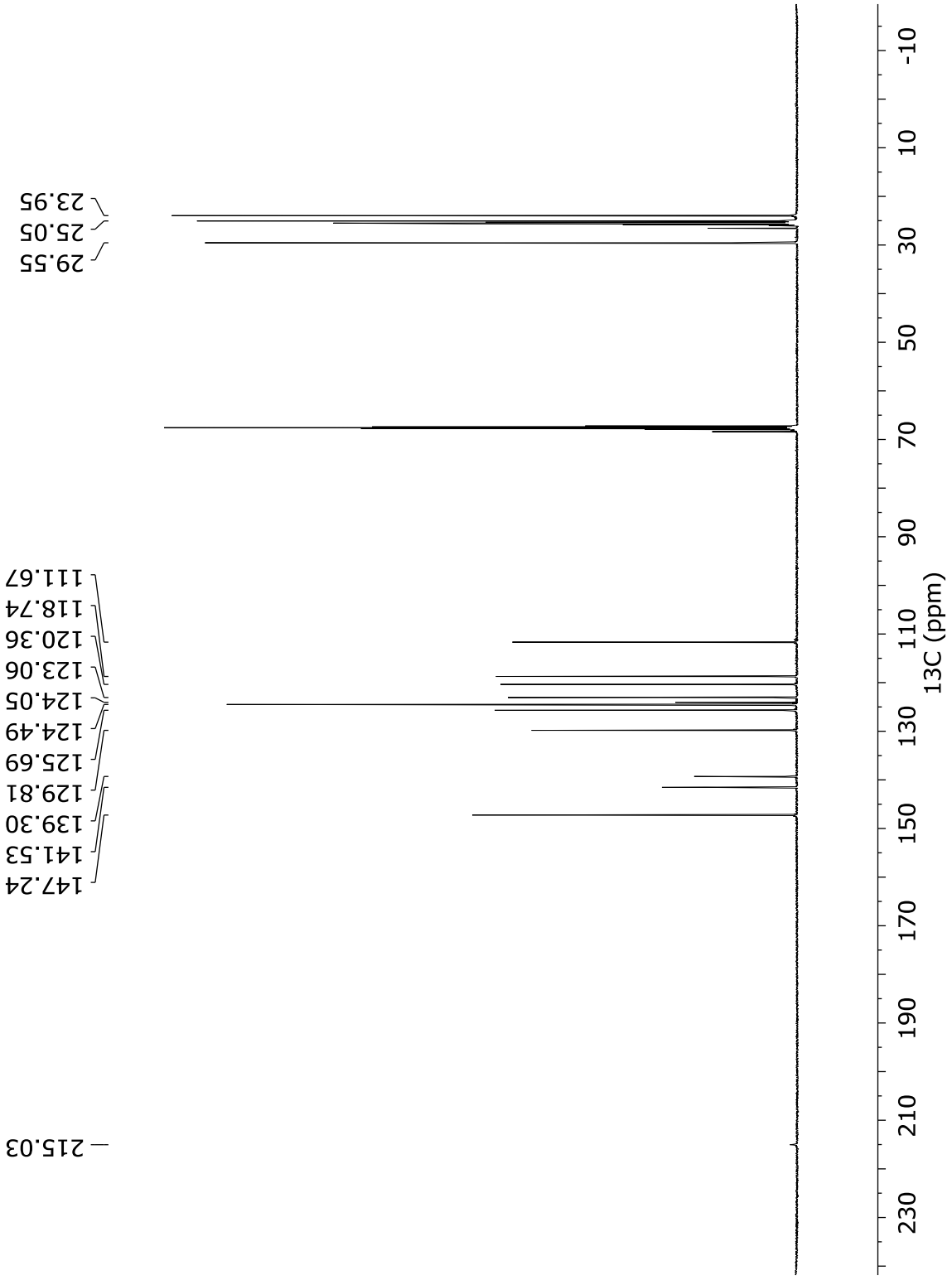

Figure A.4.3: ^{13}C {^{1}H} APT NMR (126 MHz, THF-d_8) spectrum of compound **4.1**.

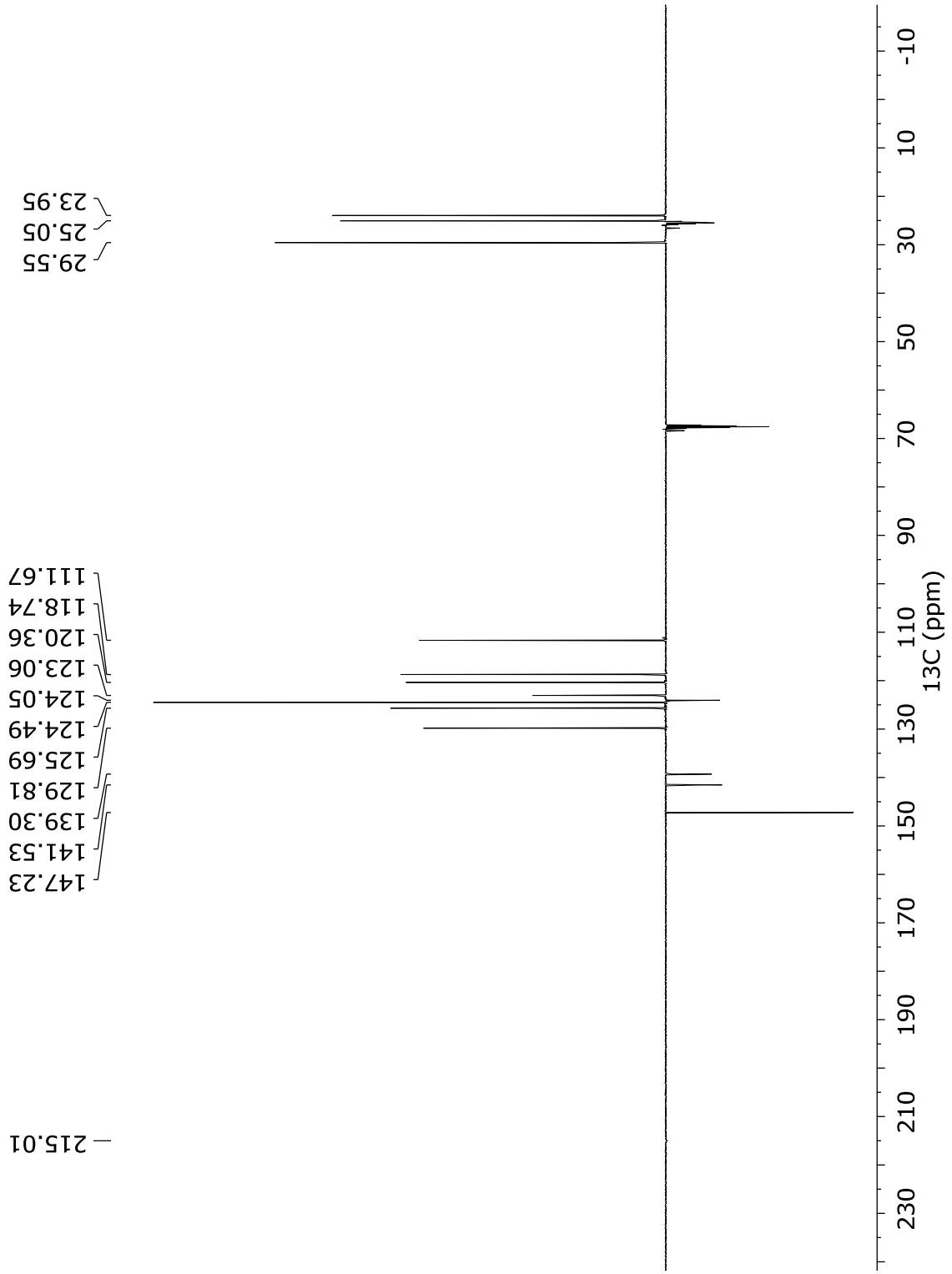

Figure A.4.4: ^{1}H-^{1}H COSY NMR (500 MHz, THF-d_8) spectrum of compound **4.1**.

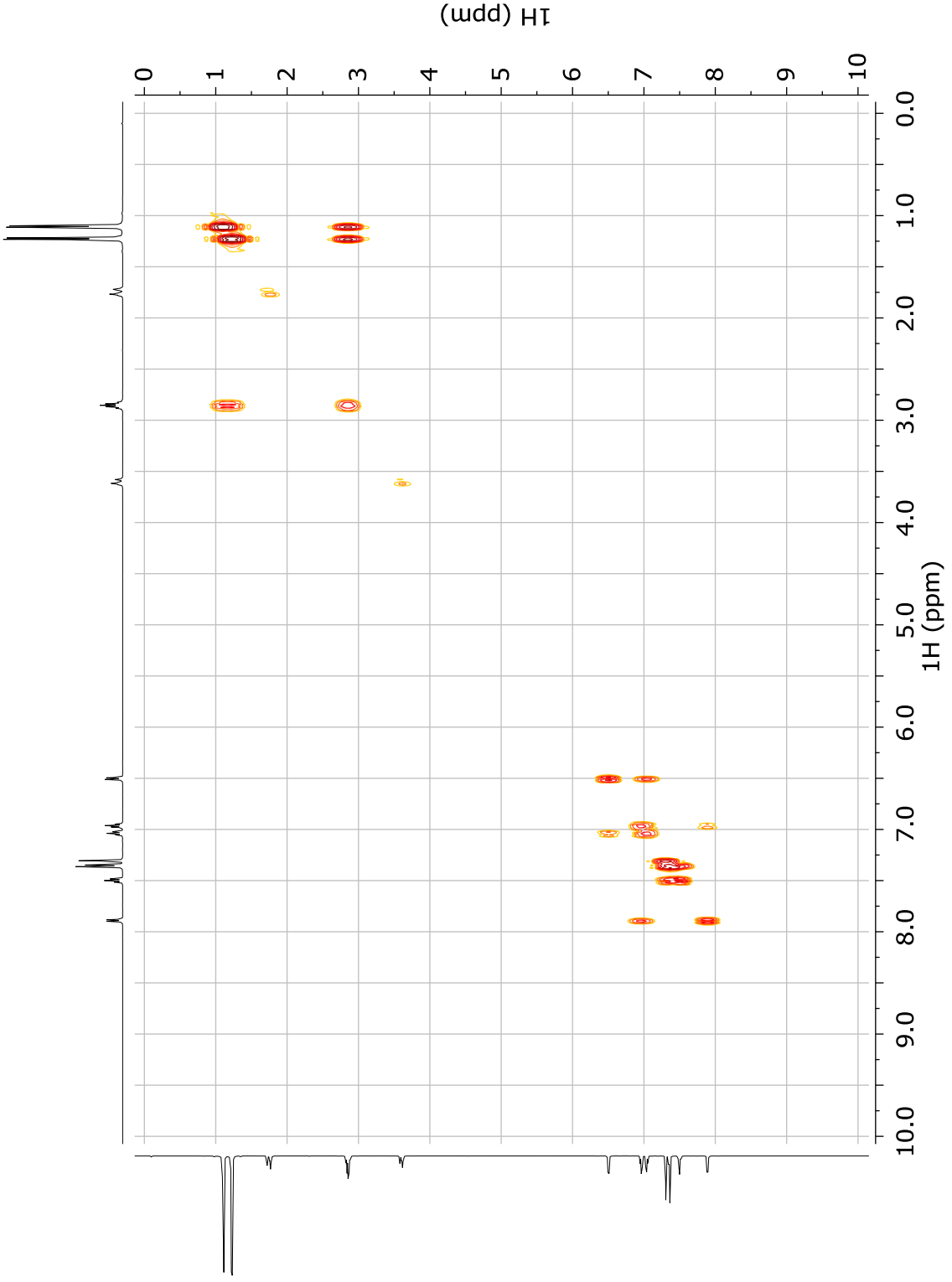

Figure A.4.5: ^{1}H-^{1}H NOESY NMR (500 MHz, THF-d_8) spectrum of compound **4.1**.

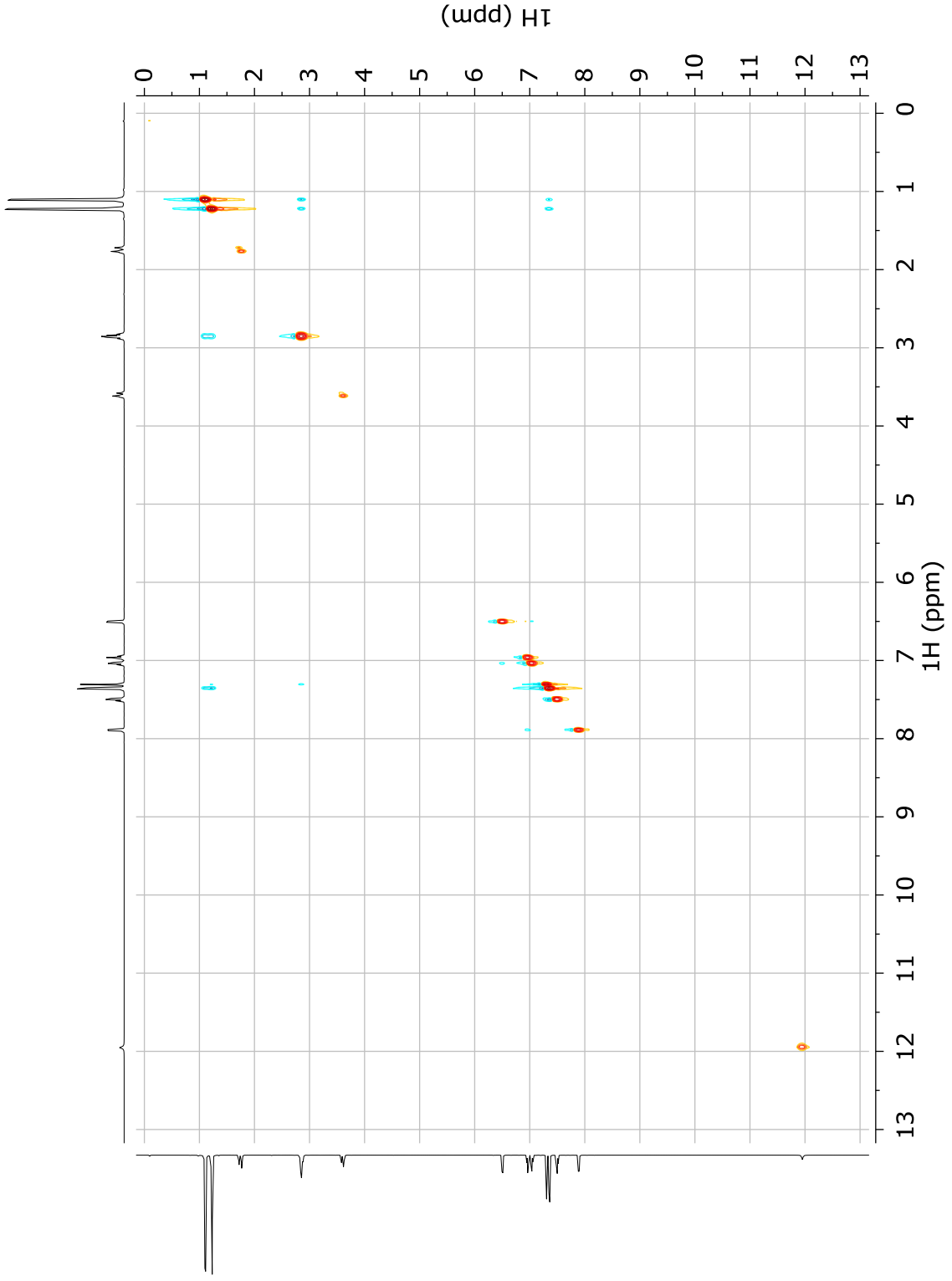

Figure A.4.6: ^{1}H-^{13}C HSQC NMR (500 MHz, THF-d_8) spectrum of compound **4.1**.

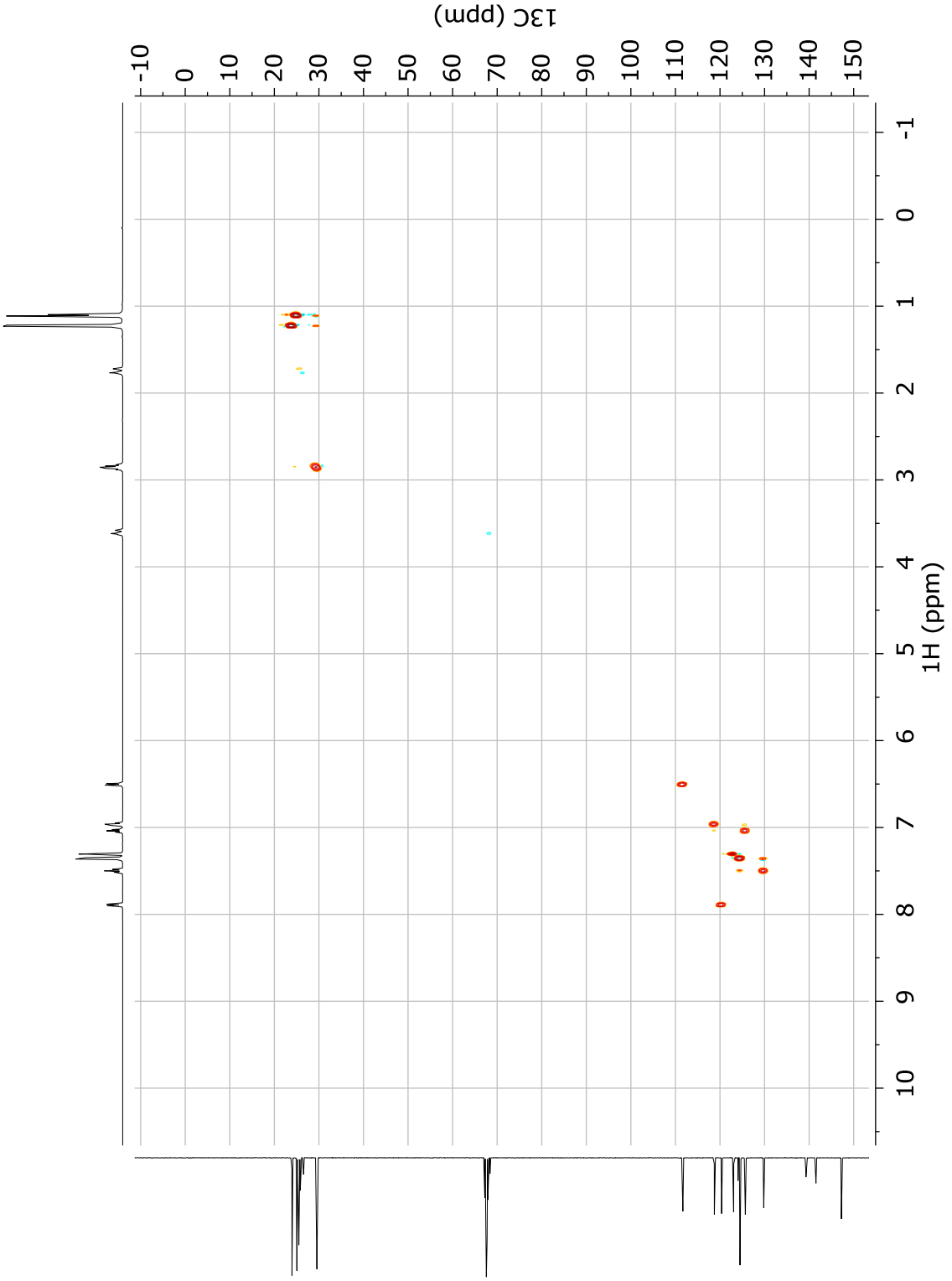

Figure A.4.7: ^{1}H-^{13}C HMBC NMR (500 MHz, THF-d_8) spectrum of compound **4.1**.

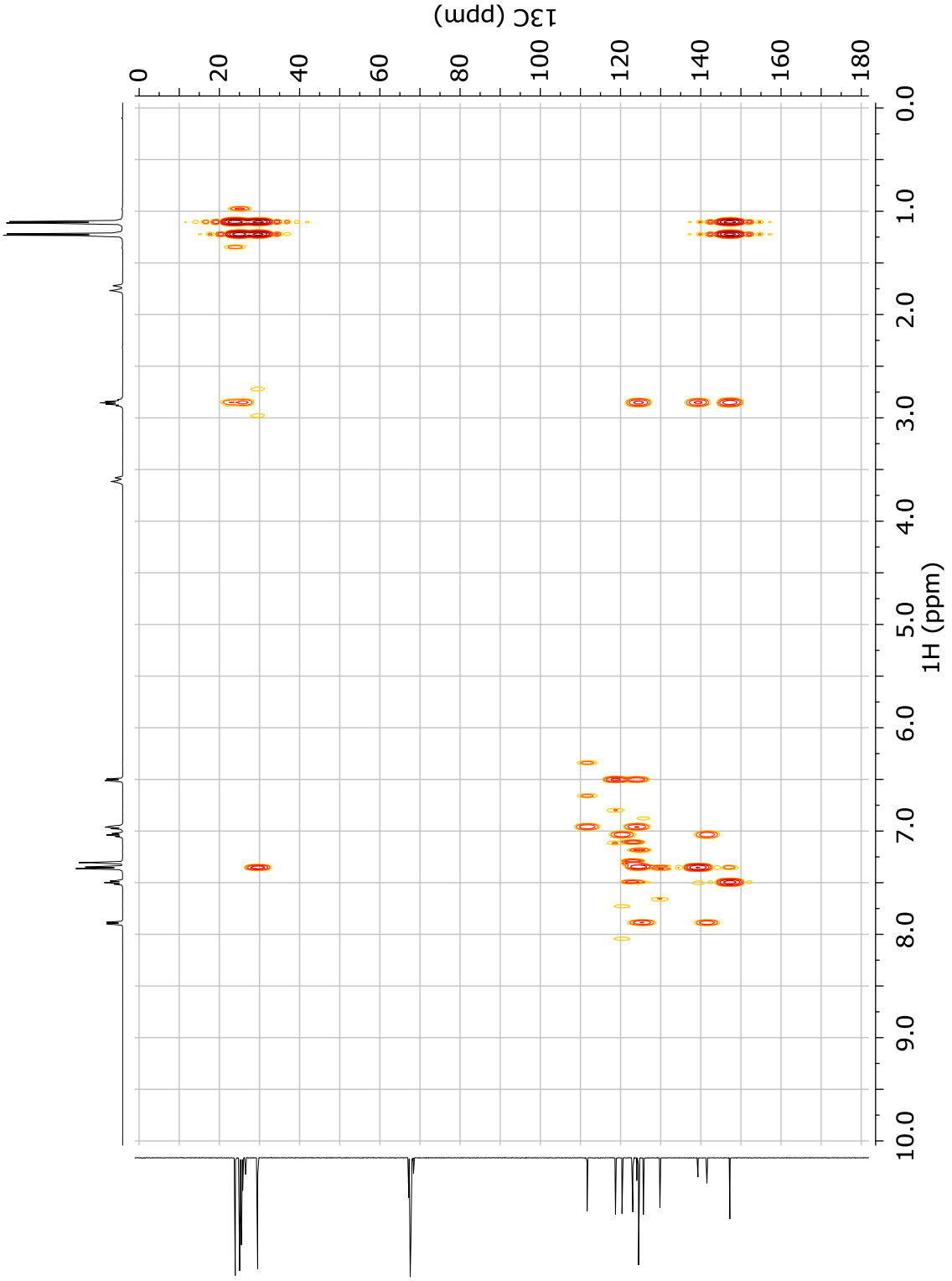

Figure A.4.8: ^{1}H NMR (500 MHz, THF-d_8) spectrum of compound **4.2**.

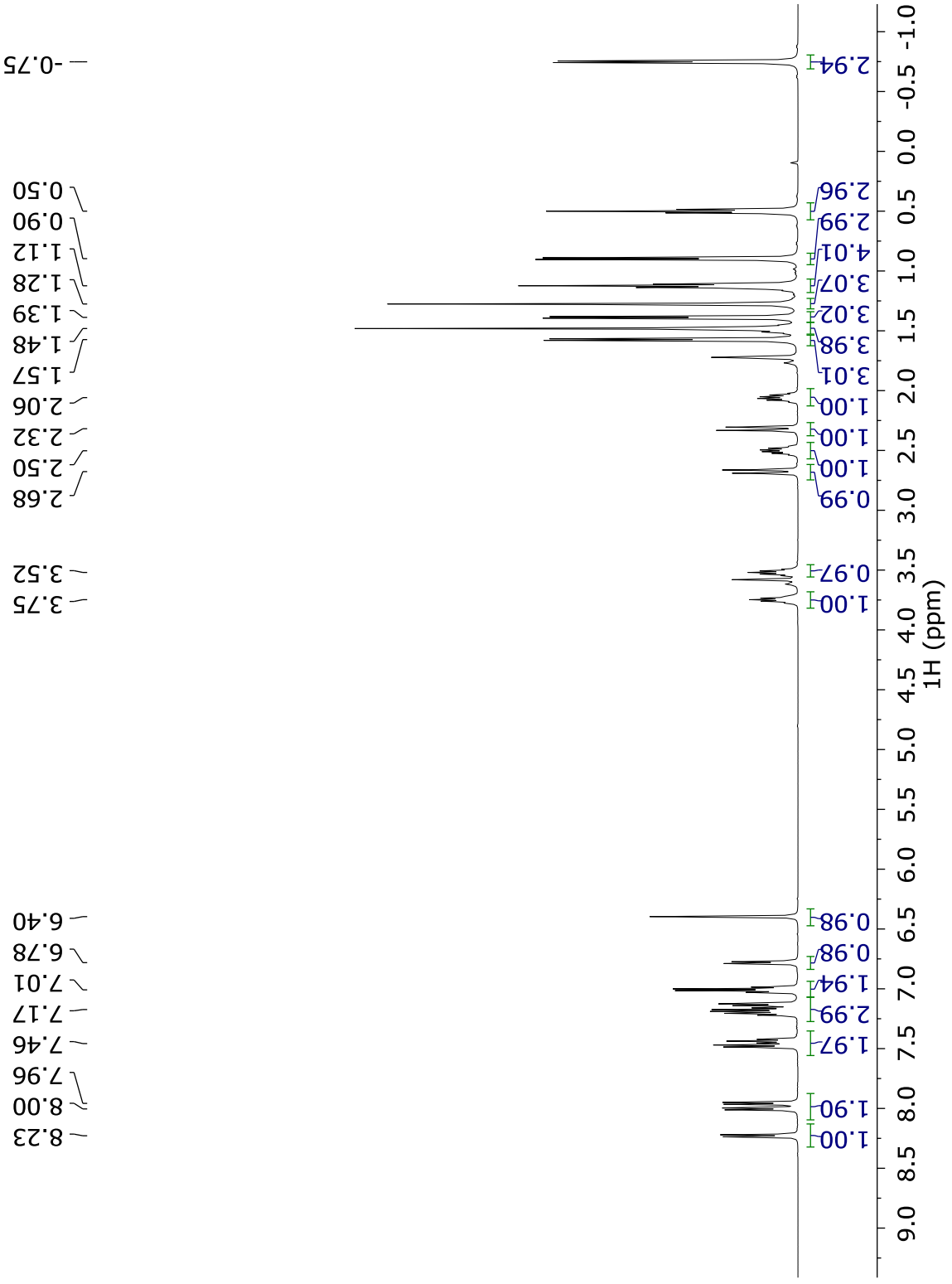

Figure A.4.9: ^{13}C NMR (126 MHz, THF-d_8) spectrum of compound **4.2**.

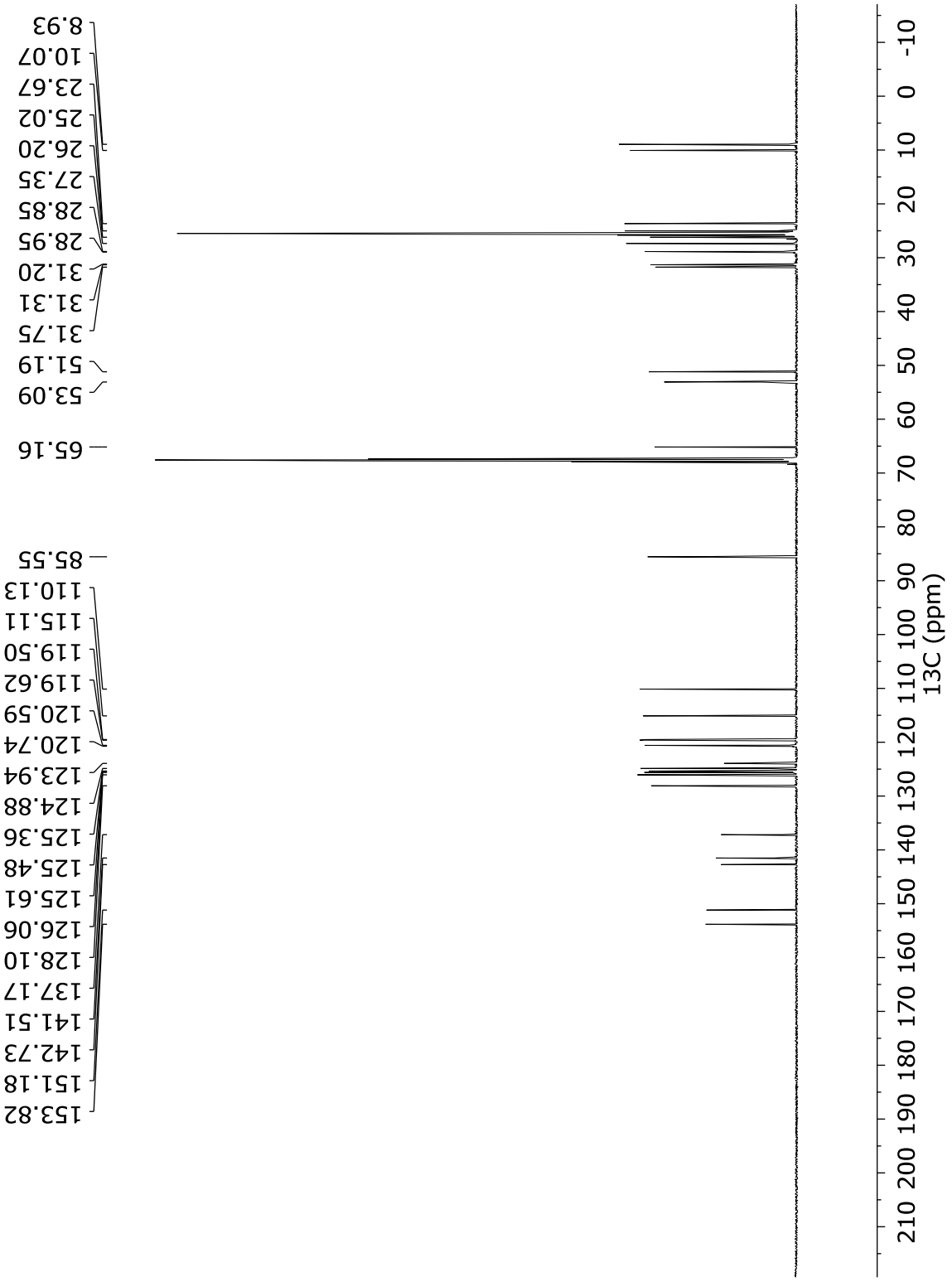

Figure A.4.10: ^{13}C APT NMR (126 MHz, THF-d_8) spectrum of compound **4.2**.

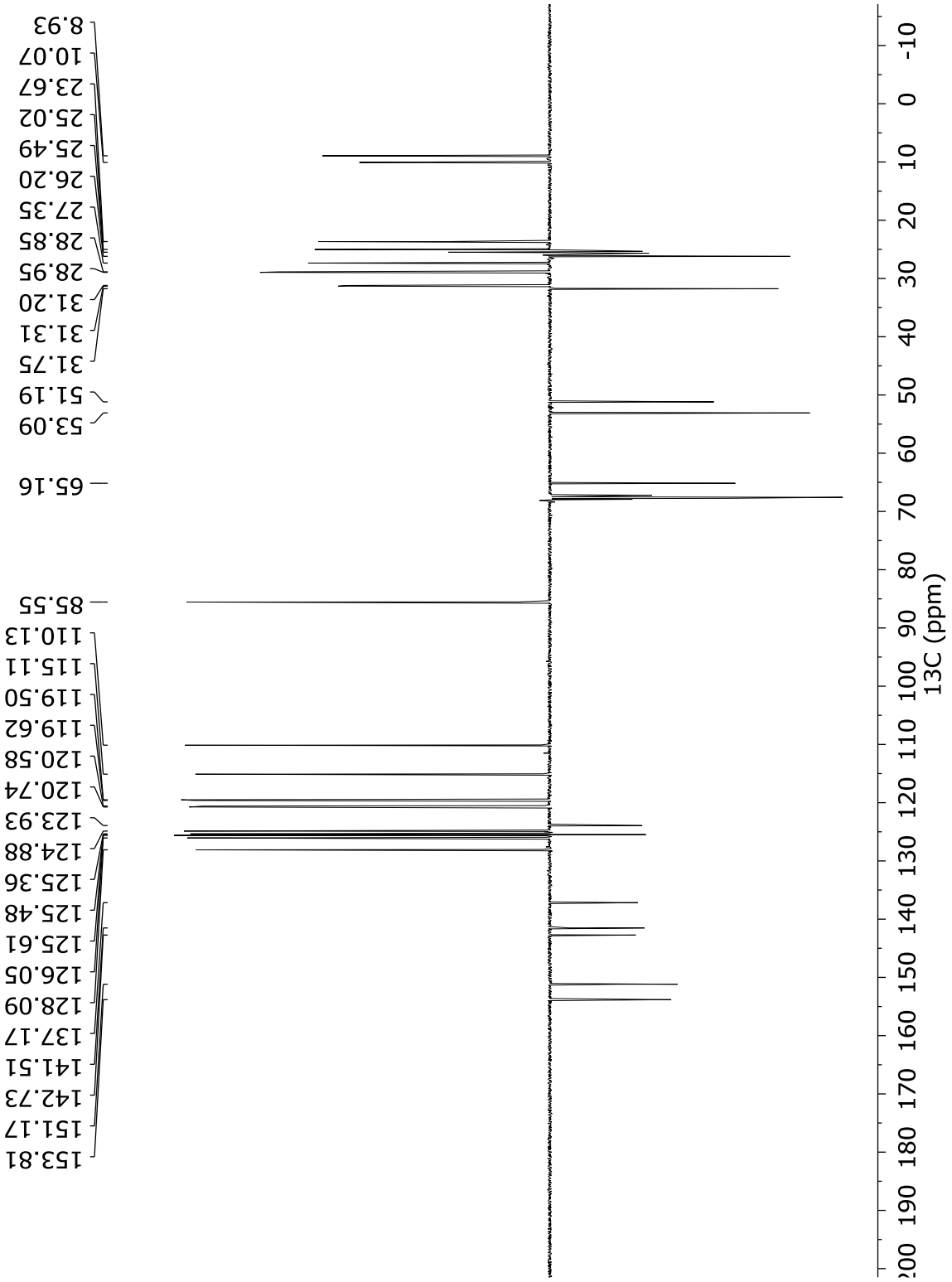

Figure A.4.11: ^{1}H-^{1}H COSY NMR (500 MHz, THF-d_8) spectrum of compound **4.2**.

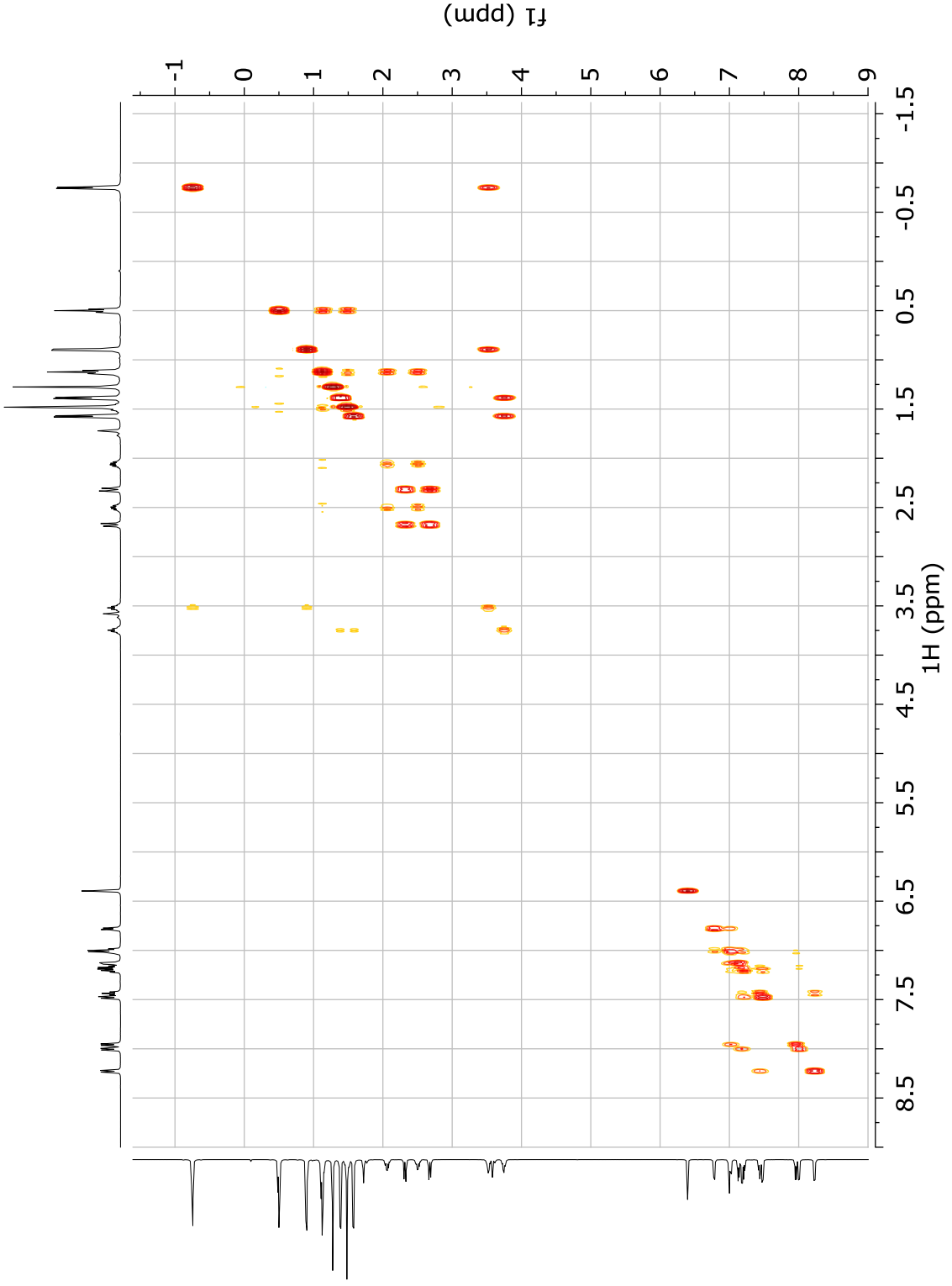

Figure A.4.12: ^{1}H-^{1}H NOESY NMR (500 MHz, THF-d_8) spectrum of compound **4.2**.

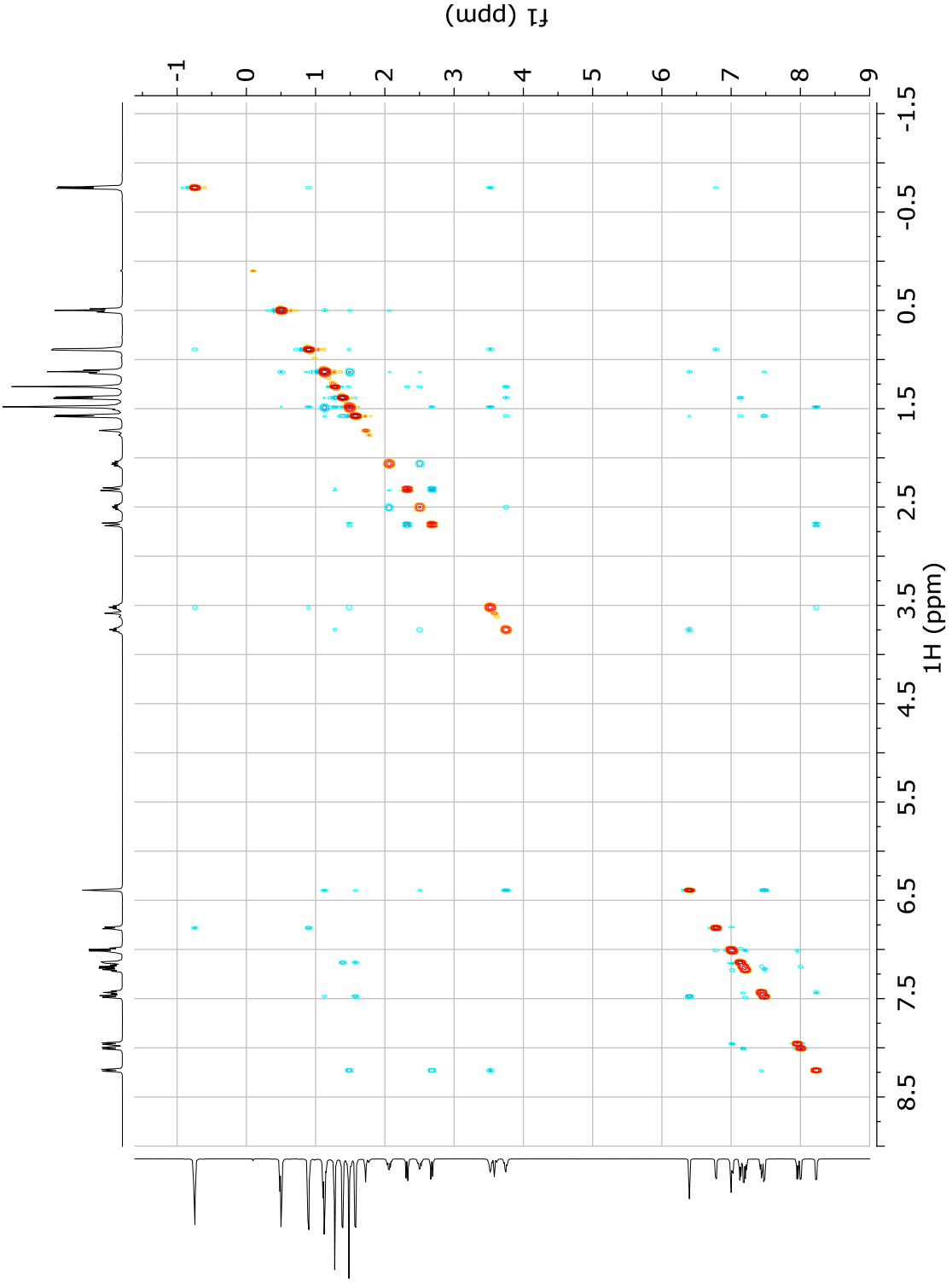

Figure A.4.13: ^{1}H-^{13}C HSQC NMR (500 MHz, THF-d_8) spectrum of compound **4.2**.

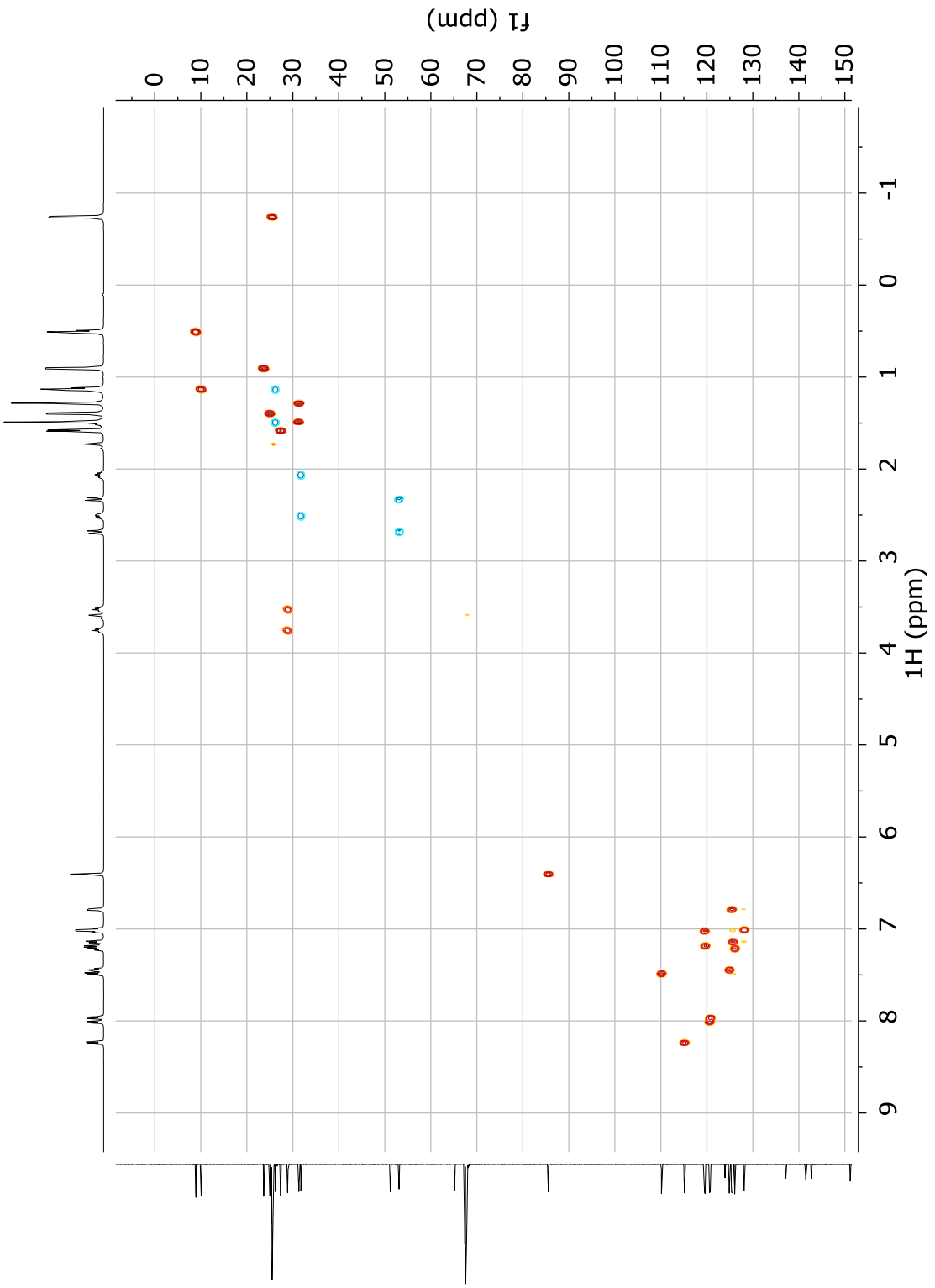

Figure A.4.14: ^{1}H-^{13}C HMBC NMR (500 MHz, THF-d_8) spectrum of compound **4.2**.

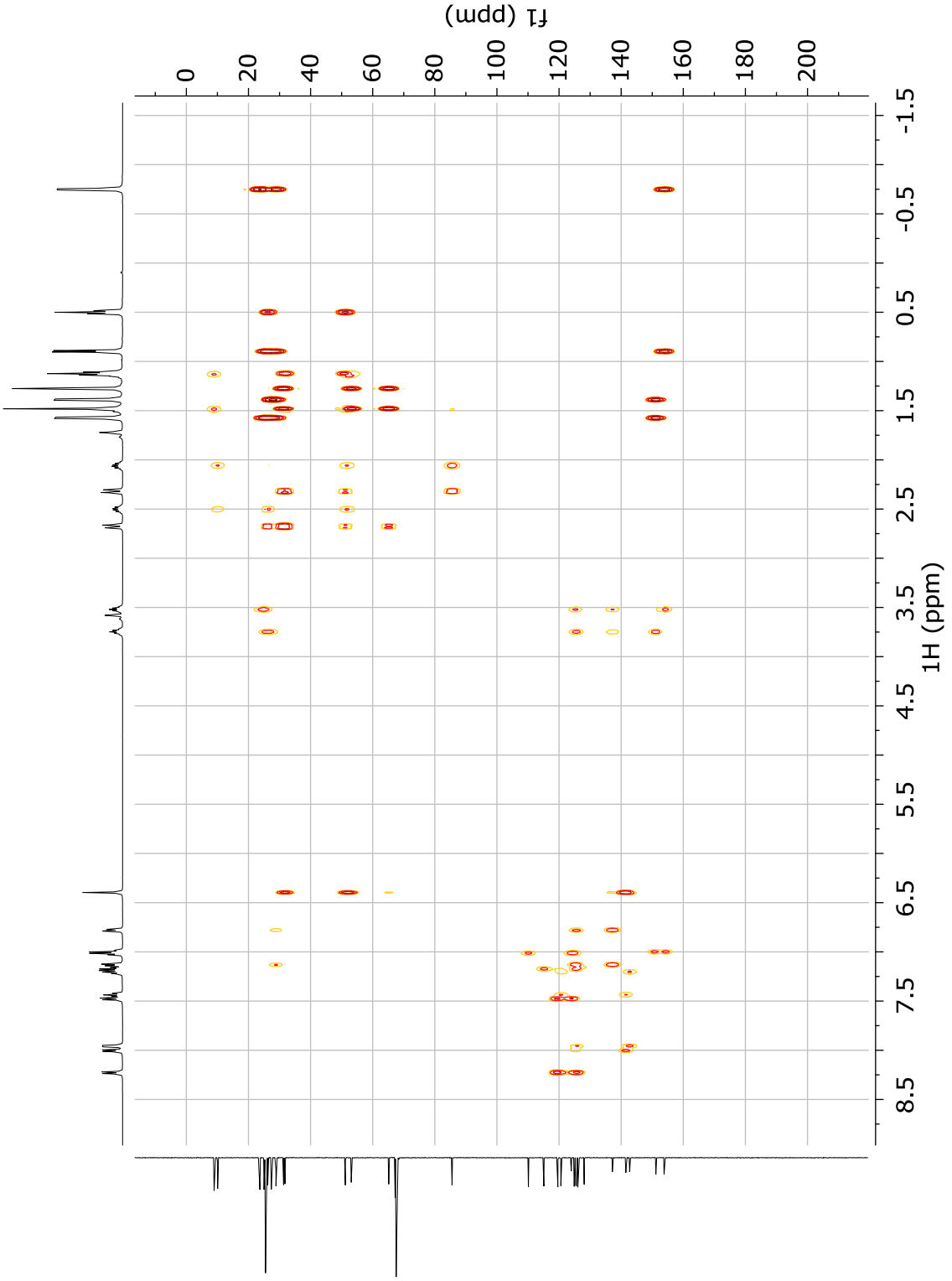

Figure A.4.15: ^{1}H NMR (500 MHz, THF-d_8) spectrum of compound **4.3**.

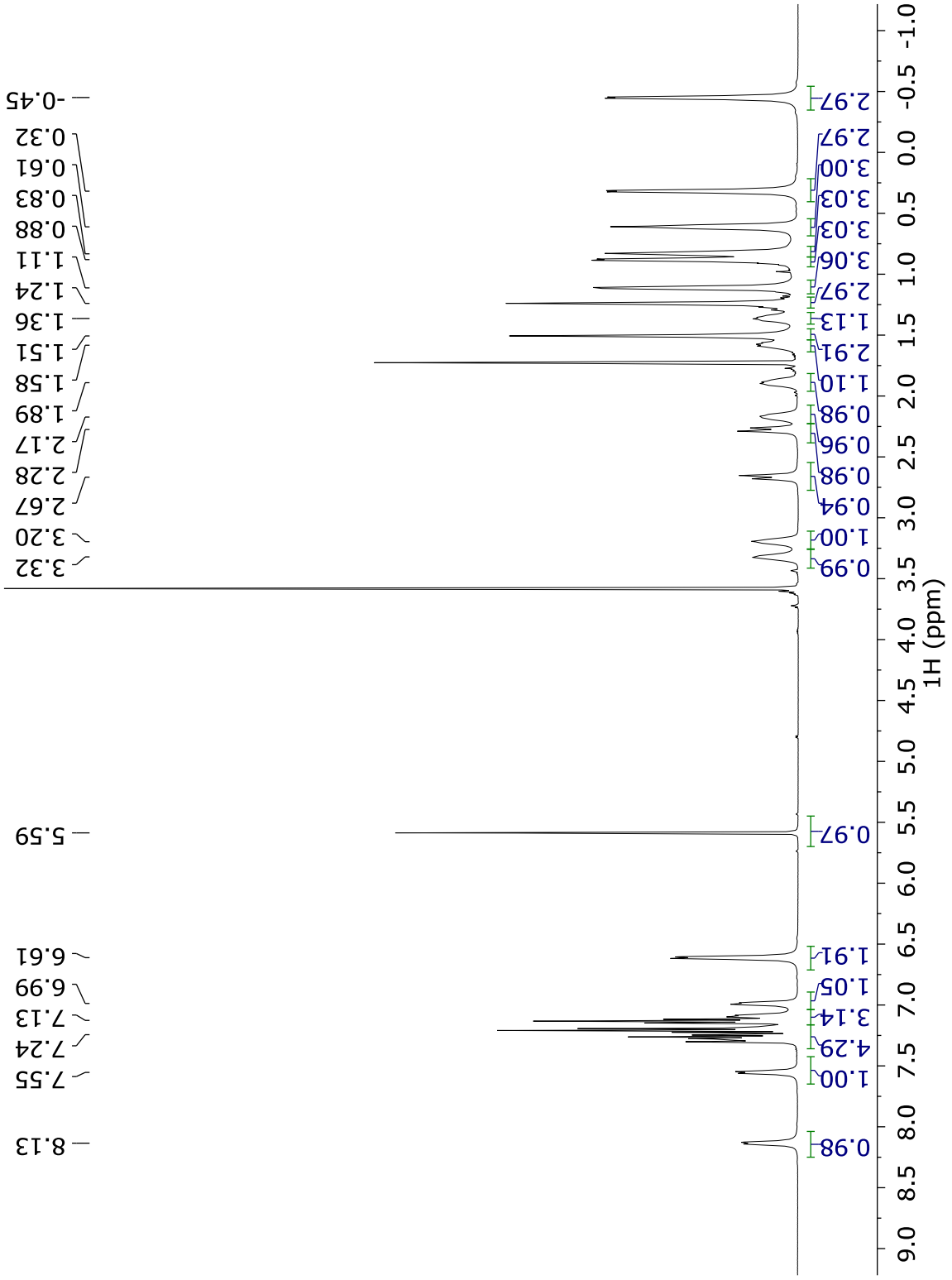

Figure A.4.16: ^{13}C NMR (126 MHz, THF-d_8) spectrum of compound **4.3**.

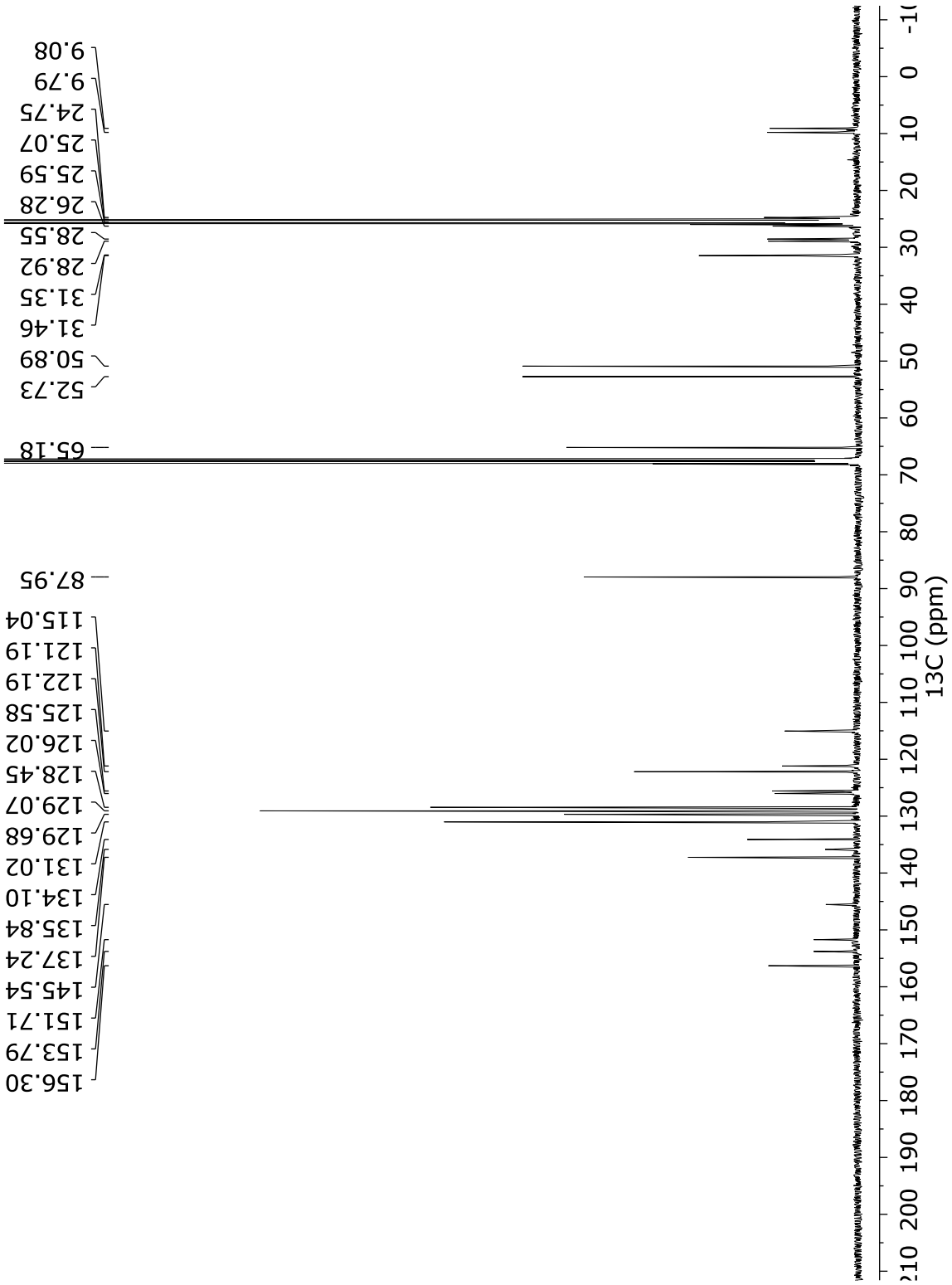

Figure A.4.17: ^{13}C APT NMR (126 MHz, THF-d_8) spectrum of compound **4.3**.

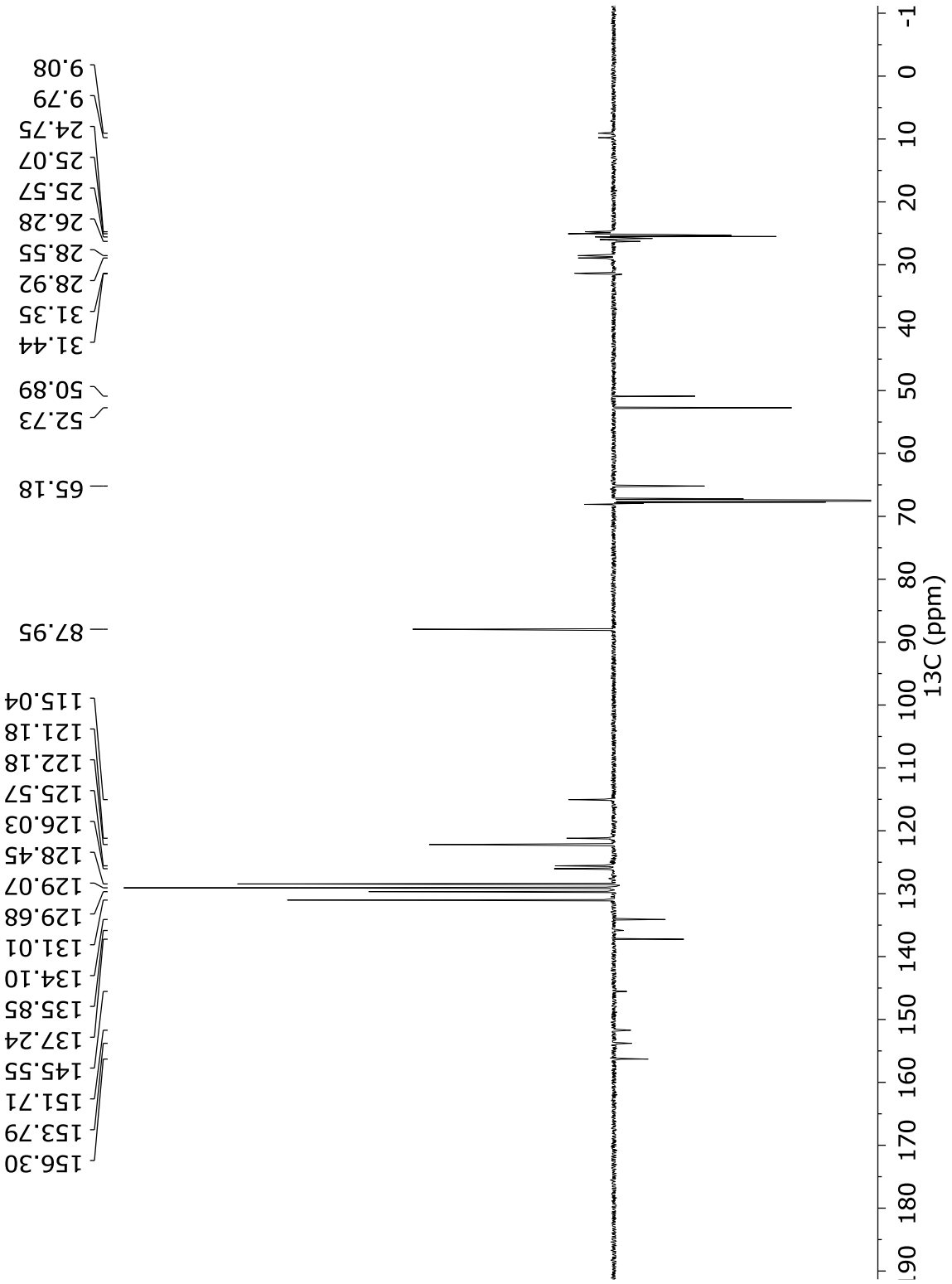

Figure A.4.18: ^{1}H-^{1}H COSY NMR (500 MHz, THF-d_8) spectrum of compound **4.3**.

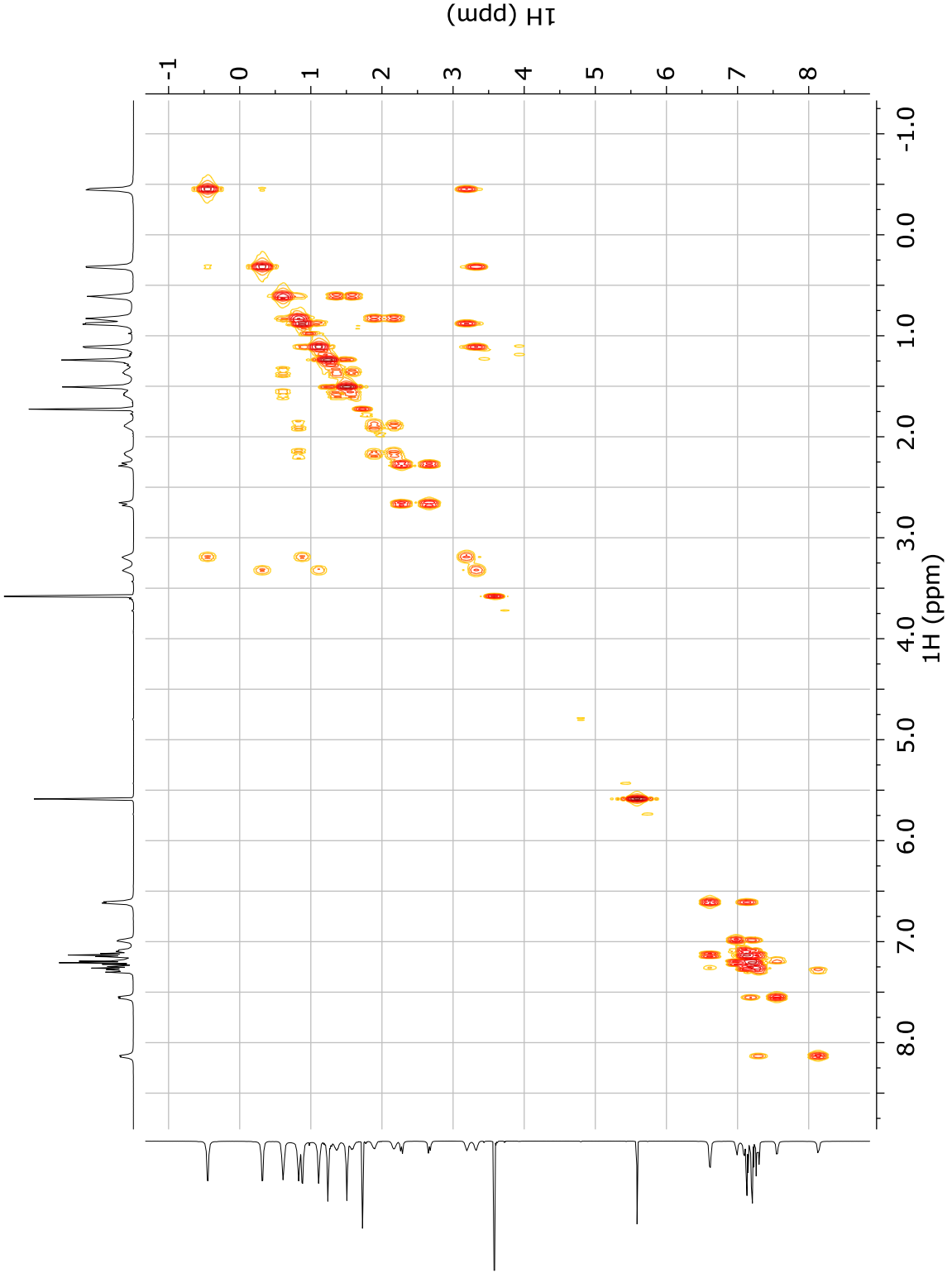

Figure A.4.19: ^{1}H-^{1}H NOESY NMR (500 MHz, THF-d_8) spectrum of compound **4.3**.

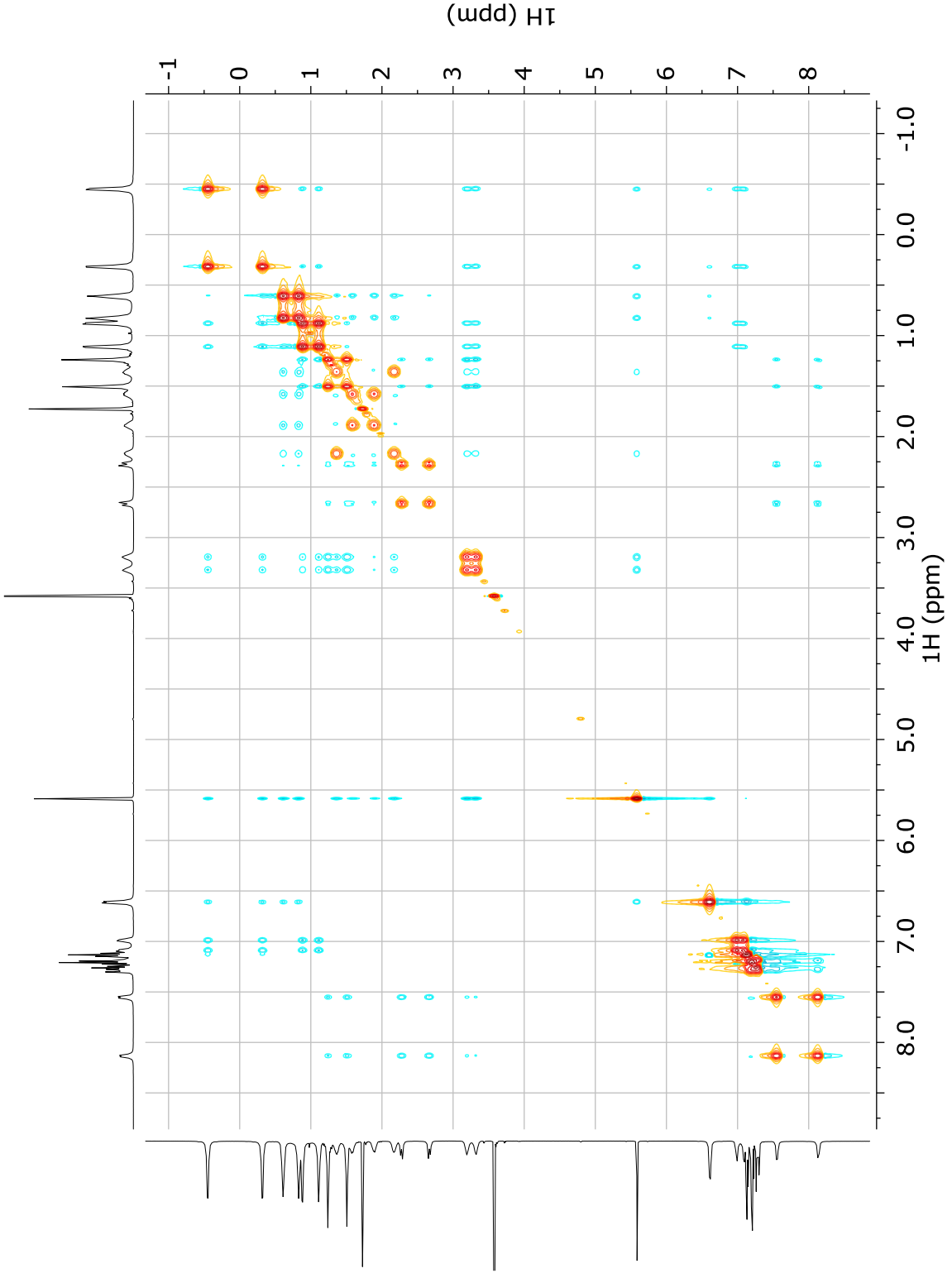

Figure A.4.20: ^{1}H-^{13}C HSQC NMR (500 MHz, THF-d_8) spectrum of compound **4.3**.

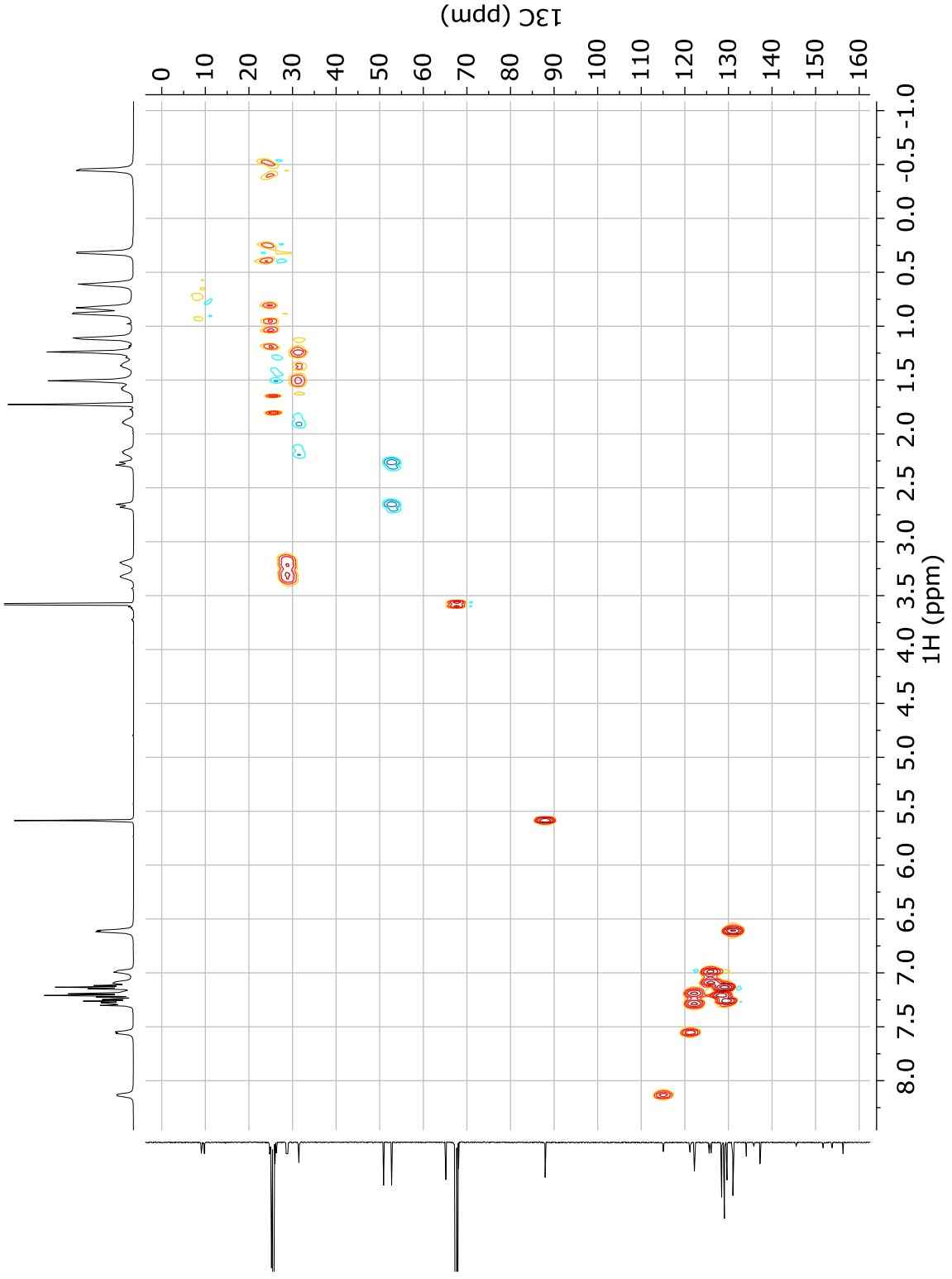

Figure A.4.21: ^{1}H-^{13}C HMBC NMR (500 MHz, THF-d_8) spectrum of compound **4.3**.

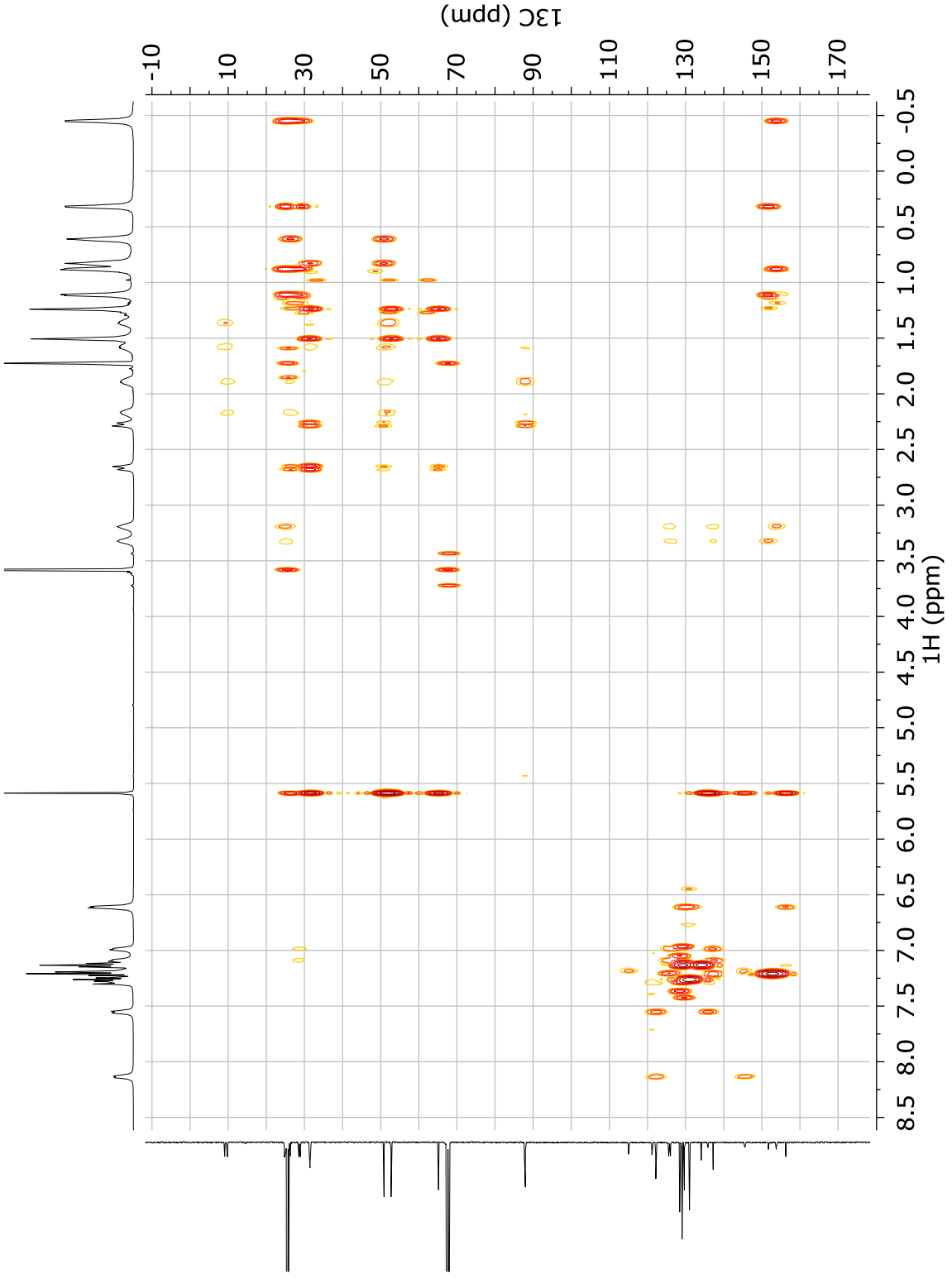

Figure A.4.22: ^{1}H NMR (500 MHz, THF-d_8) spectrum of compound **4.4**.

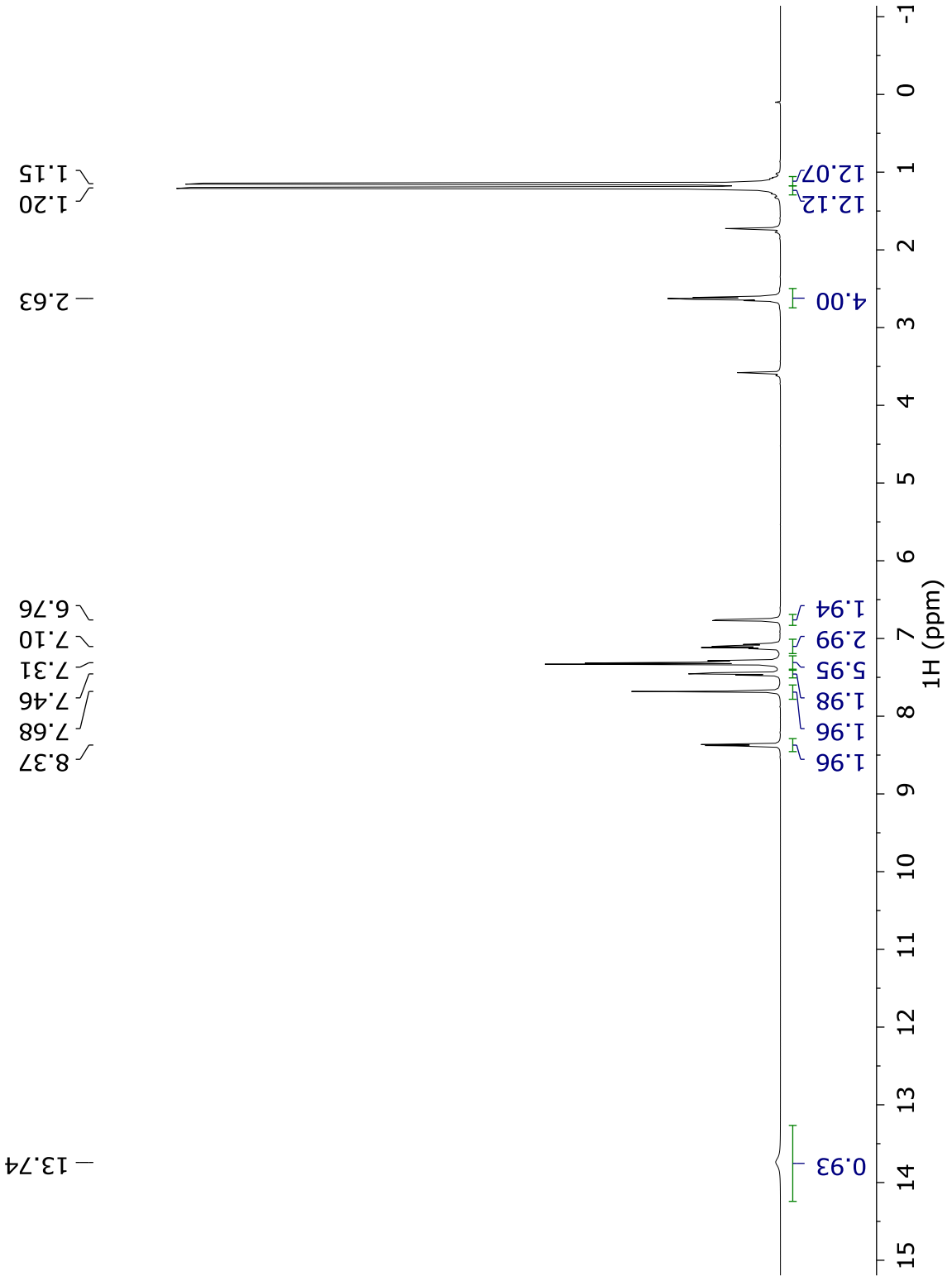

Figure A.4.23: ^{13}C NMR (126 MHz, THF-d_8) spectrum of compound **4.4**.

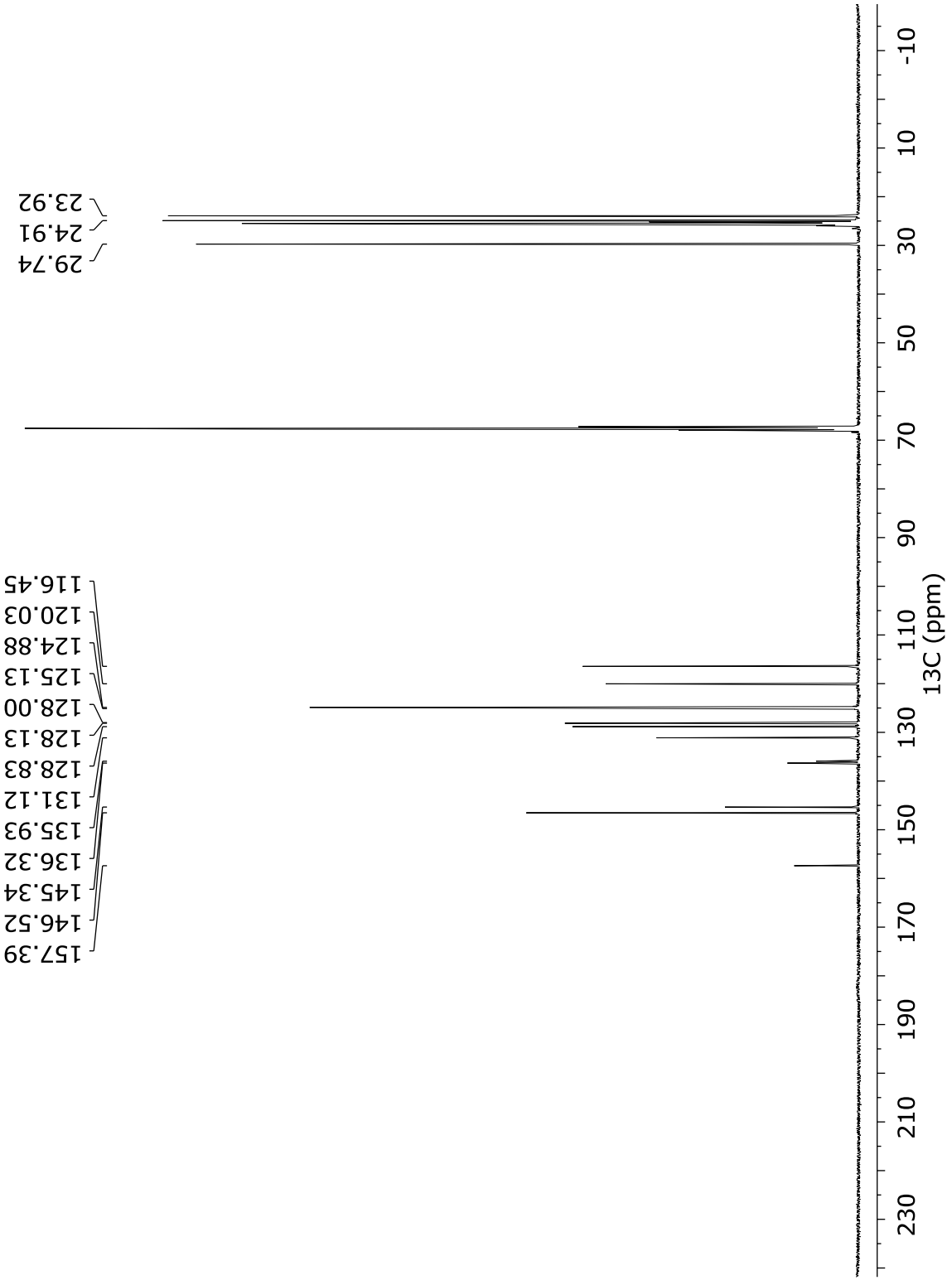

Figure A.4.24: ^{13}C APT NMR (126 MHz, THF-d_8) spectrum of compound **4.4**.

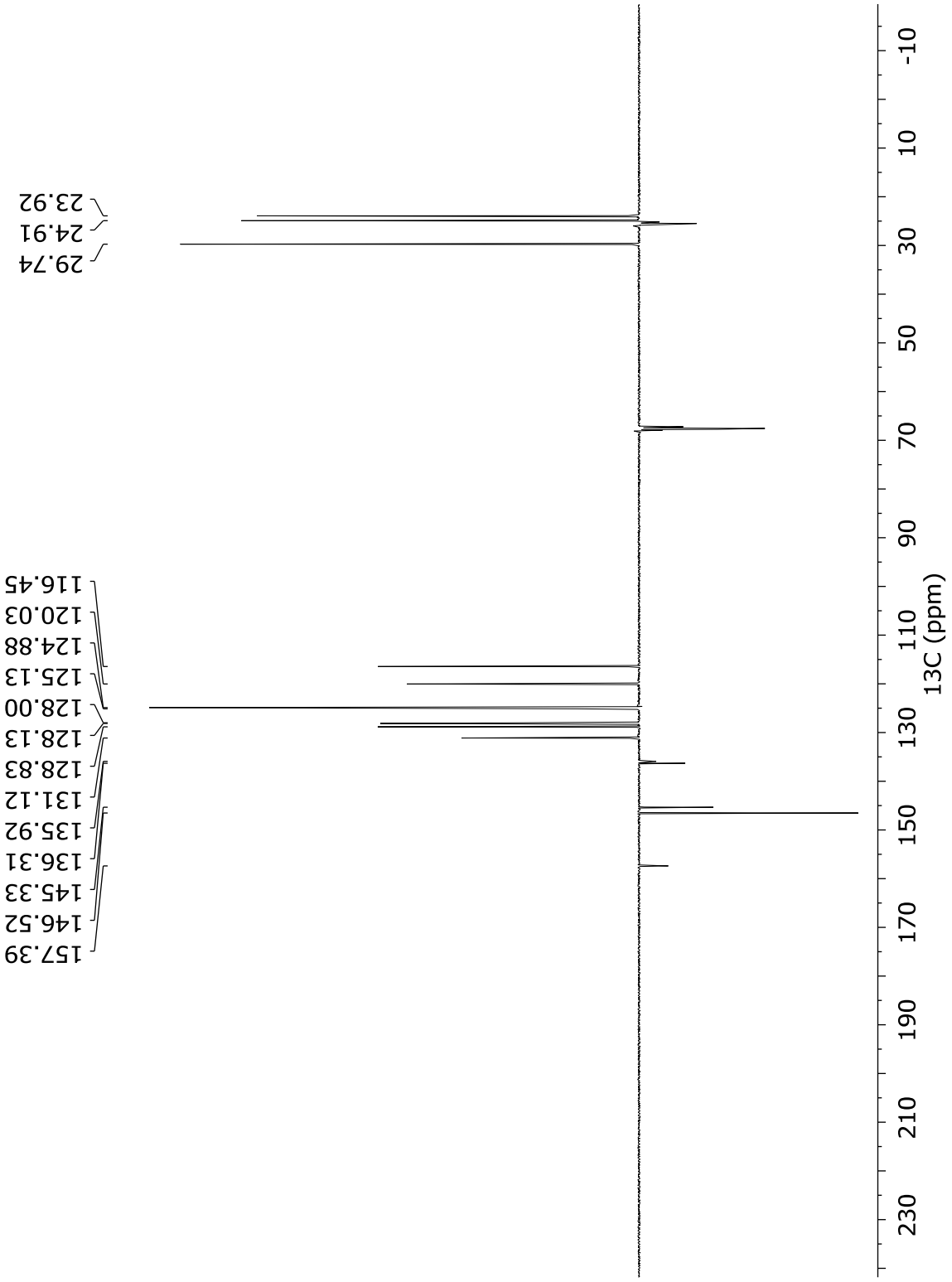

Figure A.4.25: ^{1}H-^{1}H COSY NMR (500 MHz, THF-d_8) spectrum of compound **4.4**.

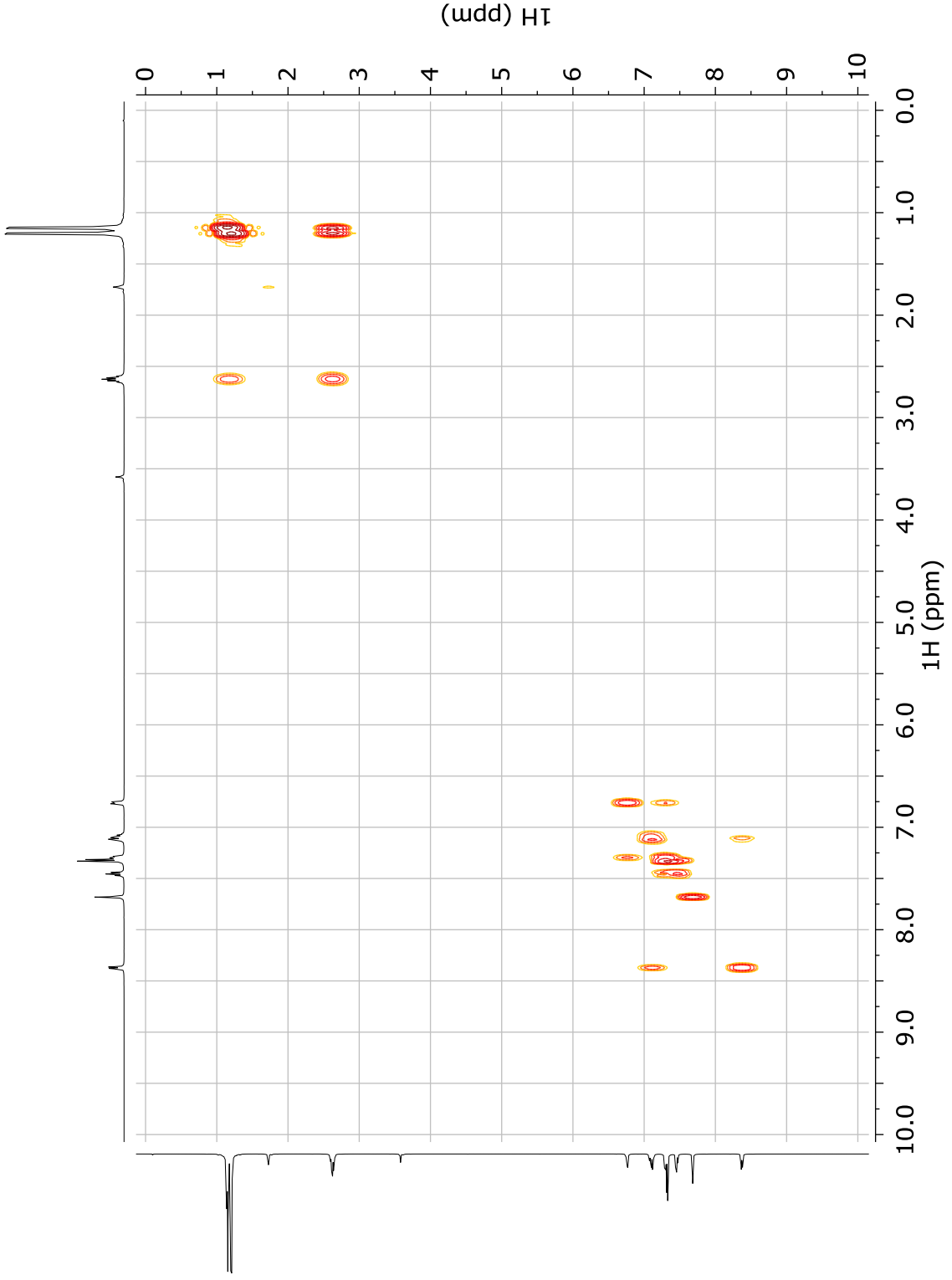

Figure A.4.26: ^{1}H-^{1}H NOESY NMR (500 MHz, THF-d_8) spectrum of compound **4.4**.

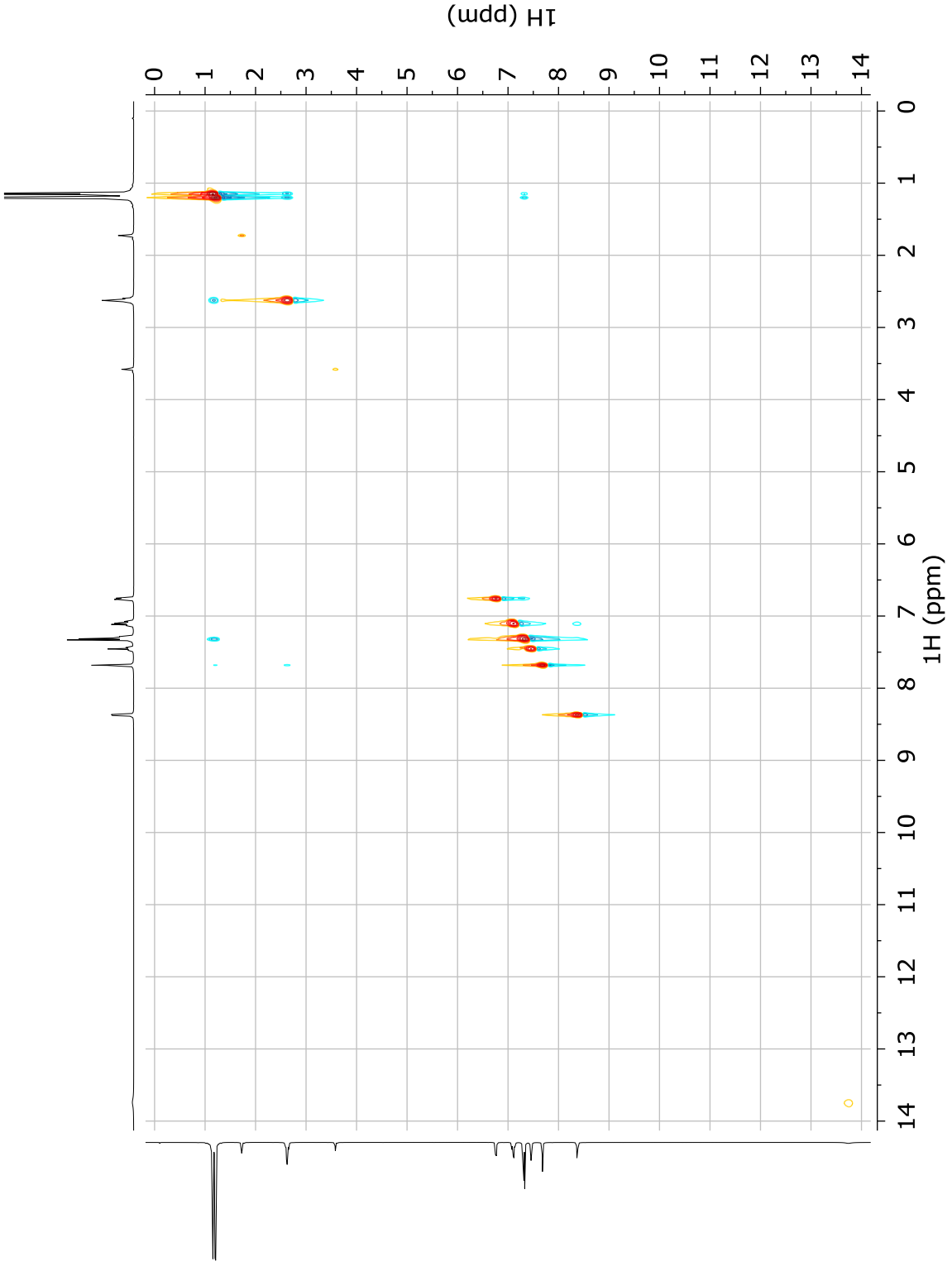

Figure A.4.27: ^{1}H-^{13}C HSQC NMR (500 MHz, THF-d_8) spectrum of compound **4.4**.

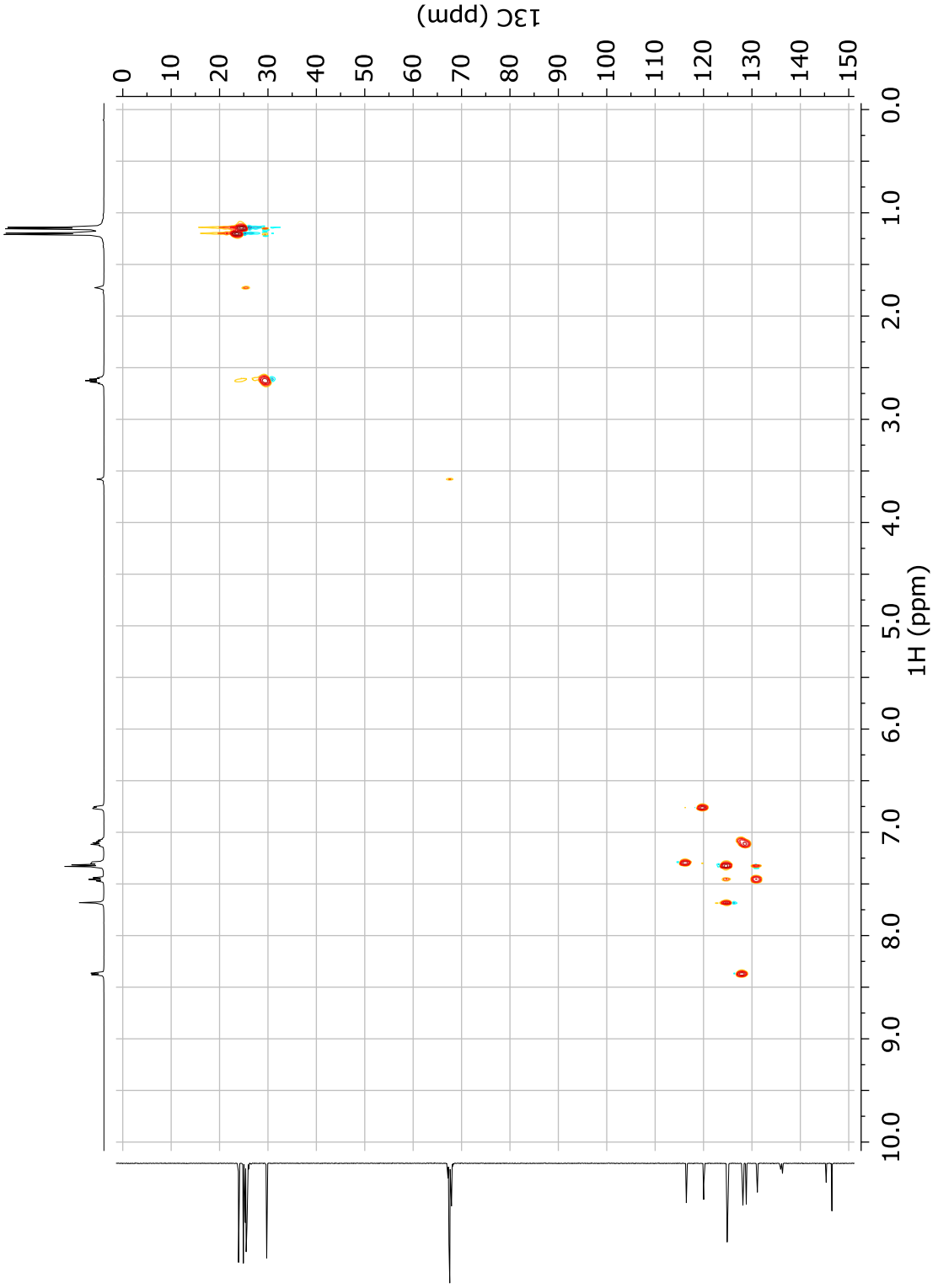

Figure A.4.28: ^{1}H-^{13}C HMBC NMR (500 MHz, THF-d_8) spectrum of compound **4.4**.

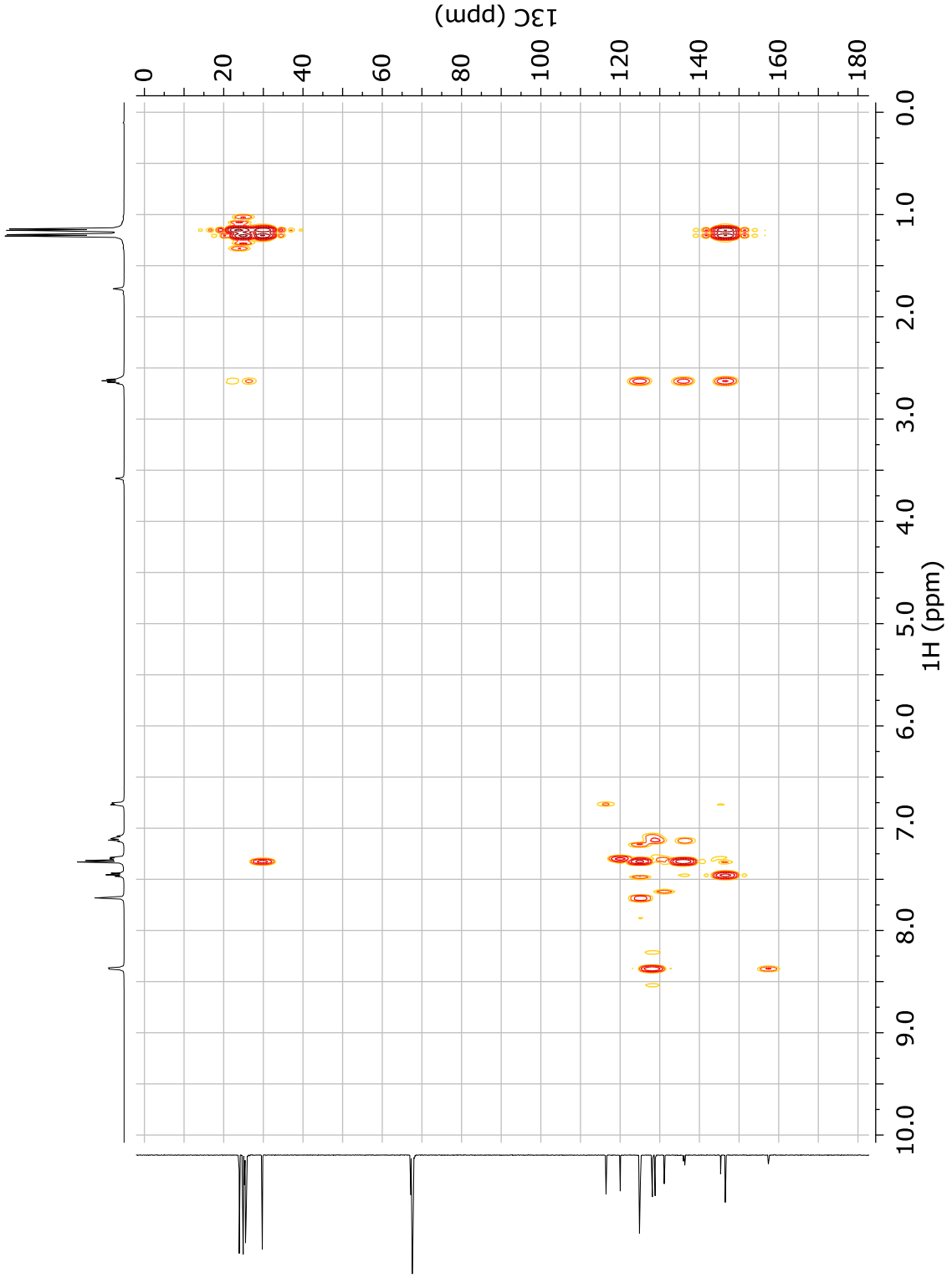

Figure A.4.29: ^{1}H NMR (500 MHz, C_6D_6) spectrum of compound **4.1** after exposure of solid sample to ambient conditions for 1 week. Spectrum of **4.1** added as reference.

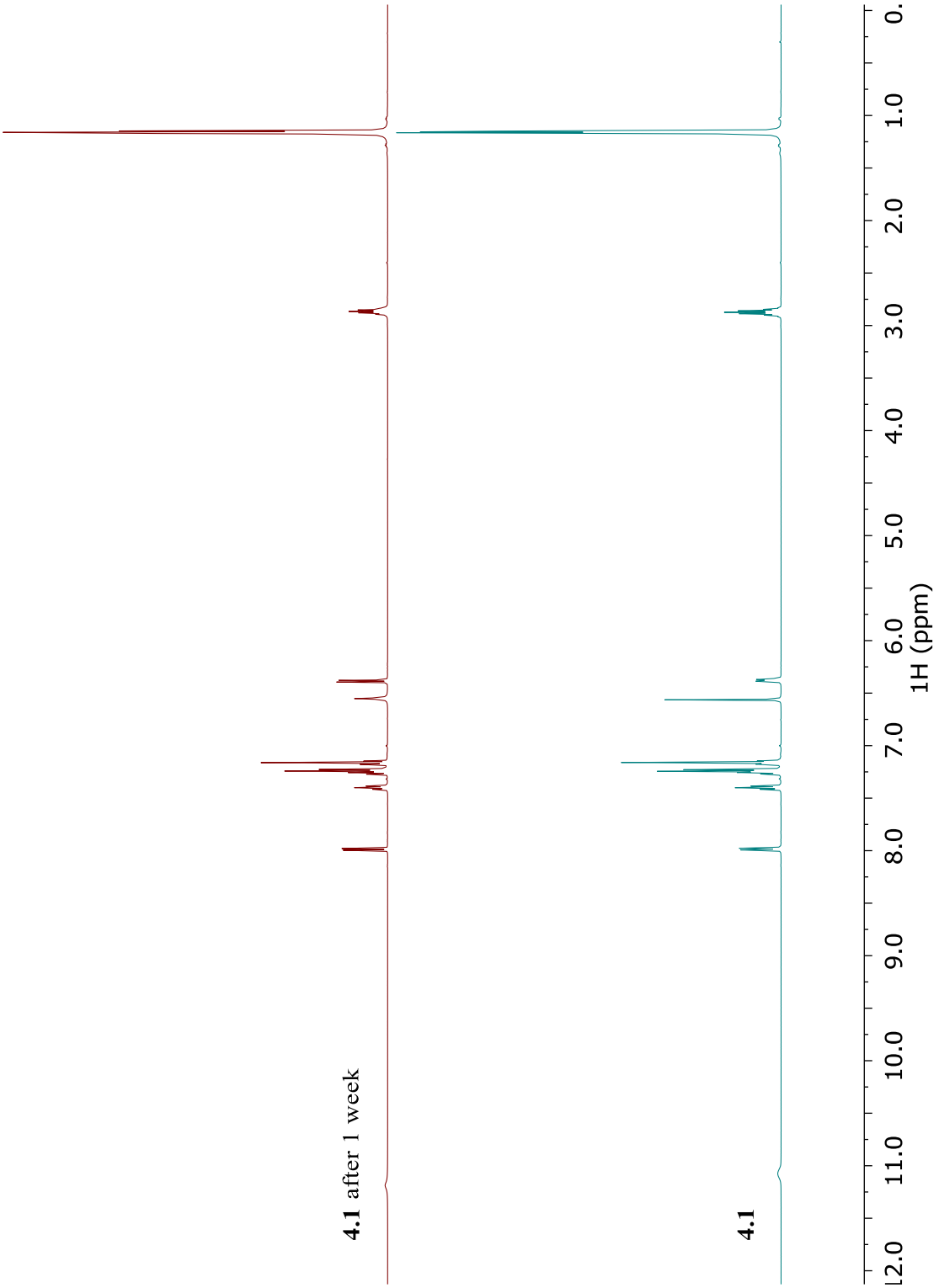

Figure A.4.30: ^{1}H NMR (500 MHz, C_6D_6) spectrum of compound **4.2** after exposure of solid sample to ambient conditions for 1 week. Spectrum of **4.2** added as reference.

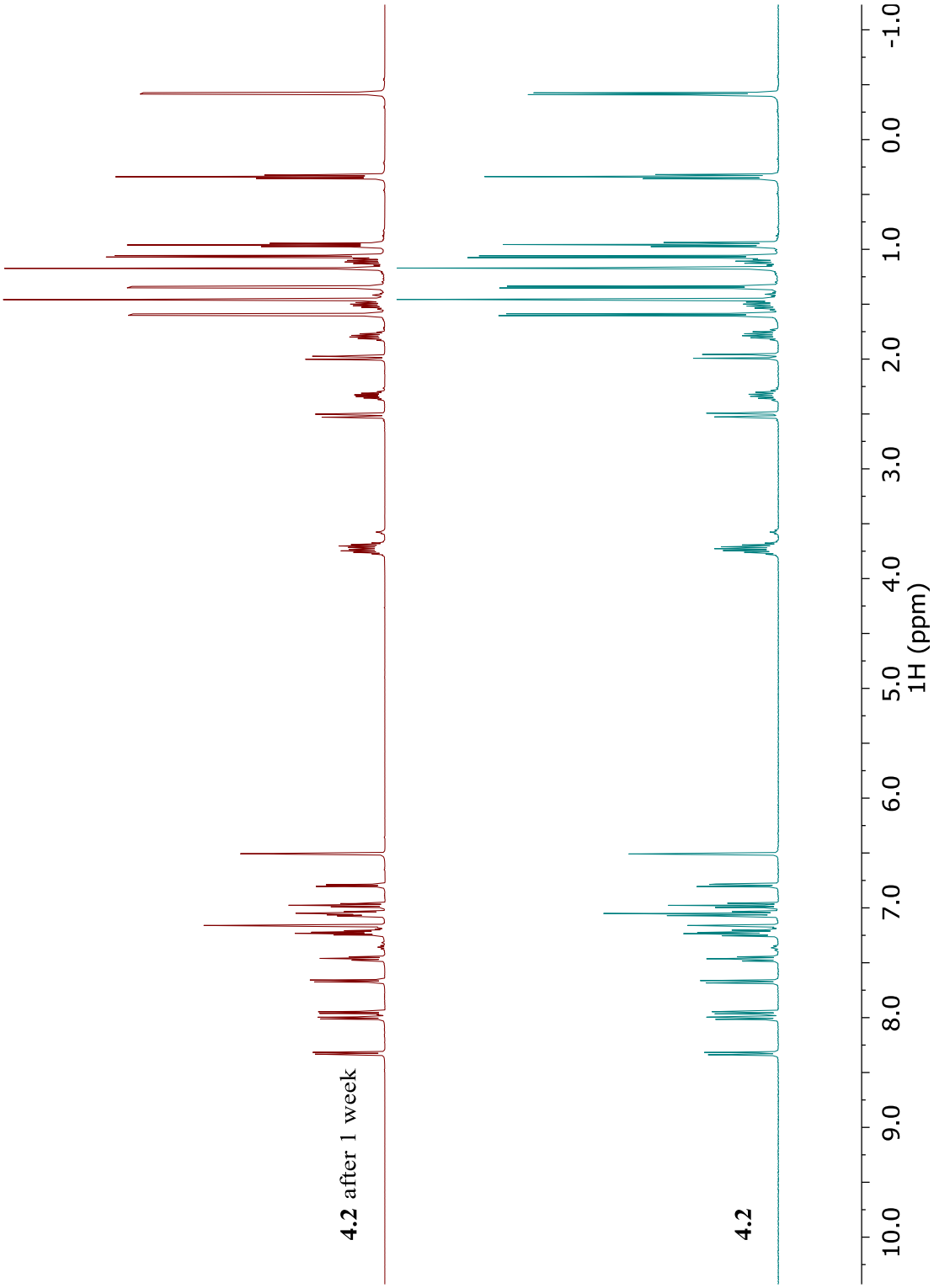

Figure A.4.31: ^{1}H NMR (500 MHz, C_6D_6) spectrum of compound **4.3** after exposure of solid sample to ambient conditions for 1 week. Spectrum of **4.3** added as reference.

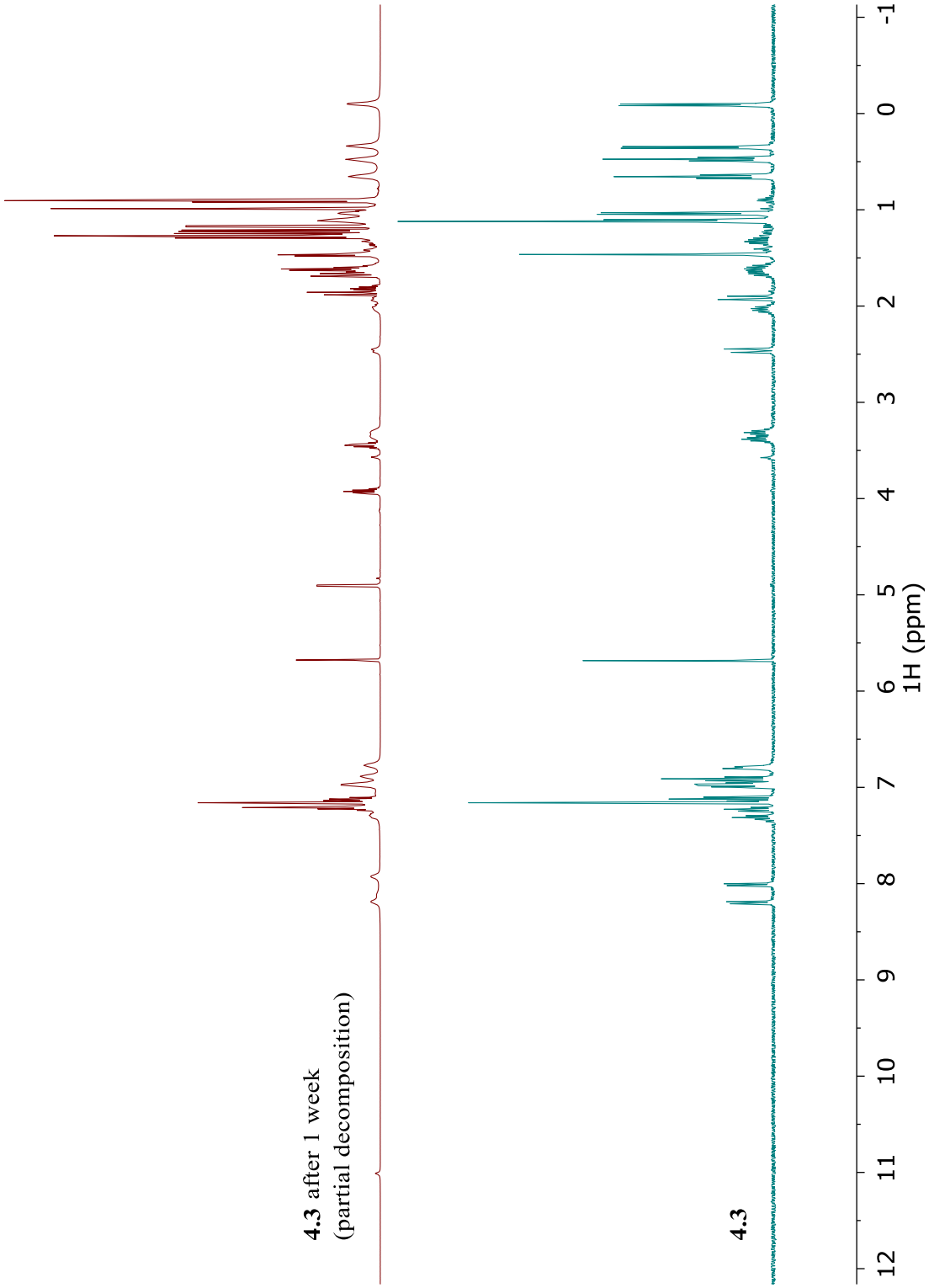

Figure A.4.32: : ^{1}H NMR (500 MHz, THF-d_8) spectrum of compound **4.4** after exposure of solid sample to ambient conditions for 1 week. Spectrum of **4.4** added as reference.

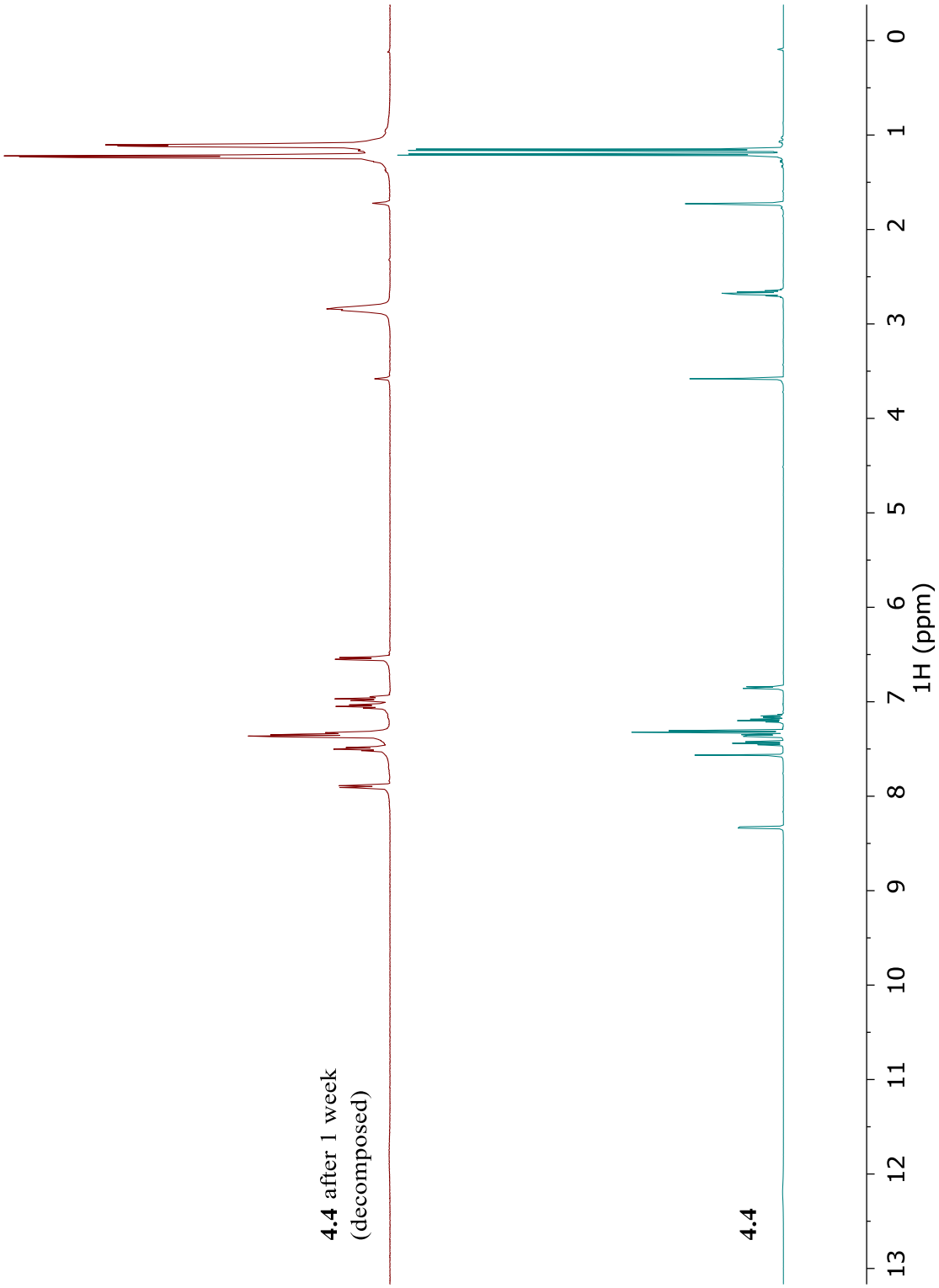

Section A.5: NMR Spectra for Compounds Included in **Chapter 5**

Figure A.5.1: ^{1}H NMR (400 MHz, $CDCl_3$) spectrum of recrystallized **5.1**

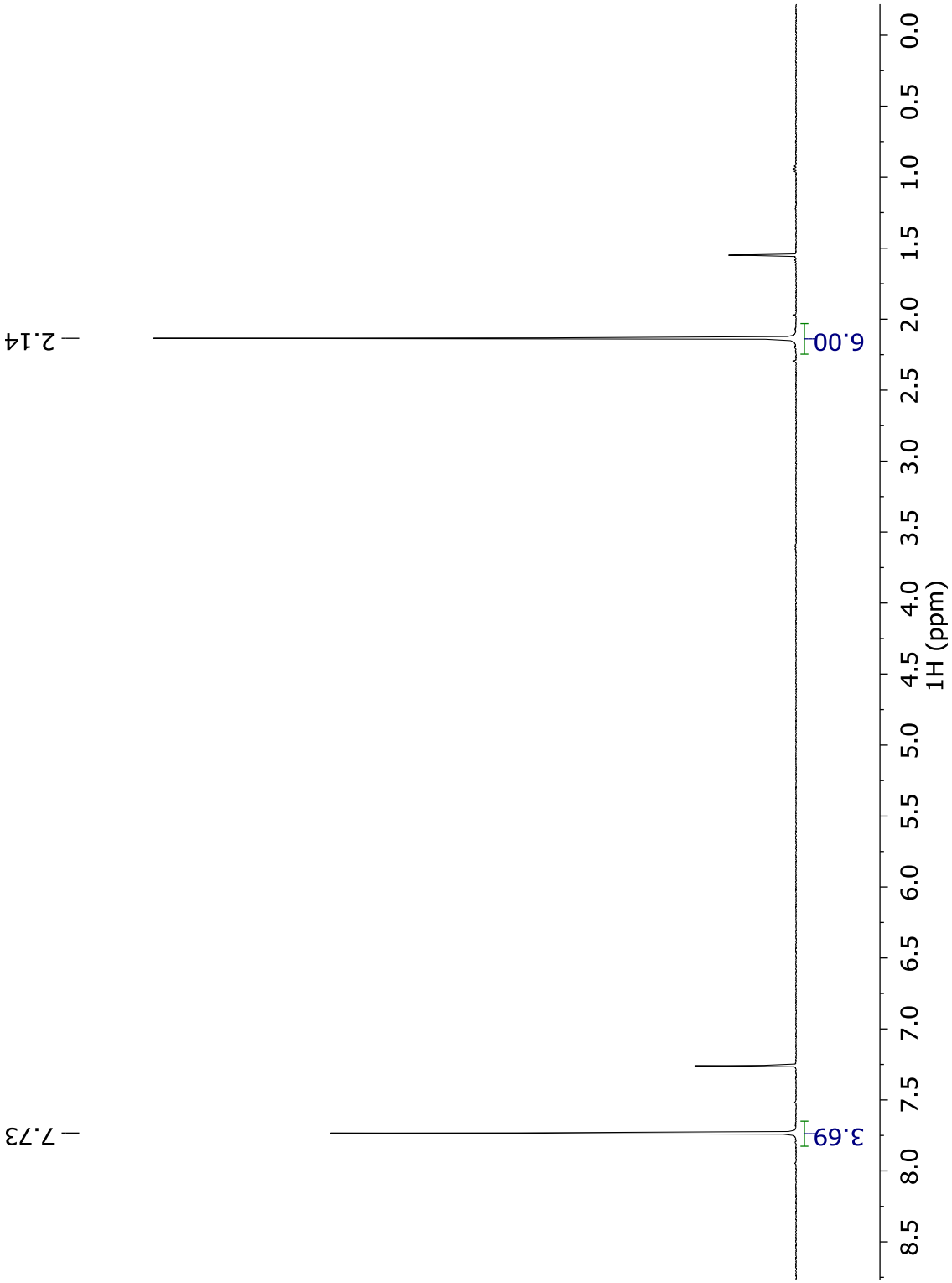

Figure A.5.2: ^{13}C NMR (126 MHz, $CDCl_3$) spectrum of recrystallized **5.1**

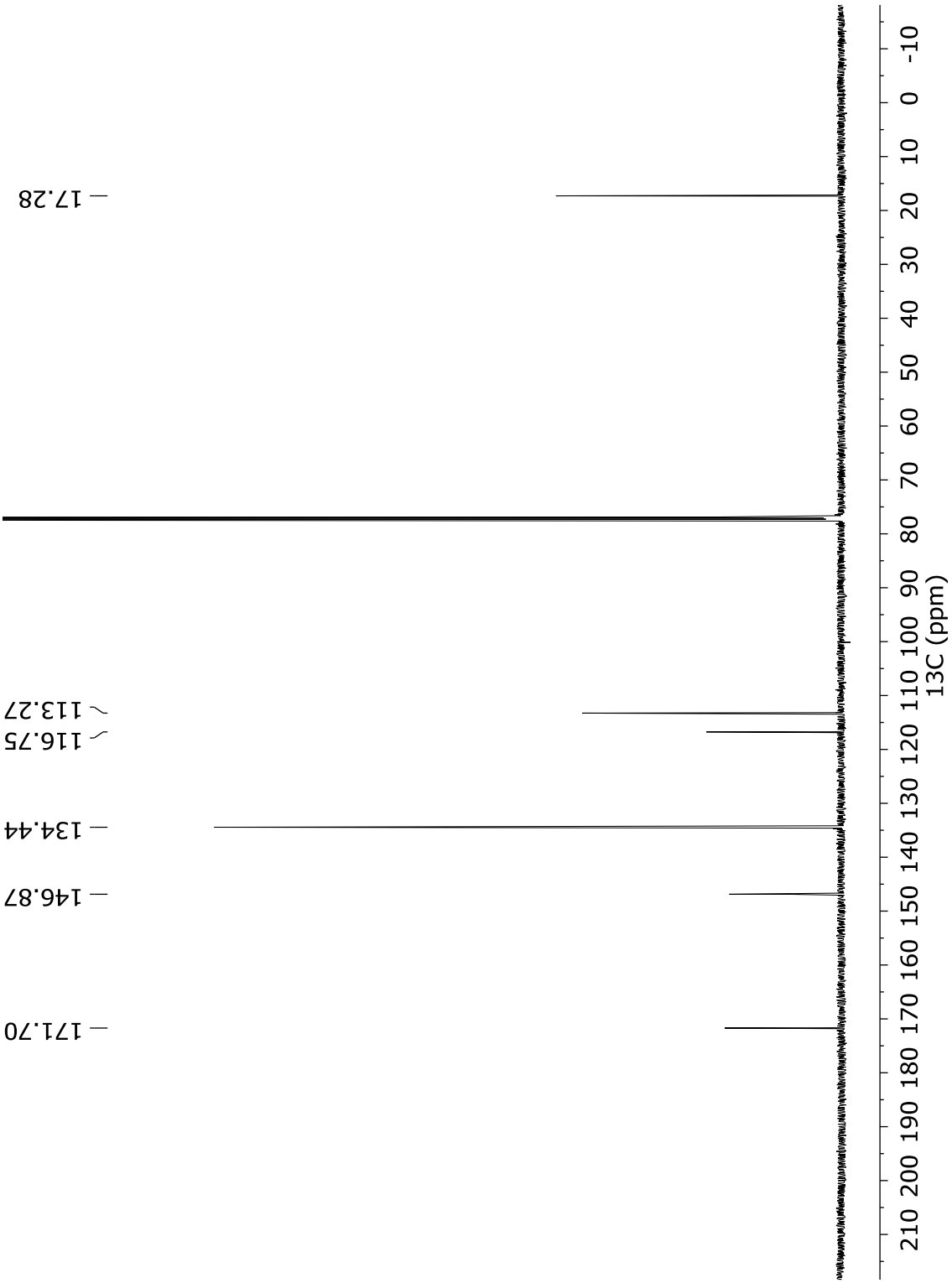

Figure A.5.3: ^{1}H NMR (400 MHz, $CDCl_3$) spectrum of 2,4,6-tribromo-3,5-dimethylaniline.

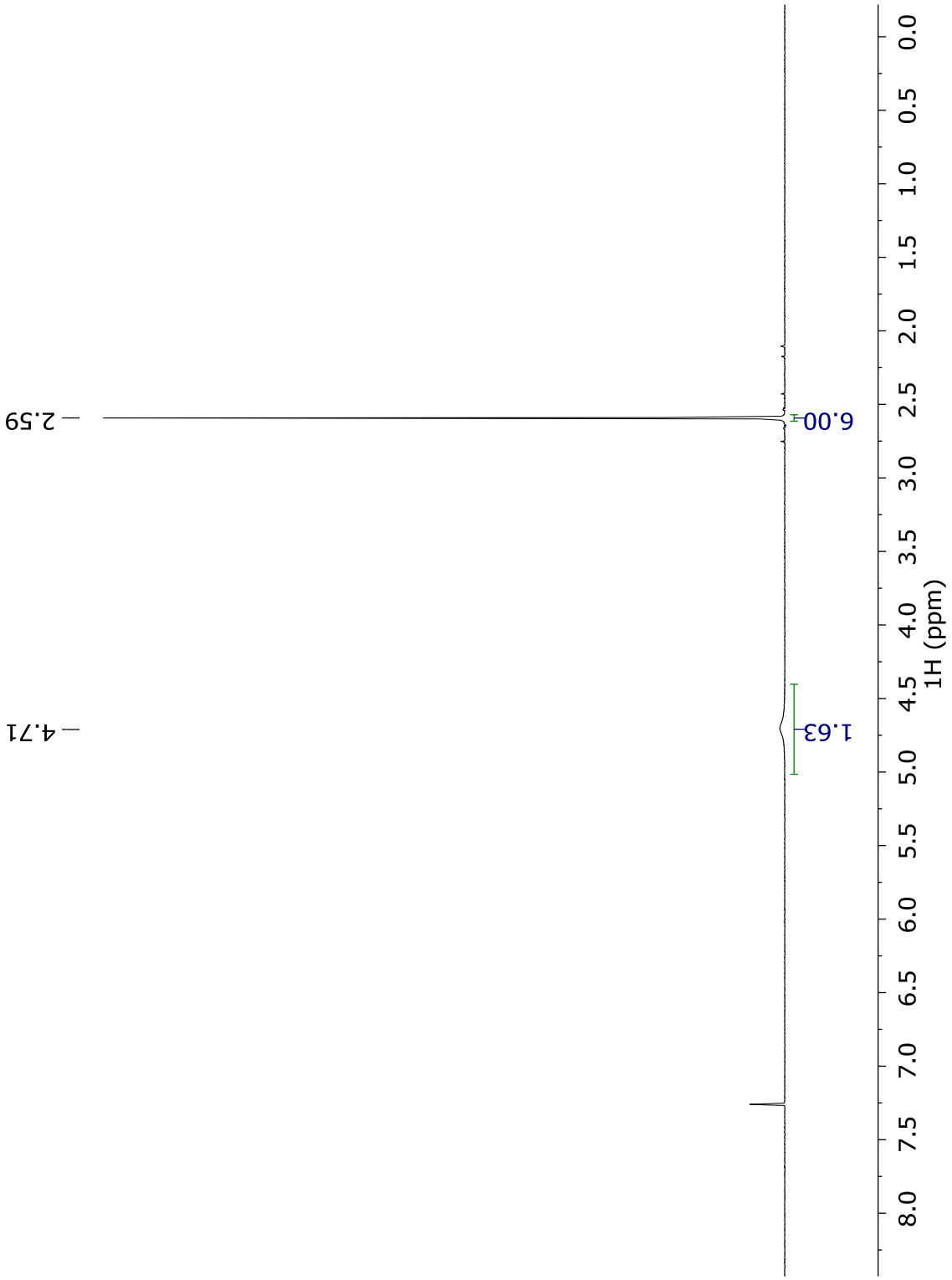

Figure A.5.4: ^{1}H NMR (500 MHz, $CDCl_3$) spectrum of **5.2**, with trace 2,4,6-tribromo-3,5-dimethylaniline.

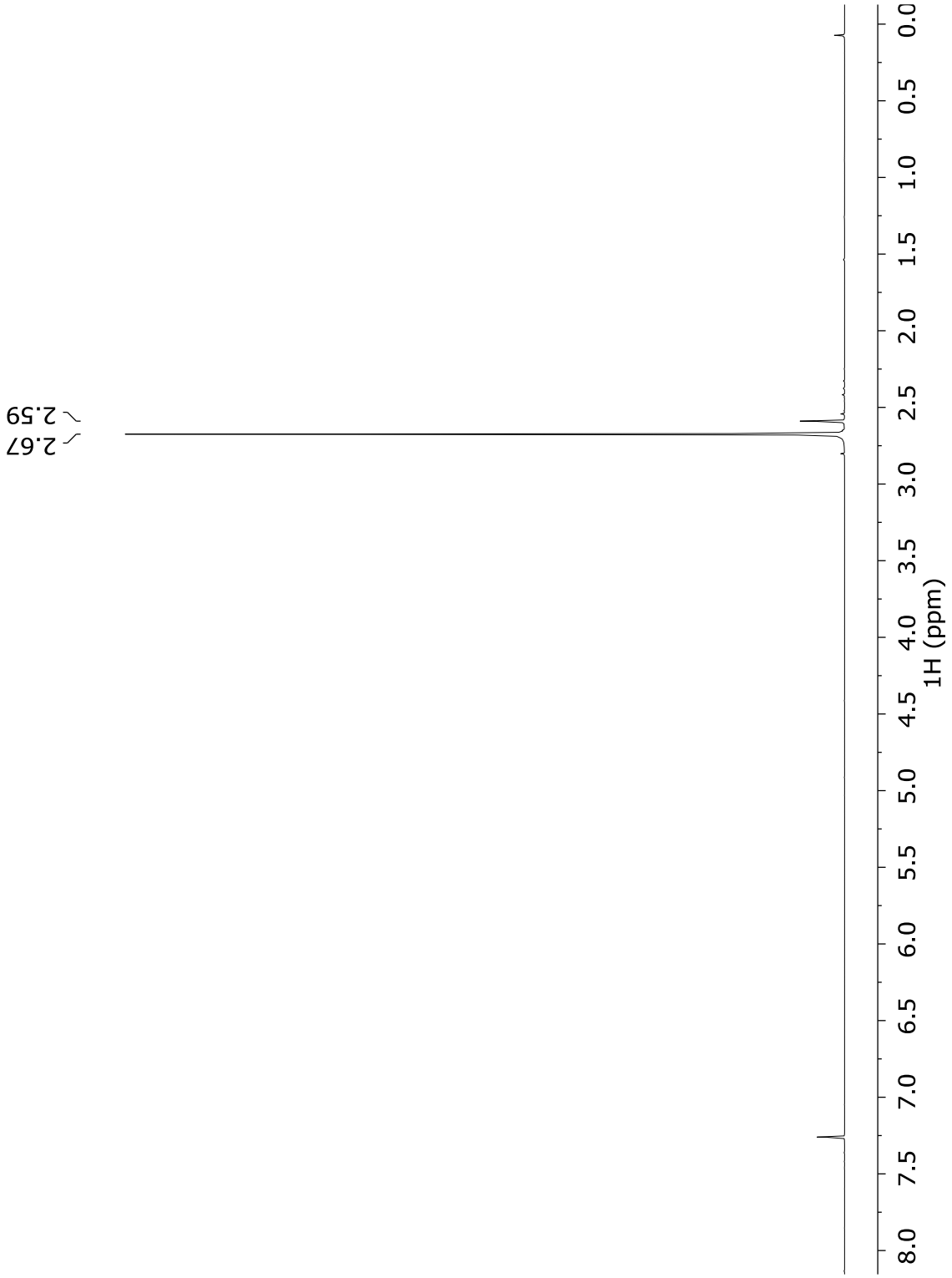

Figure A.5.5: ^{13}C NMR (126 MHz, $CDCl_3$) spectrum of **5.2**, with trace 2,4,6-tribromo-3,5-dimethylaniline.

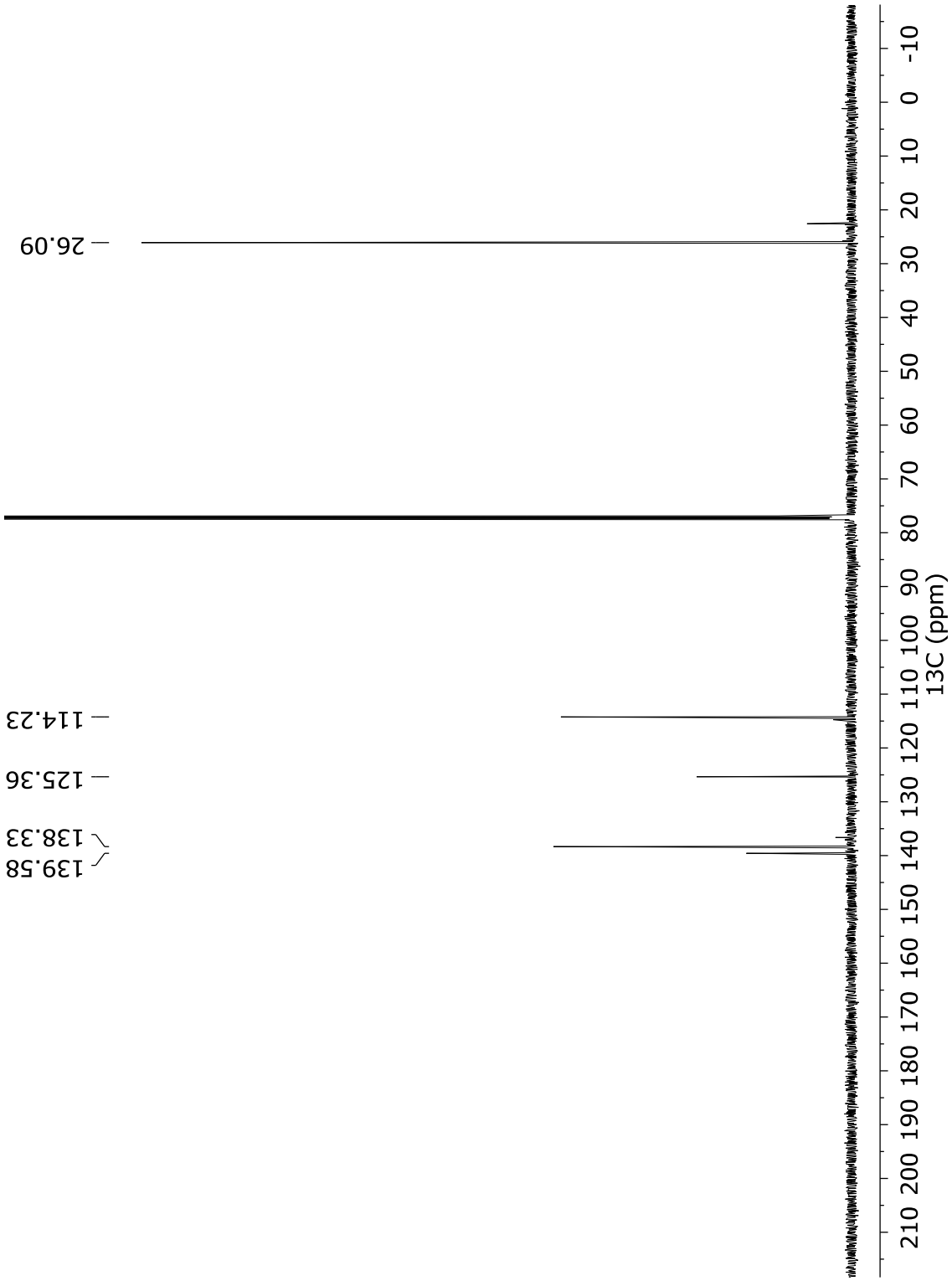

Figure A.5.6: ^{1}H NMR (400 MHz, $CDCl_3$) spectrum of **5.3**.

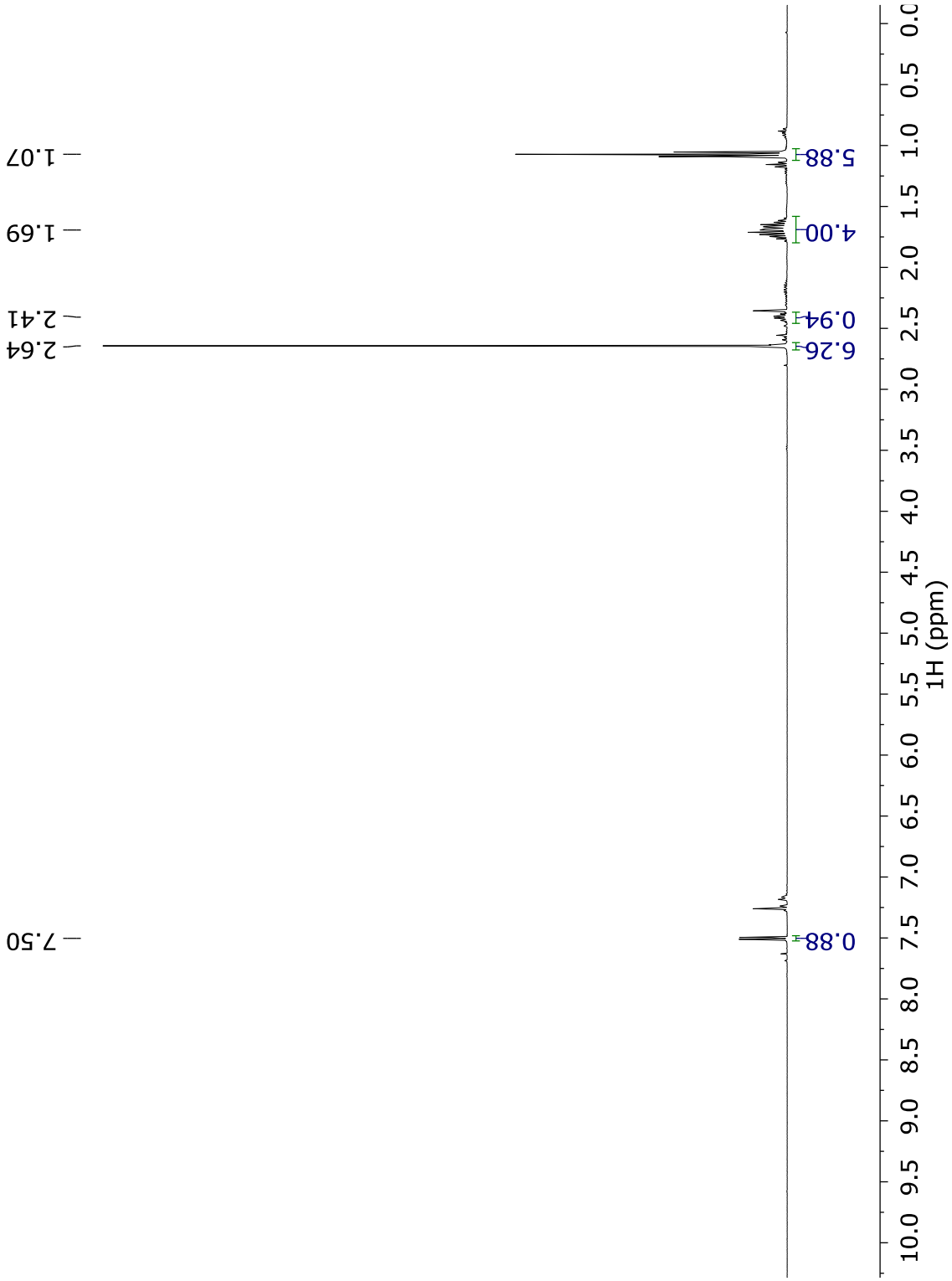

Figure A.5.7: ^{1}H NMR (400 MHz, $CDCl_3$) spectrum of crude **5.4**. Ratio of **5.4**:**5.3** of approximately 2:1.

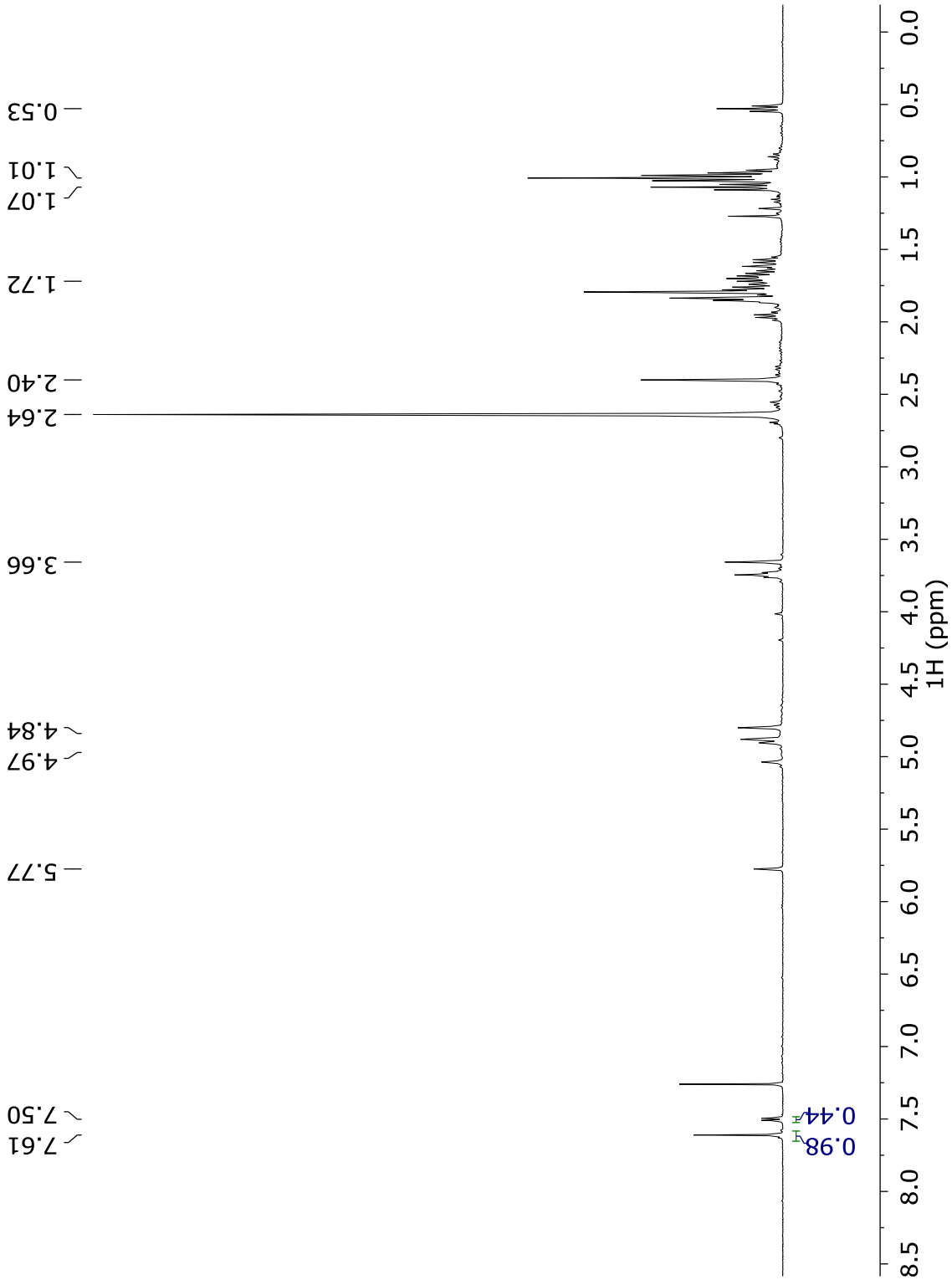

Figure A.5.8: ^{1}H NMR (400 MHz, $CDCl_3$) spectrum of 3,3-diethyl-5-methylhex-5-en-2-one.

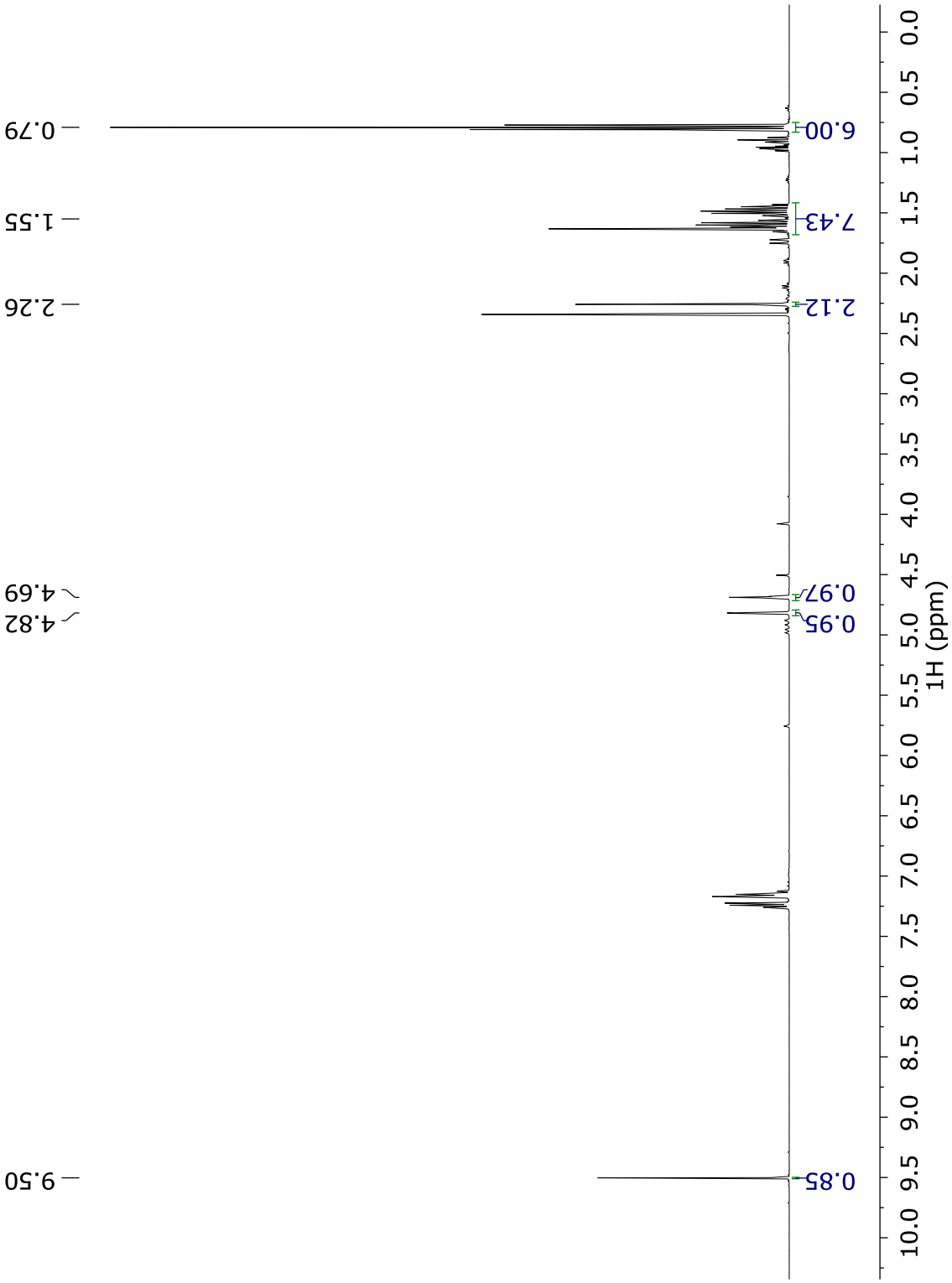

Figure A.5.9: ^{1}H NMR (400 MHz, $CDCl_3$) spectrum of **5.5**.

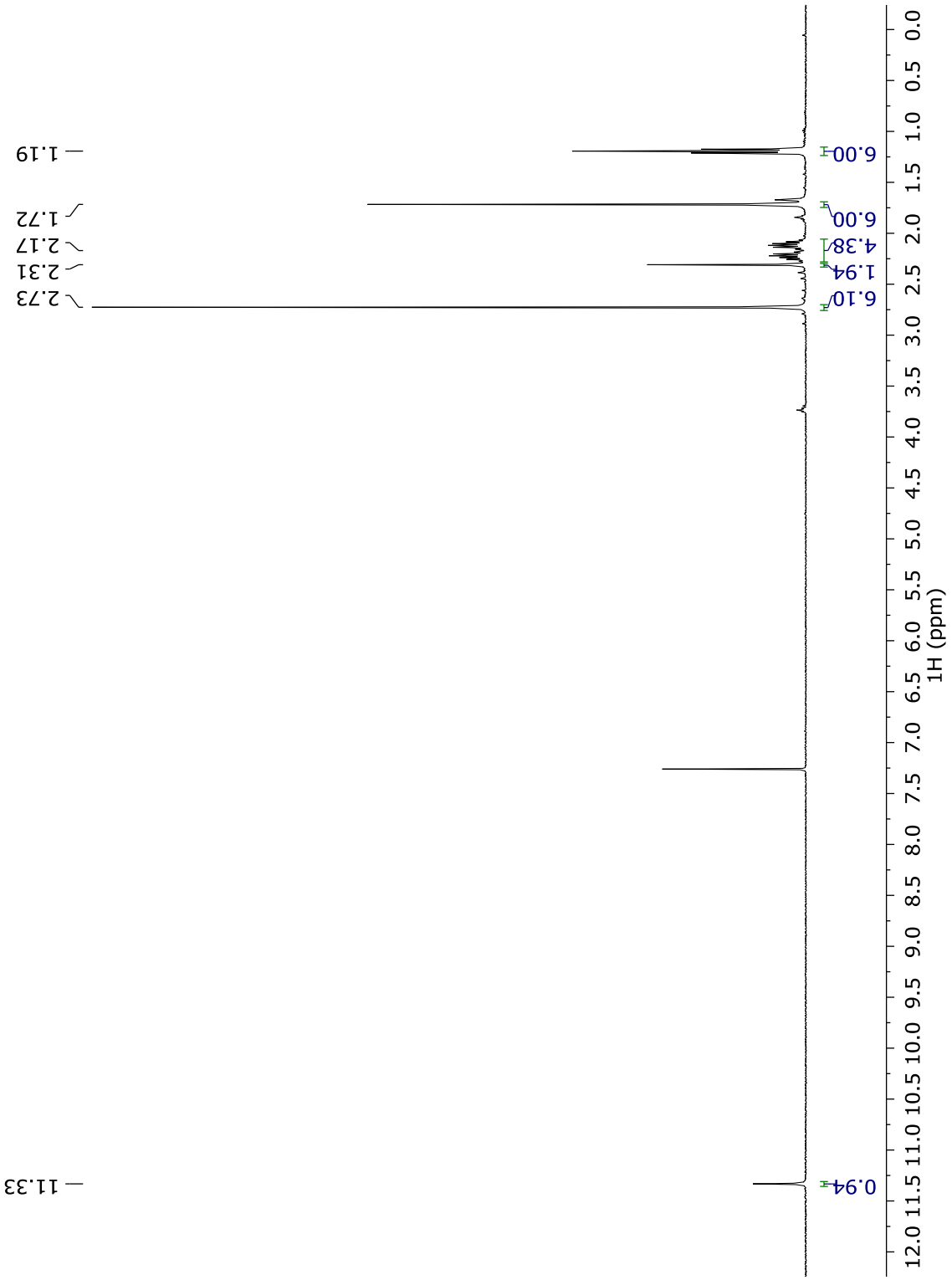

Figure A.5.10: ^{13}C NMR (126 MHz, $CDCl_3$) spectrum of **5.5**.

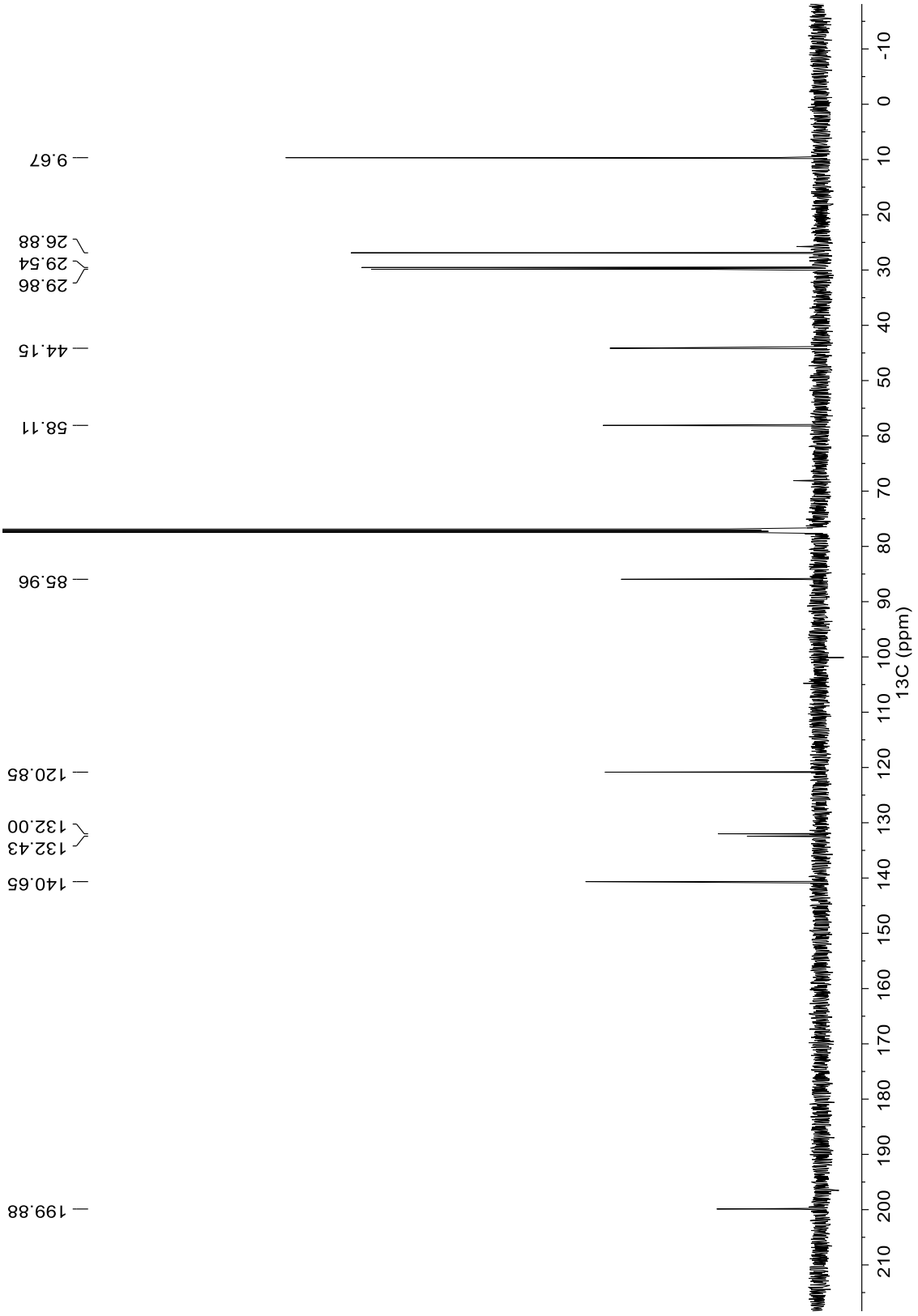

Section A.6: DOSY NMR Spectra and Data Refinement

Figure A.6.11: 2D ^{1}H DOSY-NMR spectrum of carbazole (THF-d_8, 298 K, 75 mM).

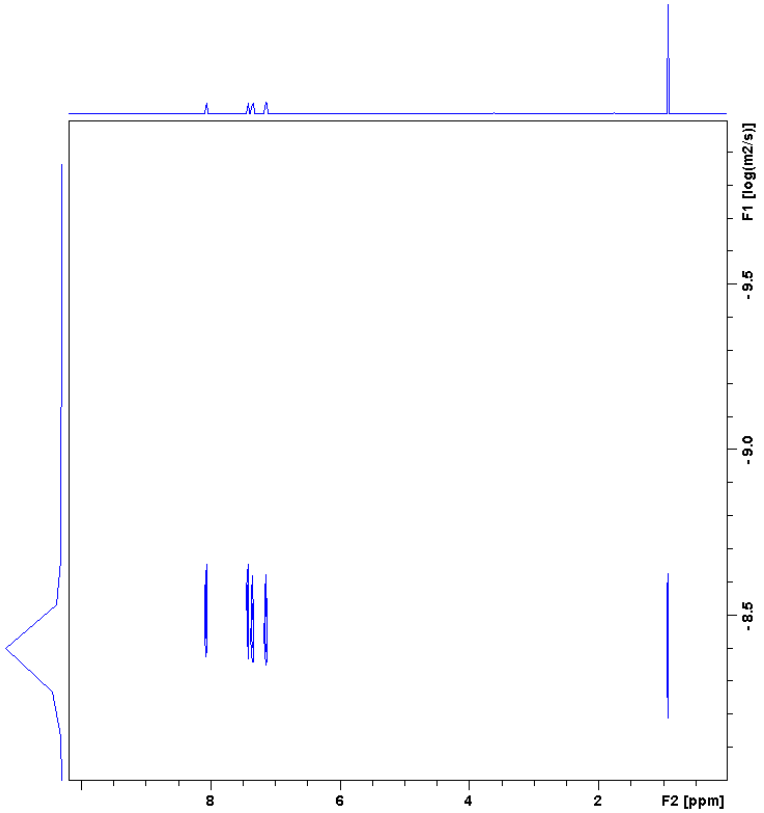

Figure A.6.12: Calculated relaxation curve fits and molecular weight of carbazole.

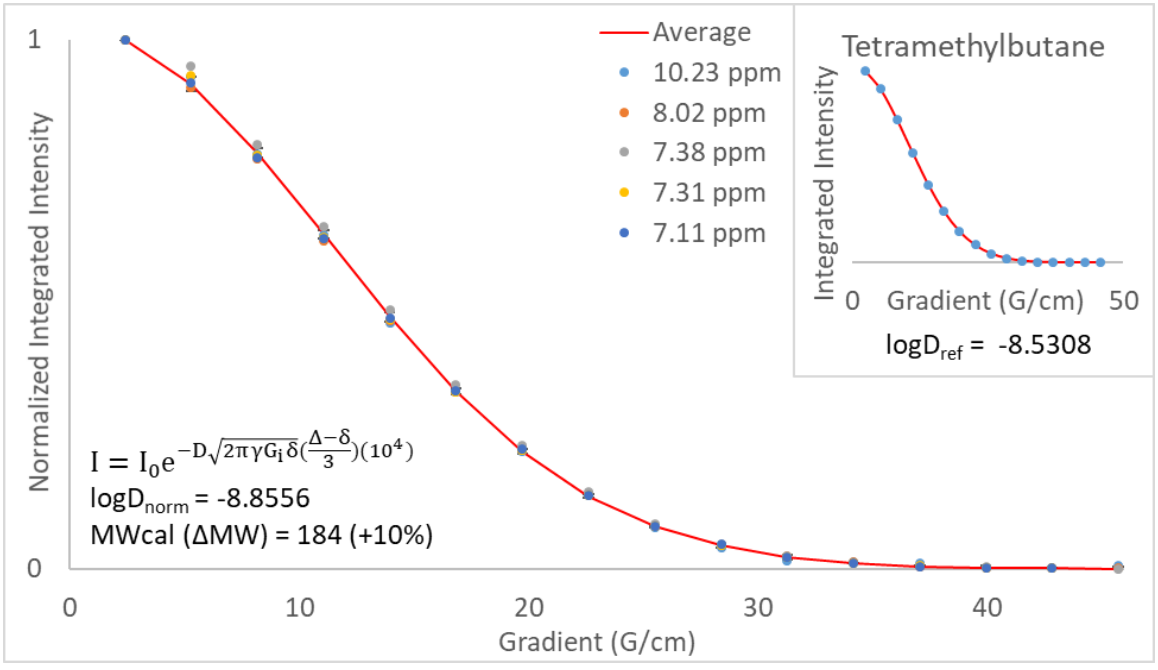

Figure A.6.13: 2D ^{1}H DOSY-NMR spectrum of Ph-BIM (THF-d_8, 298 K, 75 mM).

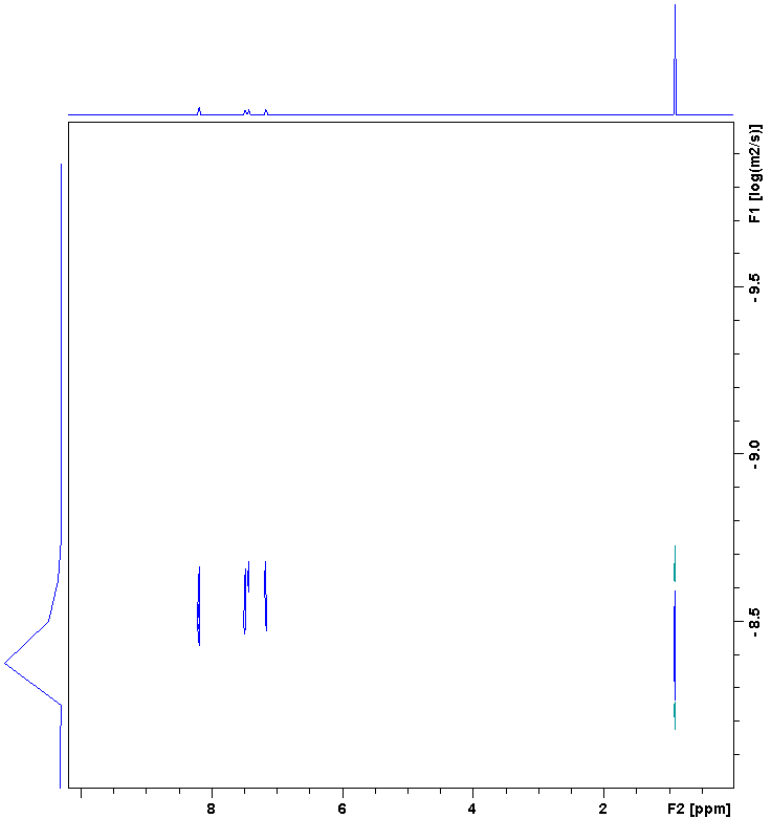

Figure A.6.14: Calculated relaxation curve fits and molecular weight of Ph-BIM.

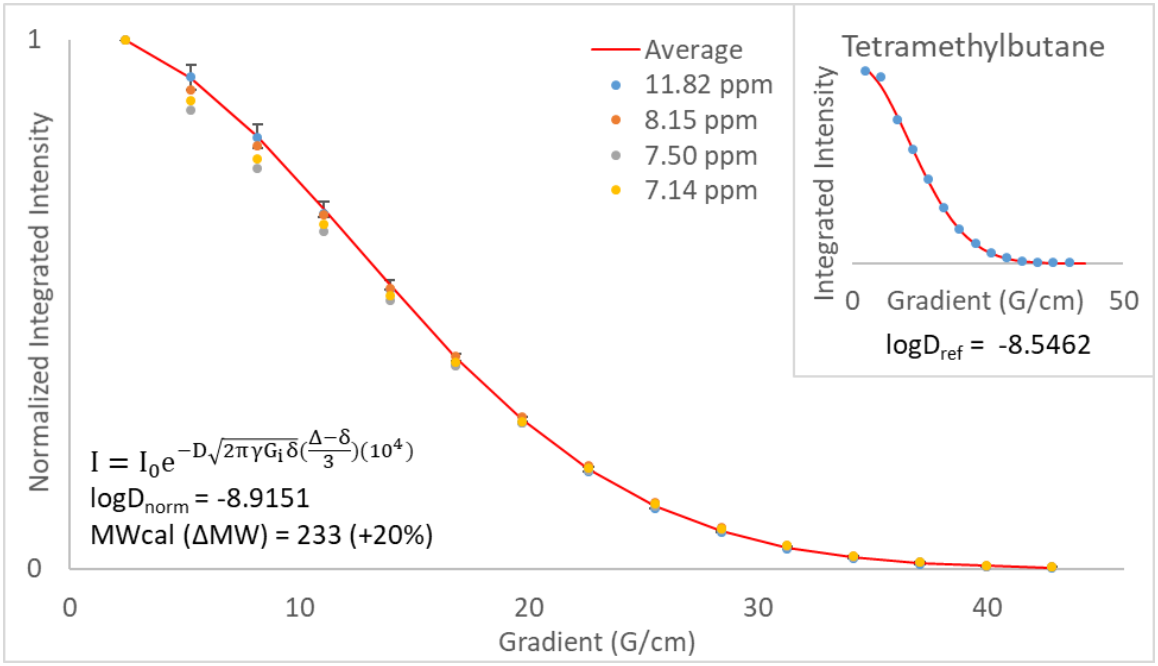

Figure A.6.15: 2D ^{1}H DOSY-NMR spectrum of IPr (THF-d_8, 298 K, 75 mM).

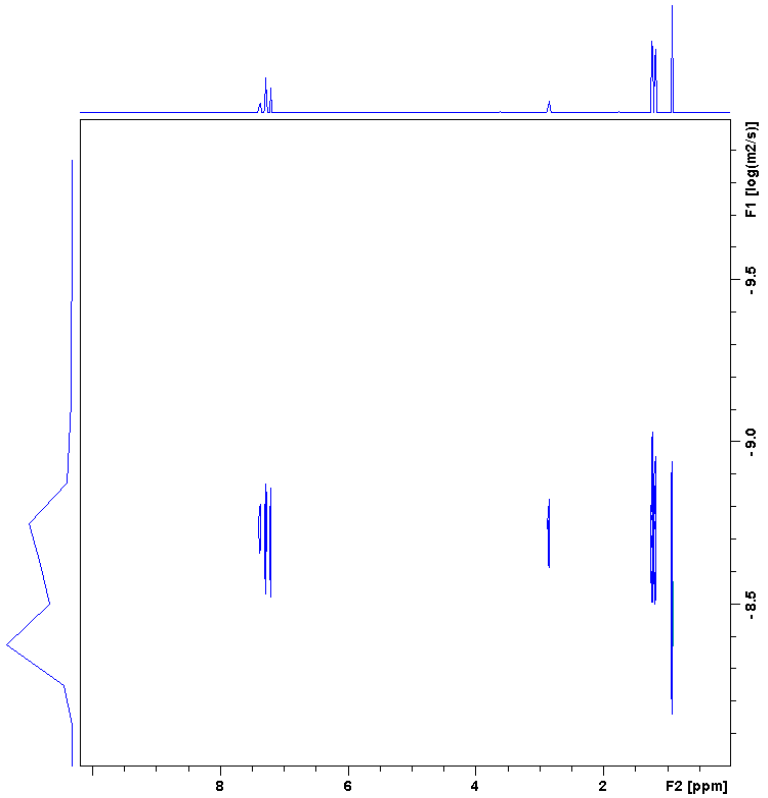

Figure A.6.16: Calculated relaxation curve fits and molecular weight of IPr.

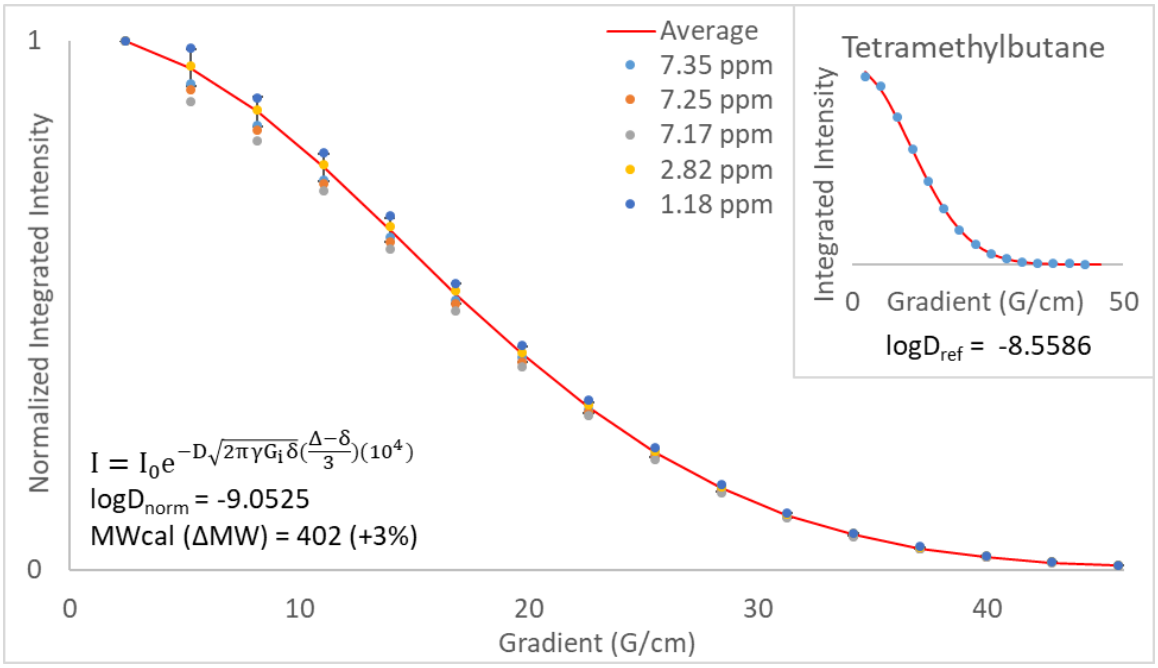

Figure A.6.17: 2D ^{1}H DOSY-NMR spectrum of ^{Et}CAAC (THF-d_8, 298 K, 75 mM).

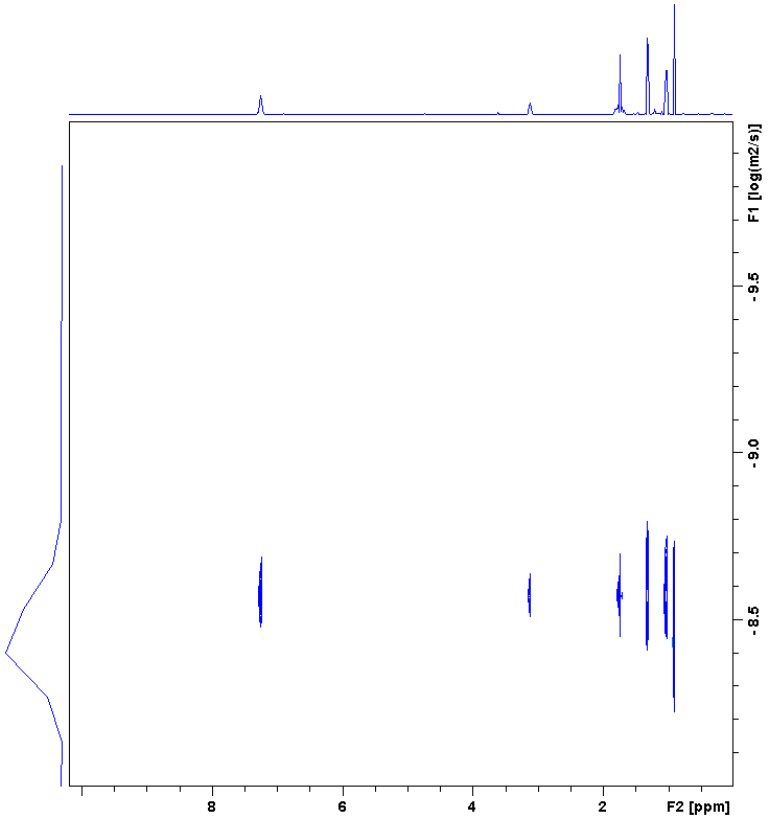

Figure A.6.18: Calculated relaxation curve fits and molecular weight of ^{Et}CAAC.

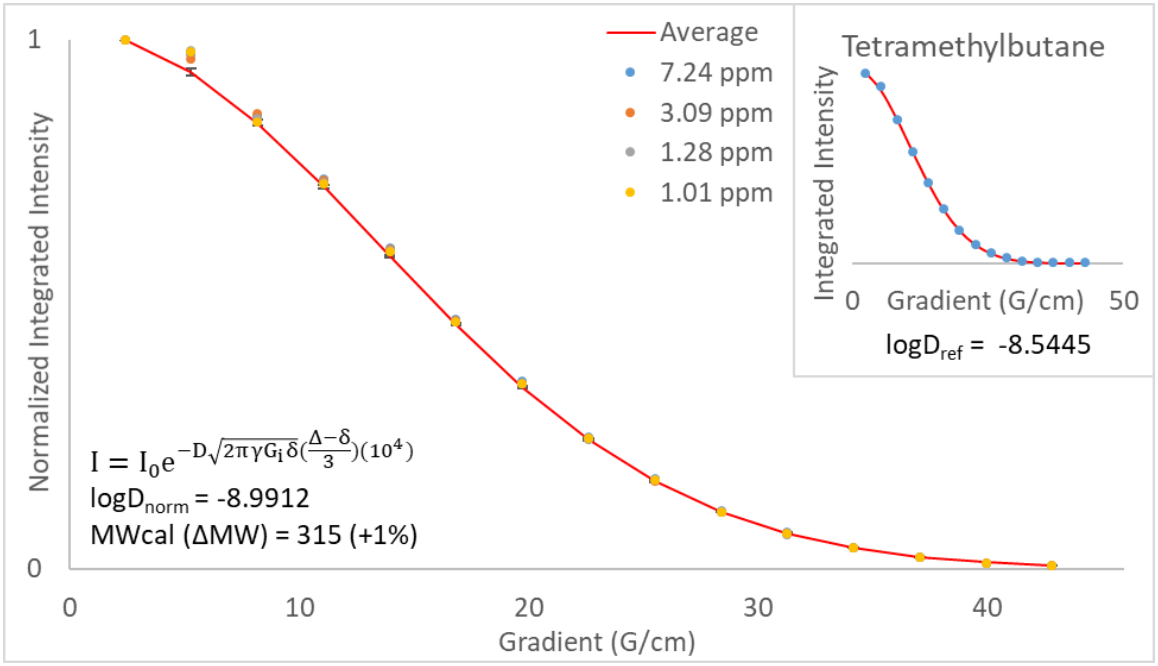

Figure A.6.19: 2D ^{1}H DOSY-NMR spectrum of **4.1** (THF-d_8, 298 K, 75 mM).

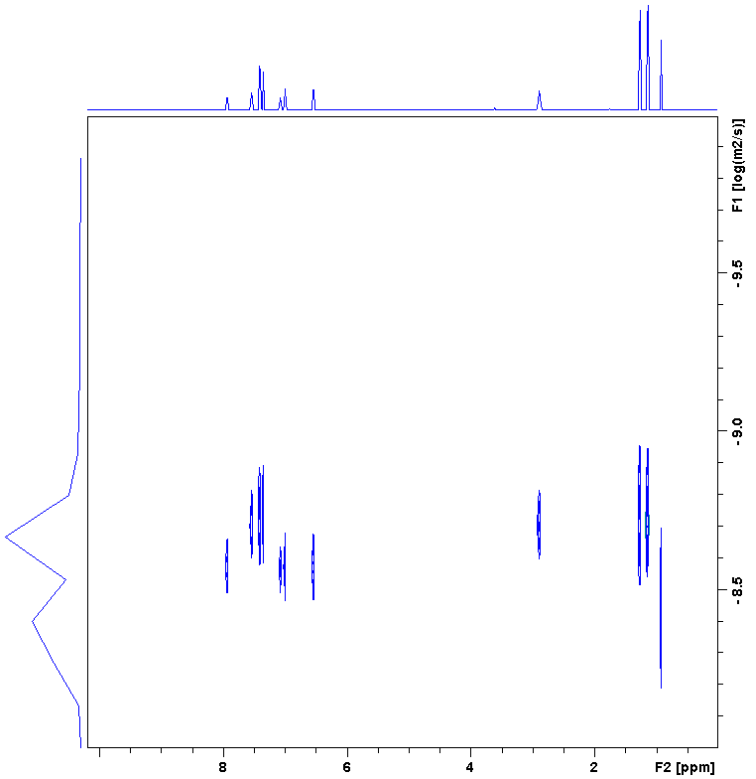

Figure A.6.20: Calculated relaxation curve fits and molecular weights of **4.1**.

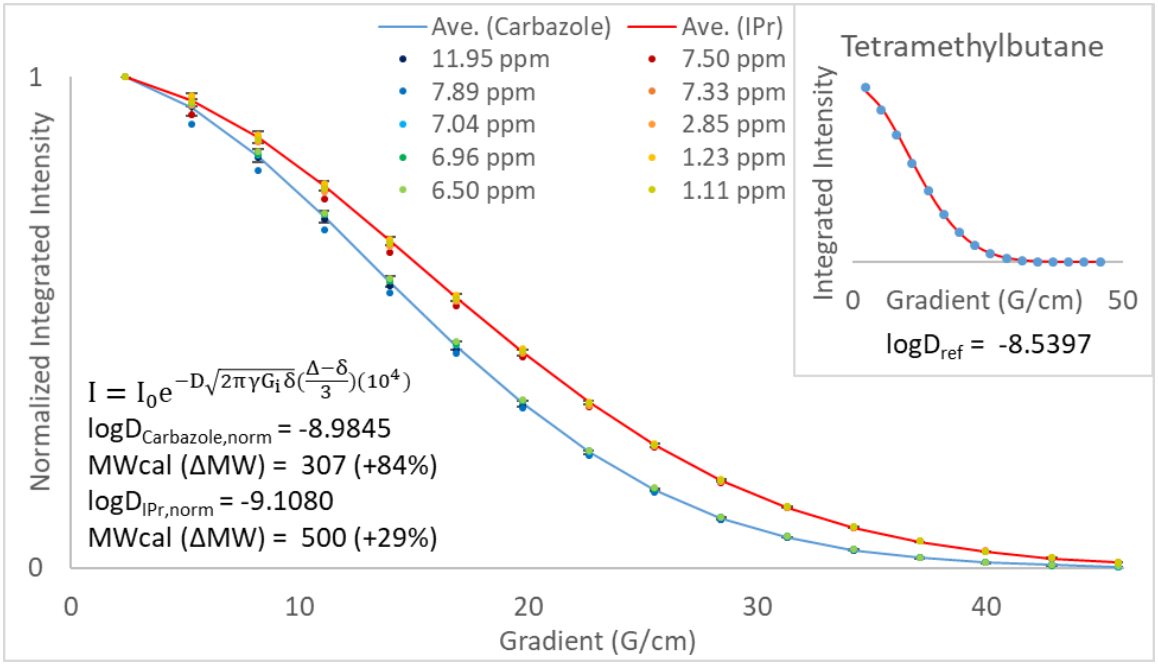

Figure A.6.21: 2D ^{1}H DOSY-NMR spectrum of **4.2** (THF-d_8, 298 K, 50 mM).

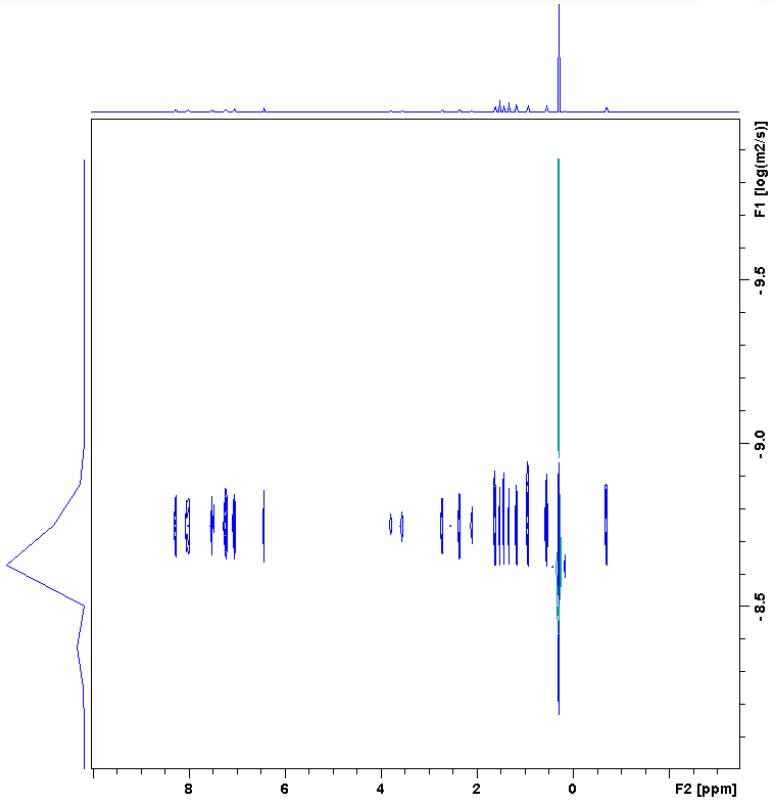

Figure A.6.22: Calculated relaxation curve fits and molecular weight of **4.2**.

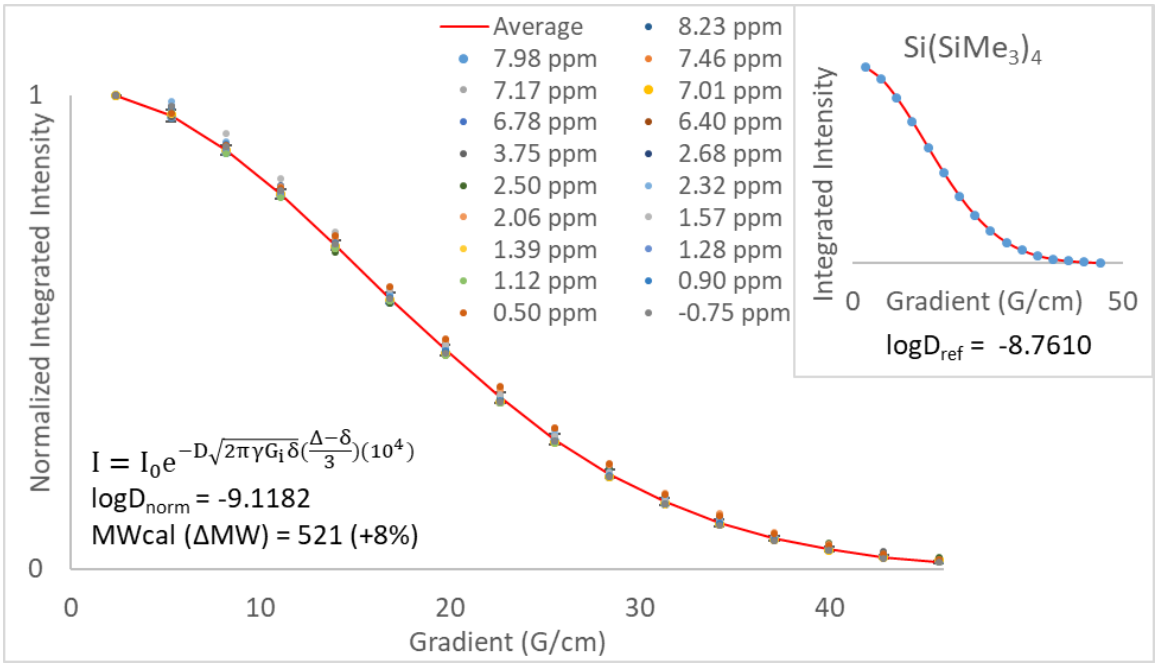

Figure A.6.23: 2D ^{1}H DOSY-NMR spectrum of **4.3** (THF-d_8, 298 K, 50 mM).

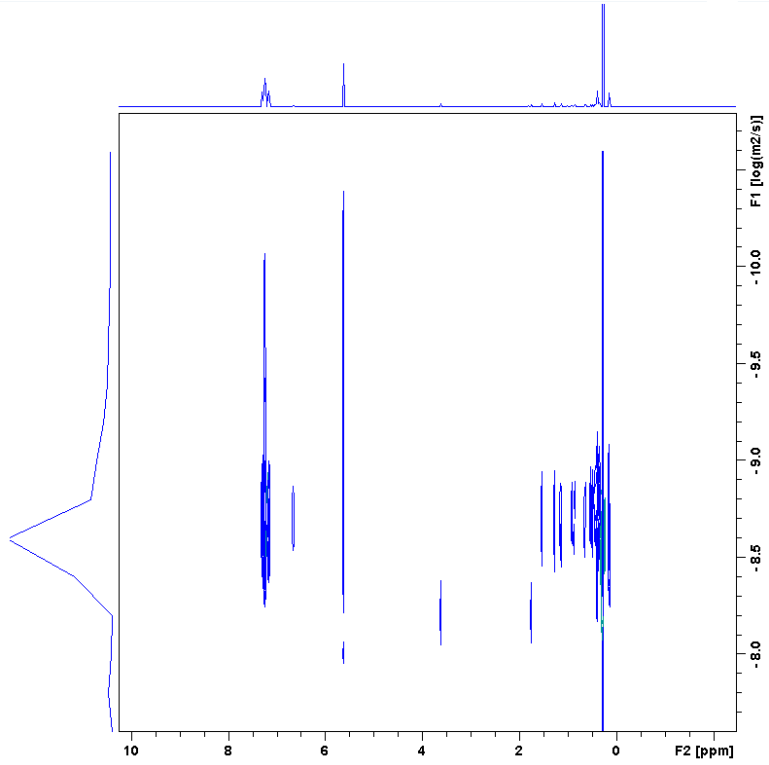

Figure A.6.24: Calculated relaxation curve fits and molecular weight of **4.3**.

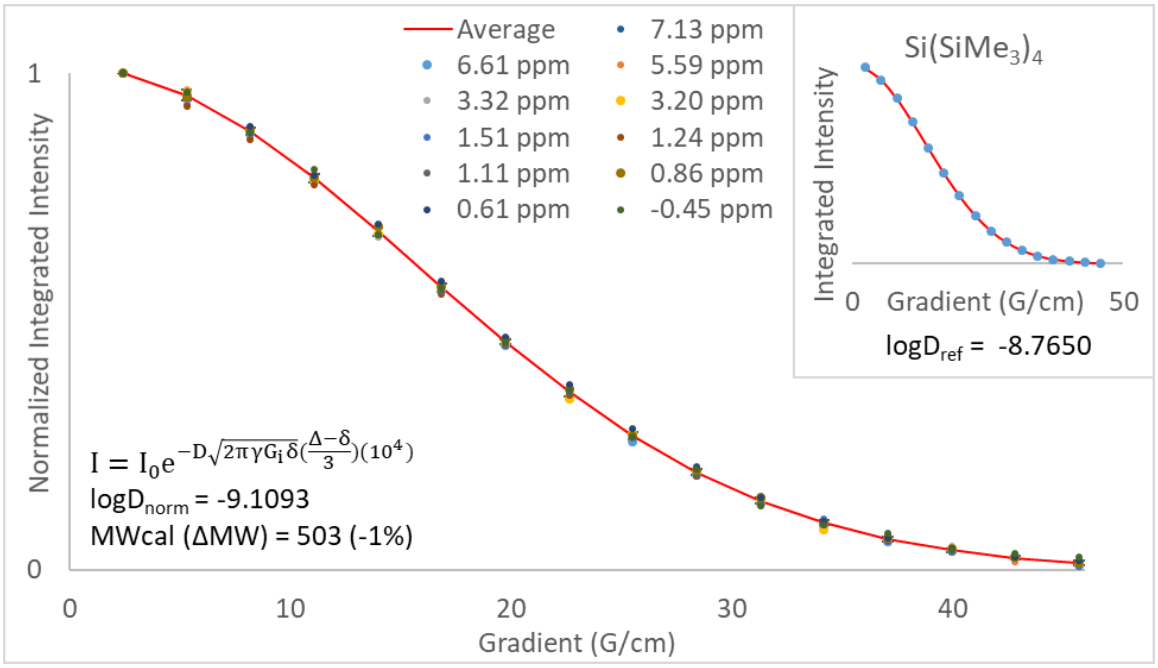

Figure A.6.25: 2D ^{1}H DOSY-NMR spectrum of **4.4** (THF-d_8, 298 K, 75 mM).

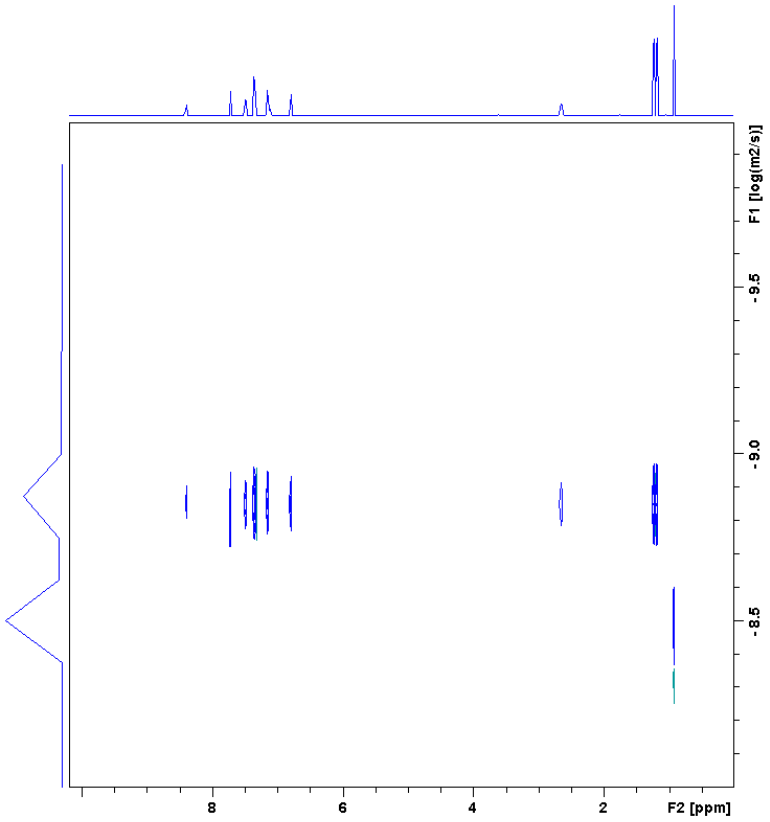

Figure A.6.26: Calculated relaxation curve fits and molecular weight of **4.4**.

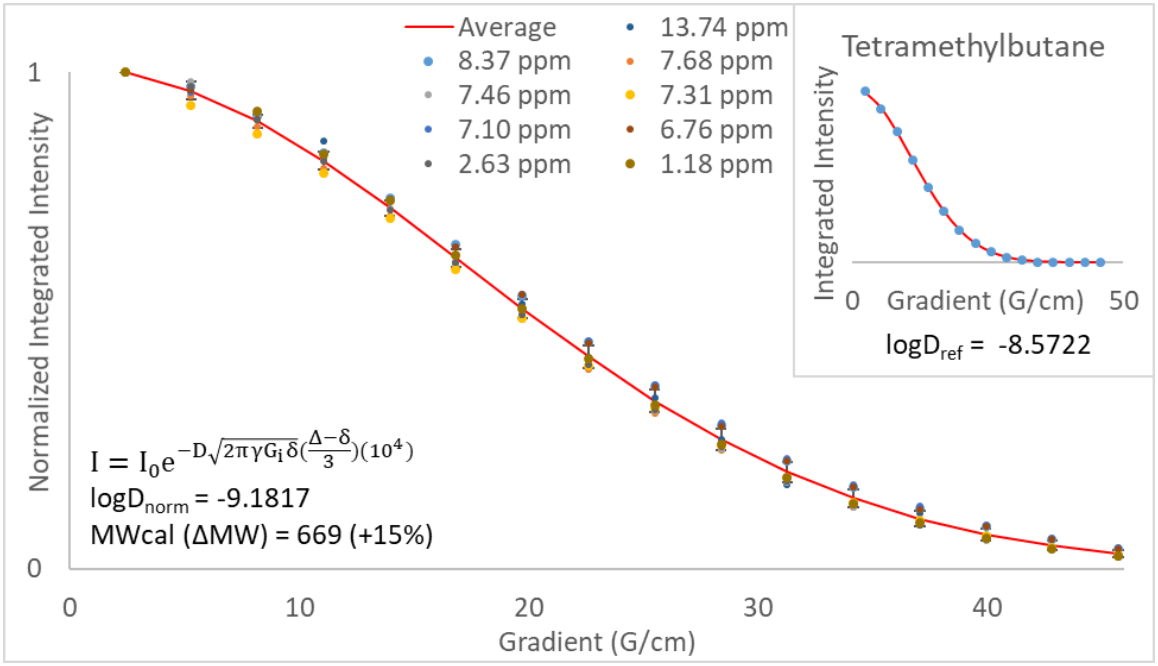

Figure A.6.27: 2D ^{1}H DOSY-NMR spectrum of **3.1** (THF-d_8, 298 K, 50 mM).

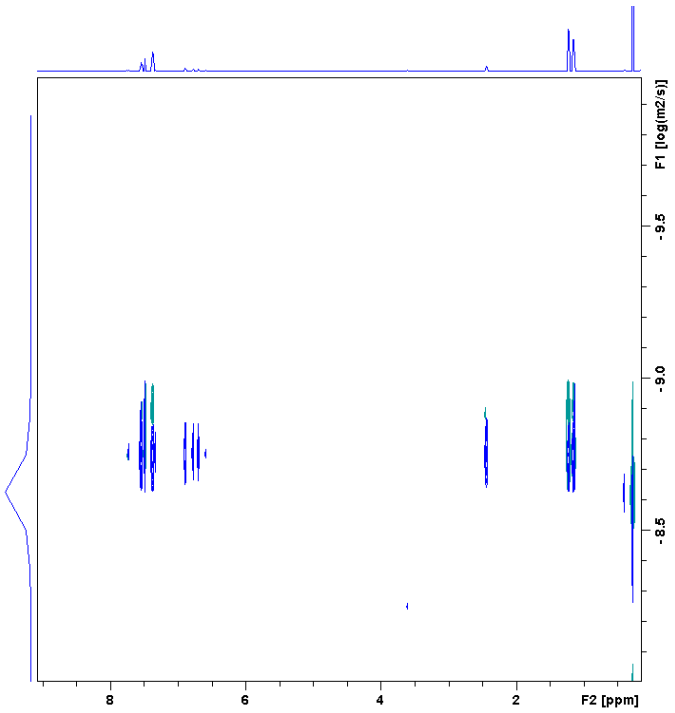

Figure A.6.28: Calculated relaxation curve fits and molecular weight of **3.1**.

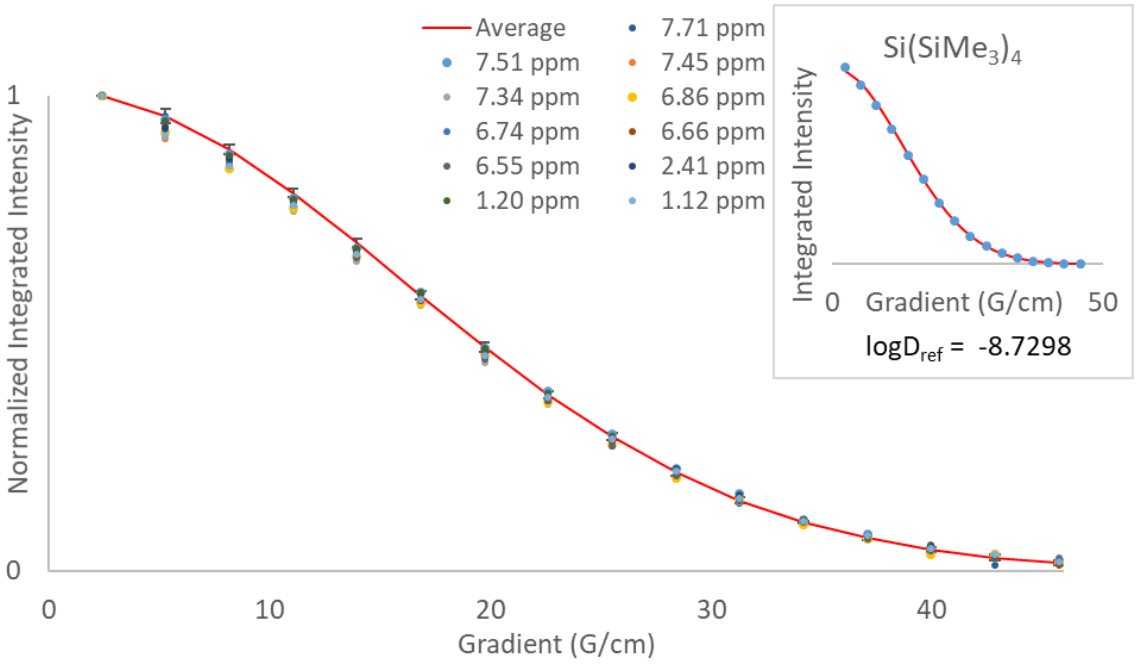

Section A.7: NMR Analysis of Solution Phase Dynamics

Scheme A.7.1: Equilibrium of **4.1** and a mixture of carbazole and IPr.

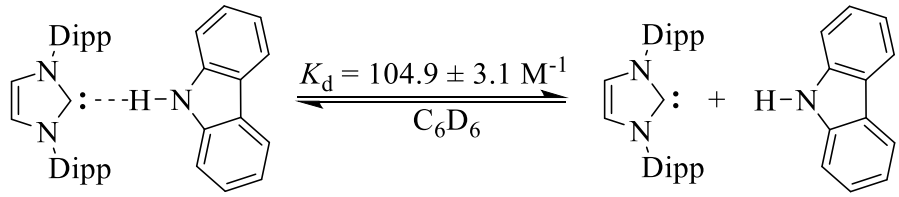

Table A.7.1: Dilution plan using a stock solution of **4.1** at 50 mM in benzene-d_6.

Conc. of 4.1 (mM)	**50**	**40**	**30**	**20**	**10**	**5**	**4**	**3**	**2**	**1**	**0.5**
Vol. Stock (mL)	0.70	0.56	0.42	0.28	0.14	0.070	0.056	0.042	0.028	0.014	0.007
Vol. C_6D_6 (mL)	0.00	0.14	0.28	0.42	0.56	0.63	0.64	0.66	0.67	0.69	0.69

Figure A.7.1: ^{1}H NMR (500 MHz, C_6D_6) spectra of **4.1** analyzed over a concentration range of 50-0.5 mM. Spectrum of carbazole included for reference.

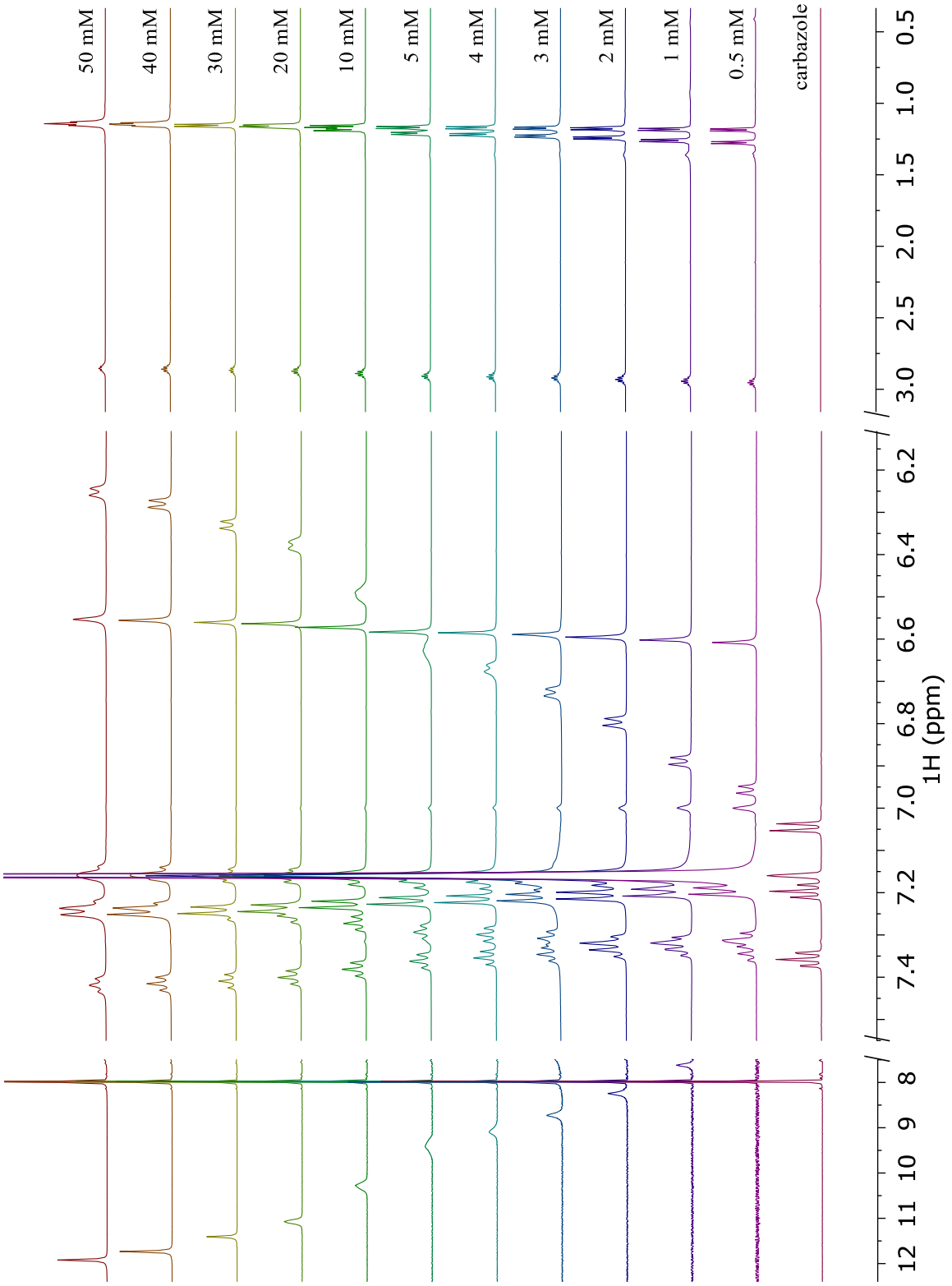

Figure A.7.2: Plot of ^{1}H resonance over concentration range of **4.1** in C_6D_6 and calculated association constants.[3] Marked value (*) excluded due to $\Delta\delta < 0.05$ ppm.

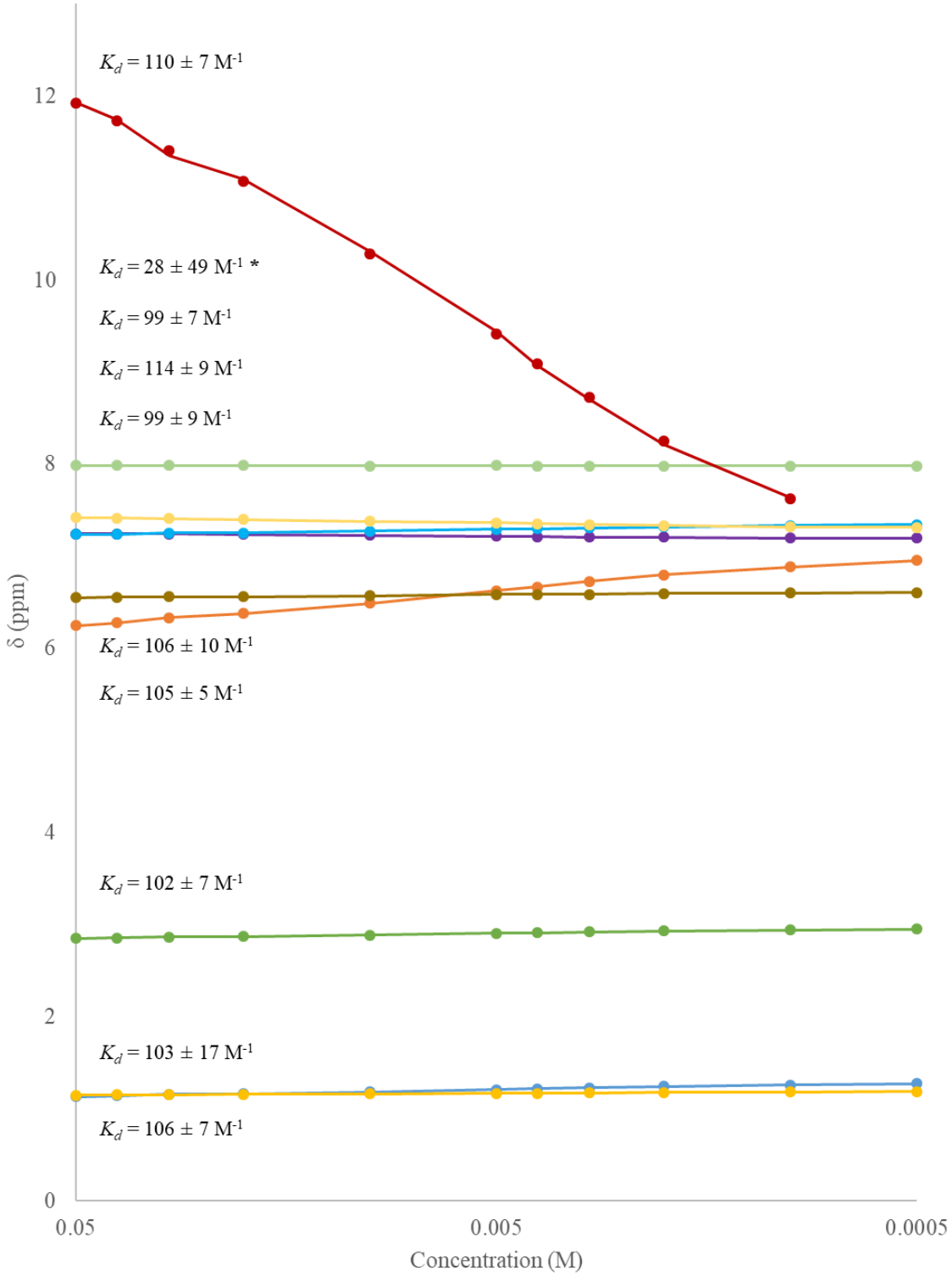

Scheme A.7.2: Equilibrium of **4.4** and a mixture of Ph-BIM and IPr.

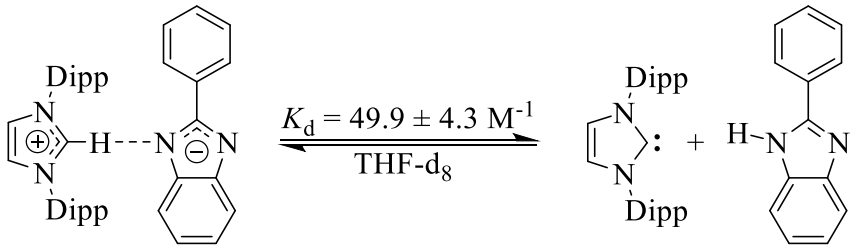

Table A.7.2: Dilution plan using a stock solution of **4.4** at 50 mM in THF-d_8.

Conc. of 4.4 (mM)	**50**	**40**	**30**	**20**	**10**	**5**	**4**	**3**	**2**	**1**	**0.5**
Vol. Stock (mL)	0.70	0.56	0.42	0.28	0.14	0.070	0.056	0.042	0.028	0.014	0.007
Vol. THF-d_8 (mL)	0.00	0.14	0.28	0.42	0.56	0.63	0.64	0.66	0.67	0.69	0.69

Figure A.7.3: ^{1}H NMR (500 MHz, THF-d_8) spectra of **4.4** analyzed over a concentration range of 50-0.5 mM. Spectrum of Ph-BIM included for reference.

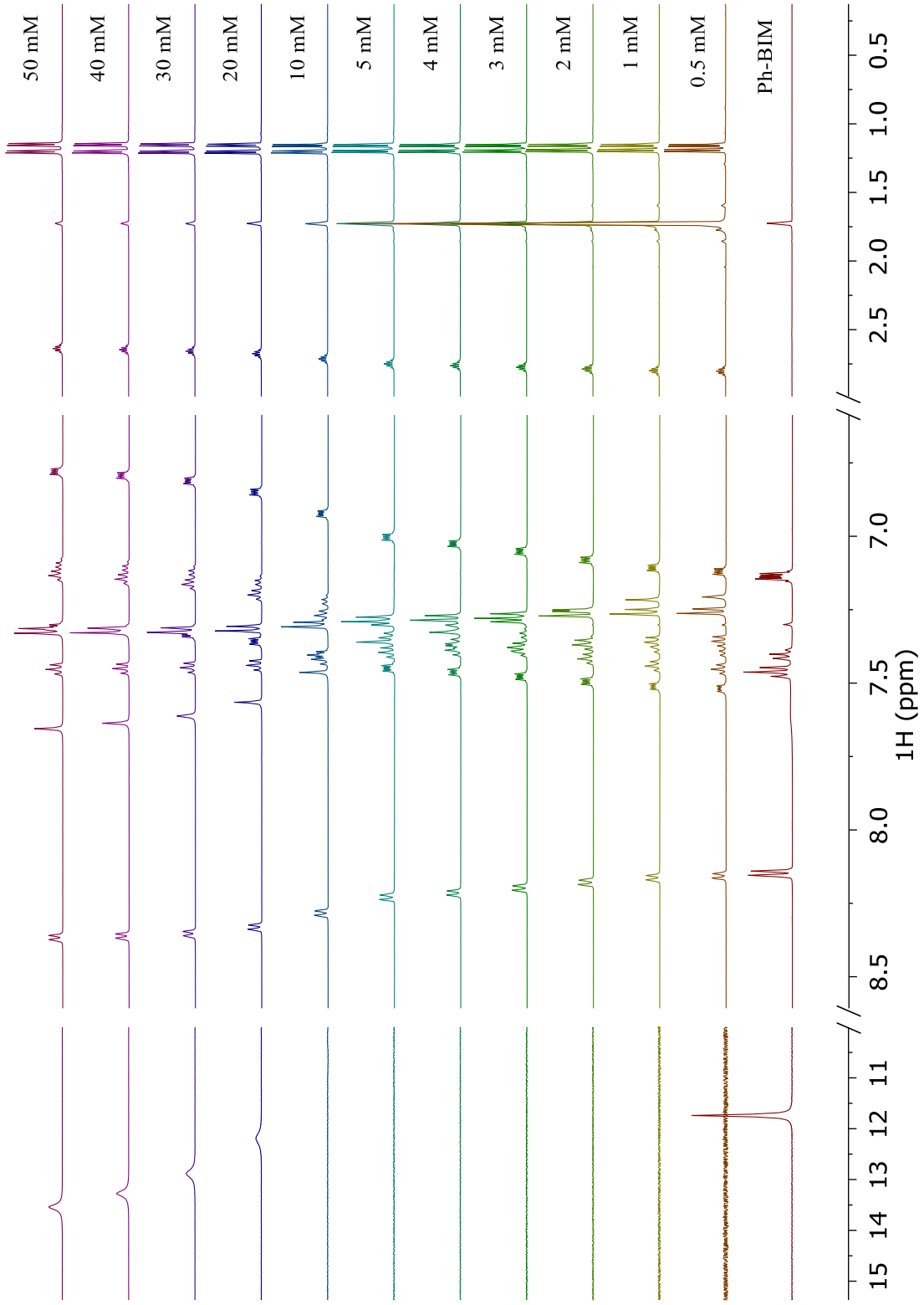

Figure A.7.4: Plot of ^{1}H resonance over concentration range of **4.4** in THF-d_8 and calculated association constants.[3] Marked values (*****) excluded due to $\Delta\delta < 0.05$ ppm.

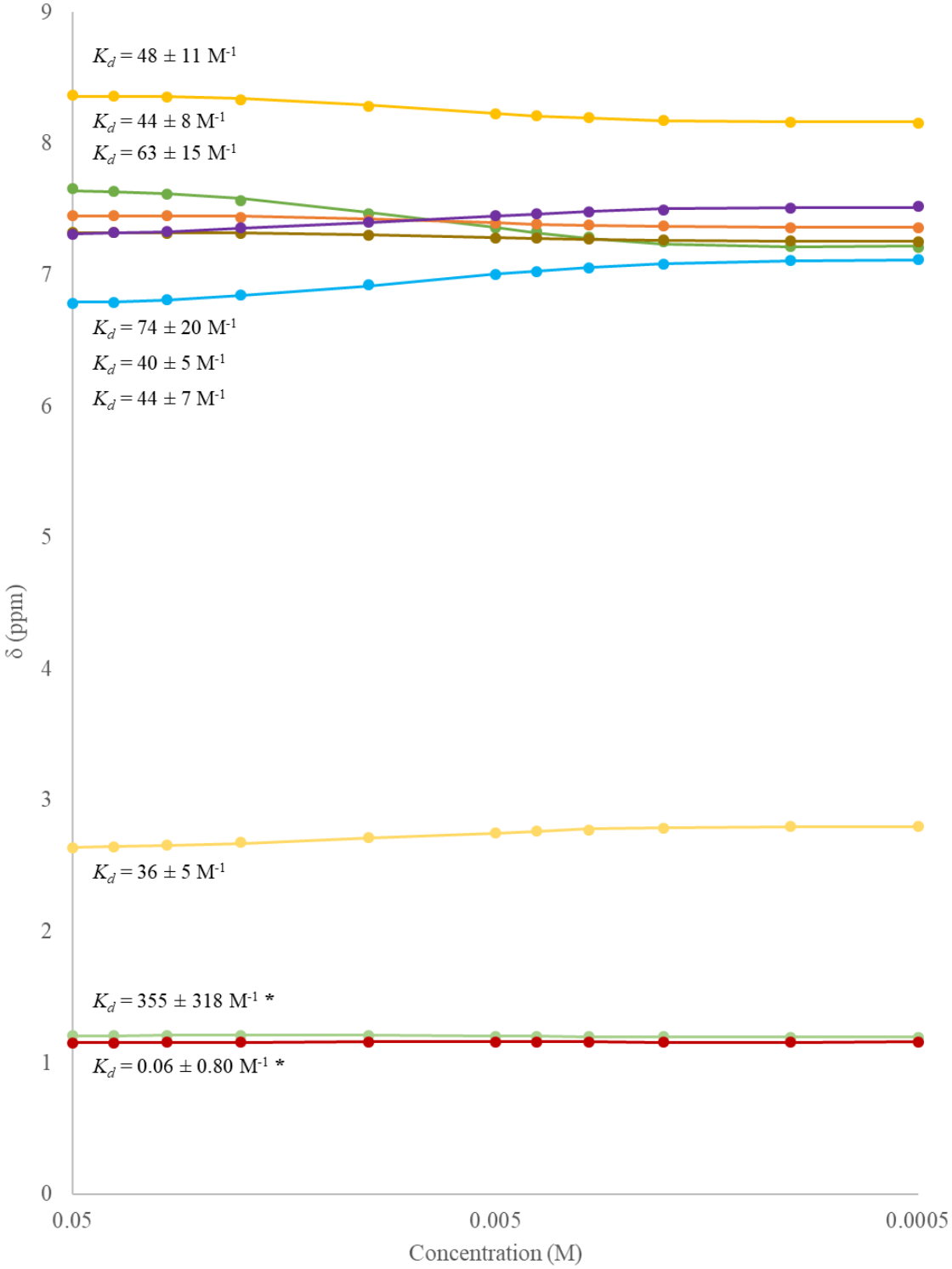

Scheme A.7.3: Equilibrium of **4.3** and carbazole to **4.2** and Ph-BIM.

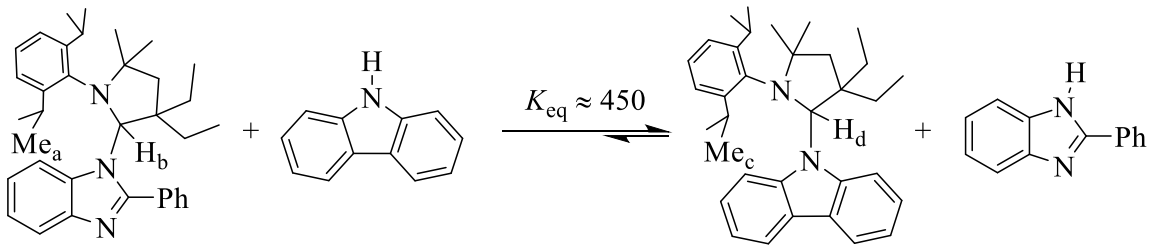

Table A.7.3: Integrations for diagnostic chemical shifts of **4.2** and **4.3** used in the determination of K_{eq}.

ppm	6.40 (H_d)	5.59 (H_b)	-0.45 (H_a)	-0.75 (H_c)	Ave. ratio **4.2**:**4.3**	K_{eq}	$1/K_{eq}$
Integral	7.24	0.35	1.00	21.62	21.2	450	0.0022

Figure A.7.5: NMR spectrum (500 MHz, THF-d_8, 298 K) of 1:1 mixture of **4.3** and carbazole at 50 mM. Spectra of **4.2**, **4.3**, and Ph-BIM provided for reference.

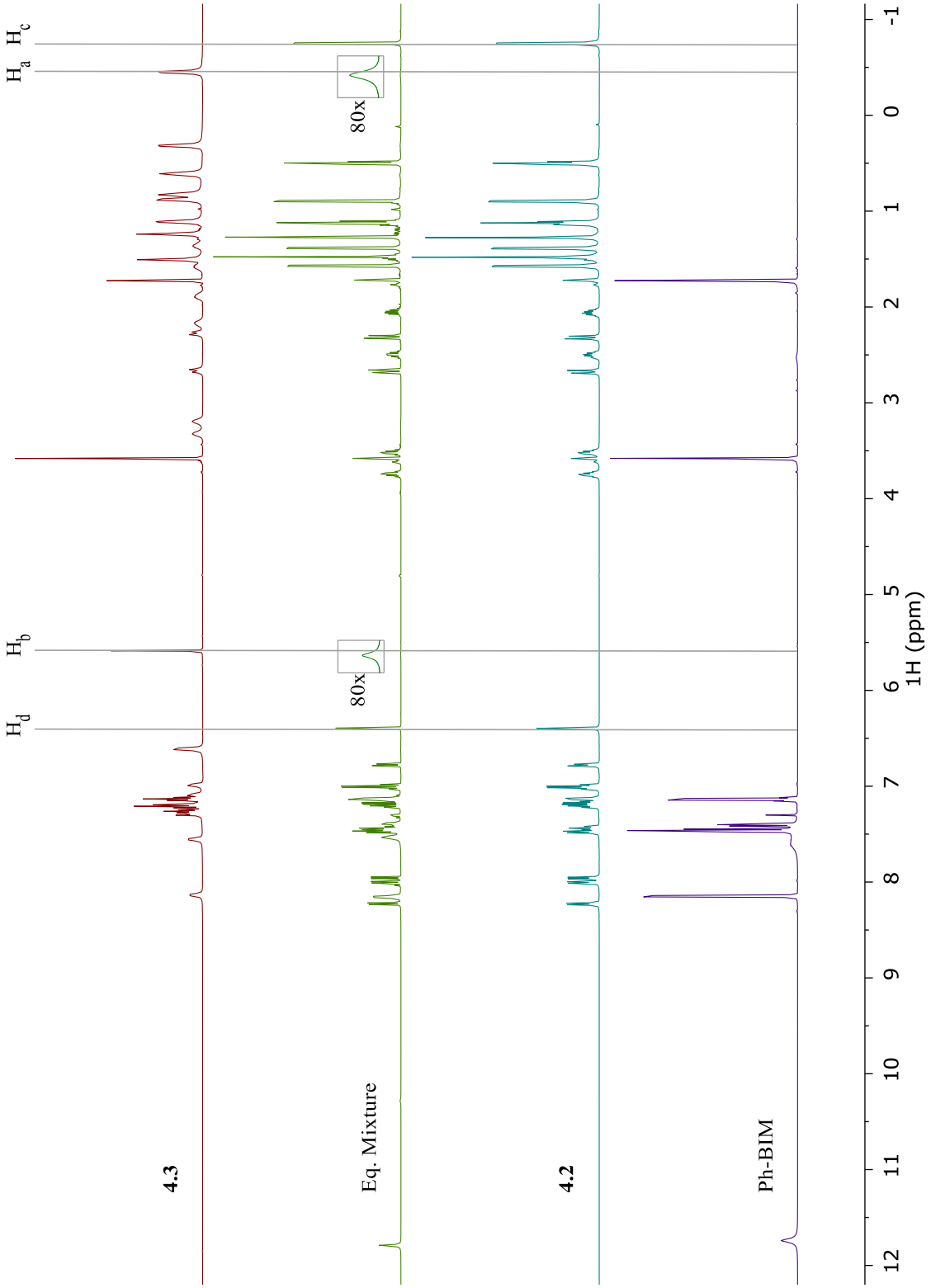

Scheme A.7.4: Equilibrium of **4.2** and Ph-BIM to **4.3** and carbazole.

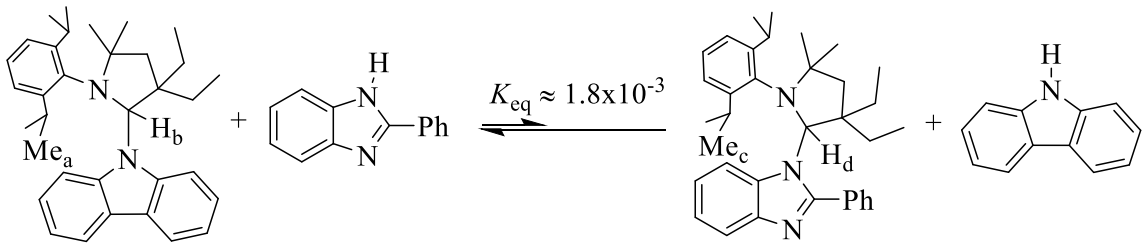

Table A.7.4: Integrations for diagnostic chemical shifts of **4.2** and **4.3** used in the determination of K_{eq}.

ppm	6.40 (H_b)	5.59 (H_d)	-0.45 (H_c)	-0.75 (H_a)	Ave. ratio **4.2**:**4.3**	K_{eq}	1/K_{eq}
Integral	7.59	0.31	1.00	22.75	23.7	0.0018	560

Figure A.7.6: NMR spectrum (500 MHz, THF-d_8, 298 K) of 1:1 mixture of **4.2** and Ph-BIM at 50 mM. Spectra of **4.2**, **4.3**, and Ph-BIM provided for reference.

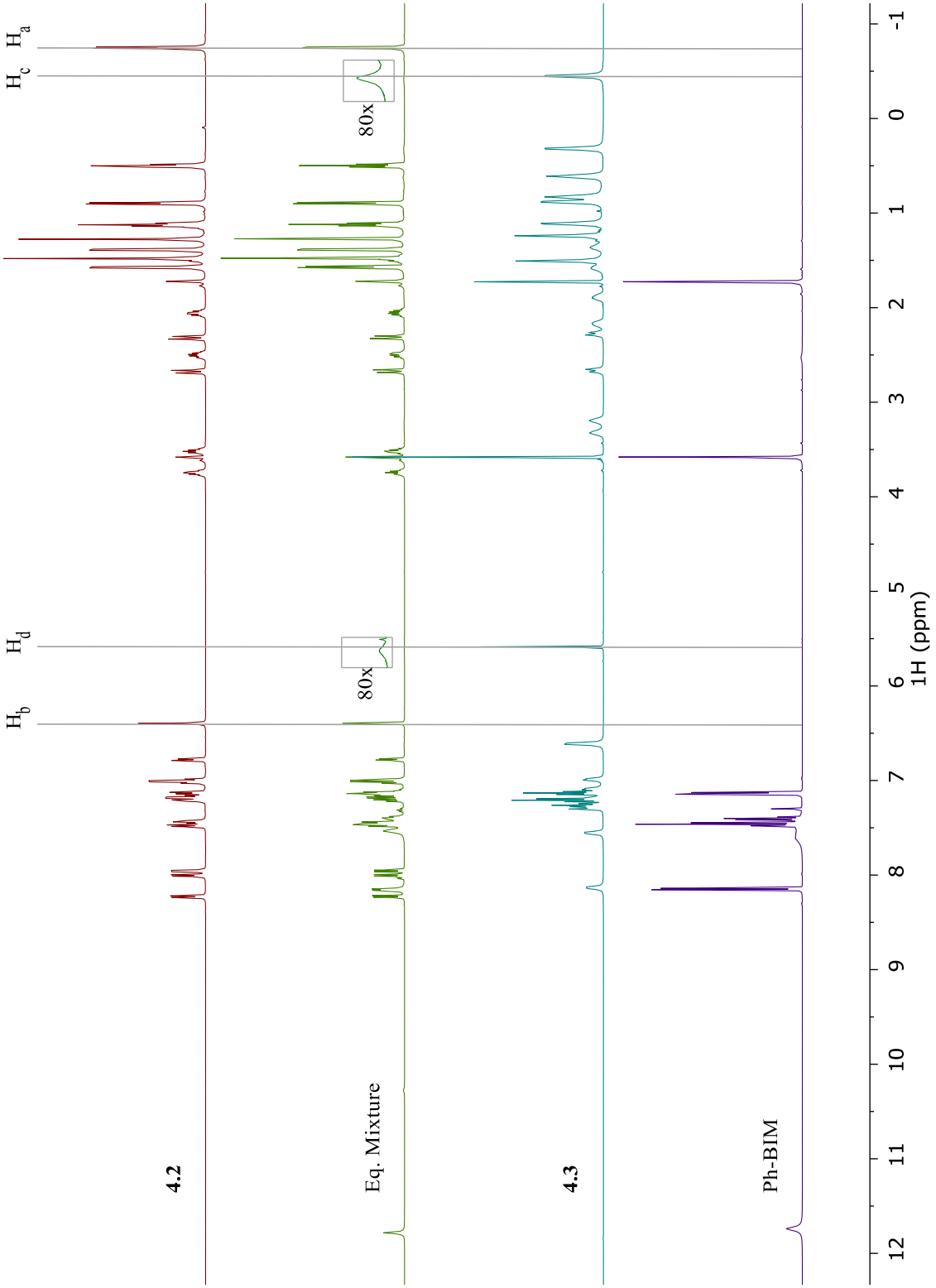

Section A.8: References

(1) Turner, G. L.; Smith, K. A.; Kirkpatrick, R. J.; Oldfieldt, E. Structure and Cation Effects on Phosphorus-31 NMR Chemical Shifts and Chemical-Shift Anisotropies of Orthophosphates. *J. Magn. Reson.* **1986**, *70*, 408–415.

(2) Neufeld, R.; Stalke, D. Accurate Molecular Weight Determination of Small Molecules via DOSY-NMR by Using External Calibration Curves with Normalized Diffusion Coefficients. *Chem. Sci.* **2015**, *6*, 3354–3364.

(3) Chu, M.; Scioneaux, A. N.; Hartley, C. S. Solution-Phase Dimerization of an Oblong Shape-Persistent Macrocycle. *J. Org. Chem.* **2014**, *79*, 9009–9017.

Appendix B: Photophysical Data

General Condiderations:

Absorbance spectra were recorded on Cary 5000 spectrophotometer and corrected for solvent background absorbance and instrument drift. Emission spectra were recorded on Cary Eclipse spectrophotometer with excitation and emission slits set to 2.5 nm and 5.0 nm, respectively, and λ_{ex} = 290nm for all spectra. All spectra were recorded at room temperature using 1 cm path length quartz cuvettes with solutions prepared under inert atmosphere. Solutions for molar absorptivity and solvent dependence analyses were obtained through standard parallel dilution technique from a stock solution of the analyte. Analyses involving addition of excess free carbene were accomplished likewise from separate stock solutions of analyte and free carbene.

Figure B.1: Molar absorptivity of **4.1** with varying concentration in THF.

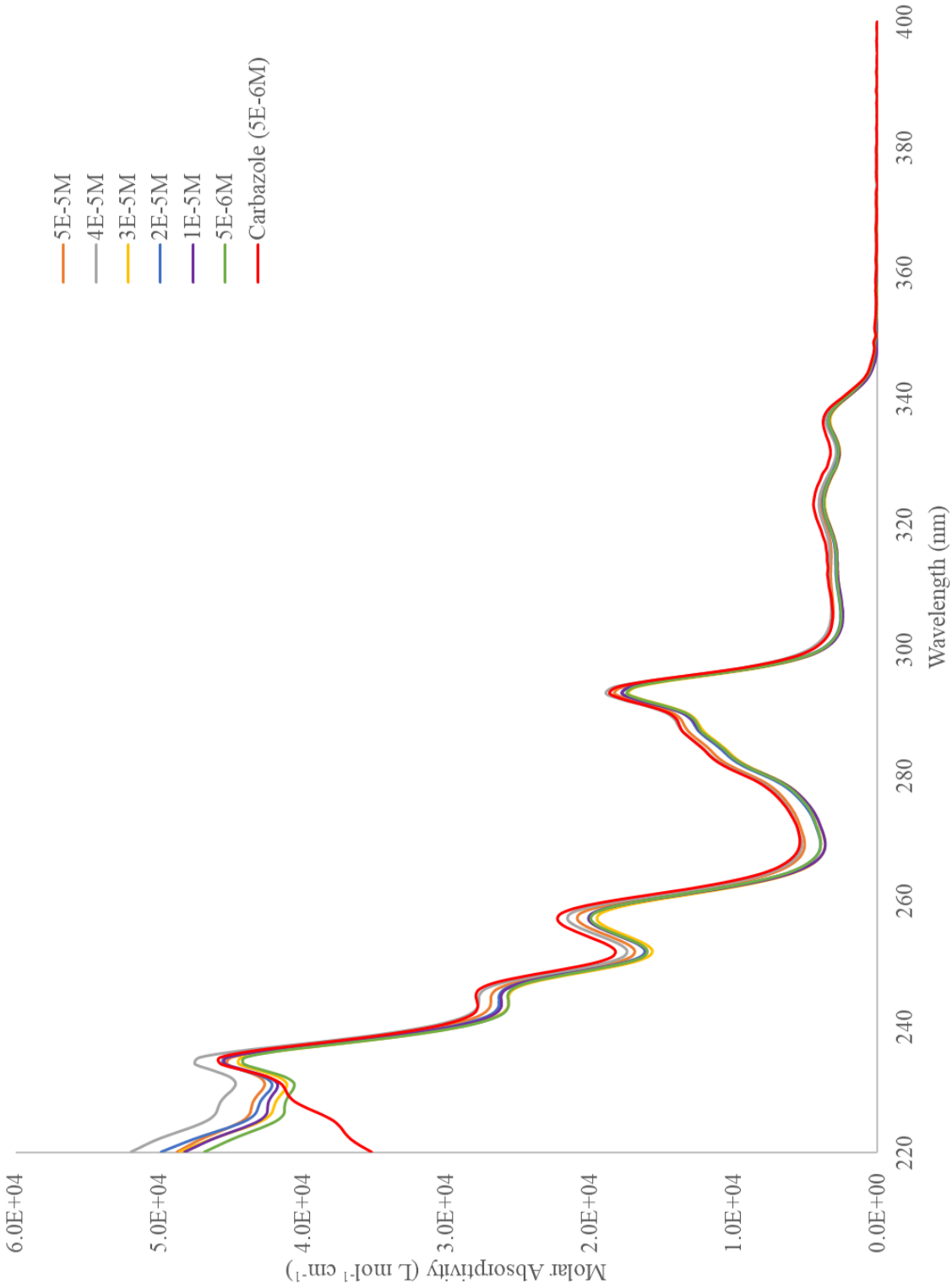

Figure B.2: Absorbance and emission spectra for **4.1** with varying solvent at $5x10^{-6}$ M.

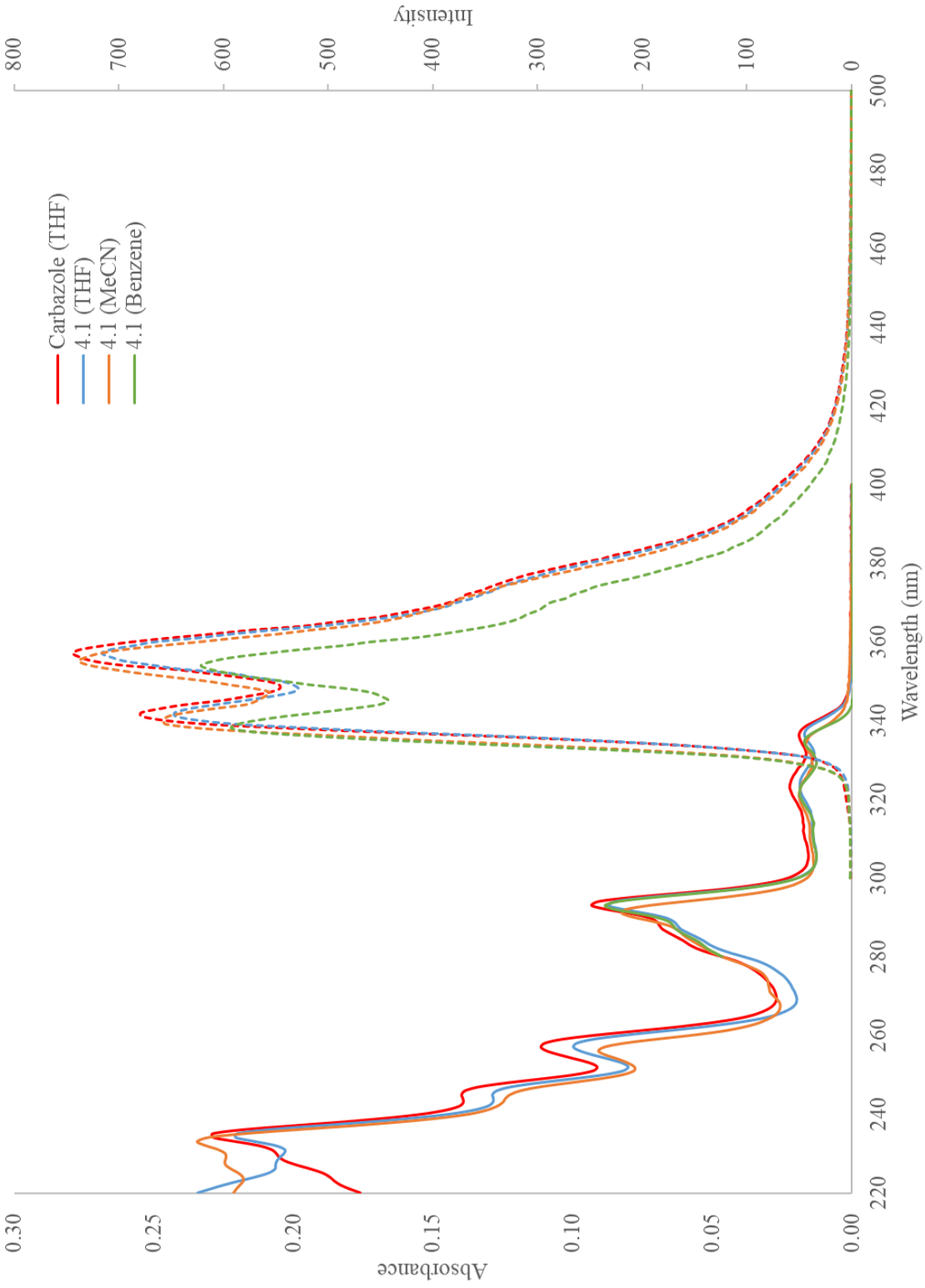

Figure B.3: Absorbance and emission spectra for **4.1** at $5x10^{-6}$ M in THF with varying amount of IPr.

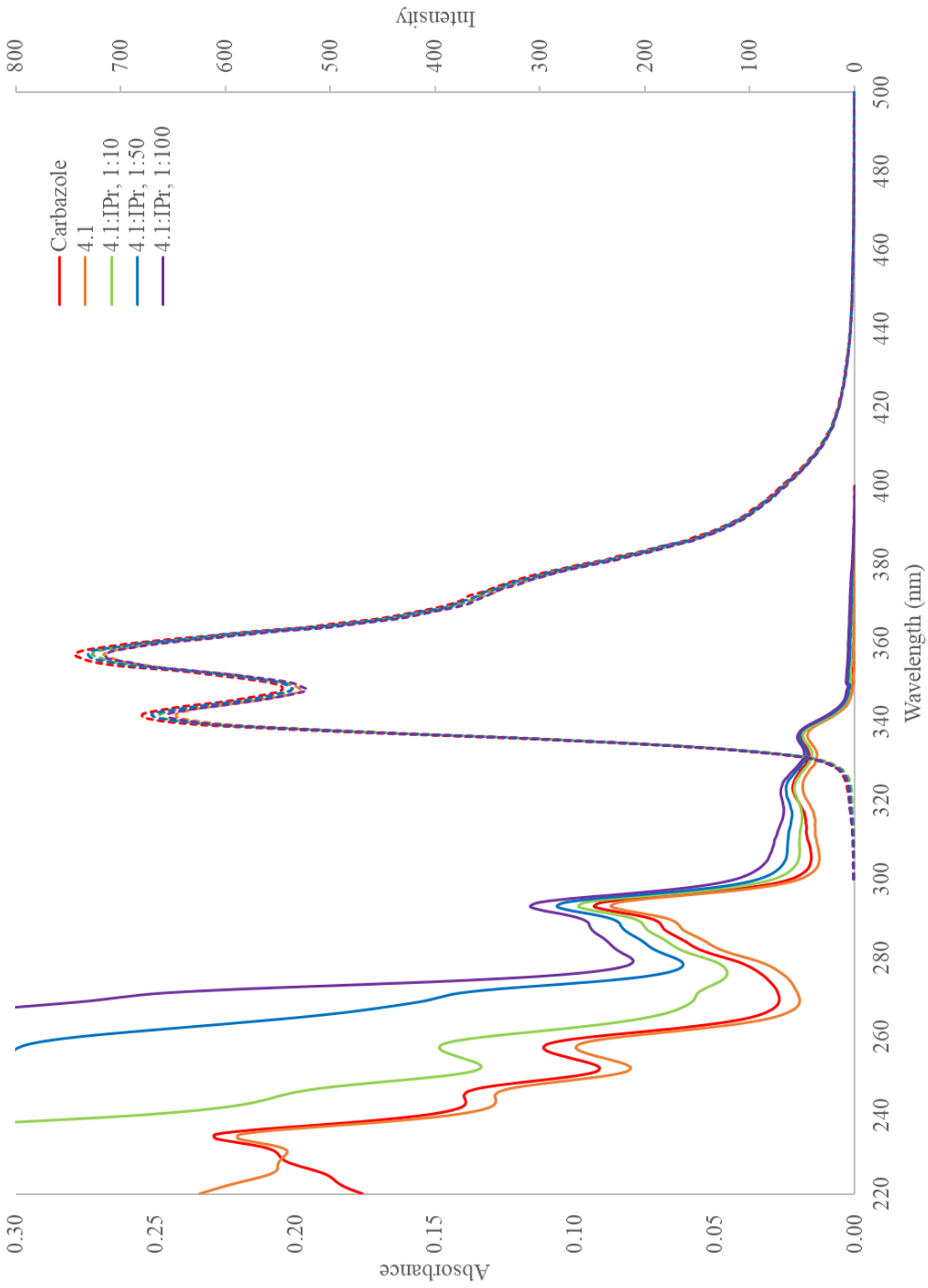

Figure B.4: Molar absorptivity of **4.2** with varying concentration in THF.

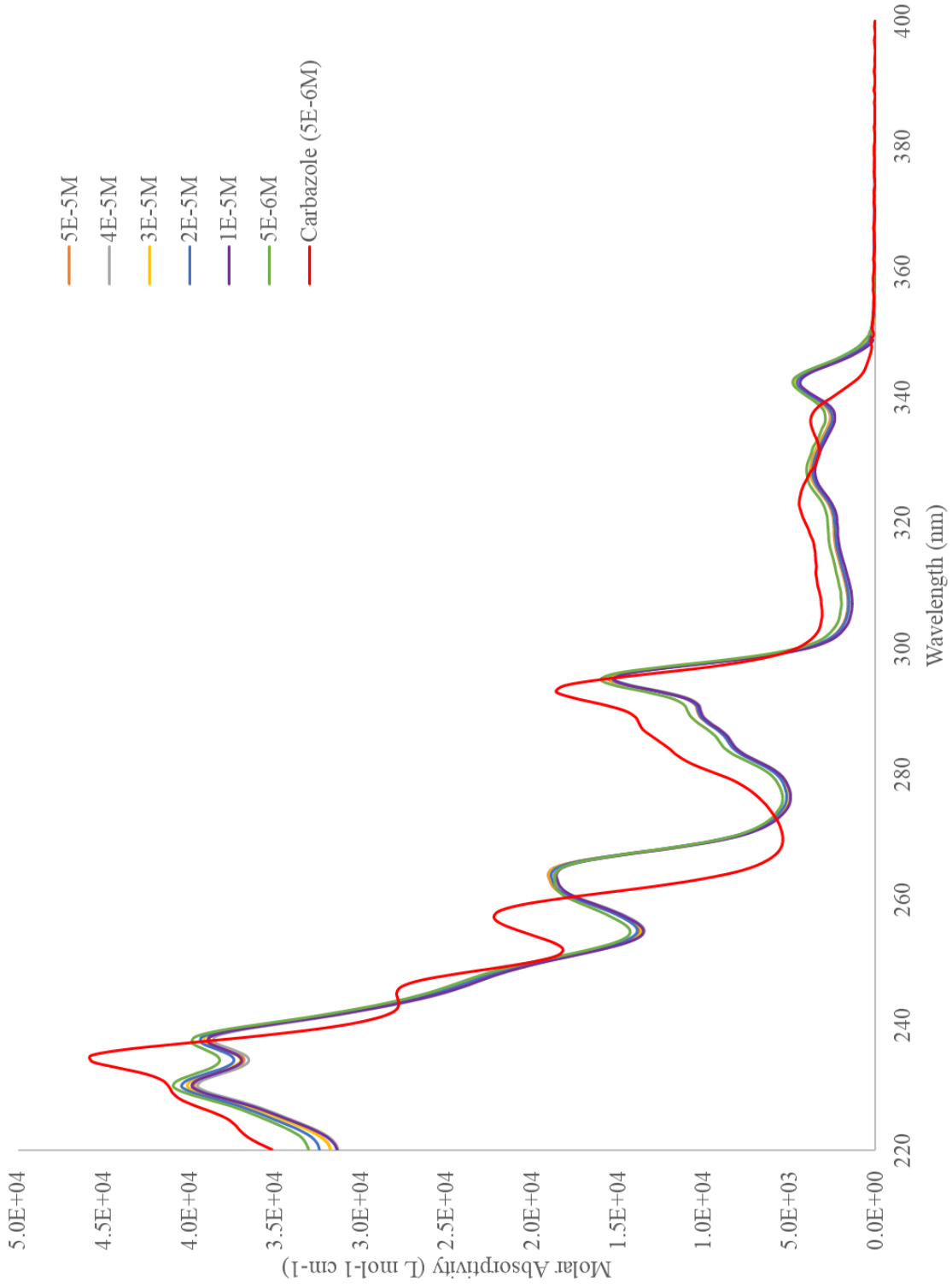

Figure B.5: Absorbance and emission spectra for **4.2** at $5x10^{-6}$ M with varying solvent.

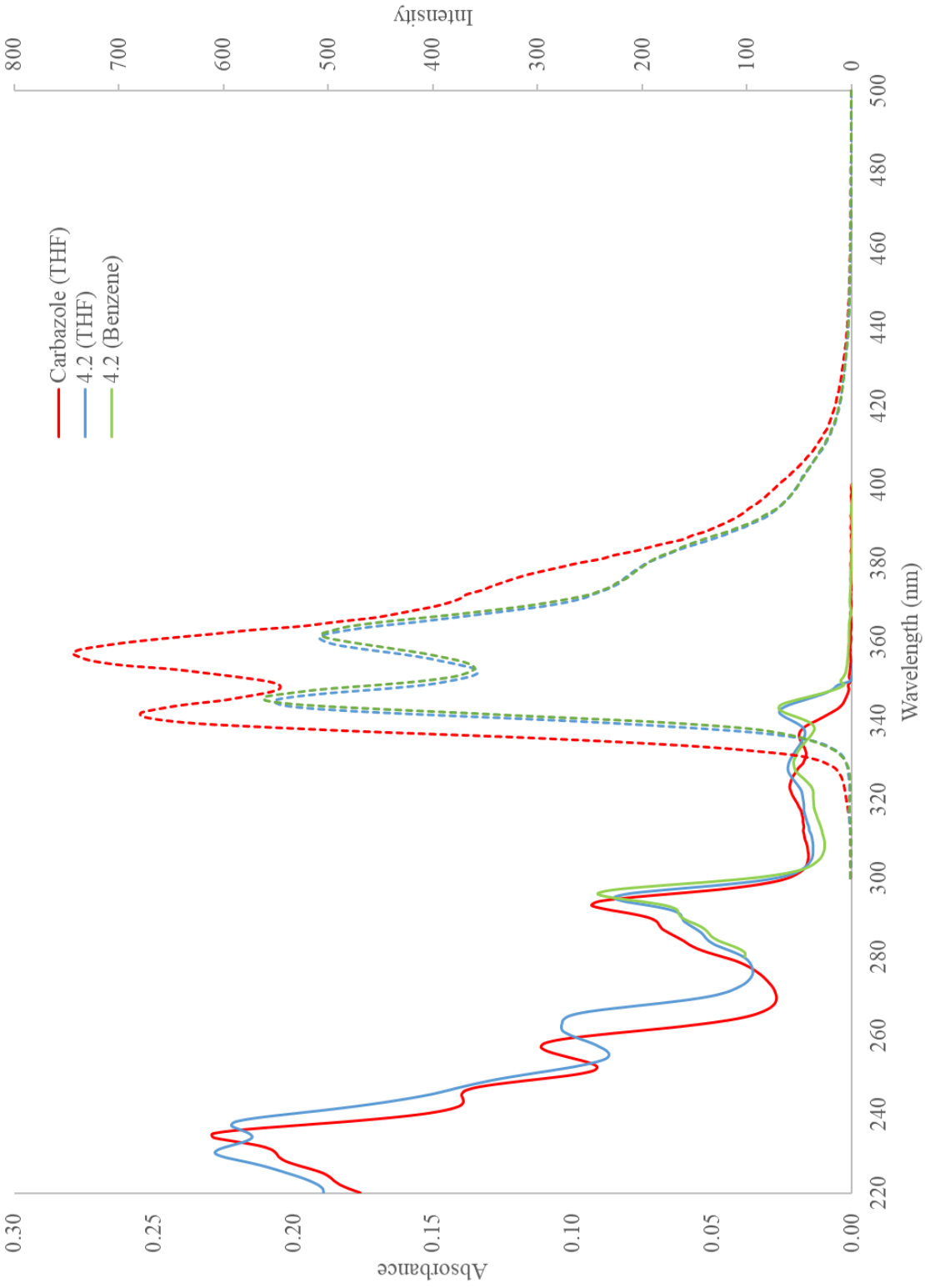

Figure B.6: Absorbance and emission spectra for **4.2** at $5x10^{-6}$ M in THF with varying amount of ^{Et}CAAC.

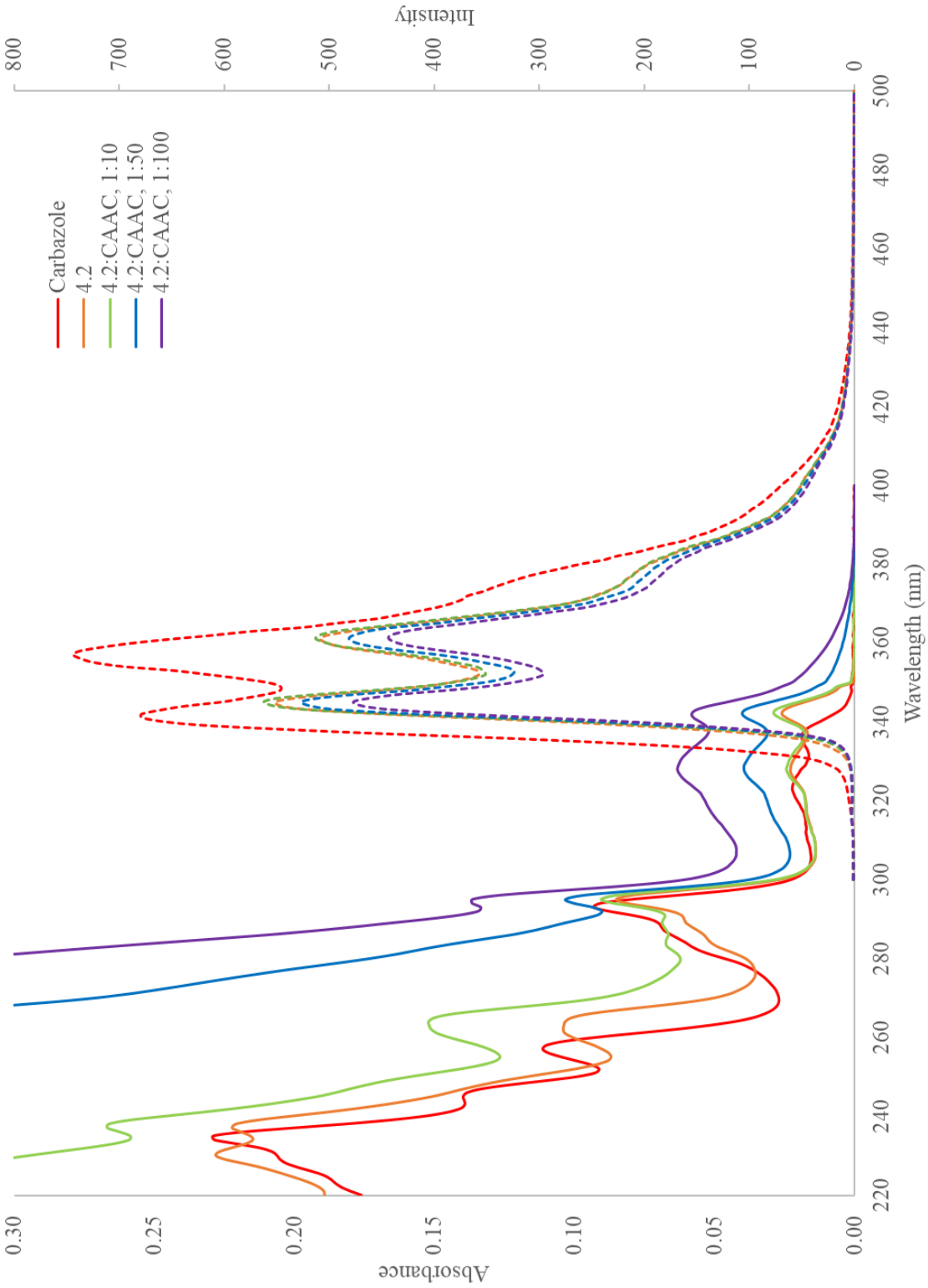

Figure B.7: Molar absorptivity of **4.3** in THF with varying concentration.

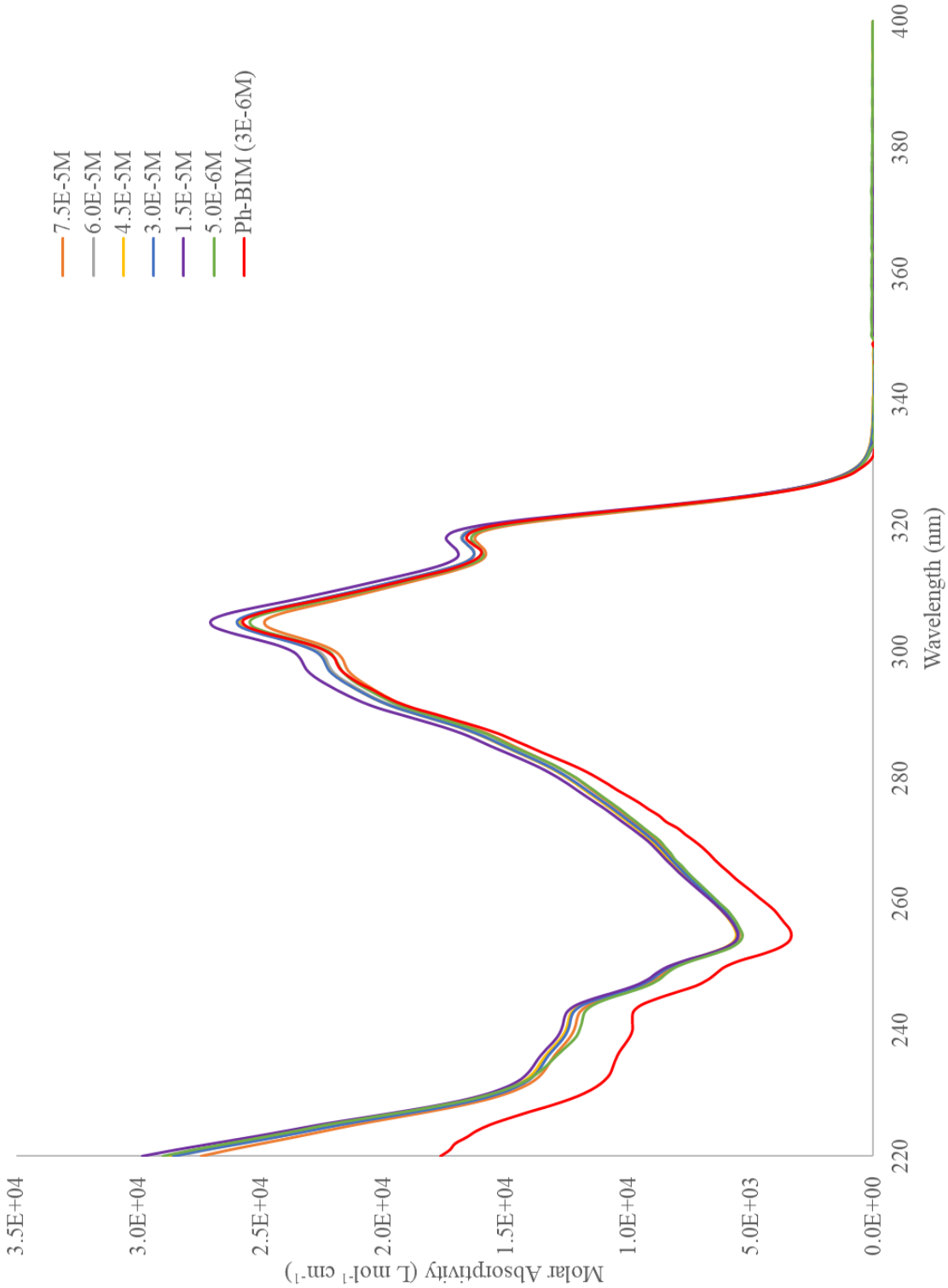

Figure B.8: Absorbance and emission spectra for **4.3** at $3x10^{-6}$ M with varying solvent.

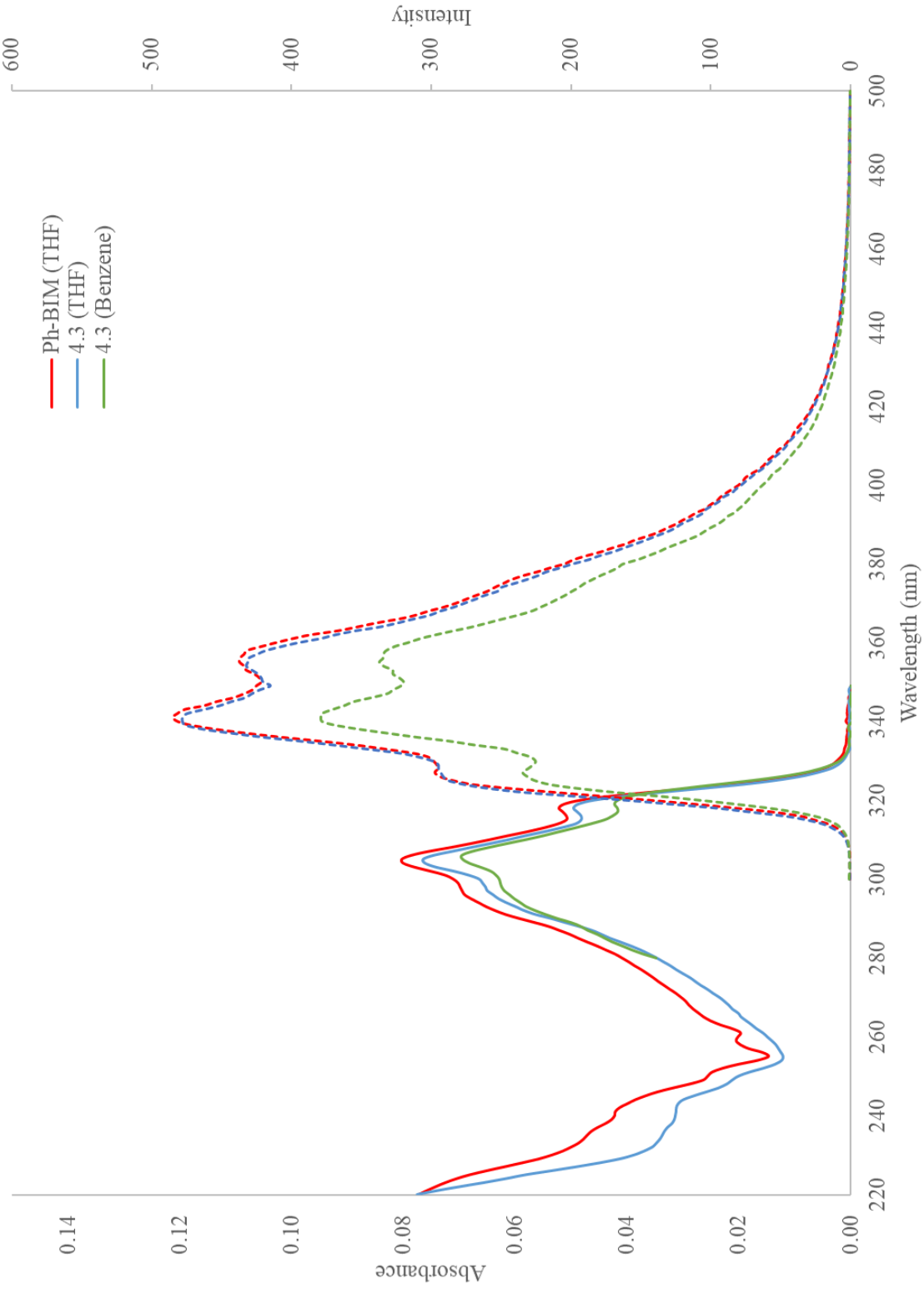

Figure B.9: Absorbance and emission spectra for **4.3** at $3x10^{-6}$ M in THF with varying amount of ^{Et}CAAC.

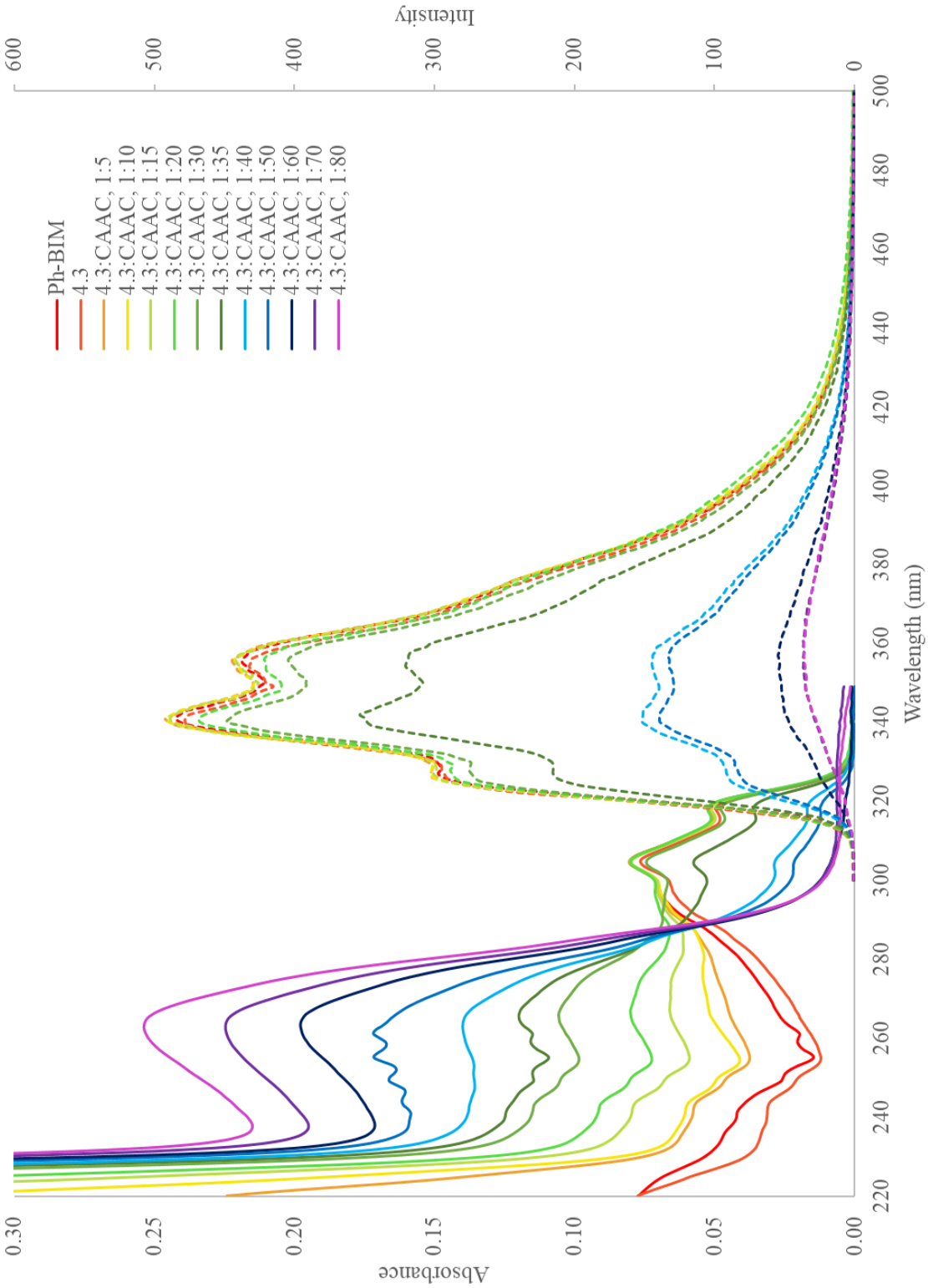

Figure B.10: Excitation spectrum (355 nm) of **4.3** at $3x10^{-6}$ M with $2.7x10^{-4}$ M ^{Et}CAAC in THF showing that emission quenching of **4.3** is not due to a change in excitation band.

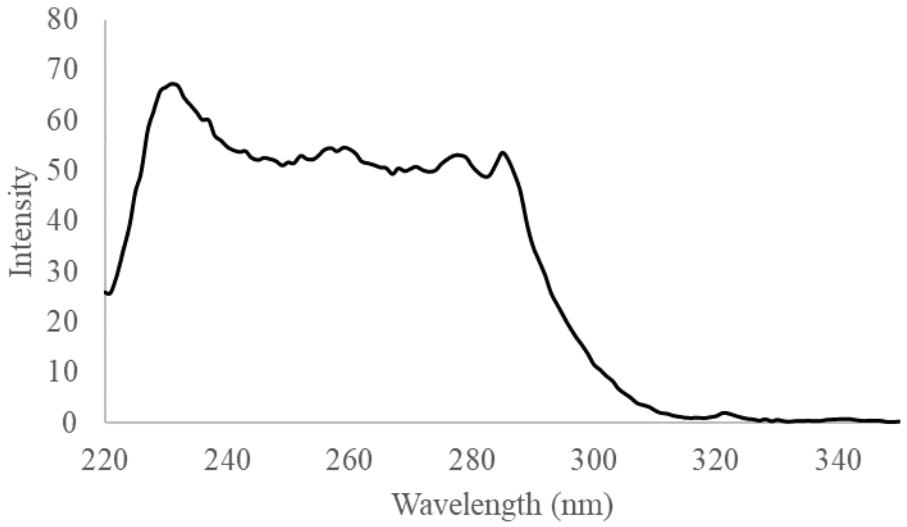

Figure B.11: Molar absorptivity of **4.4** in THF with varying concentration.

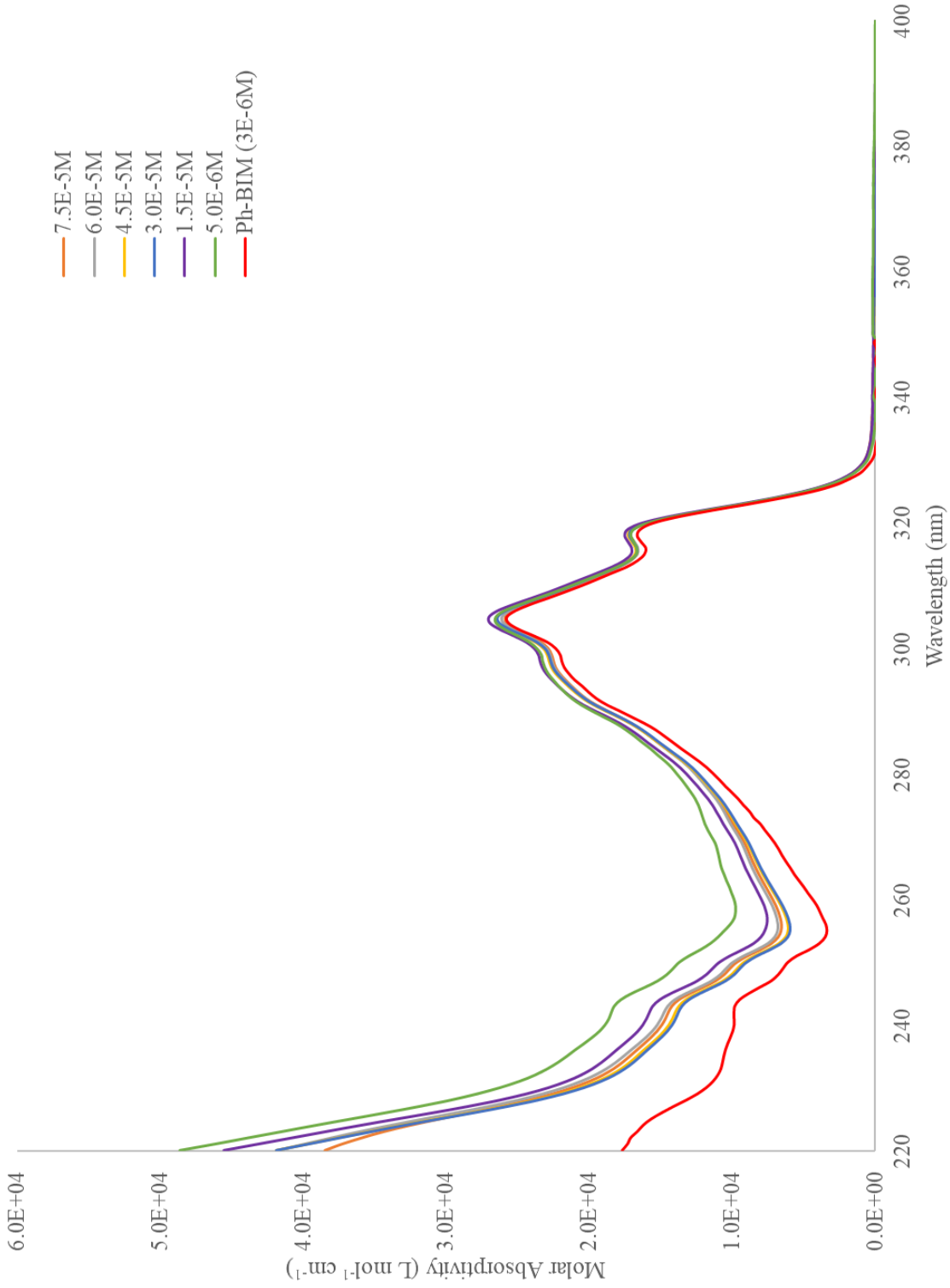

Figure B.12: Absorbance and emission spectra for **4.4** at $3x10^{-6}$ M with varying solvent.

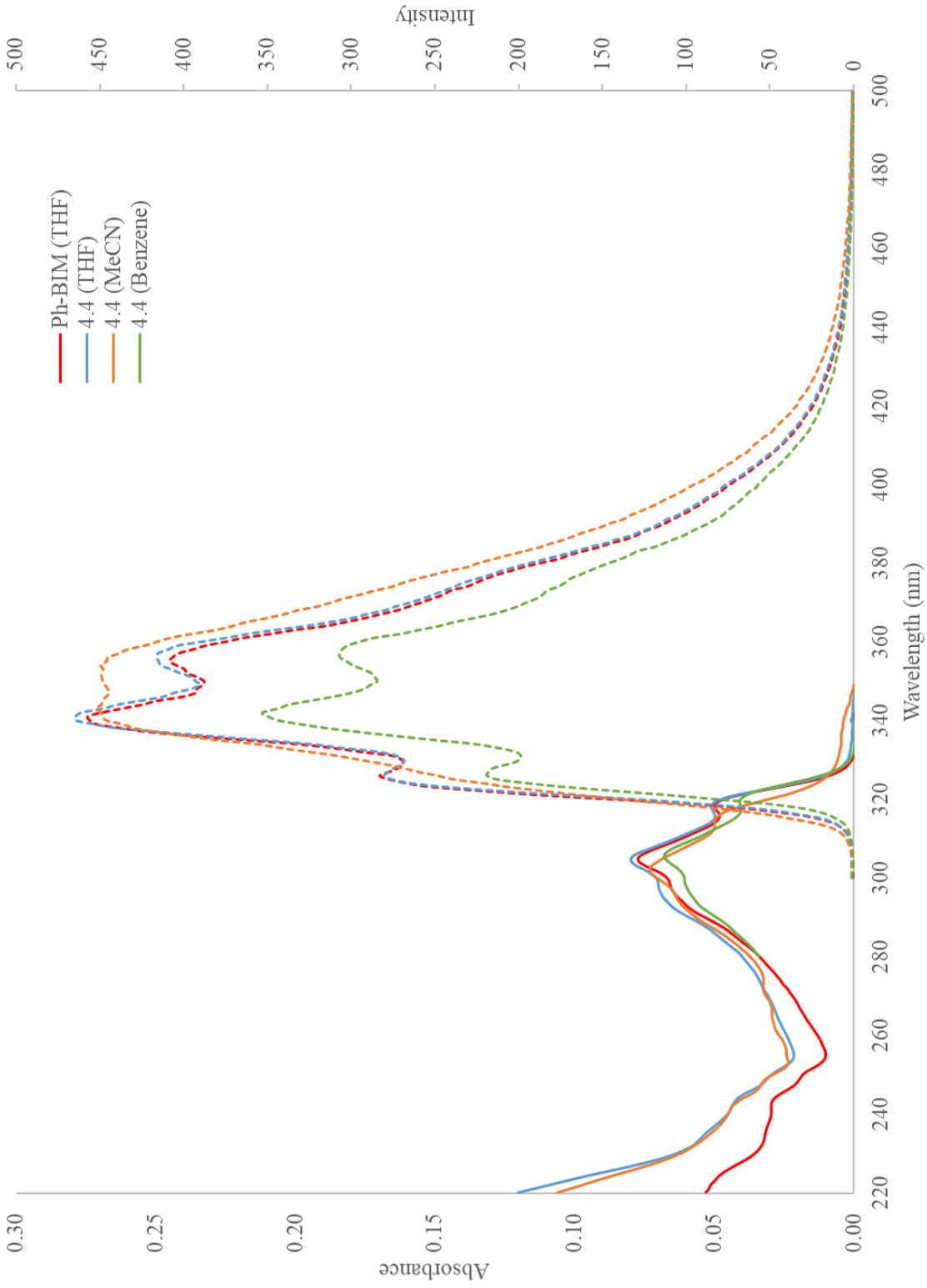

Figure B.13: Absorbance and emission spectra for **4.4** at $3x10^{-6}$ M in THF with varying amount of IPr.

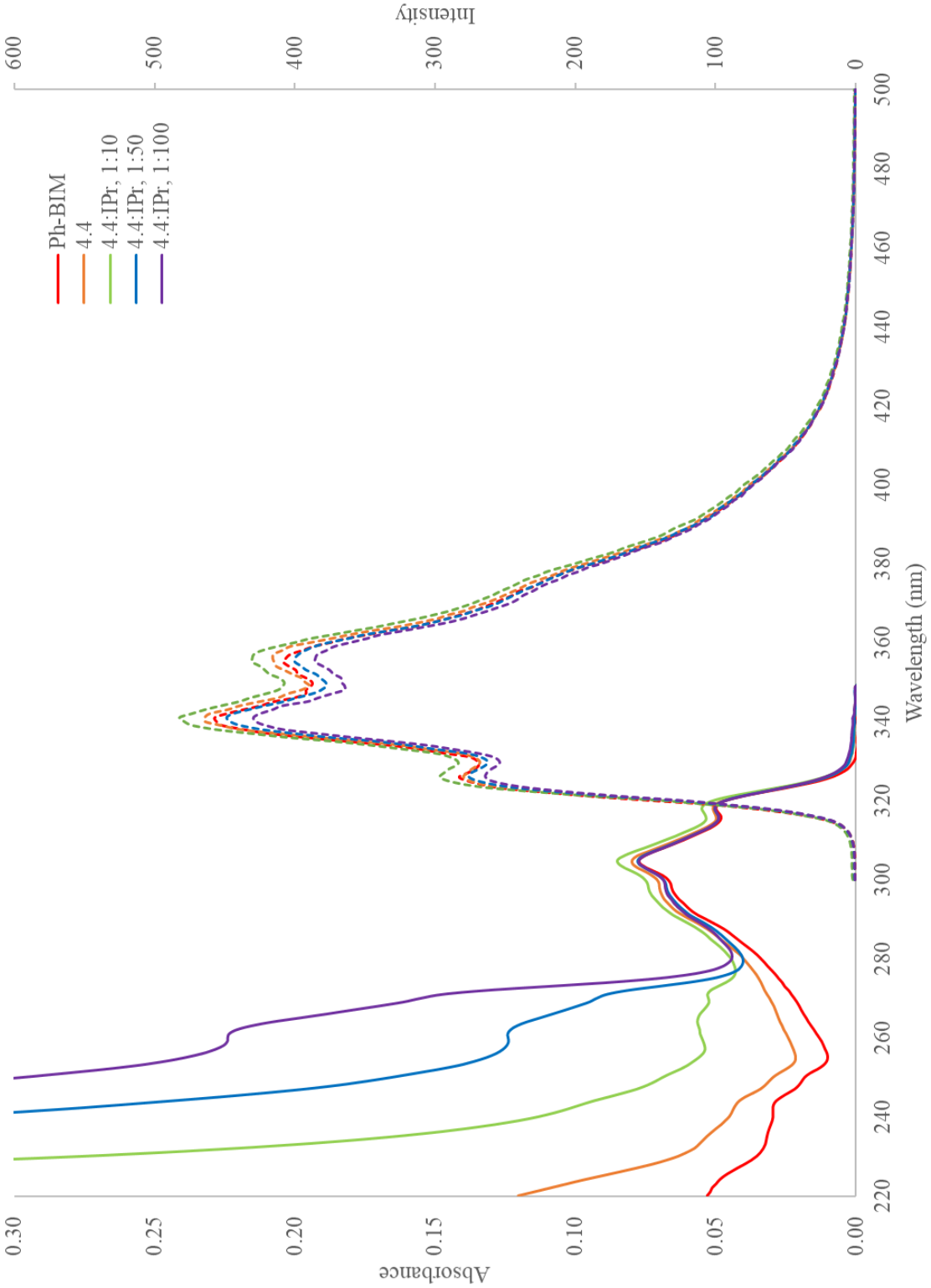

Figure B.14: Emission under 365 nm irradiation of (top) 50 mM solutions of carbazole, **4.1**, and **4.2** in THF and (bottom) solid carbazole, **4.1**, and **4.2**.

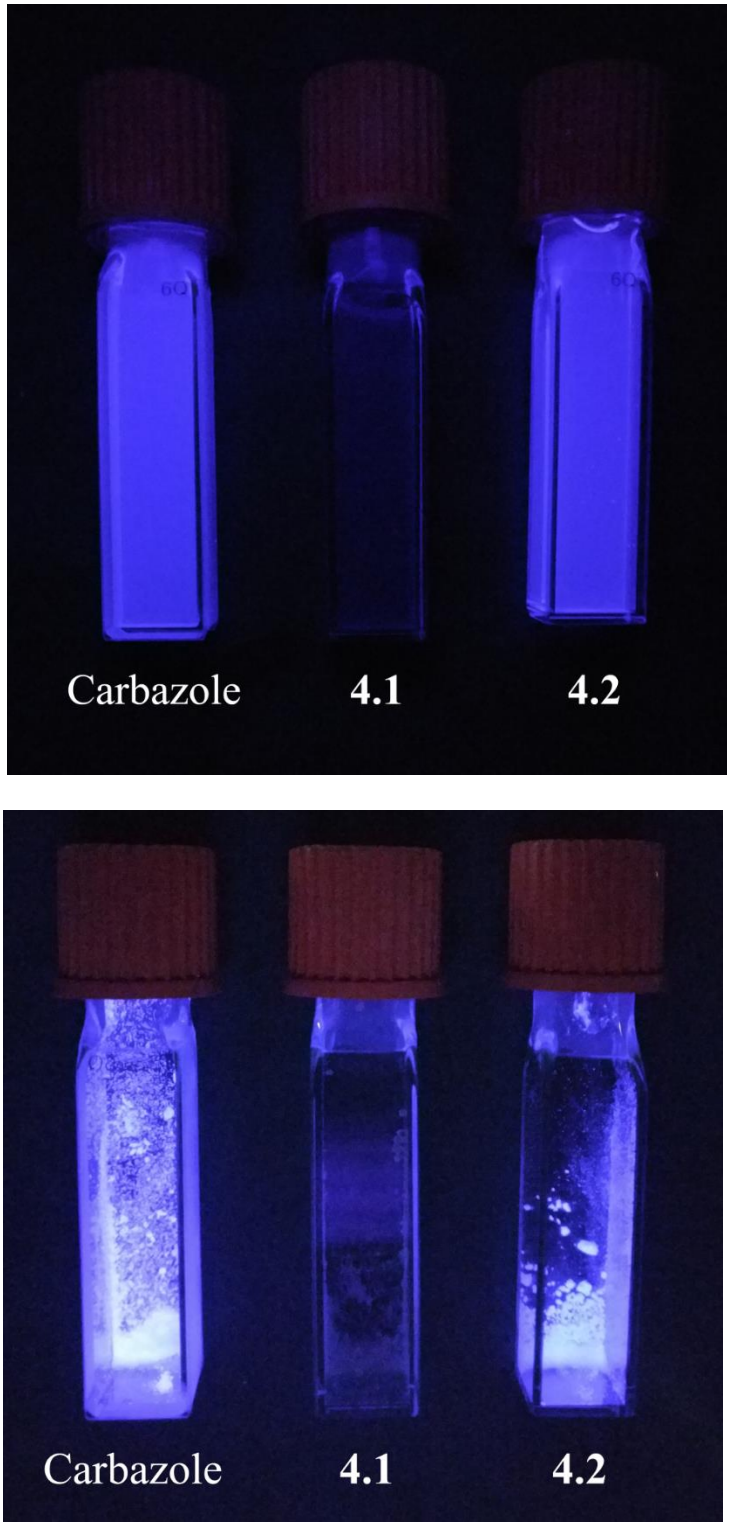

Figure B.15: Emission under 365 nm irradiation of (top) 50 mM solutions of 2-phenylbenzimidazole, **4.4**, and **4.3** in THF and (bottom) solid 2-phenylbenzimidazole, **4.4**, and **4.3**.

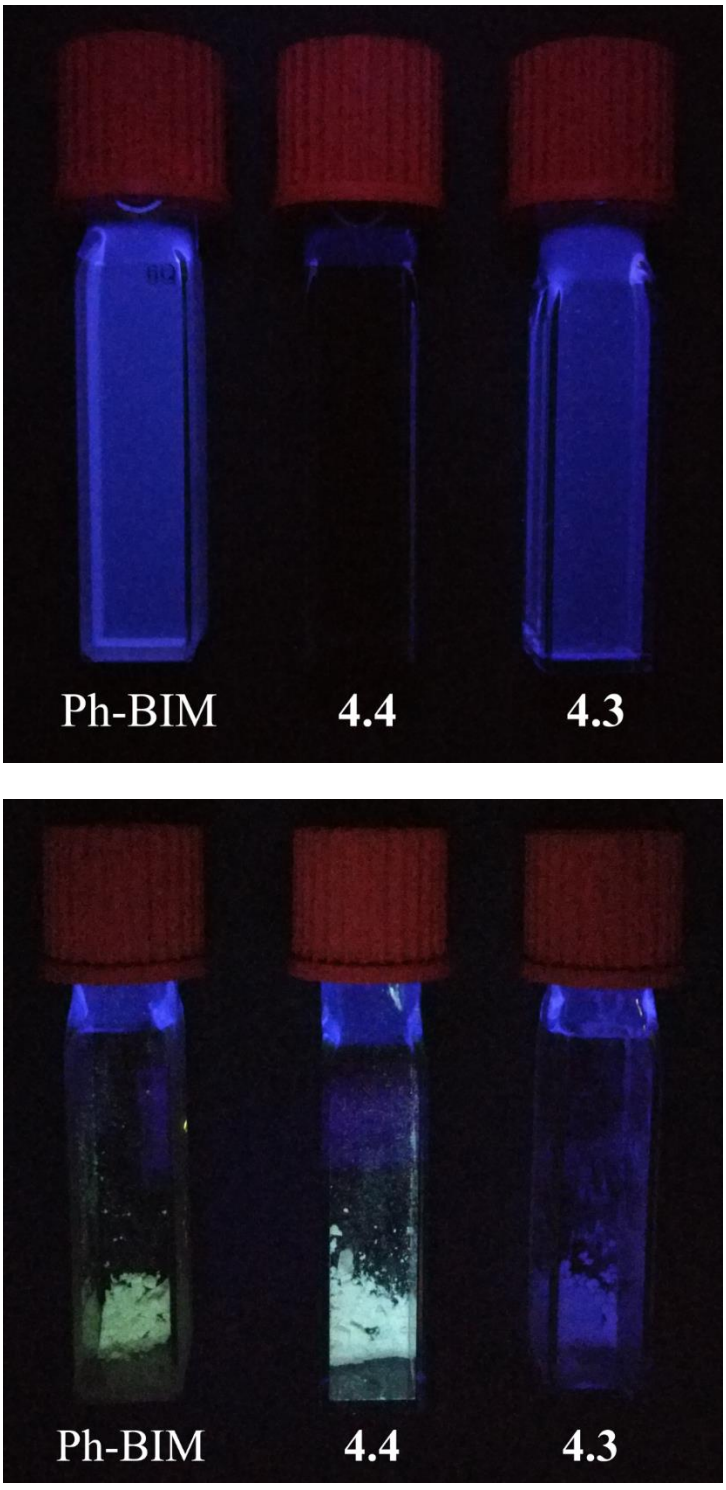

Figure B.16: Absorbance and emission spectra of $3x10^{-6}$ M anthracene in THF doped with excess free carbenes, $3x10^{-4}$ M IPr or ^{Et}CAAC (λ_{ex} = 358 nm), as a control for carbene-induced quenching of non-NH containing fluorophores even in large excess of carbene.

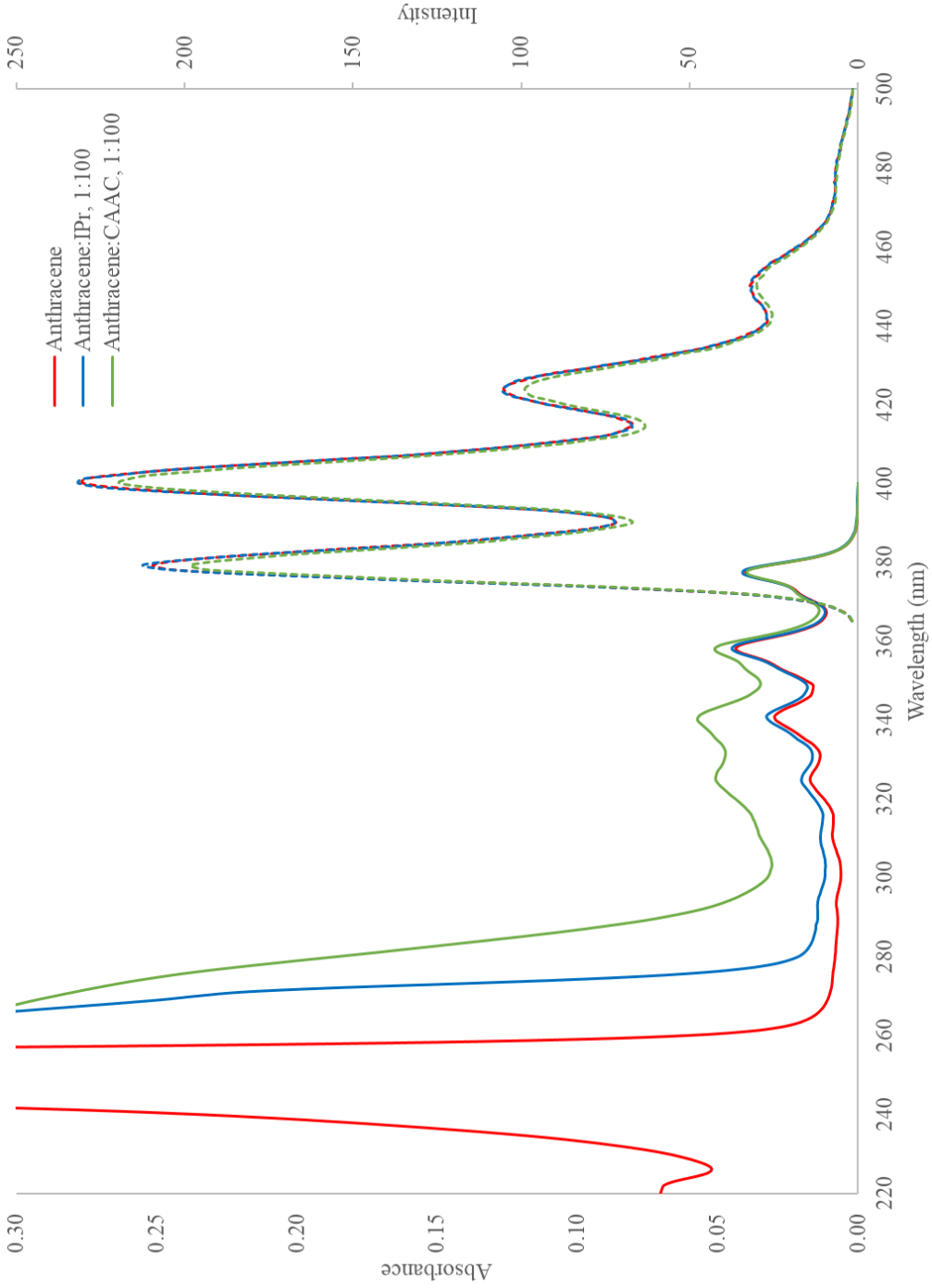

Appendix C: Crystallographic Data

To conserve space, only crystal data, structure refinement parameters, and XYZ coordinates are included. All structures have been added to the Cambridge Structural Database.

Table C.1: List of crystal structures presented in Appendix C and Cambridge Crystallographic Data Centre (CCDC) identification numbers.

1531806	zirconophosphaalkene coordination polymer (**2.1**)
1531807	zirconophosphaalkene dimer (**2.2**)
	product of rearrangement reaction between **2.1** and Mes_2BF (**2.3**)
	2-*tert*-butyl-1,3-benzazaphosphole-IPr adduct (**3.3**)
	2-*tert*-butyl-1,3-benzazaphosphole-^{Et}CAAC adduct (**3.4**)
1901811	2-phenylbenzimidazole-^{Et}CAAC insertion product (**4.1**)
1901813	2-phenylbenzimidazole-IPr adduct (**4.4**)

Figure C.1: ORTEP diagram of zirconophosphaalkene coordination polymer (**2.1**) (ellipsoids set at 50% probability; hydrogen atoms, co-crystallized THF, and second coordination polymer chain omitted for clarity).

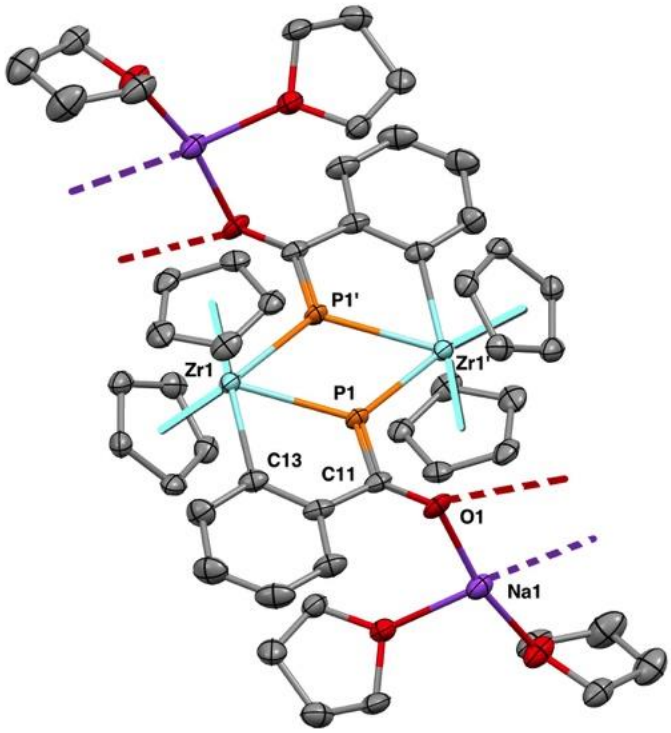

Table C.2: Crystal data and structure refinement for zirconophosphaalkene coordination polymer (**2.1**).

Empirical formula	C29 H38 Na O4 P Zr	
Formula weight	595.77	
Temperature	100.0 K	
Wavelength	0.71073 Å	
Crystal system	Triclinic	
Space group	P-1	
Unit cell dimensions	a = 10.3925(15) Å	α= 93.428(5)°.

	b = 16.372(2) Å β= 100.442(4)°.
	c = 16.948(3) Å γ = 98.703(4)°.
Volume	2792.0(7) $Å^3$
Z	4
Density (calculated)	1.417 Mg/m^3
Absorption coefficient	0.499 mm^{-1}
F(000)	1240
Crystal size	0.22 x 0.16 x 0.14 mm^3
Theta range for data collection	1.680 to 24.999°.
Index ranges	-12<=h<=12, -19<=k<=19, -20<=l<=20
Reflections collected	43409
Independent reflections	9838 [R(int) = 0.0554]
Completeness to theta = 24.999°	99.9 %
Absorption correction	Semi-empirical from equivalents
Max. and min. transmission	0.0926 and 0.0666
Refinement method	Full-matrix least-squares on F^2
Data / restraints / parameters	9838 / 0 / 649
Goodness-of-fit on F^2	1.098
Final R indices [I>2sigma(I)]	R1 = 0.0596, wR2 = 0.1531
R indices (all data)	R1 = 0.0847, wR2 = 0.1745
Extinction coefficient	n/a
Largest diff. peak and hole	1.544 and -0.637 $e.Å^{-3}$

Table C.3: Atomic coordinates (x 10^4) and equivalent isotropic displacement parameters ($Å^2$ x 10^3) for zirconophosphaalkene coordination polymer (**2.1**).

	x	y	z	U(eq)
Zr(2)	5585(1)	3818(1)	10570(1)	26(1)
Zr(1)	10420(1)	10583(1)	3831(1)	27(1)
P(1)	8781(1)	10048(1)	4761(1)	28(1)
P(2)	3820(1)	4757(1)	10112(1)	31(1)
Na(2)	-279(2)	4625(1)	9030(1)	36(1)
Na(1)	4929(2)	8983(1)	4657(1)	38(1)
O(4)	1214(3)	4626(2)	10156(2)	35(1)
O(1)	6243(3)	10219(2)	4759(2)	36(1)
O(2)	5400(4)	8263(3)	3530(2)	40(1)
O(5)	239(4)	3497(3)	8282(3)	46(1)
O(6)	-1567(4)	4804(3)	7803(2)	49(1)
O(3)	3766(4)	7702(3)	4835(3)	47(1)
O(7)	2097(6)	4753(3)	5246(3)	72(2)
C(39)	1065(6)	2353(4)	11191(3)	39(1)
C(13)	8219(5)	10778(3)	3229(3)	34(1)
C(40)	1108(5)	3100(4)	10847(3)	36(1)
C(11)	7229(5)	10310(3)	4402(3)	30(1)
C(12)	7100(5)	10645(3)	3600(3)	32(1)
C(32)	6688(6)	3424(4)	11930(3)	41(1)
C(26)	5075(5)	3200(3)	9109(3)	33(1)

C(41)	2298(5)	3521(3)	10681(3)	29(1)
C(36)	3484(5)	3197(3)	10850(3)	28(1)
C(30)	4676(6)	2559(3)	9558(3)	37(1)
C(42)	2287(5)	4320(3)	10309(3)	29(1)
C(31)	5772(6)	3928(4)	12100(3)	41(1)
C(7)	11296(6)	11990(4)	3407(4)	43(2)
C(14)	7976(6)	11046(4)	2463(4)	42(1)
C(37)	3393(6)	2437(4)	11202(4)	38(1)
C(9)	10826(5)	11981(3)	4665(3)	35(1)
C(5)	9582(5)	9482(3)	2651(3)	36(1)
C(38)	2221(6)	2020(4)	11357(4)	43(1)
C(18)	6444(5)	8432(4)	3088(3)	38(1)
C(6)	12368(6)	11758(4)	3921(4)	40(1)
C(8)	10353(6)	12140(3)	3884(4)	40(1)
C(29)	5783(6)	2370(4)	10049(4)	41(1)
C(49)	-2600(7)	5799(5)	7076(4)	55(2)
C(35)	6187(6)	4728(4)	11900(3)	38(1)
C(3)	11537(6)	9378(4)	3459(4)	38(1)
C(2)	11783(6)	9968(4)	2927(3)	39(1)
C(33)	7684(5)	3931(4)	11637(3)	40(1)
C(17)	5848(6)	10791(4)	3235(4)	42(1)
C(25)	2511(6)	7515(4)	5073(4)	45(2)
C(4)	10149(6)	9073(3)	3283(3)	36(1)

C(43)	1324(6)	3017(4)	8487(4)	45(2)
C(19)	5821(6)	8727(4)	2293(4)	45(2)
C(10)	12098(5)	11750(4)	4700(4)	38(1)
C(16)	5669(6)	11043(4)	2462(4)	50(2)
C(50)	-2831(6)	5035(4)	7580(4)	45(2)
C(1)	10579(5)	10039(4)	2424(3)	36(1)
C(34)	7380(5)	4732(4)	11618(3)	37(1)
C(24)	2751(7)	7037(5)	5810(5)	62(2)
C(21)	4257(6)	7909(4)	2923(4)	49(2)
C(27)	6465(6)	3412(4)	9322(4)	38(1)
C(22)	4340(6)	6970(4)	4962(5)	54(2)
C(15)	6715(6)	11167(4)	2069(4)	49(2)
C(45)	-786(6)	2156(4)	8408(4)	50(2)
C(28)	6900(6)	2902(4)	9899(4)	46(2)
C(51)	2994(8)	4170(5)	5293(5)	62(2)
C(20)	4328(6)	8438(4)	2232(4)	46(2)
O(8)	-1307(8)	446(5)	10595(4)	118(3)
C(48)	-1225(7)	5752(5)	6899(5)	66(2)
C(46)	-848(6)	2875(4)	7896(4)	51(2)
C(44)	705(6)	2230(4)	8769(4)	46(2)
C(52)	3032(8)	3828(5)	6102(4)	67(2)
C(23)	4039(7)	6729(5)	5757(5)	70(2)
C(47)	-960(7)	4913(5)	7122(4)	54(2)

C(54)	1430(9)	4694(5)	5913(5)	74(2)
C(53)	1678(8)	3909(5)	6268(5)	66(2)
C(57)	-3340(10)	-239(7)	9825(7)	95(3)
C(58)	-2286(13)	-279(7)	10508(6)	115(4)
C(56)	-2676(14)	356(7)	9359(6)	120(5)
C(55)	-1418(12)	729(8)	9844(6)	114(4)

Figure C.2: ORTEP diagram of zirconophosphaalkene dimer (**2.2**) (ellipsoids set at 50% probability; hydrogen atoms omitted for clarity).

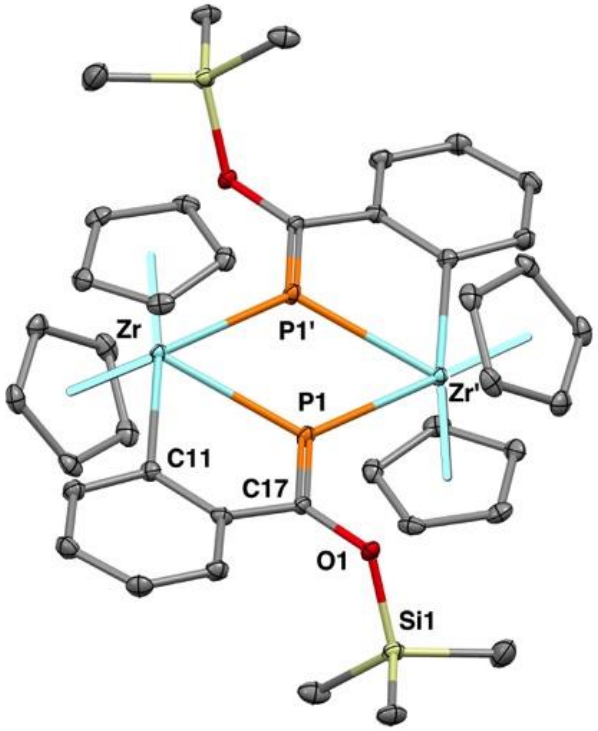

Table C.4: Crystal data and structure refinement for zirconophosphaalkene dimer (**2.2**).

Empirical formula	C40 H46 O2 P2 Si2 Zr2	
Formula weight	859.33	
Temperature	100.0 K	
Wavelength	0.71073 Å	
Crystal system	Monoclinic	
Space group	P 21/n	
Unit cell dimensions	a = 10.6157(18) Å	α= 90°.
	b = 17.277(2) Å	β= 105.752(5)°.
	c = 10.7644(16) Å	γ = 90°.

Volume	1900.1(5) $Å^3$
Z, Z’	2, 0.5
Density (calculated)	1.502 Mg/m^3
Absorption coefficient	0.730 mm^{-1}
F(000)	880
Crystal size	0.32 x 0.29 x 0.26 mm^3
Crystal color, habit	Orange block
Theta range for data collection	2.292 to 28.320°.
Index ranges	-13<=h<=14, -23<=k<=22, -14<=l<=14
Reflections collected	17868
Independent reflections	4720 [R(int) = 0.0683]
Completeness to theta = 26.000°	99.9 %
Absorption correction	Semi-empirical from equivalents
Max. and min. transmission	0.2627 and 0.2064
Refinement method	Full-matrix least-squares on F^2
Data / restraints / parameters	4720 / 0 / 220
Goodness-of-fit on F^2	1.063
Final R indices [I>2sigma(I)]	R1 = 0.0363, wR2 = 0.0946
R indices (all data)	R1 = 0.0402, wR2 = 0.0986
Extinction coefficient	n/a
Largest diff. peak and hole	0.909 and -0.534 $e.Å^{-3}$

Table C.5: Atomic coordinates (x 10^4) and equivalent isotropic displacement parameters ($Å^2$ x 10^3) for zirconophosphaalkene dimer (**2.2**).

	x	y	z	U(eq)
Zr(1)	5315(1)	6194(1)	6110(1)	10(1)
P(1)	6014(1)	5186(1)	4535(1)	13(1)
Si(1)	8537(1)	5153(1)	2425(1)	15(1)
O(1)	8311(1)	5043(1)	3891(1)	14(1)
C(16)	8024(2)	6222(1)	5022(2)	13(1)
C(6)	6674(2)	5378(1)	7959(2)	17(1)
C(11)	7204(2)	6679(1)	5571(2)	14(1)
C(17)	7524(2)	5473(1)	4448(2)	12(1)
C(14)	9729(2)	7199(1)	5469(2)	18(1)
C(10)	7325(2)	6093(1)	8038(2)	17(1)
C(7)	5456(2)	5514(1)	8233(2)	17(1)
C(9)	6513(2)	6669(1)	8322(2)	17(1)
C(18)	7427(2)	5928(1)	1577(2)	23(1)
C(15)	9288(2)	6469(1)	5017(2)	16(1)
C(13)	8911(2)	7682(1)	5926(2)	18(1)
C(12)	7686(2)	7417(1)	5981(2)	17(1)
C(20)	10273(2)	5414(1)	2556(2)	22(1)
C(4)	4424(2)	7541(1)	5671(2)	19(1)
C(5)	4532(2)	7266(1)	4484(2)	19(1)
C(8)	5365(2)	6309(1)	8459(2)	18(1)

C(2)	2967(2)	6552(1)	5056(2)	20(1)
C(1)	3640(2)	6648(1)	4106(2)	19(1)
C(3)	3444(2)	7105(1)	6021(2)	19(1)
C(19)	8210(2)	4196(1)	1618(3)	31(1)

Figure C.3: ORTEP diagram of **2.3** (ellipsoids set at 50% probability; hydrogen atoms omitted for clarity).

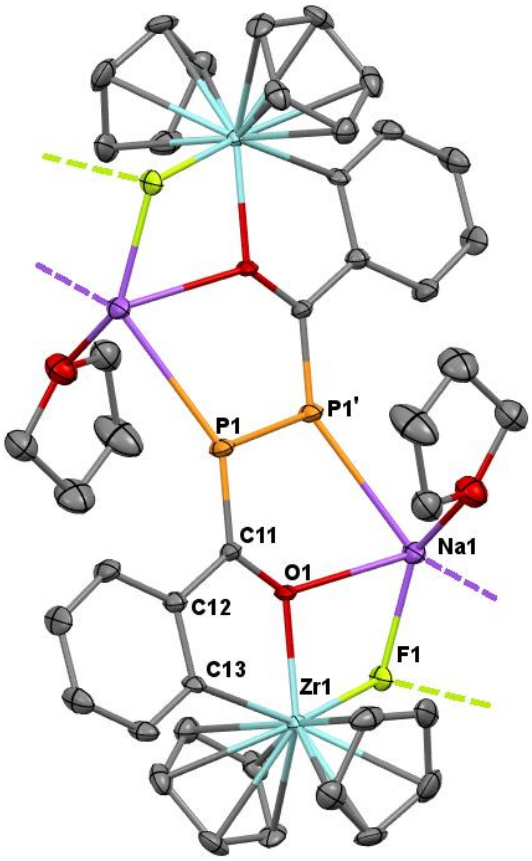

Table C.6: Crystal data and structure refinement for **2.3**.

Empirical formula	C42 H44 F2 Na2 O4 P2 Zr2	
Formula weight	941.13	
Temperature	100.0 K	
Wavelength	0.71073 Å	
Crystal system	Monoclinic	
Space group	P 21/c	
Unit cell dimensions	a = 9.678(2) Å	α= 90°.

	b = 8.310(2) Å β= 90.567(8)°.
	c = 23.859(5) Å γ = 90°.
Volume	1918.9(8) $Å^3$
Z	2
Density (calculated)	1.629 Mg/m^3
Absorption coefficient	0.702 mm^{-1}
F(000)	956
Crystal size	0.12 x 0.1 x 0.08 mm^3
Theta range for data collection	1.707 to 25.000°.
Index ranges	-11<=h<=11, -9<=k<=9, -25<=l<=28
Reflections collected	10400
Independent reflections	3373 [R(int) = 0.0543]
Completeness to theta = 25.000°	99.9 %
Absorption correction	Semi-empirical from equivalents
Max. and min. transmission	0.1496 and 0.1200
Refinement method	Full-matrix least-squares on F^2
Data / restraints / parameters	3373 / 0 / 244
Goodness-of-fit on F^2	1.030
Final R indices [I>2sigma(I)]	R1 = 0.0364, wR2 = 0.0773
R indices (all data)	R1 = 0.0564, wR2 = 0.0839
Extinction coefficient	n/a
Largest diff. peak and hole	0.792 and -0.499 $e.Å^{-3}$

Table C.7: Atomic coordinates (x 10^4) and equivalent isotropic displacement parameters ($Å^2$x 10^3) for **2.3**.

	x	y	z	U(eq)
Zr(1)	8797(1)	3345(1)	6247(1)	13(1)
P(1)	4458(1)	4397(1)	5331(1)	20(1)
Na(1)	8360(1)	4462(2)	4809(1)	20(1)
F(1)	9700(2)	4564(3)	5560(1)	21(1)
O(1)	7137(2)	4083(3)	5678(1)	15(1)
O(2)	7449(3)	2259(4)	4284(1)	30(1)
C(13)	6676(4)	2563(4)	6623(1)	14(1)
C(12)	5519(4)	3123(4)	6328(1)	17(1)
C(4)	10467(4)	1056(5)	6447(2)	27(1)
C(7)	10549(4)	4779(5)	6854(2)	24(1)
C(16)	3965(4)	2232(5)	7049(2)	28(1)
C(10)	8362(4)	4763(5)	7178(2)	24(1)
C(17)	4175(4)	2992(5)	6542(2)	23(1)
C(8)	9826(4)	6016(5)	6588(2)	22(1)
C(14)	6395(4)	1757(5)	7128(1)	21(1)
C(15)	5076(4)	1571(5)	7334(2)	26(1)
C(11)	5809(4)	3900(4)	5779(1)	15(1)
C(9)	8468(4)	5991(5)	6779(2)	23(1)
C(2)	9508(5)	1131(5)	5582(2)	30(1)
C(18)	6669(5)	1140(5)	4612(2)	31(1)

C(5)	9156(4)	397(5)	6480(2)	26(1)
C(6)	9632(4)	3997(5)	7220(1)	25(1)
C(3)	10691(4)	1541(5)	5893(2)	31(1)
C(21)	6887(5)	2198(6)	3722(2)	34(1)
C(1)	8562(4)	421(5)	5937(2)	28(1)
C(20)	5374(5)	1801(6)	3778(2)	42(1)
C(19)	5300(6)	867(7)	4313(2)	54(2)

Figure C.4: ORTEP diagram of 2-*tert*-butyl-1,3-benzazaphosphole-IPr adduct (**3.3**) (ellipsoids set at 50% probability; non-hydrogen bonded hydrogen atoms omitted for clarity).

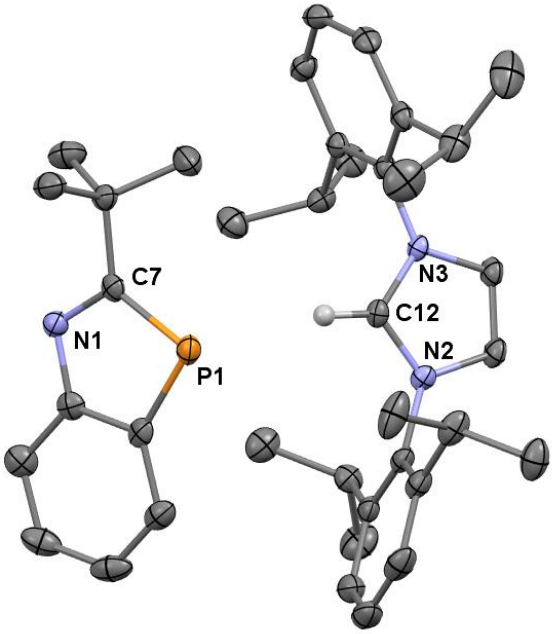

Table C.8: Crystal data and structure refinement for 2-*tert*-butyl-1,3-benzazaphosphole-IPr adduct (**3.3**).

Empirical formula	C38 H50 N3 P	
Formula weight	579.78	
Temperature	100.0 K	
Wavelength	0.71073 Å	
Crystal system	Monoclinic	
Space group	P 21/n	
Unit cell dimensions	a = 9.5977(7) Å	α= 90°.
	b = 31.843(2) Å	β= 98.272(4)°.

	c = 12.3174(10) Å γ = 90°.
Volume	3725.3(5) $Å^3$
Z	4
Density (calculated)	1.034 Mg/m^3
Absorption coefficient	0.101 mm^{-1}
F(000)	1256
Crystal size	0.3 x 0.29 x 0.27 mm^3
Theta range for data collection	1.789 to 25.377°.
Index ranges	-7<=h<=11, -38<=k<=37, -14<=l<=14
Reflections collected	24027
Independent reflections	6784 [R(int) = 0.0657]
Completeness to theta = 25.242°	99.8 %
Absorption correction	Semi-empirical from equivalents
Max. and min. transmission	0.7452 and 0.6760
Refinement method	Full-matrix least-squares on F^2
Data / restraints / parameters	6784 / 0 / 394
Goodness-of-fit on F^2	1.016
Final R indices [I>2sigma(I)]	R1 = 0.0474, wR2 = 0.0964
R indices (all data)	R1 = 0.0854, wR2 = 0.1096
Extinction coefficient	n/a
Largest diff. peak and hole	0.199 and -0.268 $e.Å^{-3}$
SQUEEZE	99e/uc total on two -1 sites

Table C.9: Atomic coordinates (x 10^4) and equivalent isotropic displacement parameters ($Å^2$ x 10^3) for 2-*tert*-butyl-1,3-benzazaphosphole-IPr adduct (**3.3**).

	x	y	z	U(eq)
P(1)	10223(1)	6187(1)	7129(1)	23(1)
N(3)	5065(2)	6370(1)	7523(1)	16(1)
N(2)	4326(2)	5987(1)	6111(1)	17(1)
N(1)	8801(2)	6902(1)	6736(1)	20(1)
C(12)	3920(2)	6208(1)	6928(2)	17(1)
C(27)	5029(2)	6658(1)	8435(2)	16(1)
C(32)	4807(2)	7082(1)	8189(2)	18(1)
C(7)	9656(2)	6690(1)	7500(2)	19(1)
C(15)	3393(2)	5741(1)	5320(2)	20(1)
C(1)	8577(2)	6668(1)	5781(2)	20(1)
C(16)	3053(2)	5336(1)	5628(2)	23(1)
C(8)	9971(2)	6877(1)	8649(2)	21(1)
C(28)	5220(2)	6495(1)	9504(2)	21(1)
C(20)	2906(2)	5920(1)	4303(2)	21(1)
C(36)	4639(2)	7255(1)	7032(2)	21(1)
C(38)	5758(2)	7588(1)	6926(2)	29(1)
C(21)	3564(2)	5151(1)	6749(2)	27(1)
C(13)	6239(2)	6251(1)	7065(2)	21(1)
C(6)	9263(2)	6274(1)	5809(2)	20(1)
C(14)	5775(2)	6012(1)	6186(2)	21(1)

C(29)	5137(2)	6782(1)	10348(2)	24(1)
C(30)	4876(2)	7202(1)	10135(2)	25(1)
C(31)	4729(2)	7352(1)	9074(2)	22(1)
C(19)	2040(2)	5671(1)	3558(2)	28(1)
C(24)	3256(2)	6370(1)	4040(2)	23(1)
C(22)	4450(2)	4755(1)	6664(2)	34(1)
C(11)	8773(2)	6758(1)	9287(2)	30(1)
C(2)	7711(2)	6802(1)	4823(2)	28(1)
C(9)	10053(2)	7356(1)	8589(2)	34(1)
C(4)	8256(2)	6164(1)	3916(2)	32(1)
C(17)	2185(2)	5102(1)	4841(2)	30(1)
C(25)	2137(2)	6668(1)	4371(2)	30(1)
C(37)	3152(2)	7426(1)	6690(2)	30(1)
C(3)	7555(2)	6550(1)	3907(2)	32(1)
C(18)	1690(2)	5267(1)	3828(2)	32(1)
C(5)	9090(2)	6027(1)	4850(2)	26(1)
C(26)	3421(3)	6437(1)	2836(2)	38(1)
C(23)	2324(3)	5064(1)	7369(2)	40(1)
C(10)	11356(2)	6702(1)	9249(2)	35(1)
C(33)	5485(2)	6033(1)	9727(2)	30(1)
C(34)	6513(3)	5957(1)	10783(2)	45(1)
C(35)	4101(3)	5799(1)	9767(2)	43(1)

Figure C.5: ORTEP diagram of 2-*tert*-butyl-1,3-benzazaphosphole-^{Et}CAAC adduct (**3.4**) (ellipsoids set at 50% probability; non-hydrogen bonded hydrogen atoms omitted for clarity).

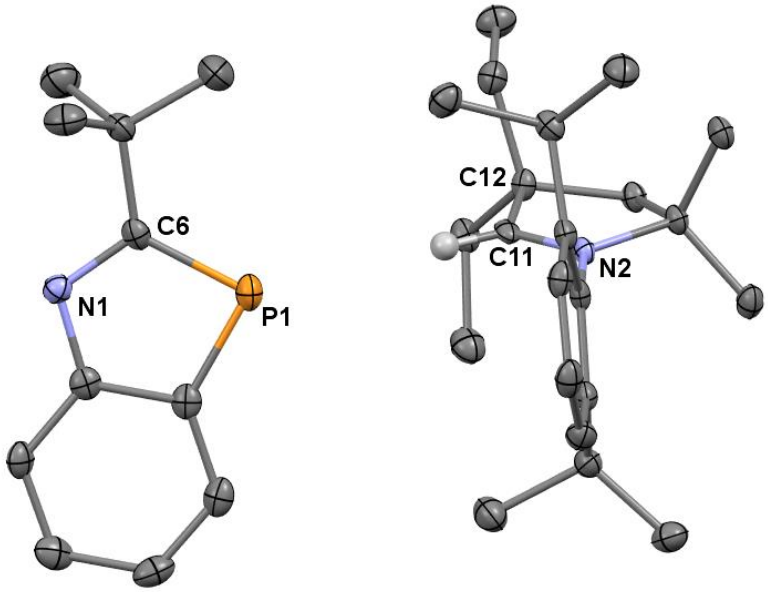

Table C.10: Crystal data and structure refinement for 2-*tert*-butyl-1,3-benzazaphosphole-^{Et}CAAC adduct (**3.4**).

Empirical formula	C33 H49 N2 P	
Formula weight	504.71	
Temperature	100.0 K	
Wavelength	0.71073 Å	
Crystal system	Monoclinic	
Space group	P 21/c	
Unit cell dimensions	a = 12.2320(12) Å	α= 90°.
	b = 12.7535(13) Å	β= 107.004(5)°.
	c = 20.343(2) Å	γ = 90°.

Volume	3034.8(6) $Å^3$
Z	4
Density (calculated)	1.105 Mg/m^3
Absorption coefficient	0.113 mm^{-1}
F(000)	1104
Crystal size	0.32 x 0.3 x 0.28 mm^3
Theta range for data collection	1.741 to 24.999°.
Index ranges	-14<=h<=14, -14<=k<=15, -17<=l<=24
Reflections collected	15339
Independent reflections	5338 [R(int) = 0.0535]
Completeness to theta = 24.999°	99.9 %
Absorption correction	Semi-empirical from equivalents
Max. and min. transmission	0.7452 and 0.7026
Refinement method	Full-matrix least-squares on F^2
Data / restraints / parameters	5338 / 0 / 336
Goodness-of-fit on F^2	1.012
Final R indices [I>2sigma(I)]	R1 = 0.0477, wR2 = 0.0930
R indices (all data)	R1 = 0.0932, wR2 = 0.1101
Extinction coefficient	n/a
Largest diff. peak and hole	0.233 and -0.245 $e.Å^{-3}$

Table C.11: Atomic coordinates (x 10^4) and equivalent isotropic displacement parameters ($Å^2$ x 10^3) for 2-*tert*-butyl-1,3-benzazaphosphole-^{Et}CAAC adduct (**3.4**).

	x	y	z	U(eq)
P(1)	3376(1)	8820(1)	7083(1)	20(1)
N(2)	2697(2)	4321(1)	7783(1)	12(1)
N(1)	1205(2)	8229(1)	6814(1)	17(1)
C(12)	4004(2)	5617(2)	8314(1)	14(1)
C(33)	1598(2)	8423(2)	7509(1)	17(1)
C(21)	2308(2)	3289(2)	7486(1)	13(1)
C(13)	2803(2)	6118(2)	8086(1)	15(1)
C(1)	2754(2)	8759(2)	7767(1)	17(1)
C(14)	1918(2)	5232(2)	7879(1)	15(1)
C(11)	3757(2)	4550(2)	8014(1)	14(1)
C(22)	2257(2)	2460(2)	7934(1)	14(1)
C(5)	946(2)	8252(2)	7963(1)	20(1)
C(20)	990(2)	5468(2)	7212(1)	20(1)
C(27)	2617(2)	2539(2)	8711(1)	17(1)
C(17)	4881(2)	6191(2)	8028(1)	18(1)
C(25)	1707(2)	2173(2)	6508(1)	20(1)
C(26)	2060(2)	3168(2)	6773(1)	15(1)
C(23)	1911(2)	1487(2)	7631(1)	18(1)
C(30)	2266(2)	4014(2)	6295(1)	18(1)
C(19)	1366(2)	4938(2)	8433(1)	19(1)

C(2)	3206(2)	8943(2)	8476(1)	21(1)
C(6)	2052(2)	8403(2)	6530(1)	16(1)
C(7)	1802(2)	8196(2)	5762(1)	20(1)
C(28)	1662(2)	2168(2)	9009(1)	26(1)
C(24)	1625(2)	1346(2)	6928(1)	21(1)
C(29)	3717(2)	1910(2)	9026(1)	23(1)
C(4)	1413(2)	8430(2)	8657(1)	24(1)
C(32)	1229(2)	4205(2)	5675(1)	24(1)
C(15)	4476(2)	5481(2)	9102(1)	19(1)
C(3)	2547(2)	8785(2)	8912(1)	24(1)
C(18)	4672(2)	6080(2)	7258(1)	25(1)
C(9)	1537(2)	7022(2)	5631(1)	29(1)
C(16)	4879(2)	6507(2)	9484(1)	25(1)
C(8)	761(2)	8830(2)	5362(1)	32(1)
C(31)	3315(2)	3728(2)	6063(1)	26(1)
C(10)	2813(2)	8487(2)	5503(1)	34(1)

Figure C.6: ORTEP diagram of 2-phenylbenzimidazole-^{Et}CAAC adduct (**4.3**) (ellipsoids set at 50% probability; hydrogen atoms omitted for clarity).

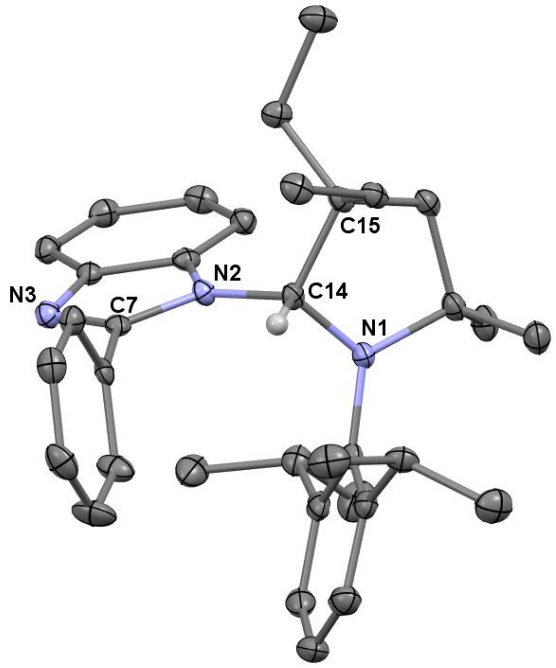

Table C.12: Crystal data and structure refinement for 2-phenylbenzimidazole-^{Et}CAAC adduct (**4.3**).

Empirical formula	C35 H45 N3	
Formula weight	507.74	
Temperature	100.0 K	
Wavelength	0.71073 Å	
Crystal system	Triclinic	
Space group	P-1	
Unit cell dimensions	a = 10.8286(8) Å	α= 81.132(2)°.
	b = 11.9086(9) Å	β= 76.324(2)°.
	c = 12.5098(9) Å	γ = 66.007(2)°.

Volume	1428.95(18) $Å^3$
Z	2
Density (calculated)	1.180 Mg/m^3
Absorption coefficient	0.068 mm^{-1}
F(000)	552
Crystal size	0.37 x 0.35 x 0.33 mm^3
Theta range for data collection	1.876 to 24.998°.
Index ranges	-12<=h<=12, -14<=k<=14, -14<=l<=11
Reflections collected	20424
Independent reflections	5019 [R(int) = 0.0434]
Completeness to theta = 24.998°	100.0 %
Absorption correction	Semi-empirical from equivalents
Max. and min. transmission	0.7454 and 0.7027
Refinement method	Full-matrix least-squares on F^2
Data / restraints / parameters	5019 / 0 / 351
Goodness-of-fit on F^2	1.030
Final R indices [I>2sigma(I)]	R1 = 0.0406, wR2 = 0.0898
R indices (all data)	R1 = 0.0591, wR2 = 0.1007
Extinction coefficient	n/a
Largest diff. peak and hole	0.199 and -0.234 $e.Å^{-3}$

Table C.13: Atomic coordinates (x 10^4) and equivalent isotropic displacement parameters ($Å^2$ x 10^3) for 2-phenylbenzimidazole-^{Et}CAAC adduct (**4.3**).

	x	y	z	U(eq)
N(2)	4537(1)	6663(1)	6611(1)	12(1)
N(1)	2834(1)	8510(1)	7513(1)	14(1)
N(3)	6028(1)	4673(1)	6714(1)	15(1)
C(7)	4731(2)	5435(1)	6809(1)	13(1)
C(1)	5860(2)	6674(1)	6384(1)	13(1)
C(8)	3586(2)	4990(1)	7142(1)	14(1)
C(9)	3153(2)	4594(1)	6363(1)	17(1)
C(5)	8184(2)	5106(2)	6290(1)	17(1)
C(15)	2927(2)	8530(1)	5572(1)	14(1)
C(6)	6763(2)	5433(1)	6450(1)	14(1)
C(28)	1173(2)	7994(1)	9053(1)	16(1)
C(20)	2972(2)	9727(1)	5854(1)	16(1)
C(16)	4007(2)	7967(2)	4550(1)	16(1)
C(2)	6360(2)	7614(1)	6160(1)	16(1)
C(14)	3150(1)	7698(1)	6660(1)	13(1)
C(30)	4897(2)	7662(2)	8964(1)	19(1)
C(29)	2470(2)	8084(1)	8644(1)	15(1)
C(22)	2547(2)	9820(1)	7112(1)	16(1)
C(24)	3459(2)	7663(1)	9333(1)	17(1)
C(3)	7769(2)	7272(2)	6022(1)	18(1)

C(33)	18(2)	8430(2)	8404(1)	19(1)
C(4)	8674(2)	6035(2)	6083(1)	18(1)
C(18)	1478(2)	8792(1)	5365(1)	16(1)
C(26)	1879(2)	7067(2)	10788(1)	23(1)
C(27)	914(2)	7476(2)	10119(1)	21(1)
C(19)	1268(2)	7706(2)	5041(1)	20(1)
C(10)	2177(2)	4073(1)	6690(1)	20(1)
C(13)	3023(2)	4869(2)	8252(1)	22(1)
C(23)	1042(2)	10697(1)	7457(1)	21(1)
C(25)	3128(2)	7172(2)	10400(1)	21(1)
C(17)	3715(2)	8694(2)	3455(1)	23(1)
C(21)	3407(2)	10340(2)	7545(1)	21(1)
C(31)	5985(2)	6343(2)	8992(1)	25(1)
C(35)	-1290(2)	9422(2)	8990(1)	26(1)
C(11)	1637(2)	3940(2)	7794(1)	24(1)
C(12)	2052(2)	4342(2)	8576(1)	28(1)
C(34)	-323(2)	7373(2)	8173(1)	26(1)
C(32)	5173(2)	8450(2)	9667(2)	30(1)

Figure C.7: ORTEP diagram of 2-phenylbenzimidazole-IPr adduct (**4.4**) (ellipsoids set at 50% probability; non-hydrogen bonded hydrogen atoms and remaining 5 independent units within supercell omitted for clarity).

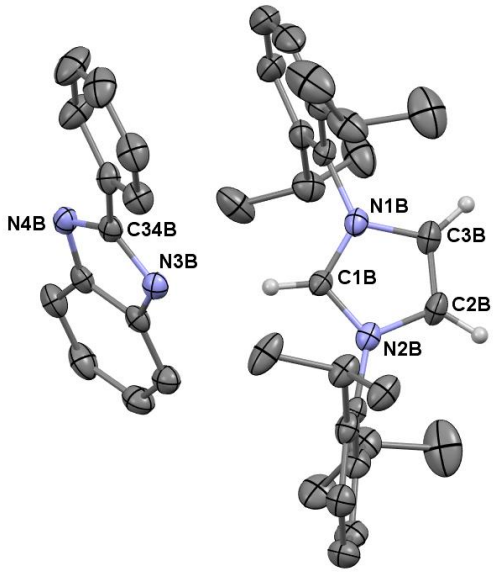

Figure C.8: Extended Structure of 2-phenylbenzimidazole-IPr adduct (**4.4**) showing intermolecular chain propagating perpendicular to 011 plane.

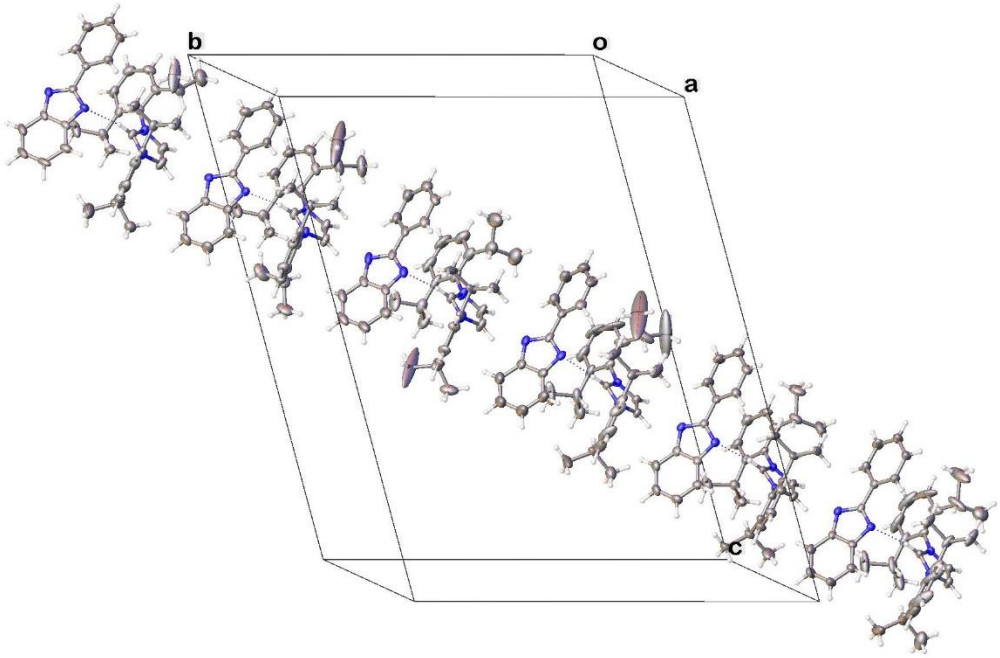

Figure C.9: Numbering diagram for individual units (Z = A-F) of 2-phenylbenzimidazole-IPr adduct (**4.4**).

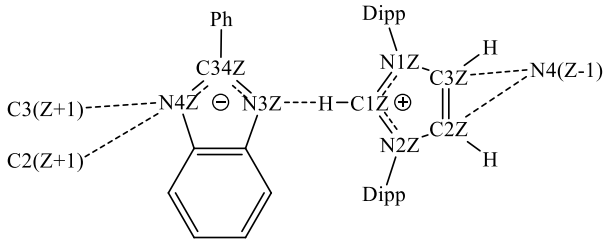

Table C.14: Selected distances (Å) and angles (deg) for each of the independent units of 2-phenylbenzimidazole-IPr adduct (**4.4**) within the supercell. Averages and standard deviations for critical distance and angle measurements provided.

Z	C34-N3	C34-N4	C1-N1	C1-N2	C1-N3	C3(Z)-N4(Z-1)	C2(Z)-N4(Z-1)	N1-C1-N2
A	1.353(5)	1.349(5)	1.340(4)	1.327(5)	3.100(5)	3.154(6)	3.496(5)	107.8(3)
B	1.352(5)	1.348(5)	1.340(4)	1.339(5)	3.087(6)	3.137(6)	3.487(6)	107.9(3)
C	1.356(5)	1.349(6)	1.337(4)	1.334(5)	3.090(6)	3.095(6)	3.404(5)	107.4(3)
D	1.338(6)	1.345(6)	1.344(5)	1.333(5)	3.080(6)	3.116(7)	3.442(6)	107.9(3)
E	1.348(5)	1.350(5)	1.337(5)	1.318(5)	3.054(6)	3.127(7)	3.351(6)	107.7(3)
F	1.350(5)	1.361(5)	1.330(5)	1.342(5)	3.084(6)	3.127(6)	3.397(6)	108.0(3)
Ave	1.350	1.350	1.338	1.332	3.083	3.126	3.430	107.8
SD	0.006	0.006	0.005	0.009	0.016	0.020	0.056	0.2

Table C.15: Crystal data and structure refinement for PhBIM-IPr adduct (**4.4**).

Empirical formula	C40 H46 N4
Formula weight	582.81
Temperature	100.0 K
Wavelength	1.54178 Å

Crystal system	Triclinic	
Space group	P-1	
Unit cell dimensions	a = 16.6802(7) Å	α= 106.262(2)°.
	b = 22.0707(9) Å	β= 94.104(2)°.
	c = 29.4908(11) Å	γ = 100.781(2)°.
Volume	10149.7(7) $Å^3$	
Z, Z’	12, 6	
Density (calculated)	1.144 Mg/m^3	
Absorption coefficient	0.511 mm^{-1}	
F(000)	3768	
Crystal size	0.3 x 0.23 x 0.2 mm^3	
Theta range for data collection	1.574 to 68.474°.	
Index ranges	-20<=h<=20, -26<=k<=26, -35<=l<=35	
Reflections collected	157114	
Independent reflections	36662 [R(int) = 0.0653]	
Completeness to theta = 67.679°	98.8 %	
Absorption correction	Semi-empirical from equivalents	
Max. and min. transmission	0.7531 and 0.6828	
Refinement method	Full-matrix least-squares on F^2	
Data / restraints / parameters	36662 / 0 / 2424	
Goodness-of-fit on F^2	1.051	
Final R indices [I>2sigma(I)]	R1 = 0.0984, wR2 = 0.2505	

R indices (all data)	R1 = 0.1651, wR2 = 0.3106
Extinction coefficient	n/a
Largest diff. peak and hole	1.708 and -0.956 e.Å^{-3}

Table C.16: Atomic coordinates (x 10^4) and equivalent isotropic displacement parameters (Å^2 x 10^3) for 2-phenylbenzimidazole-IPr adduct (**4.4**).

	x	y	z	U(eq)
N(1A)	2123(2)	-4637(1)	9654(1)	21(1)
N(2A)	3375(2)	-4228(2)	9985(1)	29(1)
C(1A)	2807(2)	-4207(2)	9655(1)	22(1)
C(2A)	3042(2)	-4686(2)	10202(1)	31(1)
C(3A)	2256(2)	-4936(2)	9994(1)	26(1)
C(4A)	1352(2)	-4736(2)	9357(1)	25(1)
C(5A)	823(2)	-4332(2)	9534(2)	40(1)
C(6A)	83(3)	-4407(3)	9268(3)	74(2)
C(7A)	-137(4)	-4852(5)	8848(3)	98(3)
C(8A)	399(5)	-5261(4)	8665(2)	88(3)
C(9A)	1168(3)	-5222(2)	8923(2)	47(1)
C(10A)	1024(3)	-3824(2)	10019(2)	54(1)
C(11A)	1016(4)	-3143(3)	9987(3)	95(3)
C(12A)	417(5)	-4002(3)	10357(3)	92(3)
C(13A)	1735(4)	-5679(3)	8757(2)	78(2)
C(14A)	1522(7)	-5982(4)	8199(2)	142(5)

C(15A)	1612(5)	-6212(3)	8956(2)	82(2)
C(16A)	4248(3)	-3905(2)	10076(2)	42(1)
C(17A)	4526(3)	-3413(2)	10492(2)	49(1)
C(18A)	5397(4)	-3160(3)	10591(2)	73(2)
C(19A)	5908(4)	-3392(4)	10275(3)	86(3)
C(20A)	5601(3)	-3873(4)	9857(2)	72(2)
C(21A)	4758(3)	-4153(3)	9742(2)	47(1)
C(22A)	3975(4)	-3153(2)	10849(2)	63(2)
C(23A)	4197(6)	-2414(3)	11055(2)	98(3)
C(24A)	3964(4)	-3433(3)	11275(3)	76(2)
C(25A)	4358(3)	-4350(3)	8882(2)	49(1)
C(26A)	4434(3)	-4667(3)	9280(2)	44(1)
C(27A)	4959(3)	-5173(3)	9154(2)	62(2)
N(3C)	2754(2)	3319(2)	5731(1)	30(1)
N(4C)	1890(2)	3924(2)	5511(1)	32(1)
C(28C)	2895(3)	3914(2)	6069(1)	33(1)
C(29C)	3423(3)	4165(2)	6494(2)	49(1)
C(30C)	3437(5)	4779(3)	6769(2)	73(2)
C(31C)	2934(5)	5150(3)	6631(2)	74(2)
C(32C)	2389(4)	4911(2)	6212(2)	53(1)
C(33C)	2366(3)	4280(2)	5933(1)	35(1)
C(34C)	2150(2)	3363(2)	5416(1)	28(1)
C(35C)	1803(3)	2825(2)	4976(1)	32(1)

C(36C)	2278(3)	2391(2)	4762(2)	41(1)
C(37C)	1952(4)	1917(3)	4332(2)	59(2)
C(38C)	1153(4)	1860(3)	4128(2)	64(2)
C(39C)	683(4)	2274(3)	4344(2)	64(2)
C(40C)	1010(3)	2759(2)	4765(2)	46(1)
N(3A)	2813(2)	-3188(2)	9114(1)	23(1)
N(4A)	1850(2)	-2668(2)	8888(1)	27(1)
C(28A)	2890(2)	-2605(2)	9454(1)	24(1)
C(29A)	3419(3)	-2322(2)	9884(1)	33(1)
C(30A)	3348(3)	-1726(2)	10168(2)	45(1)
C(31A)	2753(3)	-1412(2)	10030(2)	48(1)
C(32A)	2231(3)	-1681(2)	9610(1)	36(1)
C(33A)	2298(2)	-2285(2)	9317(1)	26(1)
C(34A)	2191(2)	-3191(2)	8792(1)	22(1)
C(35A)	1908(2)	-3730(2)	8349(1)	26(1)
C(36A)	2387(3)	-4184(2)	8193(1)	32(1)
C(37A)	2151(3)	-4662(2)	7758(2)	42(1)
C(38A)	1431(4)	-4705(2)	7483(2)	51(1)
C(39A)	940(3)	-4280(2)	7637(2)	49(1)
C(40A)	1179(3)	-3787(2)	8068(2)	36(1)
N(1B)	2042(2)	-1318(1)	8000(1)	25(1)
N(2B)	3326(2)	-984(1)	8302(1)	24(1)
C(1B)	2746(2)	-915(2)	7993(1)	23(1)

C(2B)	2974(3)	-1448(2)	8506(1)	31(1)
C(3B)	2175(3)	-1656(2)	8321(1)	31(1)
C(4B)	1253(2)	-1363(2)	7742(1)	26(1)
C(5B)	756(2)	-947(2)	7956(1)	30(1)
C(6B)	-2(3)	-998(2)	7707(2)	37(1)
C(7B)	-257(3)	-1444(2)	7270(2)	42(1)
C(8B)	242(3)	-1858(2)	7065(2)	45(1)
C(9B)	1013(3)	-1833(2)	7297(1)	34(1)
C(10B)	1025(3)	-454(2)	8442(2)	35(1)
C(11B)	1076(3)	233(2)	8418(2)	46(1)
C(12B)	443(4)	-602(2)	8798(2)	56(1)
C(13B)	1560(3)	-2294(2)	7080(2)	46(1)
C(14B)	1365(4)	-2557(3)	6532(2)	67(2)
C(15B)	1453(4)	-2859(2)	7278(2)	64(2)
C(16B)	4197(2)	-681(2)	8387(1)	24(1)
C(17B)	4509(3)	-189(2)	8817(1)	29(1)
C(18B)	5356(3)	35(2)	8906(1)	35(1)
C(19B)	5872(3)	-202(2)	8586(1)	35(1)
C(20B)	5544(3)	-675(2)	8158(1)	32(1)
C(21B)	4703(2)	-931(2)	8052(1)	27(1)
C(22B)	3947(3)	81(2)	9172(1)	37(1)
C(23B)	4239(3)	809(2)	9401(2)	43(1)
C(24B)	3898(4)	-265(3)	9559(2)	66(2)

C(25B)	4238(3)	-1126(2)	7197(1)	44(1)
C(26B)	4349(3)	-1449(2)	7586(1)	31(1)
C(27B)	4889(3)	-1945(2)	7441(1)	38(1)
N(3E)	2910(2)	10058(2)	2471(1)	30(1)
N(4E)	2080(2)	10699(2)	2266(1)	28(1)
C(28E)	3091(3)	10653(2)	2815(1)	32(1)
C(29E)	3665(3)	10889(2)	3225(2)	42(1)
C(30E)	3700(3)	11513(2)	3511(2)	48(1)
C(31E)	3194(3)	11899(2)	3396(2)	45(1)
C(32E)	2628(3)	11675(2)	2989(2)	39(1)
C(33E)	2576(2)	11043(2)	2690(1)	28(1)
C(34E)	2315(2)	10128(2)	2167(1)	25(1)
C(35E)	1941(2)	9592(2)	1734(1)	28(1)
C(36E)	2329(3)	9085(2)	1552(2)	40(1)
C(37E)	1984(3)	8604(2)	1135(2)	48(1)
C(38E)	1247(3)	8611(2)	903(1)	42(1)
C(39E)	853(3)	9103(2)	1073(2)	46(1)
C(40E)	1206(3)	9597(2)	1488(2)	39(1)
N(1C)	1978(2)	1955(1)	6331(1)	23(1)
N(2C)	3240(2)	2318(1)	6654(1)	22(1)
C(1C)	2111(2)	1626(2)	6655(1)	25(1)
C(2C)	2900(2)	1849(2)	6856(1)	24(1)
C(3C)	2671(2)	2377(2)	6337(1)	21(1)

C(4C)	1205(2)	1878(2)	6044(1)	30(1)
C(5C)	994(3)	1372(3)	5614(2)	49(1)
C(6C)	248(4)	1313(4)	5353(2)	78(2)
C(06F)	309(4)	2739(3)	7021(2)	63(2)
C(06W)	1055(4)	3502(3)	6621(3)	88(3)
C(7C)	-259(4)	1718(4)	5501(2)	80(2)
C(8C)	-43(3)	2201(3)	5922(2)	58(2)
C(9C)	706(3)	2295(2)	6213(2)	38(1)
C(10C)	1559(4)	903(3)	5452(2)	77(2)
C(11C)	1286(6)	304(5)	5424(7)	288(12)
C(13C)	4091(2)	2662(2)	6768(1)	26(1)
C(14C)	4326(3)	3137(2)	7210(2)	34(1)
C(15C)	5168(3)	3422(2)	7323(2)	53(1)
C(16C)	5719(3)	3255(3)	7015(2)	70(2)
C(17C)	5465(3)	2806(3)	6578(2)	59(2)
C(18C)	4632(2)	2477(2)	6443(2)	34(1)
C(19C)	3725(3)	3339(2)	7553(2)	45(1)
C(20C)	3849(7)	4076(3)	7740(2)	113(4)
C(21C)	3791(3)	3072(2)	7975(2)	51(1)
C(22C)	4361(3)	1974(3)	5968(2)	43(1)
C(23C)	4926(4)	1491(3)	5854(2)	62(2)
C(24C)	4294(4)	2293(3)	5569(2)	64(2)
C(048)	942(3)	2827(2)	6687(2)	49(1)

C(12C)	1707(18)	919(9)	5016(7)	560(30)
N(3B)	2777(2)	92(2)	7446(1)	24(1)
N(4B)	1839(2)	639(2)	7225(1)	26(1)
C(28B)	2842(2)	666(2)	7804(1)	24(1)
C(29B)	3339(2)	919(2)	8243(1)	30(1)
C(30B)	3258(3)	1510(2)	8538(1)	36(1)
C(31B)	2701(3)	1845(2)	8400(2)	39(1)
C(32B)	2205(3)	1600(2)	7963(2)	35(1)
C(33B)	2271(2)	1000(2)	7666(1)	26(1)
C(34B)	2177(2)	115(2)	7122(1)	23(1)
C(35B)	1914(2)	-397(2)	6664(1)	27(1)
C(36B)	2418(3)	-828(2)	6493(1)	32(1)
C(37B)	2196(3)	-1287(2)	6051(2)	40(1)
C(38B)	1484(3)	-1333(2)	5778(2)	47(1)
C(39B)	961(3)	-923(3)	5949(2)	52(1)
C(40B)	1182(3)	-455(2)	6390(2)	41(1)
N(1D)	2021(2)	5189(2)	4568(1)	34(1)
N(2D)	3266(2)	5610(2)	4921(1)	28(1)
C(1D)	2699(2)	5640(2)	4590(1)	28(1)
C(2D)	2945(3)	5132(2)	5116(2)	39(1)
C(3D)	2168(3)	4871(2)	4900(2)	42(1)
C(4D)	1247(2)	5096(2)	4281(2)	37(1)
C(5D)	730(3)	5527(2)	4442(2)	45(1)

C(6D)	-16(3)	5414(3)	4153(2)	59(2)
C(7D)	-227(3)	4898(4)	3737(2)	70(2)
C(8D)	286(3)	4482(3)	3593(2)	60(2)
C(9D)	1048(3)	4578(3)	3868(2)	47(1)
C(10D)	946(3)	6073(2)	4900(2)	48(1)
C(11D)	1016(4)	6721(3)	4799(3)	80(2)
C(12D)	324(3)	5994(3)	5247(2)	58(1)
C(13D)	1609(3)	4103(3)	3702(2)	54(1)
C(14D)	1519(6)	3805(3)	3147(2)	95(3)
C(15D)	1418(5)	3529(3)	3882(3)	82(2)
C(16D)	4086(2)	6021(2)	5072(1)	24(1)
C(17D)	4241(3)	6471(2)	5527(1)	31(1)
C(18D)	5046(3)	6824(2)	5675(1)	36(1)
C(19D)	5650(3)	6738(2)	5382(1)	38(1)
C(20D)	5466(2)	6297(2)	4931(1)	34(1)
C(21D)	4678(2)	5921(2)	4767(1)	25(1)
C(22D)	3576(3)	6592(3)	5851(2)	50(1)
C(23D)	3435(10)	7255(7)	5915(5)	317(12)
C(24D)	3787(3)	6514(3)	6325(2)	64(2)
C(25D)	4514(3)	5799(3)	3896(2)	52(1)
C(26D)	4496(3)	5440(2)	4270(1)	34(1)
C(27D)	5094(3)	4979(2)	4195(2)	40(1)
N(3D)	2883(2)	6677(2)	4068(1)	33(1)

N(4D)	2007(2)	7279(2)	3872(1)	40(1)
C(28D)	3064(3)	7284(2)	4402(1)	34(1)
C(29D)	3644(3)	7538(2)	4803(2)	46(1)
C(30D)	3679(4)	8168(2)	5082(2)	55(1)
C(31D)	3150(4)	8531(2)	4967(2)	58(2)
C(32D)	2572(3)	8285(2)	4568(2)	48(1)
C(33D)	2527(3)	7647(2)	4281(2)	37(1)
C(34D)	2263(3)	6719(2)	3772(1)	31(1)
C(35D)	1879(3)	6174(2)	3342(1)	33(1)
C(36D)	2318(3)	5713(2)	3122(2)	37(1)
C(37D)	1969(3)	5237(2)	2704(2)	41(1)
C(38D)	1181(3)	5196(2)	2507(2)	48(1)
C(39D)	737(4)	5635(2)	2731(2)	53(1)
C(40D)	1088(3)	6125(2)	3146(2)	45(1)
N(1E)	2057(2)	8496(2)	2886(1)	31(1)
N(2E)	3278(2)	8927(2)	3251(1)	30(1)
C(1E)	2720(2)	8964(2)	2926(1)	29(1)
C(2E)	2961(2)	8421(2)	3429(2)	35(1)
C(3E)	2198(2)	8162(2)	3205(2)	35(1)
C(4E)	1320(2)	8367(2)	2564(1)	29(1)
C(5E)	785(2)	8794(2)	2672(1)	28(1)
C(6E)	74(3)	8652(2)	2351(2)	41(1)
C(7E)	-84(3)	8114(3)	1953(2)	48(1)

C(8E)	447(3)	7701(2)	1864(2)	45(1)
C(9E)	1160(3)	7818(2)	2165(2)	38(1)
C(10E)	929(3)	9370(2)	3117(2)	39(1)
C(11E)	811(4)	9980(2)	3014(2)	65(2)
C(12E)	371(4)	9233(2)	3484(2)	51(1)
C(13E)	1750(3)	7357(2)	2057(2)	62(2)
C(14E)	2007(12)	7276(8)	1593(6)	380(17)
C(15E)	1427(4)	6722(3)	2092(3)	85(2)
C(16E)	4081(2)	9361(2)	3418(1)	28(1)
C(17E)	4206(3)	9786(2)	3878(2)	34(1)
C(18E)	4984(3)	10177(2)	4036(1)	36(1)
C(19E)	5603(3)	10151(2)	3746(2)	39(1)
C(20E)	5460(2)	9733(2)	3291(1)	31(1)
C(21E)	4685(2)	9315(2)	3108(1)	27(1)
C(22E)	3517(3)	9819(3)	4196(2)	51(1)
C(23E)	2937(4)	10194(3)	4070(2)	81(2)
C(24E)	3839(4)	10036(3)	4725(2)	68(2)
C(25E)	4607(3)	9236(2)	2247(1)	34(1)
C(26E)	4549(2)	8858(2)	2610(1)	29(1)
C(27E)	5158(3)	8406(2)	2544(2)	34(1)
N(3F)	2816(2)	13456(2)	819(1)	25(1)
N(4F)	1968(2)	14066(2)	582(1)	30(1)
C(28F)	2969(2)	14065(2)	1151(1)	27(1)

C(29F)	3527(3)	14322(2)	1567(1)	37(1)
C(30F)	3534(3)	14955(2)	1837(1)	45(1)
C(31F)	3020(3)	15316(2)	1698(2)	47(1)
C(32F)	2472(3)	15065(2)	1281(2)	45(1)
C(33F)	2445(3)	14429(2)	1002(1)	29(1)
C(34F)	2226(2)	13500(2)	498(1)	23(1)
C(35F)	1864(2)	12954(2)	69(1)	24(1)
C(36F)	2252(3)	12434(2)	-81(1)	31(1)
C(37F)	1927(3)	11939(2)	-497(2)	41(1)
C(38F)	1214(3)	11948(2)	-759(2)	40(1)
C(39F)	825(3)	12449(2)	-607(2)	41(1)
C(40F)	1150(3)	12943(2)	-200(1)	33(1)
N(1F)	2097(2)	11975(2)	1325(1)	27(1)
N(2F)	3314(2)	12434(2)	1704(1)	30(1)
C(1F)	2757(2)	12433(2)	1352(1)	27(1)
C(2F)	2993(3)	11966(2)	1909(2)	39(1)
C(3F)	2235(2)	11680(2)	1674(2)	34(1)
C(4F)	1365(2)	11821(2)	982(1)	26(1)
C(5F)	814(2)	12235(2)	1068(1)	29(1)
C(6F)	131(3)	12084(2)	725(2)	36(1)
C(7F)	23(3)	11557(2)	324(2)	41(1)
C(8F)	572(3)	11152(2)	258(2)	40(1)
C(9F)	1259(2)	11270(2)	592(1)	32(1)

C(10F)	917(3)	12794(2)	1517(2)	38(1)
C(11F)	784(4)	13406(2)	1414(2)	59(2)
C(12F)	317(3)	12609(2)	1851(2)	47(1)
C(13F)	1860(3)	10813(2)	537(2)	46(1)
C(14F)	2482(6)	10959(4)	219(4)	166(6)
C(15F)	1441(4)	10107(3)	337(2)	72(2)
C(16F)	4132(2)	12827(2)	1837(1)	30(1)
C(17F)	4306(3)	13291(2)	2290(1)	38(1)
C(18F)	5110(3)	13636(2)	2423(2)	42(1)
C(19F)	5687(3)	13544(2)	2127(2)	45(1)
C(20F)	5498(3)	13088(2)	1677(2)	37(1)
C(21F)	4709(2)	12707(2)	1523(1)	28(1)
C(22F)	3672(4)	13438(3)	2633(2)	57(1)
C(23F)	3667(6)	14200(3)	2789(2)	101(3)
C(24F)	3881(3)	13320(2)	3087(2)	45(1)
C(25F)	4481(3)	12529(2)	641(2)	38(1)
C(26F)	4507(2)	12208(2)	1035(2)	32(1)
C(27F)	5111(3)	11754(2)	949(2)	41(1)

Bibliography

1. Alidori, S.; Heift, D.; Santiso-Quinones, G.; Benkå, Z.; Grützmacher, H.; Caporali, M.; Gonsalvi, L.; Rossin, A.; Peruzzini, M. Synthesis and Characterization of Terminal [Re(XCO)(CO) 2(Triphos)] (X=N, P): Isocyanate versus Phosphaethynolate Complexes. *Chem. - Eur. J.* **2012**, *18*, 14805–14811.
2. Alkorta, I.; Rozas, I.; Elguero, J. Non-Conventional Hydrogen Bonds. *Chem. Soc. Rev.* **1998**, *27*, 163–170.
3. Anschütz, L.; Delijski, Z. M. Studien an Aromatischen Thionylaminen. *Justus Liebig's Ann. der Chemie* **1932**, *493*, 241–250.
4. Arduengo, A. J.; Harlow, R. L.; Kline, M. A Stable Crystalline Carbene. *J. Am. Chem. Soc.* **1991**, *113*, 361–363.
5. Arduengo, Anthony J., I.; Gamper, S. F.; Tamm, M.; Calabrese, J. C.; Davidson, F.; Craig, H. A. A Bis(Carbene)—Proton Complex: Structure of a C—H—C Hydrogen Bond. *J. Am. Chem. Soc.* **1995**, *117*, 572–573.
6. Arduengo, Anthony J., I.; Krafczyk, R.; Schmutzler, R.; Craig, H. A.; Goerlich, J. R.; Marshall, W. J.; Unverzagt, M. Imidazolylidenes, Imidazolinylidenes and Imidazolidines. *Tetrahedron* **1999**, *55*, 14523–14534.
7. Artyukhov, V. Y.; Morev, A. V.; Morozova, Y. P.; Pomogaev, V. A. Investigation of the Heavy-Atom Effect on the Spectral-Luminescent Properties of Dichloroanilines. *Russ. Phys. J.* **2002**, *45*, 1203–1207.
8. Bąk, K. M.; Chabuda, K.; Montes, H.; Quesada, R.; Chmielewski, M. J. 1,8-Diamidocarbazoles: An Easily Tuneable Family of Fluorescent Anion Sensors and Transporters. *Org. Biomol. Chem.* **2018**, *16*, 5188–5196.

9. Bannwarth, C.; Ehlert, S.; Grimme, S. GFN2-XTB – an Accurate and Broadly Parametrized Self-Consistent Tight-Binding. *ChemRxiv* **2018**, http://doi.org/10.26434/chemrxiv.7246238.v1.

10. Bansal, R. K.; Gupta, N.; Heinicke, J.; Nikonov, G. N.; Saguitova, F.; Sharma, D. C. 1H-1,3-Benzazaphospholes: The Organometallic Route and a New Three-Step Synthesis with Reductive Ring Closure. *Synthesis* **1999**, No. 2, 264–269.

11. Baxter, S. G.; Cowley, A. H.; Davis, R. E.; Riley, P. E. Crystal Structure and Low-Temperature 1H NMR Spectrum of Tetramesityldiphosphine. Evidence for the Anti-Conformational Preference in Tetraaryldiphosphines. *J. Am. Chem. Soc.* **1981**, *103*, 1699–1702.

12. Becker, G. Bildung Und Eigenschaften von Acylphosphinen. I. Monosubstitutionsreaktionen an Substituierten Disilylphosphinen Mit Pivaloylchlorid. *Z. Anorg. Alleg. Chem.* **1976**, *423*, 242–254.

13. Becker, G.; Heckmann, G.; Hübler, K.; Schwarz, W. Alkylidinphosphane Und -arsane. II. Über Die Oxydation Des Lithoxy-methylidinphosphans P≡C-O-Li Mit Schwefeldioxid Und Iod. *Z. Anorg. Alleg. Chem.* **1995**, *621*, 34–46.

14. Becker, G.; Schwarz, W.; Seidler, N.; Westerhausen, M. Acyl- Und Alkylidenphosphane. XXXIII. Lithoxy-methylidenphosphan · DME Und -methylidinphosphan · 2 DME — Synthese Und Struktur. *Z. Anorg. Alleg. Chem.* **1992**, *612*, 72–82.

15. Berlman, I. B. Empirical Study of Heavy-Atom Collisional Quenching of the Fluorescence State of Aromatic Compounds in Solution. *J. Phys. Chem.* **1973**, *77*, 562–567.

16. Binger, P.; Biedenbach, B.; Mynott, R.; Regitz, M. Synthese von Bis(Cyclopentadienyl)-1-Metalla-3-Phosphaindenen (M = Titan, Zirkonium). *Chem. Ber.* **1988**, *121*, 1455–1456.

17. Bolton, O.; Lee, K.; Kim, H. J.; Lin, K. Y.; Kim, J. Activating Efficient Phosphorescence from Purely Organic Materials by Crystal Design. *Nat. Chem.* **2011**, *3*, 205–210.

18. Bordwell, F. G.; Drucker, G. E.; Fried, H. E. Acidities of Carbon and Nitrogen Acids: The Aromaticity of the Cyclopentadienyl Anion. *J. Org. Chem.* **1981**, *46*, 632–635.

19. Bordwell, Frederick, G. Equilibrium Acidities in Dimethyl Sulfoxide Solution. *Acc. Chem. Res.* **1988**, *21*, 456–463.

20. Brown, A. B.; Gibson, T. L.; Baum, J. C.; Ren, T.; Smith, T. M. Fluorescence-Enhancement Sensing of Ammonia and Hydrazines via Disruption of the Internal Hydrogen Bond in a Carbazolopyridinophane. *Sensors Actuators, B Chem.* **2005**, *110*, 8–12.

21. Buchwald, S. L.; Lucas, E. A.; Dewan, J. C. Synthesis, Structure, and Reactions of a Zirconocene-Benzdiyne Complex. *J. Am. Chem. Soc.* **1987**, *109*, 4396–4397.

22. Buchwald, S. L.; Watson, B. T.; Huffman, J. C. The Trimethylphosphine Adduct of the Zirconocene-Benzyne Complex: Synthesis, Reactions, and X-Ray Crystal Structure. *J. Am. Chem. Soc.* **1986**, *108*, 7411–7413.

23. Camp, C.; Settineri, N.; Lefèvre, J.; Jupp, A. R.; Goicoechea, J. M.; Maron, L.; Arnold, J. Uranium and Thorium Complexes of the Phosphaethynolate Ion. *Chem. Sci.* **2015**, *6*, 6379–6384.

24. Catalán, J.; De Paz, J. L. G.; del Valle, J. C.; Kasha, M. Inter-Ring Torsional Modulation in Molecular Lasers. Ultraviolet Lasing via Amplified Spontaneous Emission Spectroscopy of Phenylimidazoles. *J. Phys. Chem. A* **1997**, *101*, 5284–5291.

25. Catalán, J.; Mena, E.; Fabero, F.; Amat-Guerri, F. The Role of the Torsion of the Phenyl Moiety in the Mechanism of Stimulated Ultraviolet Light Generation in 2-Phenylbenzazoles. *J. Chem. Phys.* **1992**, *96*, 2005–2016.

26. Chu, J.; Munz, D.; Jazzar, R.; Melaimi, M.; Bertrand, G. Synthesis of Hemilabile Cyclic (Alkyl)(Amino)Carbenes (CAACs) and Applications in Organometallic Chemistry. *J. Am. Chem. Soc.* **2016**, *138*, 7884–7887.

27. Chu, M.; Scioneaux, A. N.; Hartley, C. S. Solution-Phase Dimerization of an Oblong Shape-Persistent Macrocycle. *J. Org. Chem.* **2014**, *79*, 9009–9017.

28. Cook, J. L.; Hunter, C. A.; Low, C. M. R.; Perez-Velasco, A.; Vinter, J. G. Solvent Effects on Hydrogen Bonding. *Angew. Chem. Int. Ed.* **2007**, *46*, 3706–3709.

29. Cowan, J. A.; Clyburne, J. A. C.; Davidson, M. G.; Harris, R. L. W.; Howard, J. A. K.; Küpper, P.; Leech, M. A.; Richards, S. P. On the Interaction between N-Heterocyclic Carbenes and Organic Acids: Structural Authentication of the First N-H ... C Hydrogen Bond and Remarkably Short C-H ... O Interactions. *Angew. Chem. Int. Ed.* **2002**, *41*, 1432–1434.

30. d'Arbeloff-Wilson, S. E.; Hitchcock, P. B.; Nixon, J. F.; Kawaguchi, H.; Tatsumi, K. [2+2] Cyclo-Addition Reactions of Bis-Pentamethylcyclopentadienyl Zirconium Metal Complexes Containing Terminal Chalcogenide Ligands with

the Phospha-Alkyne PCtBu. Syntheses, Crystal and Molecular Structures of the Four Complexes. *J. Organomet. Chem.* **2003**, *672*, 1–10.

31. Del Bene, J. E.; Alkorta, I.; Elguero, J. Hydrogen-Bonded Complexes with Carbenes as Electron-Pair Donors. *Chem. Phys. Lett.* **2017**, *675*, 46–50.
32. Di, D.; Romanov, A. S.; Yang, L.; Richter, J. M.; Rivett, J. P. H.; Jones, S.; Thomas, T. H.; Abdi Jalebi, M.; Friend, R. H.; Linnolahti, M.; et al. High-Performance Light-Emitting Diodes Based on Carbene-Metal-Amides. *Science* **2017**, *356*, 159–163.
33. Dillon, K. B.; Mathey, F.; Nixon, J. F. *Phosphorus : The Carbon Copy : From Organophosphorus to Phospha-Organic Chemistry*; 1998.
34. El-Bayoumi, M. A.; Kasha, M. Energy Transfer in Hydrogen-Bonded *N* -Heterocyclic Complexes and Their Possible Role as Energy Sinks. *J. Chem. Phys.* **1961**, *34*, 2181–2182.
35. Elie, M.; Renaud, J. L.; Gaillard, S. N-Heterocyclic Carbene Transition Metal Complexes in Light Emitting Devices. *Polyhedron* **2018**, *140*, 158–168.
36. El-Sayed, M. A. The Triplet State: Its Radiative and Nonradiative Properties. *Acc. Chem. Res.* **1968**, *1*, 8–16.
37. Emsley, J. Very Strong Hydrogen Bonding. *Chem. Soc. Rev.* **1968**, *9*, 91–124.
38. Enders, D.; Niemeier, O.; Henseler, A. Organocatalysis by N-Heterocyclic Carbenes. *Chem. Rev.* **2007**, *107*, 5606–5655.
39. Fagan, P. J.; Nugent, W. A. Synthesis of Main Group Heterocycles by Metallacycle Transfer from Zirconium. *J. Am. Chem. Soc.* **1988**, *110*, 2310–2312.

40. Fagan, P. J.; Nugent, W. A.; Calabrese, J. C. Metallacycle Transfer from Zirconium to Main Group Elements: A Versatile Synthesis of Heterocycles. *J. Am. Chem. Soc.* **1994**, *116*, 1880–1889.

41. Föller, J.; Marian, C. M. Rotationally Assisted Spin-State Inversion in Carbene-Metal-Amides Is an Artifact. *J. Phys. Chem. Lett.* **2017**, *8*, 5643–5647.

42. Frey, G. D.; Lavallo, V.; Donnadieu, B.; Schoeller, W. W.; Bertrand, G. Facile Splitting of Hydrogen at a Single Carbon Center. *Science* **2007**, *316*, 439–441.

43. Furfari, S. K.; Gyton, M. R.; Twycross, D.; Cole, M. L. Air Stable NHCs: A Study of Stereoelectronics and Metallorganic Catalytic Activity. *Chem. Commun.* **2015**, *51*, 74–76.

44. Gernert, M.; Müller, U.; Haehnel, M.; Pflaum, J.; Steffen, A. A Cyclic Alkyl(Amino)Carbene as Two-Atom π-Chromophore Leading to the First Phosphorescent Linear Cu I Complexes. *Chem. - Eur. J.* **2017**, *23*, 2206–2216.

45. Giffin, N. A.; Makramalla, M.; Hendsbee, A. D.; Robertson, K. N.; Sherren, C.; Pye, C. C.; Masuda, J. D.; Clyburne, J. A. C. Anhydrous TEMPO-H: Reactions of a Good Hydrogen Atom Donor with Low-Valent Carbon Centres. *Org. Biomol. Chem.* **2011**, *9*, 3672–3680.

46. Gilliard, R. J.; Heift, D.; Benko, Z.; Keiser, J. M.; Rheingold, A. L.; Grützmacher, H.; Protasiewicz, J. D. An Isolable Magnesium Diphosphaethynolate Complex. *Dalt. Trans.* **2018**, *47*, 666–669.

47. Gillis, E. P.; Eastman, K. J.; Hill, M. D.; Donnelly, D. J.; Meanwell, N. A. Applications of Fluorine in Medicinal Chemistry. *J. Med. Chem.* **2015**, *58*, 8315–8359.

48. Grant, L. N.; Pinter, B.; Manor, B. C.; Suter, R.; Grützmacher, H.; Mindiola, D. J. A Planar Ti2P2 Core Assembled by Reductive Decarbonylation of −O−C≡P and P−P Radical Coupling. *Chem. - Eur. J.* **2017**, *23*, 6272–6276.

49. Grimme, S.; Bannwarth, C.; Shushkov, P. A Robust and Accurate Tight-Binding Quantum Chemical Method for Structures, Vibrational Frequencies, and Noncovalent Interactions of Large Molecular Systems Parametrized for All Spd-Block Elements (Z = 1-86). *J. Chem. Theory Comput.* **2017**, *13*, 1989–2009.

50. Grineva, A. A.; Filippov, O. A.; Nefedov, S. E.; Lugan, N.; César, V.; Valyaev, D. A. Direct Access to IMesF and IMesF2 by Electrophilic Fluorination of Abnormal N-Heterocyclic Carbenes. *Organometallics* **2019**, *38*, 2330–2337.

51. Hamze, R.; Peltier, J. L.; Sylvinson, D.; Jung, M.; Cardenas, J.; Haiges, R.; Soleilhavoup, M.; Jazzar, R.; Djurovich, P. I.; Bertrand, G.; et al. Eliminating Nonradiative Decay in Cu(I) Emitters: >99% Quantum Efficiency and Microsecond Lifetime. *Science* **2019**, *363*, 601–606.

52. Hans, M.; Lorkowski, J.; Demonceau, A.; Delaude, L. Efficient Synthetic Protocols for the Preparation of Common N-Heterocyclic Carbene Precursors. *Beilstein J. Org. Chem.* **2015**, *11*, 2318–2325.

53. Hart, H. Arynes and Heteroarynes. In *Supplement C2: The Chemistry of Triple-Bonded Functional Groups*; John Wiley & Sons, Ltd: Chichester, UK, 2004; pp 1017–1134.

54. Hartwig, J. F.; Bergman, R. G.; Andersen, R. A. Reactions with Arenes, Alkenes, and Heteroatom-Containing Organic Compounds. *J. Am. Chem. Soc.* **1991**, *113*, 3404–3418.

55. Heift, D.; Benkő, Z.; Grützmacher, H. Is the Phosphaethynolate Anion, (OCP)−, an Ambident Nucleophile? A Spectroscopic and Computational Study. *Dalt. Trans.* **2014**, *43*, 5920.

56. Heift, D.; Benko, Z.; Grützmacher, H. Redox-Triggered Reversible Interconversion of a Monocyclic and a Bicyclic Phosphorus Heterocycle. *Angew. Chem. Int. Ed.* **2014**, *53*, 6757–6761.

57. Heinicke, J.; Steinhauser, K.; Peulecke, N.; Spannenberg, A.; Mayer, P.; Karaghiosoff, K. Metalated 1,3-Azaphospholes: Structure and Reactivity of 2-Lithio-1-Methy1-1,3-Benzazaphosphole, an Isolable -P=C(Li)-NR Heterocycle. *Organometallics* **2002**, *21*, 912–919.

58. Heinicke, J.; Tzschach, A. 1,3-Benzoxaphosphole-Heterocyclen Mit Phosphor Der Koordinationszahl 2. *Phosphorus Sulfur Relat. Elem.* **1985**, *25*, 345–356.

59. Hollóczki, O. Unveiling the Peculiar Hydrogen Bonding Behavior of Solvated N-Heterocyclic Carbenes. *Phys. Chem. Chem. Phys.* **2016**, *18*, 126–140.

60. Hopkinson, M. N.; Richter, C.; Schedler, M.; Glorius, F. An Overview of N-Heterocyclic Carbenes. *Nature* **2014**, *510*, 485–496.

61. Igau, A.; Grutzmacher, H.; Baceiredo, A.; Bertrand, G. Analogous α,α'-Bis-Carbenoid Triply Bonded Species: Synthesis of a Stable Λ3-Phosphinocarbene-Λ5-Phosphaacetylene. *J. Am. Chem. Soc.* **1988**, *110*, 6463–6466.

62. Jazzar, R.; Bourg, J. B.; Dewhurst, R. D.; Donnadieu, B.; Bertrand, G. Intramolecular "Hydroiminiumation and -Amidiniumation" of Alkenes: A Convenient, Flexible, and Scalable Route to Cyclic Iminium and Imidazolinium Salts. *J. Org. Chem.* **2007**, *72*, 3492–3499.

63. Johnson, C. S. Diffusion Ordered Nuclear Magnetic Resonance Spectroscopy: Principles and Applications. *Prog. Nucl. Magn. Reson. Spectrosc.* **1999**, *34*, 203–256.

64. Jupp, A. R.; Goicoechea, J. M. Phosphinecarboxamide: A Phosphorus-Containing Analogue of Urea and Stable Primary Phosphine. *J. Am. Chem. Soc.* **2013**, *135*, 19131–19134.

65. Kieser, J. M.; Gilliard, R. J.; Rheingold, A. L.; Grützmacher, H.; Protasiewicz, J. D. Insertion of Sodium Phosphaethynolate, Na[OCP], into a Zirconium-Benzyne Complex. *Chem. Commun.* **2017**, *53*, 5110–5112.

66. Kieser, J. M.; Kinney, Z. J.; Gaffen, J. R.; Evariste, S.; Harrison, A. M.; Rheingold, A. L.; Protasiewicz, J. D. Three Ways Isolable Carbenes Can Modulate Emission of NH-Containing Fluorophores. *J. Am. Chem. Soc.* **2019**, *141*, 12055–12063.

67. Laughlin, F. L.; Deligonul, N.; Rheingold, A. L.; Golen, J. A.; Laughlin, B. J.; Smith, R. C.; Protasiewicz, J. D. Fluorescent Heteroacenes with Multiply-Bonded Phosphorus. *Organometallics* **2013**, *32*, 7116–7121.

68. Li, C. Y.; Kuo, Y. Y.; Tsai, J. H.; Yap, G. P. A.; Ong, T. G. Amine-Linked N-Heterocyclic Carbenes: The Importance of an Pendant Free-Amine Auxiliary in Assisting the Catalytic Reaction. *Chem. - Asian J.* **2011**, *6*, 1520–1524.

69. Liotta, C. L.; MeLaughlin, M. L.; O'Brien, B. A. The Synthesis and Reactions of Potassium Benzoylphosphide, Benzoylphosphine, and Benzoylmethylphosphine. *Tetrahedron Lett.* **1984**, *25*, 1249–1252.

70. Liu, L.; Ruiz, D. A.; Dahcheh, F.; Bertrand, G.; Suter, R.; Tondreau, A. M.; Grützmacher, H. Isolation of Au-, Co-η [1] PCO and Cu-η [2] PCO Complexes, Conversion of an Ir–η [1] PCO Complex into a Dimetalladiphosphene, and an Interaction-Free PCO Anion. *Chem. Sci.* **2016**, *7*, 2335–2341.

71. Ma, X.-B.; Regitz, M. Organophosphorus Compounds; 99. An Efficient One-Pot Synthesis of 1,1-Bis(H5-Cyclopentadienyl)-1-Zircona-3-Phosphaindenes. *Synthesis* **1995**, *1995*, 667–670.

72. Magill, A. M.; Cavell, K. J.; Yates, B. F. Basicity of Nucleophilic Carbenes in Aqueous and Nonaqueous Solvents - Theoretical Predictions. *J. Am. Chem. Soc.* **2004**, *126*, 8717–8724.

73. Mahoney, J. K.; Martin, D.; Moore, C. E.; Rheingold, A. L.; Bertrand, G. Bottleable (Amino)(Carboxy) Radicals Derived from Cyclic (Alkyl)(Amino) Carbenes. *J. Am. Chem. Soc.* **2013**, *135*, 18766–18769.

74. Majhi, P. K.; Chow, K. C. F.; Hsieh, T. H. H.; Bowes, E. G.; Schnakenburg, G.; Kennepohl, P.; Streubel, R.; Gates, D. P. Even the Normal Is Abnormal: N-Heterocyclic Carbene C 2 Binding to a Phosphaalkene without Breaking the P=C π-Bond. *Chem. Commun.* **2016**, *52*, 998–1001.

75. Mandal, D.; Dolai, R.; Kalita, P.; Narayanan, R. S.; Kumar, R.; Sobottka, S.; Sarkar, B.; Rajaraman, G.; Chandrasekhar, V.; Jana, A. “Abnormal” Addition of NHC to a Conjugate Acid of CAAC: Formation of N -Alkyl-Substituted CAAC. *Chem. - Eur. J.* **2018**, *24*, 12722–12727.

76. Martin, D.; Melaimi, M.; Soleilhavoup, M.; Bertrand, G. A Brief Survey of Our Contribution to Stable Carbene Chemistry. *Organometallics* **2011**, *30*, 5304–5313.

77. Martin, M. M.; Ware, W. R. Fluorescence Quenching of Carbazole by Pyridine and Substituted Pyridines. Radiationless Processes in the Carbazole-Amine Hydrogen Bonded Complex. *J. Phys. Chem.* **1978**, *82*, 2770–2776.

78. Martin, R. B. Comparisons of Indefinite Self-Association Models. *Chem. Rev.* **2002**, *96*, 3043–3064.

79. Mataga, N.; Tanaka, F.; Kato, M. Electronic Energy Relaxation Processes in the Intermolecular Hydrogen-Bonded Systems. *Acta Phys. Pol.* **1968**, *34*, 733–745.

80. McGlynn, S. P.; Sunseri, R.; Christodouleas, N. External Heavy-Atom Spin-Orbital Coupling Effect. I. The Nature of the Interaction. *J. Chem. Phys.* **1962**, *37*, 1818–1824.

81. Melaimi, M.; Jazzar, R.; Soleilhavoup, M.; Bertrand, G. Cyclic (Alkyl)(Amino)Carbenes (CAACs): Recent Developments. *Angew. Chem. Int. Ed.* **2017**, *56*, 10046–10068.

82. Mercs, L.; Albrecht, M. Beyond Catalysis: N-Heterocyclic Carbene Complexes as Components for Medicinal, Luminescent, and Functional Materials Applications. *Chem. Soc. Rev.* **2010**, *39*, 1903–1912.

83. Michaelis, A. Ueber Die Thionylamine. *Berichte der Dtsch. Chem. Gesellschaft* **1891**, *24*, 745–757.

84. Mignani, G. Preparation of Precursors of Carbenes of CAAC Type and Preparing Said Carbenes Therefrom. US2010113791 (A1), 2010.

85. Movassaghi, M.; Schmidt, M. A. N-Heterocyclic Carbene-Catalyzed Amidation of Unactivated Esters with Amino Alcohols. *Org. Lett.* **2005**, *7*, 2453–2456.

86. Mukherjee, S.; Thilagar, P. Recent Advances in Purely Organic Phosphorescent Materials. *Chem. Commun.* **2015**, *51*, 10988–11003.

87. Najbar, J.; Munro, I. H. External Heavy Atom Effects on the Decay of the Triplet State of Aromatic Hydrocarbons III. The Decay Functions of Fluorescence and Phosphorescence of Carbazole in the Presence of KI. *J. Lumin.* **1978**, *17*, 135–148.

88. Neilson, B. M.; Bielawski, C. W. Photoswitchable Organocatalysis: Using Light to Modulate the Catalytic Activities of N-Heterocyclic Carbenes. *J. Am. Chem. Soc.* **2012**, *134*, 12693–12699.

89. Neilson, B. M.; Lynch, V. M.; Bielawski, C. W. Photoswitchable N-Heterocyclic Carbenes: Using Light to Modulate Electron-Donating Properties. *Angew. Chem. Int. Ed.* **2011**, *50*, 10322–10326.

90. Neufeld, R.; Stalke, D. Accurate Molecular Weight Determination of Small Molecules via DOSY-NMR by Using External Calibration Curves with Normalized Diffusion Coefficients. *Chem. Sci.* **2015**, *6*, 3354–3364.

91. Öfele, K. 1,3-Dimethyl-4-Imidazolinyliden-(2)-Pentacarbonylchrom Ein Neuer Übergangsmetall-Carben-Komplex. *J. Organomet. Chem.* **1968**, *12*, P42–P43.

92. Paul, U. S. D.; Radius, U. Ligand versus Complex: C−F and C−H Bond Activation of Polyfluoroaromatics at a Cyclic (Alkyl)(Amino)Carbene. *Chem. - Eur. J.* **2017**, *23*, 3993–4009.

93. Perez, F.; Ren, Y.; Boddaert, T.; Rodriguez, J.; Coquerel, Y. A Stable N-Heterocyclic Carbene Organocatalyst for Hydrogen/Deuterium Exchange Reactions between Pseudoacids and Deuterated Chloroform. *J. Org. Chem.* **2015**, *80*, 1092–1097.

94. Peris, E. Smart N-Heterocyclic Carbene Ligands in Catalysis. *Chem. Rev.* **2018**, *118*, 9988–10031.

95. Pi, C.; Yu, X.; Zheng, W. Imidazolium 1,3-Benzazaphospholide Ion Pairs with Strong C-H···N Hydrogen Bonds - Synthesis, Structures, and Reactivity. *Eur. J. Inorg. Chem.* **2015**, *2015*, 1804–1810.

96. Puschmann, F. F.; Stein, D.; Heift, D.; Hendriksen, C.; Gal, Z. A.; Grützmacher, H.-F.; Grützmacher, H. Phosphination of Carbon Monoxide: A Simple Synthesis of Sodium Phosphaethynolate (NaOCP). *Angew. Chem. Int. Ed.* **2011**, *50*, 8420–8423.

97. Quan, Z.-J.; Wang, X.-C. The 2-Phosphaethynolate Anion: Convenient Synthesis and the Reactivity. *Org. Chem. Front.* **2014**, *1*, 1128–1131.

98. Rae, M.; Fedorov, A.; Berberan-Santos, M. N. Fluorescence Quenching with Exponential Distance Dependence: Application to the External Heavy-Atom Effect. *J. Chem. Phys.* **2003**, *119*, 2223–2231.

99. Raut, A. H.; Karir, G.; Viswanathan, K. S. Matrix Isolation Infrared and Ab Initio Study of the Interaction of N-Heterocyclic Carbene with Water and Methanol: A Case Study of a Strong Hydrogen Bond. *J. Phys. Chem. A* **2016**, *120*, 9390–9400.

100. Retbøll, M.; Edwards, A. J.; Rae, A. D.; Willis, A. C.; Bennett, M. A.; Wenger, E. Preparation of Benzyne Complexes of Group 10 Metals by Intramolecular

Suzuki Coupling of Ortho-Metalated Phenylboronic Esters: Molecular Structure of the First Benzyne-Palladium(0) Complex. *J. Am. Chem. Soc.* **2002**, *124*, 8348–8360.

101. Romero-Ale, E. E.; Olives, A. I.; Martín, M. A.; Del Castillo, B.; López-Alvarado, P.; Menéndez, J. C. Environmental Effects on the Fluorescence Behaviour of Carbazole Derivatization Reagents. *Luminescence* **2005**, *20*, 162–169.
102. Rosa, P.; Le Floch, P.; Ricard, L.; Mathey, F. Synthesis, Structure, and Reactivity of η 2 -Phosphabenzyne−Zirconocene Dimers. *J. Am. Chem. Soc.* **1997**, *119*, 9417–9423.
103. Schmidt, M. A.; Müller, P.; Movassaghi, M. On the Interactions of N,N′-Bismesitylimidazolin-2-Yl and Alcohols. *Tetrahedron Lett.* **2008**, *49*, 4316–4318.
104. Schroeder, W. A.; Wilcox, P. E.; Trueblood, K. N.; Dekker, A. O. Ultraviolet and Visible Absorption Spectra in Ethyl Alcohol. *Anal. Chem.* **1951**, *23*, 1740–1747.
105. Scott, N. M.; Nolan, S. P. Stabilization of Organometallic Species Achieved by the Use of N-Heterocyclic Carbene (NHC) Ligands. *Eur. J. Inorg. Chem.* **2005**, No. 10, 1815–1828.
106. Sessler, C. D.; Rahm, M.; Becker, S.; Goldberg, J. M.; Wang, F.; Lippard, S. J. CF2H, a Hydrogen Bond Donor. *J. Am. Chem. Soc.* **2017**, *139*, 9325–9332.
107. Shi, F.; Waldo, J. P.; Chen, Y.; Larock, R. C. Benzyne Click Chemistry: Synthesis of Benzotriazoles from Benzynes and Azides. *Org. Lett.* **2008**, *10*, 2409–2412.

108. Shi, S.; Jung, M. C.; Coburn, C.; Tadle, A.; Sylvinson, D. M. R.; Djurovich, P. I.; Forrest, S. R.; Thompson, M. E. Highly Efficient Photo- and Electroluminescence from Two-Coordinate Cu(I) Complexes Featuring Nonconventional N-Heterocyclic Carbenes. *J. Am. Chem. Soc.* **2019**, *141*, 3576–3588.

109. Shih, W. C.; Wang, C. H.; Chang, Y. T.; Yap, G. P. A.; Ong, T. G. Synthesis and Structure of an Amino-Linked N-Heterocyclic Carbene and the Reactivity of Its Aluminum Adduct. *Organometallics* **2009**, *28*, 1060–1067.

110. Simpson, M. C.; Protasiewicz, J. D. Phosphorus as a Carbon Copy and as a Photocopy: New Conjugated Materials Featuring Multiply Bonded Phosphorus. *Pure Appl. Chem.* **2013**, *85*, 801–815.

111. Smith, R. C.; Protasiewicz, J. D. Conjugated Polymers Featuring Heavier Main Group Element Multiple Bonds: A Diphosphene-PPV. *J. Am. Chem. Soc.* **2004**, *126*, 2268–2269.

112. Smith, R. C.; Protasiewicz, J. D. Systematic Investigation of PPV Analogue Oligomers Incorporating Low-Coordinate Phosphorus Centres. *Eur. J. Inorg. Chem.* **2004**, No. 5, 998–1006.

113. Spencer, T. S.; O'Donnell, C. M. Energy Transfer in a Hydrogen-Bonded Carbazole–Benzophenone Complex. *J. Am. Chem. Soc.* **1972**, *94*, 4846–4849.

114. Standard, J. M. Effects of Solvation and Hydrogen Bond Formation on Singlet and Triplet Alkyl or Aryl Carbenes. *J. Phys. Chem. A* **2017**, *121*, 381–393.

115. Stejskal, E. O.; Tanner, J. E. Spin Diffusion Measurements: Spin Echoes in the Presence of a Time-Dependent Field Gradient. *J. Chem. Phys.* **1965**, *42*, 288–292.

116. Sun, J.-K.; Zhang, W.; Guterman, R.; Lin, H. J.; Yuan, J. Porous Polycarbene-Bearing Membrane Actuator for Ultrasensitive Weak-Acid Detection and Real-Time Chemical Reaction Monitoring. *Nat. Commun.* **2018**, *9*, 1–8.

117. Sun, X.; Zhang, B.; Li, X.; Trindle, C. O.; Zhang, G. External Heavy-Atom Effect via Orbital Interactions Revealed by Single-Crystal X-Ray Diffraction. *J. Phys. Chem. A* **2016**, *120*, 5791–5797.

118. Surana, A.; Singh, S.; Bansal, R. K.; Peulecke, N.; Spannenberg, A.; Heinicke, J. Metalated 1,3-Azaphospholes: Synthesis of Lithium-1,3-Benzazaphospholides and Reactivity towards Organoelement and Organometal Halides. *J. Organometalic Chem.* **2002**, *646*, 113–124.

119. Suter, R.; Benkő, Z.; Bispinghoff, M.; Grützmacher, H. Annulated 1,3,4-Azadiphospholides: Heterocycles with Widely Tunable Optical Properties. *Angew. Chem. Int. Ed.* **2017**, *56*, 11226–11231.

120. Suter, R.; Mei, Y.; Baker, M.; Benkő, Z.; Li, Z.; Grützmacher, H. 2,4,6-Tri(Hydroxy)-1,3,5-Triphosphinine, P 3 C 3 (OH) 3 : The Phosphorus Analogue of Cyanuric Acid. *Angew. Chem. Int. Ed.* **2017**, *56*, 1356–1360.

121. Takahashi, T.; Swanson, D. R.; Negishi, E. Zirconacyclopropanes and Zirconacyclopropenes. Their Synthesis, Characterization, and Reactions. *Chem. Lett.* **1987**, *16*, 623–626.

122. Tanaka, F.; Kato, M.; Mataga, N. Electronic Energy Transfers in Intermolecular Hydrogen Bonded Systems: Sensitization of Quinoline Phosphorescence in the Carbazole—Quinoline System. *Zeitschrift für Phys. Chemie* **1970**, *70*, 104–112.

123. Teator, A. J.; Tian, Y.; Chen, M.; Lee, J. K.; Bielawski, C. W. An Isolable, Photoswitchable N-Heterocyclic Carbene: On-Demand Reversible Ammonia Activation. *Angew. Chem. Int. Ed.* **2015**, *54*, 11559–11563.

124. Tolentino, D. R.; Neale, S. E.; Isaac, C. J.; Macgregor, S. A.; Whittlesey, M. K.; Jazzar, R.; Bertrand, G. Reductive Elimination at Carbon under Steric Control. *J. Am. Chem. Soc.* **2019**, 8–11.

125. Turner, G. L.; Smith, K. A.; Kirkpatrick, R. J.; Oldfieldt, E. Structure and Cation Effects on Phosphorus-31 NMR Chemical Shifts and Chemical-Shift Anisotropies of Orthophosphates. *J. Magn. Reson.* **1986**, *70*, 408–415.

126. Urnéžius, E.; Protasiewicz, J. D. Synthesis and Structural Characterization of New Hindered Aryl Phosphorus Centers (Aryl = 2,6-Dimesitylphenyl). *Main Gr. Chem.* **1996**, *1*, 369–372.

127. Van Wagenen, B. C.; Livinghouse, T. On the Generation of Stabilized Low-Valent Metallocene Derivatives. The Direct Synthesis and Reductive Coupling Reactions of 1-Methylthioalkyne-Zirconocene Complexes. *Tetrahedron Lett.* **1989**, *30*, 3495–3498.

128. Vougioukalakis, G. C.; Grubbs, R. H. Ruthenium-Based Olefin Metathesis Catalysts Coordinated with Unsymmetrical N-Heterocyclic Carbene Ligands: Synthesis, Structure, and Catalytic Activity. *Chem. - Eur. J.* **2008**, *14*, 7545–7556.

129. Walba, H.; Isensee, R. W. Acidity Constants of Some Arylimidazoles and Their Cations. *J. Org. Chem.* **1961**, *26*, 2789–2791.

130. Wanzlick, H. -W; Schönherr, H. -J. Direct Synthesis of a Mercury Salt-Carbene Complex. *Angew. Chem. Int. Ed.* **1968**, *7*, 141–142.

131. Washington, M. P.; Gudimetla, V. B.; Laughlin, F. L.; Deligonul, N.; He, S.; Payton, J. L.; Simpson, M. C.; Protasiewicz, J. D. Phosphorus Can Also Be a "Photocopy." *J. Am. Chem. Soc.* **2010**, *132*, 4566–4567.

132. Weber, L. Metallophosphaalkenes—from Exotics to Versatile Building Blocks in Preparative Chemistry. *Angew. Chem. Int. Ed.* **1996**, *35*, 271–288.

133. Weber, L. Recent Developments in the Chemistry of Metallophosphaalkenes. *Coord. Chem. Rev.* **2005**, *249*, 741–763.

134. Weber, L.; Kleinebekel, S.; Rühlicke, A.; Stammler, H. Syntheses and Structures of C-Monoamino-P-Ferriophosphaalkenes. *Eur. J. Inorg. Chem* **2000**, *1*, 1185–1191.

135. Westerhausen, M.; Schneiderbauer, S.; Piotrowski, H.; Suter, M.; Nöth, H. Synthesis of Alkaline Earth Metal Bis(2-Phosphaethynolates). *J. Organomet. Chem.* **2002**, *643–644*, 189–193.

136. Wolf, S.; Plenio, H. Synthesis of (NHC)Rh(Cod)Cl and (NHC)RhCl(CO)2 Complexes - Translation of the Rh- into the Ir-Scale for the Electronic Properties of NHC Ligands. *J. Organomet. Chem.* **2009**, *694*, 1487–1492.

137. Wolfgang A. Herrmann. N-Heterocyclic Carbenes: A New Concept in Organometallic Catalysis. *Angew. Chem. Int. Ed.* **2002**, *41*, 1290–1309.

138. Wright, V. A.; Patrick, B. O.; Schneider, C.; Gates, D. P. Phosphorus Copies of PPV: π-Conjugated Polymers and Molecules Composed of Alternating Phenylene and Phosphaalkene Moieties. *J. Am. Chem. Soc.* **2006**, *128*, 8836–8844.

139. Wu, S.; Rheingold, A. L.; Golen, J. A.; Grimm, A. B.; Protasiewicz, J. D. Synthesis of a Luminescent Azaphosphole. *Eur. J. Inorg. Chem.* **2016**, *2016*, 768–773.

140. Wu, S.; Rheingold, A. L.; Protasiewicz, J. D. Luminescent Materials Containing Multiple Benzoxaphosphole Units. *Chem. Commun.* **2014**, *50*, 11036–11038.

141. Yam, V. W.-W.; Lee, J. K.-W.; Ko, C.-C.; Zhu, N. Photochromic Diarylethene-Containing Ionic Liquids and N-Heterocyclic Carbenes. *J. Am. Chem. Soc.* **2009**, *131*, 912–913.

142. Yan, X.; Xi, C. Conversion of Zirconacyclopentadienes into Metalloles: Fagan-Nugent Reaction and Beyond. *Acc. Chem. Res.* **2015**, *48*, 935–946.

143. Yoshifuji, M.; Shima, I.; Inamoto, N.; Hirotsu, K.; Higuchi, T. Synthesis and Structure of Bis(2,4,6-Tri-Tert-Butylphenyl)Diphosphene: Isolation of a True "Phosphobenzene." *J. Am. Chem. Soc.* **1981**, *103*, 4587–4589.

144. Zafrani, Y.; Yeffet, D.; Sod-Moriah, G.; Berliner, A.; Amir, D.; Marciano, D.; Gershonov, E.; Saphier, S. Difluoromethyl Bioisostere: Examining the "Lipophilic Hydrogen Bond Donor" Concept. *J. Med. Chem.* **2017**, *60*, 797–804.

145. Zhizhin, A. A.; Zarubin, D. N.; Ustynyuk, N. A. An Imido-Transfer Reaction of Aldehydes with N-Sulfinylamines Using Vanadium and Molybdenum Oxochlorides as Catalysts. *Tetrahedron Lett.* **2008**, *49*, 699–702.

146. Zhizhko, P. A.; Pichugov, A. V.; Bushkov, N. S.; Allouche, F.; Zhizhin, A. A.; Zarubin, D. N.; Ustynyuk, N. A. Catalytic Oxo/Imido Heterometathesis by a Well-Defined Silica-Supported Titanium Imido Complex. *Angew. Chem. Int. Ed.* **2018**, *57*, 10879–10882.

147. Zhizhko, P. A.; Zhizhin, A. A.; Belyakova, O. A.; Zubavichus, Y. V.; Kolyagin, Y. G.; Zarubin, D. N.; Ustynyuk, N. A. Oxo/Imido Heterometathesis Reactions Catalyzed by a Silica-Supported Tantalum Imido Complex. *Organometallics* **2013**, *32*, 3611–3617.

148. Zhizhko, P. A.; Zhizhin, A. A.; Zarubin, D. N.; Ustynyuk, N. A.; Lemenovskii, D. A.; Shelimov, B. N.; Kustov, L. M.; Tkachenko, O. P.; Kirakosyan, G. A. Oxo/Imido Heterometathesis of N-Sulfinylamines and Carbonyl Compounds Catalyzed by Silica-Supported Vanadium Oxochloride. *J. Catal.* **2011**, *283*, 108–118.